UNIVERSITAT POLITÈCNICA DE CATALUNYA
BARCELONATECH
Departament de Teoria del Senyal
i Comunicacions

Ph.D. Thesis

MIMO designs for filter bank multicarrier and multiantenna systems based on OQAM

Author:

Màrius Caus López
Email: marius.caus@upc.edu

Thesis advisor:

Prof. Ana I. Pérez Neira
Professor at Universitat Politècnica de Catalunya
Associate Researcher at Centre Tecnològic de Telecomunicacions de Catalunya
Email: ana.isabel.perez@upc.edu

Date: November 2013

La veritat està trencada a miques i a bocins.
I per això m'emparo en el modest —i equívoc—
rètol de l'agnosticisme.

Salvador Espriu

Abstract

From the perspective of increasingly data rate requirements in mobile communications, it is deemed necessary to do further research so that the future goals can be reached. To that end, the radio-based communications are resorting to multicarrier modulations and spatial diversity. Until today, the orthogonal frequency division multiplexing (OFDM) modulation is regarded as the dominant technology. On one hand, the OFDM modulation is able to accommodate multiantenna configurations in a very straightforward manner. On the other hand, the poor stopband attenuation exhibited by the OFDM modulation, highlights that a definitely tight synchronization is required. In addition, the cyclic prefix (CP) has to be sufficiently long to avoid inter-block interference, which may substantially reduce the spectral efficiency.

In order to overcome the OFDM drawbacks, the filter bank multicarrier modulation based on OQAM (FBMC/OQAM) is introduced. This modulation does not need any CP and benefits from pulse shaping techniques. This aspect becomes crucial in cognitive radio networks and communication systems where nodes are unlikely to be synchronized. In principle, the poor frequency confinement exhibited by OFDM should tip the balance towards FBMC/OQAM. However, the perfect reconstruction property of FBMC/OQAM systems does not hold in presence of multipath fading. This means that the FBMC/OQAM modulation is affected by inter-symbol and inter-carrier interference, unless the channel is equalized to some extent. This observation highlights that the FBMC/OQAM extension to MIMO architectures becomes a big challenge due to the need to cope with both modulation- and multiantenna-induced interference.

The goal of this thesis is to study how the FBMC/OQAM modulation scheme can benefit from the degrees of freedom provided by the spatial dimension. In this regard, the first attempt to put the research on track is based on designing signal processing techniques at reception. In this case the emphasis is on single-input-multiple-output (SIMO) architectures. Next, the possibility of pre-equalizing the channel at transmission is investigated. It is considered that multiple antennas are placed at the transmit side giving rise to a multiple-input-single-output (MISO) configuration. In this scenario, the research is not only focused on counteracting the channel but also on distributing the power among subcarriers. Finally, the joint transmitter and receiver design in multiple-input-

multiple-output (MIMO) communication systems is covered.

From the theory developed in this thesis, it is possible to conclude that the techniques originally devised in the OFDM context can be easily adapted to FBMC/OQAM systems if the channel frequency response is flat within the subchannels. However, metrics such as the peak to average power ratio or the sensitivity to the carrier frequency offset constraint the number of subcarriers, so that the frequency selectivity may be appreciable at the subcarrier level. Then, the flat fading assumption is not satisfied and the specificities of FBMC/OQAM systems have to be considered. In this situation, the proposed techniques allow FBMC/OQAM to remain competitive with OFDM. In addition, for some multiantenna configurations and propagation conditions FBMC/OQAM turns out to be the best choice. The simulation-based results together with the theoretical analysis conducted in this thesis contribute to make progress towards the application of FBMC/OQAM to MIMO channels. The signal processing techniques that are described in this dissertation allow designers to exploit the potentials of FBMC/OQAM and MIMO to improve the link reliability as well as the spectral efficiency.

Resum

Des de la perspectiva que les tasses de dades requerides per les comunicacions mòbils incrementaran progressivament, s'estima necessari realitzar investigacions per tal d'assolir els futurs objectius. Amb aquesta finalitat, les comunicacions ràdio estan recorrent a la utilització de modulacions multi-portadora i a la diversitat en espai. Fins avui la modulació *orthogonal frequency division multiplexing* (OFDM) és considerada com la tecnologia dominant. D'una banda la modulació OFDM permet la utilització de múltiples antenes d'una manera senzilla. D'altre banda, la baixa atenuació que OFDM exhibeix fora de la banda pas, posa de manifest que la sincronització ha d'estar molt ben ajustada. A més, el prefixe cíclic (PC) que evita la interferència entre blocs, redueix de manera substancial l'eficiència espectral.

Amb l'objectiu de vèncer els inconvenients dels sistemes OFDM introduïm la modulació *filter bank multicarrier modulation based on OQAM* (FBMC/OQAM). Aquesta modulació no necessita cap PC i utilitza formes d'ona ben confinades en el domini temporal i freqüencial. Aquest aspecte esdevé crucial en xarxes de ràdio cognitiva i en sistemes de comunicació on els nodes no estan sincronitzats. En principi, la baixa atenuació que OFDM exhibeix fora de la banda de pas hauria de decantar la balança en favor de FBMC/OQAM. Tanmateix, la propietat que garanteix que la senyal transmesa pugui ser perfectament recuperada pel receptor, no es compleix quan hi ha propagació multicamí. Tret que el canal sigui equalitzat, això significa que hi ha interferència entre portadores. Aquesta observació posa de manifest que l'aplicació de FBMC/OQAM en arquitectures on hi ha diverses antenes esdevé un gran repte, ja que a mesura que s'afegeixen antenes s'incrementa la interferència.

L'objectiu d'aquesta tesis és estudiar com la modulació FBMC/OQAM pot beneficiar-se de la diversitat en espai. El primer intent que s'ha fet per encarrilar la recerca en la direcció desitjada, ha estat dissenyar tècniques de processat de senyal en recepció. En aquest cas s'ha posat èmfasi en arquitectures *single-input-multiple-output* (SIMO). En el pas següent, s'ha investigat la possibilitat d'equalitzar el canal en la banda del transmissor. Tanmateix, s'ha considerat que només el transmissor està equipat amb múltiples antenes originant una configuració *multiple-input-single-output* (MISO). En aquest escenari la recerca no només està orientada a combatre el canal sinó també a

distribuir la potència entre les sub-portadores. Finalment s'inclou el disseny conjunt del receptor i de l'emissor en un sistema de comunicacions *multiple-input-multiple-output* (MIMO).

De la teoria que s'ha desenvolupat en aquesta tesis, és possible concloure que les tècniques concebudes en el context d'OFDM poden ser fàcilment adaptades als sistemes FBMC/OQAM, si la resposta freqüencial del canal es plana en la banda dels sub-canals. Tanmateix, la relació entre potència màxima i potència mitja o la sensibilitat a les desviacions de la portadora limiten el nombre de sub-portadores, de tal manera que la selectivitat en freqüència del canal pot ser perceptible. Llavors, la hipòtesis de resposta plana no es compleix i les característiques de la modulació FBMC/OQAM han de ser considerades. En aquesta situació, les tècniques proposades permeten que FBMC/OQAM sigui tan competitiu com OFDM. Depenent de les condicions de propagació i del nombre d'antenes resulta que FBMC/OQAM és la millor opció. Els resultats de les simulacions juntament amb l'anàlisi teòric que s'ha portat a terme, contribueixen a aconseguir avenços en l'aplicació de FBMC/OQAM en arquitectures amb múltiples antenes. Les tècniques de processat de senyal descrites en aquesta dissertació permeten explotar els potencials de FBMC/OQAM i MIMO, per millorar la fiabilitat de l'enllaç així com l'eficiència espectral.

Resumen

Desde la perspectiva que las tasas de datos requeridas por las comunicaciones móviles incrementarán progresivamente, se estima necesario realizar investigaciones para conseguir los futuros objetivos. Con este fin, las comunicaciones radio están recorriendo a la utilización de modulaciones multi-portadora y a la diversidad en espacio. Hasta hoy la modulación *orthogonal frequency division multiplexing* (OFDM) es considerada como la tecnología dominante. De una banda la modulación OFDM permite la utilización de múltiples antenas de una manera sencilla. De otra banda, la baja atenuación que OFDM exhibe fuera de la banda de paso, pone de manifiesto que la sincronización tiene que estar muy bien ajustada. Además, el prefijo cíclico (PC) que evita la interferencia entre bloques, reduce de manera substancial la eficiencia espectral.

Con el objetivo de vencer los inconvenientes de los sistemas OFDM introducimos la modulación *filter bank multicarrier modulation based on OQAM* (FBMC/OQAM). Esta modulación no necesita ningún PC y utiliza formas de onda bien confinadas en el dominio temporal y de la frecuencia. Este aspecto es crucial en redes de radio cognitiva y en sistemas de comunicación donde los nodos no están sincronizados. En principio, la baja atenuación que OFDM exhibe fuera de la banda de paso debería decantar la balanza en favor de FBMC/OQAM. Sin embargo, la propiedad que garantiza que la señal transmitida pueda ser perfectamente recuperada en recepción, es destruida cuando hay propagación multicamino. Salvo que el canal sea ecualizado, esto significa que hay interferencia entre portadoras. Esta observación pone de manifiesto que la aplicación de FBMC/OQAM en arquitecturas donde hay varias antenas es un gran reto, ya que a medida que se añaden antenas se incrementa la interferencia.

El objetivo de esta tesis es estudiar como la modulación FBMC/OQAM puede beneficiarse de la diversidad en espacio. El primer intento que se ha hecho para encarrilar la investigación en la dirección deseada, ha estado diseñar técnicas de procesado de señal en recepción. En este caso se ha puesto el énfasis en arquitecturas *single-input-multiple-output* (SIMO). En el paso siguiente, se ha investigado la posibilidad de ecualizar el canal en la banda del transmisor. Sin embargo, se ha considerado que solo el transmisor está equipado con múltiples antenas originando una configuración *multiple-input-single-output* (MISO). En este escenario la investigación no solo está orientada a

combatir el canal sino también a distribuir la potencia entre las sub-portadoras. Finalmente se ha incluyendo el diseño conjunto del transmisor y del receptor en un sistema de comunicaciones *multiple-input-multiple-output* (MIMO).

De la teoría que se ha desarrollado en esta tesis, es posible concluir que las técnicas concebidas en el contexto de OFDM pueden ser fácilmente adaptadas a los sistemas FBMC/OQAM, si la respuesta del canal en frecuencia es plana en la banda de los sub-canales. No obstante, la relación entre potencia máxima y potencia media o la sensibilidad a las desviaciones de la portadora limitan el número de sub-portadoras, de tal manera que la selectividad del canal puede ser perceptible. Entonces, la hipótesis de respuesta plana no se cumple y las características de la modulación FBMC/OQAM tienen que ser consideradas. En esta situación, las técnicas propuestas permiten que FBMC/OQAM sea tan competitivo como OFDM. Dependiendo de las condiciones de propagación y del número de antenas resulta que FBMC/OQAM es la mejor opción. Los resultados de las simulaciones juntamente con el análisis teórico que se ha llevada a cabo, contribuyen a lograr avances en la aplicación de FBMC/OQAM en arquitecturas con múltiples antenas. Las técnicas de procesado de señal descritas en esta disertación permiten explotar los potenciales de FBMC/OQAM y MIMO, para mejorar la fiabilidad del enlace así como la eficiencia espectral.

Acknowledgements

With these lines I want to express my deepest gratitude towards the institutions and the people that have significantly contributed to the elaboration of this thesis.

First of all I would like to thank my supervisor, the Prof. Ana Pérez Neira for her guidance, patience and support in all moments of this thesis development. I am truly indebted to Ana for being a great mentor and for transmitting me her passion for research. I feel very lucky to have had the opportunity to work with Ana. I would like to mention that during the doctorate we have had lots of interesting and nice conversations, not always related to work, which I have really enjoyed.

Another reason I am grateful to Ana is for encouraging me to learn from other people. In this sense, I have had the pleasure to collaborate with outstanding researchers. I thank Markku Renfors, Marco Moretti and Ana García Armada who have helped to shape my thinking and develop my research skills. I especially owe a debt of gratitude to Markku Renfors for making my stay at the Tampere University of Technology so pleasant. I certainly had a wonderful time.

I am very grateful for the funding that I have received from the Govierno de España to pursue my PhD studies.

I would like to express my thankfulness to all my current and former colleagues who I shared office with in D5-214: Josep F., Eva L., Javier R., Sandra L., Adriano P., Adrián A., Guillem P., Miriam L., Marta C., Frank S., Juan Manuel C. and Rupayan C. Thank you for sharing your views, experience and concerns about pursuing a Ph. D and for your predisposition to meet me outside office hours just to have a good time. Embarking on a doctoral degree has given me the chance to know a lot of people. Among them I would like to mention: Maria G., Miguel Ángel V., Javier A., Giuseppe C., Jaime G., Marc M., Omid G. and Tatjana P. with whom I have also spent a good time at some point during my Ph. D. studies.

I appreciate the interest that Toni Pascual has showed about the progress of my research. Thanks Toni. I am extremely grateful to Carlos F. Bader and Xavier Mestre to allow me to participate and be involved in the Emptahic project. It is an awesome forum to inspire further research.

Without my friends the period of time that I spent working on my thesis would have been much

more boring and monotonous. I have had some of the most memorable and funniest moments with you.

Last, but not least, an enormous debt of gratitude is owed to my parents for their unconditional support and love.

Contents

Abstract **v**

Resum **vii**

Resumen **ix**

Table of contents **xiii**

Acronyms **xvii**

Notation **xxi**

List of figures **xxiii**

List of tables **xxvi**

1 Why FBMC/OQAM? **1**

1.1 Background and motivation 1

1.2 Outline of the dissertation 6

1.3 Research contributions 8

2 FBMC/OQAM system model **11**

2.1 SISO architecture 11

2.2 MIMO architecture 18

2.3 Study cases 20

2.3.1 OFDM vs. FBMC/OQAM 21

3 Equalization and detection **23**

3.1 Equalization in SIMO PTP communications 23

3.1.1 MDIR receiver 24

3.1.2 MDIR impairments . . . 26
3.1.3 Simulation results . . . 27
3.2 Equalization in the asynchronous SIMO-MAC . . . 29
3.2.1 MDIR receiver . . . 30
3.2.2 ZF receiver . . . 32
3.2.3 Simulation results . . . 34
3.2.4 Complexity analysis . . . 36
3.3 Interference aware detection . . . 36
3.3.1 Direct decision method (DDM) . . . 39
3.3.2 Refined direct decision method (RDDM) . . . 40
3.3.3 Comparison of different estimation techniques . . . 41
3.3.4 Application to single frequency networks . . . 42
3.3.5 Numerical results . . . 43
3.4 Chapter summary . . . 48
3.A Solution of problem 3.12 . . . 49
3.B Demonstration that the IN term has zero mean . . . 51

4 Precoding techniques in MISO PTP communications 53
4.1 System model . . . 53
4.2 Precoding with fixed power distribution . . . 55
4.2.1 ZF transmitter . . . 55
4.2.2 SLNR-based precoding . . . 57
4.2.3 MDIR transmitter . . . 58
4.2.4 MMSE transmitter . . . 58
4.2.5 Simulation results . . . 58
4.3 Precoding with power allocation . . . 61
4.3.1 Optimal precoding . . . 61
4.3.2 Suboptimal precoding . . . 62
4.3.3 Simulation results . . . 62
4.4 Chapter summary . . . 65
4.A Solution of problem 4.13 . . . 66
4.B Solution of problem 4.17 . . . 66
4.C Solution of problem 4.18 . . . 67
4.D Solution of problem 4.19 . . . 69

5 Power allocation algorithms **73**
5.1 SINR balancing in MISO PTP communications . . . 73
5.1.1 Simulation results . . . 75
5.2 Sum-rate maximization in MISO PTP communications . . . 78
5.2.1 Step 1 . . . 81
5.2.2 Step 2 . . . 81
5.2.3 Step 3 . . . 83
5.2.4 Simulation results . . . 84
5.3 Discrete sum-rate maximization in MISO PTP communications . . . 88
5.3.1 Interference aware bit-filling algorithm . . . 91
5.3.2 Ideal bit-filling algorithm . . . 94
5.3.3 Simulation results . . . 95
5.4 Sum-rate maximization in the SIMO-BC . . . 98
5.4.1 Step 1 . . . 103
5.4.2 Step 2 . . . 104
5.4.3 Step 3 . . . 105
5.4.4 Simulation results . . . 106
5.5 Chapter summary . . . 110
5.A Solution of problem 5.1 . . . 112
5.B Solution of problem 5.16 . . . 112
5.C Solution of problem 5.18 . . . 114
5.D Maximum transmittable power per-subcarrier . . . 115
5.E Solution of problem 5.81 . . . 116

6 MIMO designs for low frequency selective channels **119**
6.1 MIMO designs in PTP communications . . . 120
6.1.1 Linear processing design in MIMO-FBMC/OQAM systems . . . 122
6.1.2 Linear processing design in MIMO-OFDM systems . . . 123
6.1.3 Widely linear processing design in MIMO-FBMC/OQAM systems . . . 124
6.1.4 Widely linear processing versus linear processing . . . 126
6.1.5 MIMO-FBMC/OQAM versus MIMO-OFDM . . . 127
6.1.6 Simulation results . . . 128
6.2 MIMO designs in the BC . . . 130
6.2.1 Block diagonalization . . . 132
6.2.2 Spatial Tomlinson Harashima precoder . . . 132
6.2.3 Simulation results . . . 136

6.3 Chapter summary . . . 138
6.A Demonstration of Lemma 6.28 . . . 139
6.B Demonstration that $\tilde{\boldsymbol{\lambda}}_q$ is majorized by $\tilde{\boldsymbol{\beta}}_q$ . . . 140
6.C Demonstration that $\beta_{1q} > \lambda_{1q}$ and $\beta_{N_R q} < \lambda_{N_R q}$ . . . 143
6.D Demonstration of Lemma 6.31 . . . 144
6.E Demonstration of Lemma 6.33 . . . 144

7 MIMO designs for highly frequency selective channels 147
7.1 Mathematical model for narrowband precoders and broadband equalizers . . . 147
7.2 Mathematical model for broadband precoders and narrowband equalizers . . . 149
7.3 Single-stream transmission . . . 150
7.3.1 Maximization of the SLNR: space-time processing at transmission . . . 151
7.3.2 Maximization of the SINR: space-time processing at reception . . . 153
7.4 Multi-stream transmission . . . 156
7.4.1 Suboptimal subband processing . . . 156
7.4.2 Widely linear vs. linear processing . . . 158
7.4.3 Iterative design . . . 160
7.5 Simulation results . . . 162
7.6 Chapter summary . . . 165
7.A Solution of problem 7.46 . . . 167
7.B Solution of problem 7.56 . . . 169

8 Conclusions and future work 173
8.1 Conclusions . . . 173
8.2 Future lines of research . . . 175
8.2.1 Resource allocation . . . 176
8.2.2 Design of MIMO precoding and decoding matrices . . . 176

Bibliography 179

Publications in journals 195

Acronyms

AFB	Analysis filter bank
AM	Amplitude Modulation
AWGN	Additive white Gaussian noise
BC	Broadcast channel
BD	Block diagonalization
BER	Bit error rate
BS	Base station
CFO	Carrier frequency offset
CFR	Channel frequency response
CIR	Channel impulse response
CP	Cyclic prefix
CPO	Carrier phase offset
CSI	Channel state information
CMT	Cosine modulated multitone
DC	Difference of concave
DDM	Direct decision method
DFT	Discrete Fourier transform
DIR	Desired impulse response
EMFB	Exponentially-modulated filter bank
E-UTRA	Evolved UMTS Terrestrial Radio Access
FBMC	Filter bank multicarrier
FFT	Fast Fourier Transform
FIR	Finite impulse response
FMT	Filtered multitone
GFDM	Generalized frequency division multiplexing

IAI	Inter-antenna interference
IBI	Inter-block interference
IC	Interference channel
ICI	Inter-carrier interference
IDFT	Inverse DFT
IFFT	Inverse FFT
IN	Interference plus noise
IS	Interference suppression
ISI	Inter-symbol interference
IUI	Inter-user interference
LLR	Log-likelihood ratio
MA	Margin adaptive
MAC	Multiple access channel
MAI	Multiple access interference
MCM	Multicarrier modulation
MDIR	Matched desired impulse response
MIMO	Multiple-input-multiple-output
MISO	Multiple-input-single-output
ML	Maximum likelihood
MLSE	Maximum likelihood sequence estimator
MM	Margin maximization
MMSE	Minimum mean square error
MSE	Mean square error
MTP	Multipoint-to-point
OFDM	Orthogonal frequency division multiplexing
OQAM	Offset quadrature amplitude modulation
PPN	Polyphase network
PHYDYAS	PHYsical layer for DYnamic spectrum AccesS and cognitive radio
PTP	Point-to-point

PTM	Point-to-multipoint
P/S	Parallel to serial
QAM	Quadrature amplitude modulation
RA	Rate adaptive
RDDM	Refined direct decision method
RM	Rate maximization
Rx	Receiver
SC-FDE	Single carrier frequency domain equalization
SDMA	Space-division multiple access
SER	Symbol error rate
SFB	Synthesis filter bank
SFN	Single frequency network
SIMO	Single-input-multiple-output
SINR	Signal to interference plus noise ratio
SISO	Single-input-single-output
SLNR	Signal to leakage plus noise ratio
SMT	Staggered modulated multitone
SNR	Signal to noise ratio
S/P	Serial to parallel
STHP	Spatial Tomlinson Harashima precoder
SVD	Singular value decomposition
TMUX	Transmultiplexer
TO	Time offset
Tx	Transmitter
UMTS	Universal Mobile Telecommunications System
UPA	Uniform power allocation
UT	User terminal
WiMAX	Worldwide Interoperability for Microwave Access
ZF	Zero forcing

Notation

Notation for scalars

x	Scalar
$\lfloor x \rfloor$	Largest integer not greater than x
$\lceil x \rceil$	Smalest integer not less than x
$\Re\{x\}$	Real part of x
$\Im\{x\}$	Imaginary part of x
$\|x\|$	Absolute value of x
$\mathbb{E}\{x\}$	Statistical expectation of x
$(x)^*$	Complex conjugate of x
j	Imaginary unit $\sqrt{-1}$
$\log_n(x)$	n-base logarithm of x
e^x	Exponential function evaluated on x
$\delta_{q,m}$	Kronecker delta: $\delta_{q,m} = \begin{cases} 1 & m = q \\ 0 & \text{otherwise} \end{cases}$
$\frac{\partial f(x)}{\partial x}$	Partial derivative of function $f(x)$ with respect to x
$\mathcal{CN}(m, c)$	Complex circularly symmetric Gaussian variable with mean m and variance c
$\mathcal{N}(m, c)$	Real Gaussian variable with mean m and variance c

Notation for sets

$\mathbb{R}$	Set of real numbers
$\mathbb{C}$	Set of complex numbers
$\|X\|$	Cardinality of the set X
$X^{M \times N}$	Set of $M \times N$ matrices whose entries belong to the set X
$X \bigcup Y$	Union of sets X and Y
$X \bigcap Y$	Intersection of sets X and Y

Notation for sequences

$x[n]$	Discrete-time sequence
n	Sampling index
$(.)_{\downarrow N}$	Downsampling by factor N
$(.)_{\uparrow N}$	Upsampling by factor N
$X(z)$	Z-transform of $x[n]$
z	Z-transform variable
z^{-1}	Unit delay
$X(e^{jw})$	Frequency response of the sequence $x[n]$
$*$	Convolution operation

Vector and matrix notation

$\mathbf{x}$	Column vector
$[\mathbf{x}]_i$	ith element of the vector $\mathbf{x}$
$\|\mathbf{x}\|_n$	n-norm of vector $\mathbf{x}$
$\mathbf{X}$	Matrix
$\mathbf{I}_N$	$N \times N$ identity matrix
$[\mathbf{X}]_{ij}$	Element of matrix $\mathbf{X}$ located at the ith row and the jth column
$\det(\mathbf{X})$	Determinant of $\mathbf{X}$
$\mathbf{X}^T$	Transpose of $\mathbf{X}$
$\mathbf{X}^H$	Complex transpose of $\mathbf{X}$
$\mathbf{X}^{-1}$	Inverse of $\mathbf{X}$
$\text{diag}(\{\mathbf{x}\})$	Diagonal matrix which entries are collected in $\mathbf{x}$
$\text{tr}(\mathbf{X})$	Trace of matrix $\mathbf{X}$
$\|\mathbf{X}\|_F$	Frobenius norm of matrix $\mathbf{X}$
$\otimes$	Kronecker product
$\frac{\partial f(\mathbf{x})}{\partial \mathbf{x}}$	Partial derivative of function $f(\mathbf{x})$ with respect to vector $\mathbf{x}$
$\mathcal{CN}(\mathbf{m}, \mathbf{C})$	Complex circularly symmetric Gaussian vector with mean $\mathbf{m}$ and covariance matrix $\mathbf{C}$
$\mathcal{N}(\mathbf{m}, \mathbf{C})$	Real Gaussian vector with mean $\mathbf{m}$ and covariance matrix $\mathbf{C}$

List of Figures

2.1 Block diagram of the FBMC/OQAM transceiver. 12
2.2 Efficient implementation of the transmitter. 13
2.3 Staggering process. 14
2.4 Power spectral density corresponding to the signal transmitted in the tenth subchannel when the air-interface is based on FBMC/OQAM and OFDM. 14
2.5 Efficient implementation of the receiver. 15
2.6 De-staggering process. 16
2.7 FBMC/OQAM application to MIMO communication systems 20
2.8 Magnitude of the channel frequency response evaluated between subcarrier 200 and subcarrier 209. The subcarrier spacing has been set to 10.94 KHz. The channel realizations obey the ITU Vehicular A, ITU Pedestrian A and the ITU Vehicular B guidelines. 21

3.1 MDIR subcarrier receiver adapted to FBMC/OQAM systems. 26
3.2 R against $\frac{E_b}{N_0}$. The system parameters and the propagations conditions are set according to Scenario 3 (see Table 2.3). 27
3.3 BER against $\frac{E_b}{N_0}$. The simulated systems correspond to FBMC/OQAM with per-subcarrier MDIR receiver and OFDM with CP. System parameters are set according to Scenario 1 and 3 (see Table 2.3). 28
3.4 FBMC/OQAM-based SIMO multiple access channel. 32
3.5 Blockwise subcarrier allocation strategy with frequency guards. 34
3.6 BER against $\frac{E_b}{N_0}$. The simulated systems correspond to OFDM with multi-user MMSE receiver and to FBMC/OQAM with per-subcarrier MDIR receiver and per-subcarrier ZF receiver. System parameters are set according to Scenario 1 (see Table 2.3). 35
3.7 Transmitter and receiver block diagram. 37
3.8 Receiver scheme with variance estimation. 40

3.9 Single frequency network with frequency reuse equal to one. 43
3.10 BER vs. $\frac{E_b}{N_0}$ when the receiver is based either on perfect IN variance estimation or on perfect interference cancellation. The propagation conditions obey the VehA and the VehB channel models. 44
3.11 Average NIR versus $\frac{E_b}{N_0}$. The propagation conditions obey the VehB channel model. 45
3.12 BER versus $\frac{E_b}{N_0}$ when the receiver implements different IN variance estimation methods. The propagation conditions obey the VehA and VehB channel models. 46
3.13 SER before and after performing the initial turbo iteration versus $\frac{E_b}{N_0}$. The propagation conditions obey the VehA aand VehB channel models. 47

4.1 BER against $\frac{E_b}{N_0}$. The simulated systems correspond to FBMC/OQAM with different precoding schemes. System parameters are set according to Scenario 1 (see Table 2.3). 59
4.2 BER against $\frac{E_b}{N_0}$. The simulated systems correspond to FBMC/OQAM with different precoding schemes. System parameters are set according to Scenario 3 (see Table 2.3). 60
4.3 BER against $\frac{E_b}{N_0}$. The simulated systems correspond to OFDM. System parameters are set according to Scenario 1 and 3 (see Table 2.3). 61
4.4 Average power against the inverse of the normalized noise power. The simulated systems correspond to FBMC/OQAM with different precoding schemes. The target SINR is set to 10 dB and 15 dB. System parameters are set according to Scenario 1 (see Table 2.3). 63
4.5 Average leakage and desired signal energy against the inverse of the normalized noise power. The simulated systems correspond to FBMC/OQAM with different precoding schemes. System parameters are set according to Scenario 1 (see Table 2.3). 64

5.1 Minimum SINR against $\frac{E_s}{N_0}$. The simulated systems correspond to FBMC/OQAM. System parameters are set according to Scenario 1 and 3 (see Table 2.3). 76
5.2 BER against $\frac{E_s}{N_0}$. The simulated systems correspond to FBMC/OQAM. System parameters are set according to Scenario 1 and 3 (see Table 2.3). 76
5.3 BER against $\frac{E_s}{N_0}$. The simulated systems correspond to OFDM. System parameters are set according to Scenario 1 and 3 (see Table 2.3). 77
5.4 Subband partitioning scheme. Subcarrier signals span from the subcarrier index 1 to the index 9. 81
5.5 Performance assessment of FBMC/OQAM-based 1×2 MISO systems. The power is distributed according to alternatives 1 and 2. System parameters are set according to the scenario 3 (see Table 2.3). 86

5.6 Rate against $\frac{E_s}{N_0}$ fixing $P_T = 1W$. Different power allocation strategies are evaluated in a FBMC/OQAM-based MISO system. System parameters are set according to the scenario 3 (see Table 2.3). 86
5.7 Rate against $\frac{E_s}{N_0}$ fixing $P_T = 1W$. The FBMC/OQAM and the OFDM modulation schemes are evaluated when WF and UPA policies are implemented. System parameters are set according to the scenario a (see Table 2.3). 87
5.8 Assessment of different bit-loading algorithms in FBMC/OQAM systems. System parameters are set according to the scenario 3 (see Table 2.3). 96
5.9 Assessment of the simple bit-filling algorithm in FBMC/OQAM and OFDM systems. System parameters are set according to the scenario 1 (see Table 2.3). 97
5.10 FBMC/OQAM-based MISO broadcast channel. 99
5.11 FBMC/OQAM-based SIMO broadcast channel. 101
5.12 Evaluation of the sum-rate in the FBMC/OQAM-based 2×1 SIMO broadcast channel. Different power and subcarrier allocation strategies are simulated. System parameters are set according to the scenario 3 (see Table 2.3). 108
5.13 Evaluation of the sum-rate in the 2×1 SIMO broadcast channel. The FBMC/OQAM and the OFDM modulation schemes are evaluated when the subcarrier allocation is based on the SNR metric and the power is distributed according to WF and UPA policies. System parameters are set according to the scenario 1 (see Table 2.3). . . . 109

6.1 BER vs. $\frac{E_s}{N_0}$ for different multi-antenna configurations in FBMC/OQAM systems. System parameters are set according to Scenarios 1 and 2 (see Table 2.3). 129
6.2 BER vs. $\frac{E_s}{N_0}$ for different multi-antenna configurations in FBMC/OQAM and OFDM systems. System parameters are set according to Scenarios 1 (see Table 2.3). 130
6.3 FBMC/OQAM-based MIMO broadcast channel. 131
6.4 Block diagram of the spatial Tomlinson-Harashima precoder. 133
6.5 Block diagram of the proposed spatial Tomlinson-Harashima precoder. 135
6.6 BER vs. $\frac{E_s}{N_0}$ when BD is applied to FBMC/OQAM and OFDM systems. System parameters are set according to Scenarios 1 and 2 (see Table 2.3). 136
6.7 BER vs. $\frac{E_s}{N_0}$ when the TH concept is applied to FBMC/OQAM and OFDM systems. System parameters are set according to Scenarios 1 and 2 (see Table 2.3). 137

7.1 BER vs. $\frac{E_b}{N_0}$ for $2 \times 2 \times 1$ communication systems in OFDM and FBMC/OQAM modulation schemes. System parameters are set according to Scenarios 1 and 3 (see Table 2.3). 163

7.2 BER vs. $\frac{E_b}{N_0}$ for different multi-antenna configurations in FBMC/OQAM and OFDM modulation schemes. System parameters are set according to the Scenario 1 (see Table 2.3). 164
7.3 BER vs. $\frac{E_s}{N_0}$ for $4 \times 2 \times 2$ communication systems in OFDM and FBMC/OQAM modulation schemes. System parameters are set according to Scenarios 1 and 3 (see Table 2.3). 165
7.4 BER for a $4 \times 2 \times 2$ communication system having fixed $\frac{E_s}{N_0}$=20dB. 166

List of Tables

2.1 Intrinsic interferences for q even. 18
2.2 Intrinsic interferences for q odd. 18
2.3 System parameters and propagation conditions 20

3.1 Complexity order and memory requirements of computing the variance of the IN term in all the subcarriers. 41

Chapter 1

Why FBMC/OQAM?

1.1 Background and motivation

The wireless personal communications have recently become very popular due to the increasingly users' demands on multimedia content and mobility. It is not expected that the requirements on higher data rates will decrease, but the opposite as it is reported by the International Telecommunication Union Radiocommunication [1]. Thus, it becomes mandatory to gradually increase the capacity of the networks that provide these contents. Towards this end, it seems that the use of multicarrier modulation (MCM) schemes together with multiantenna configurations is the option that is being most favourably considered to reach the throughput goals. Among the wireless standards that include multicarrier and multiantenna techniques in the physical layer specifications, the most recent are the Evolved UMTS Terrestrial Radio Access Long Term Evolution (E-UTRA LTE) [2], the Worldwide Interoperability for Microwave Access (WiMAX) [3] and the WiFi based on the standard IEEE 802.11ac [4]. The stringent challenges that future wireless communications have to face implies that further research has to be done in order to attain the ever-increasing rate requirements.

The implementation of multiple antennas at both ends of the link is widely considered as an attractive solution to substantially improve the overall system performance. The key aspect that allows multiantenna transceiving systems to improve the wireless communications stems from the additional degrees of freedom provided by the spatial dimension. The use of multiple antennas in combination with advanced signal processing algorithms, give rise to the multiple-input-multiple-out (MIMO) technology, which is able to boost the spectral efficiency and enhance the link reliability [5–9]. The beauty of MIMO systems is that the aforementioned merits come at no extra cost in terms of bandwidth and transmit power.

In wireless communications the media is dispersive when there is no visual line of sight between

the transmitter and the receiver. This results in a channel that induces inter-symbol interference (ISI) giving rise to frequency selectivity. This may become an obstacle to benefit from the MIMO technology developed in narrowband communications, where the media is nondispersive. The strategy of transmitting the information in blocks and equalizing the channel in the frequency domain has been proven to be able to deal with ISI [10–12]. The alternative that consists in equalizing the channel in the time domain may require a digital signal processing speed that is prohibitively high, which makes the solution impractical and unattractive. The block processing described in [10, 12] can be implemented in single carrier and multicarrier modulated systems. The idea in both cases hinges on receiving a signal that is expressed as the circular convolution of the channel with the transmitted block. This property is satisfied thanks to the transmission of a cyclic prefix (CP), which should be larger than the most delayed echo of the channel. If don't, there is inter-block interference (IBI) and the system performance degrades significantly. In the literature, the single carrier and the multicarrier solutions based on the CP transmission are called single carrier frequency domain equalization (SC-FDE) and orthogonal frequency division multiplexing (OFDM), respectively. Both schemes have similar complexity because the same blocks are used. The difference of SC-FDE with respect to OFDM is that the inverse fast Fourier transform (IFFT) is moved from the transmitter to the receiver. As a consequence, in the OFDM case the symbols are detected in the frequency domain. Conversely, the decisions are carried out in the time domain when the SC-FDE scheme is implemented. Hence, the energy of a given symbol is distributed over all the frequency band when the single carrier system is considered. Hence, SC-FDE presents an increased robustness to deep spectral notches, a reduced sensitivity to carrier frequency offsets and a reduced peak to average power ratio (PAPR) when compared to OFDM. Based on this, the SC-FDE scheme seems to be the most attractive solution. However, the system performance can be substantially improved in OFDM if the modulation order and the power allocated on each subcarrier are based on the channel gains. With adaptive modulation and power allocation, the block processing based on the multicarrier concept outperforms the single carrier alternative [13]. It is worth mentioning that the PAPR problem that arise in OFDM can be circumvented by spreading the symbols over all the frequency range by using the discrete Fourier transform (DFT) [14]. As a result, SC-FDE is only suggested by IEEE 802.16. while OFDM has been included in the physical layer specifications of several standards such as: the digital video broadcasting (DVB), the digital audio broadcasting (DAB), IEEE 802.16 and IEEE.802.11. Actually, OFDM is nowadays the most prominent multicarrier modulation. Aside from the ability to mitigate the dispersion of the media, the beauty of OFDM comes from the fact that the end-to-end communication system, which accounts for the transmitter, the channel and the receiver, can be represented as a set of parallel flat fading channels. It must be mentioned that this is the key aspect that enables combining straightforwardly OFDM with MIMO techniques. In this sense, OFDM can benefit from

the theory developed in MIMO narrowband systems. Nevertheless, the orthogonality conditions, which enable independently processing each subcarrier, hinge on shaping the subcarrier signals with the rectangular window along with transmitting redundancy in the form of a CP. This highlights that OFDM presents several limitations, which are listed below:

- The CP transmission implies a reduction of the spectral efficiency as well as wastage of power.
- Any time and frequency misalignment between the transmitter and the receiver destroys the orthogonality between subcarriers and, therefore, subcarrier signals leak to unintended subcarriers. Since the rectangular window is characterized to have a sinc-like shape spectrum, the leakage severely degrades the quality of the demodulated data. As a result, it is deemed necessary to achieve a tight synchronization between nodes. The stringent synchronization requirements limit the use of OFDM in dynamic spectrum access networks where nodes are unlikely to be perfectly aligned [15].
- The poor stopband attenuation exhibited by the rectangular pulse obliges the designer to leave empty several subcarriers at the boundaries of the band. Otherwise, the OFDM signal may degrade other services transmitted on adjacent bands.
- The large side lobes that characterize the sinc pulse implies that narrowband interferences will affect several subcarrier signals.

It is obvious that the OFDM disadvantages associated to the rectangular window can be overcome to a significant extent if the subcarrier signals are shaped with well-frequency localized waveforms. The idea of shaping the subcarrier signals with a pulse different from the rectangular window has its origins at sixties. Chang was the first who devised a multichannel transmission system in which amplitude modulated (AM) data is transmitted in parallel by band-limited pulses, [16]. Therein Chang met the orthogonal conditions that resulted in a new set of pulses that enable achieving the maximum data rate in the absence of ISI and inter-carrier interference (ICI). Soon after, Saltzberg in [17] extended the scheme envisaged in [16] and proposed a parallel quadrature amplitude modulation (QAM) transmission. The modification consisted in staggering in-phase and quadrature components of symbols drawn from a QAM constellation. It must be mentioned that both schemes achieve the same bandwidth efficiency since a partially spectrum overlapping between adjacent channels is permitted. However, neither Chang's nor Saltzberg's transmultiplexer (TMUX) was regarded as a candidate in transmission data systems. Single channel transmission schemes were more appealing since they needed far less circuitry. Aiming at reducing the hardware requirements many researchers investigated the possibility of designing an equivalent digital system. In this regard, Bellanger proposed a special structure that combines a polyphase network

(PPN) and a digital Fourier processor, [18]. The idea of overcoming the circuit complexity by using the digital Fourier transform (DFT) was further studied by Hirosaki giving rise to a new digital signal processing method, [19]. Therein the Saltzberg's data transmission scheme was efficiently reformulated in the digital domain. It must be mentioned that Hirosaki's scheme works with real samples. Even though the digital Fourier processor as well as the PPN process complex data, only the real part of the incoming signal to be fed to the digital to analog converter is extracted. This processing is suitable for baseband applications. However, Coriolaro et al. demonstrated that the sampling rate can be reduced by a factor of two for bandpass transmissions, [20]. To do so, Saltzberg's scheme is rearranged into a digital virtual complex model. At this point little attention was paid to the inherent discretization of the pulses. The orthogonal conditions originally formulated for continuous-time signals do not hold when the digital model is considered. In this regard Siohan et al. and Bolcskei addressed different approaches to establish the discrete orthogonality in [21] and [22], respectively. It is worth mentioning that Vetterli [23], Vaidyanathan [24] and Karp and Fliege [25], among other authors, have also carried out studies to efficiently implement filter bank structures.

In the literature the multicarrier schemes that resort to pulse shaping techniques are called filter bank multicarrier (FBMC) systems. These systems are divided into two categories depending on the real or complex nature of symbols. In the complex case the multicarrier signal can be generated according to the filtered multitone (FMT) scheme [26, 27], or the generalized frequency division multiplexing (GFDM) scheme [28]. The FMT technique uses frequency confined pulses but the subcarrier signals are not allowed to overlap in the frequency domain. As a consequence, FMT systems fail to achieve the maximum bandwidth efficiency. The spectral efficiency loss is related with the roll-off factor of the pulses in the sense that the higher is the roll-off factor, the higher is the transition band of the pulses and consequently the higher has to be the subcarrier spacing. The GFDM system can be understood as a parallel transmission in several SC-FDE links, which are separated in frequency. Hence, each subcarrier performs a block transmission with a CP. In addition, subcarrier signals can be shaped with the desired waveform independently. Since subcarriers overlap in the frequency domain and waveforms are not orthogonal, the received signals are degraded by ICI. This highlights that the bandwidth of each subcarrier together with the design of the pulses are of paramount importance to control the energy that leaks through non-intended subcarriers. Despite of this, the GFDM scheme in [29] is considered as a candidate to address the requirements that cognitive radio and machine-to-machine communications introduce to 5th generation cellular networks.

The two techniques that lie into the second category, where transmitted signals belong to the real field, are named staggered modulated multitone (SMT) and cosine modulated multitone (CMT), [30, 31]. The CMT and SMT schemes are respectively related to the Chang's method [16]

and the Saltzberg's method [17]. In this dissertation we focus on SMT, which is also identified with the terminology FBMC/offset quadrature amplitude modulation (FBMC/OQAM) or OFDM/offset quadrature amplitude modulation (OFDM/OQAM). The reason lies in the fact that the low-rate signals multiplexed over each subband belong to the OQAM constellation, which is obtained by staggering in-phase and quadrature components of QAM symbols. The approach based on the OQAM scheme is gaining momentum because in contrast to FMT, GFDM and OFDM it achieves maximum bandwidth efficiency. That is because no redundancy is transmitted and subcarrier signals can overlap in the frequency domain as described in [17]. This allows reducing the subcarrier spacing when compared to FMT and, therefore, we can increase the number of streams that are frequency multiplexed. In view of this discussion, we have favoured the FBMC/OQAM modulation over the others filter bank multicarrier schemes.

It is important to remark that we may improve the system performance of OFDM systems by choosing a signal basis different than that built upon the rectangular pulse. To this end, several techniques to suppress the side lobes can be found in [32–37]. Even though these techniques succeed in reducing the out of band emission, the implementation complexity may increase and the capacity loss in the prefix is not solved. It must be mentioned that if subcarrier signals convey complex-valued symbols as it happens in the OFDM context, then there exists a theoretical limit that restricts the factor with which the pulses of the orthogonal basis decay. The authors in [38] show that these limits can be exceeded, thus a faster decay can be achieved, if the symbols are drawn from the OQAM constellation, which confirms that FBMC/OQAM is an attractive multicarrier modulation.

In summary, FBMC/OQAM exhibits a low out of band emission while the spectral efficiency is not degraded. Therefore, the FBMC/OQAM has the key features that are needed to transmit in a fragmented spectrum or in networks where tight synchronization cannot be attained. This may tip the balance towards FBMC/OQAM when designing the air-interface in networks where different systems coexist in the same bandwidth. With that being said, the FBMC/OQAM-based air-interface can be considered as a possible candidate for future wireless communications. Therefore, it is of paramount importance to demonstrate that the FBMC/OQAM scheme can benefit from the additional degrees of freedom provided by the spatial dimension. It is well-know that if the channel frequency selectivity is not appreciable in the frequency range of at least one subchannel, then some of the pre- and post-processing techniques originally devised for OFDM can be applied to FBMC/OQAM without destroying the orthogonality. However, the applicability of FBMC/OQAM to MIMO communication systems is a non-trivial task when the channel is frequency selective at the subcarrier level. Under this assumption the orthogonality between subcarriers is destroyed and the data symbols leak to unintended slots and subcarriers. As a consequence, the demodulated signals are affected by ISI, ICI and inter-antenna interference (IAI). In the light of the above

discussion along with the characteristics of the OQAM, we can assert that in general the optimal MIMO precoding and decoding matrices originally devised for OFDM systems are not optimal for FBMC/OQAM. Therefore, the reasons that motivate us to devise signal processing techniques specifically thought for the FBMC/OQAM modulation are twofold:

- The channel may induce interference and, therefore, aside from the noise the received signal may be degraded by ICI, ISI and IAI.
- The OQAM symbols only convey information in a single dimension.

The first point reveals that the loss of orthogonality has to be considered. The second point indicates that the real and imaginary parts of the received samples have to be independently processed so that all the second order statistics come into play. This way of performing can be viewed as a special case of widely linear processing (WLP) when the variables to be estimated are real-valued [39]. In general, WLP is used the exploit the improperness of data sequences, [40]. In this sense, applications of WLP include: prediction [41], multiuser detection with improper multiple access interference [42], suppression of rotationally variant residual multiuser interference [43], equalization [44], equalization for STBC transmission [45, 46], single antenna interference cancellation for global system for mobile communications [47, 48], transceiver structure employing widely linear filters [49, 50], multiple antenna interference cancellation [51] and improper signalling on the interference channel [52]

Since the aim of this thesis is to provide insight into the design of filter bank multicarrier and multiantenna systems based on OQAM, it is deemed necessary to take into account the issues that have been previously raised. In the European Union's 7th Framework Project PHYDYAS [53] some light has been casted into the design of FBMC/OQAM systems. However, some areas are not fully explored yet and there is room for improvement. In this sense, next section briefly introduces the research areas that have been studied in this thesis.

1.2 Outline of the dissertation

This dissertation is aimed at devising novel signal processing techniques that take advantage of the good frequency localization properties exhibited by the FBMC/OQAM modulation scheme and the additional degrees of freedom provided by multiantenna architectures. It must be mentioned that this thesis is not limited to the study of MIMO PTP communications, but other scenarios have been considered.

Chapter 2 introduces the basics of the FBMC/OQAM modulation by providing the expressions of a pure digital filter bank that works in the transmultiplexer configuration. Special emphasis is

on the efficient implementation of the transmitter and the receiver. Finally, this chapter presents a unified formulation that allows the extension of the FBMC/OQAM scheme to MIMO channels. The model has been derived in the context of point-to-point communications and it contemplates the possibility of including precoding and equalization techniques that work on a per-subcarrier basis.

Chapter 3 focuses on signal processing techniques used at reception to combat the detrimental effects induced by the channel. In particular, the chapter covers the equalization design for the FBMC/OQAM modulation scheme. The cases of study correspond to synchronous point-to-point communications and asynchronous multiple access networks. In both cases it is contemplated that the receiver may have multiple antennas. In addition, the design of interference aware detectors for coded FBMC/OQAM systems is investigated.

Chapter 4 delves into the problem of constructing linear precoders for FBMC/OQAM systems with the emphasis on multiple-input-single-output (MISO) channels. One advantage of pre-equalizing the channel at the transmit side is that the power distribution can be adjusted to adapt the channel variations. Based on this observation Chapter 4 first investigates the design of linear precoders when the power distribution is set beforehand. Next, power allocation comes into play and the problem becomes more challenging because linear precoders and power coefficients are jointly designed.

Chapter 5 provides insight into the power allocation problem for FBMC/OQAM systems when residual inter-symbol and inter-carrier interference is not negligible. In particular, we focus on the design of power allocation strategies that maximize the minimum signal to interference plus noise ratio (SINR) and strategies that maximize the sum rate. While the maximization of the minimum SINR is exclusively investigated for point-to-point communications, the sum rate maximization is analysed in the broadcast channel as well as in point-to-point communications.

Chapter 6 presents an architecture that can be understood as the fusion of the techniques introduced in Chapter 3 and Chapter 4. In other words, the transmitted symbols are linearly precoded while at the receive side the demodulated data is equalized. This chapter pursues the joint optimization of the transmitter and the receiver in low frequency selective channels where the channel frequency response is assumed flat at the subcarrier level. MIMO techniques are envisaged for point-to-point communications and for the broadcast channel.

Chapter 7 goes beyond the research carried out in Chapter 6 and proposes to jointly optimize

the transmitter and the receiver without making any assumption about the flatness of the channel. It must be mentioned that the studies are exclusively focused on point-to-point communications. To counteract the channel a novel architecture is proposed. Now precoders and equalizers work on a per-subcarrier basis and may have multiple taps. For design and complexity reasons we restrict our study to two cases. In the first one the precoders are broadband filters whereas the equalizers are narrowband combiners. By contrast, in the second case the complexity burden is placed on the receive side and the multi-tap filtering is only performed by the equalizers.

Chapter 8 draws the conclusions of this dissemination and proposes future lines of research.

1.3 Research contributions

The contents of the following articles have been used to write this thesis.

Chapter 3:

P1 ©2010 IEEE. Reprinted, with permission, from M. Caus, A.I. Pérez-Neira, "Space-time receiver for filterbank based multicarrier systems," *International ITG Workshop on Smart Antennas (WSA)*, pp.421-427, 23-24 February 2010.

P2 ©2011 IEEE. Reprinted, with permission, from M. Caus, A.I. Pérez-Neira, "Interference mitigation techniques for asynchronous multiple access communications in SIMO FBMC systems," *12th International Workshop on Signal Processing Advances in Wireless Communications (SPAWC)*, pp.331-335, 26-29 June 2011.

P3 ©2013 Caus et al. Reprinted, with permission, from M. Caus, A.I. Pérez-Neira, M. Renfors, "Low-complexity interference variance estimation methods for coded multicarrier systems: application to SFN," *EURASIP Journal on Advances in Signal Processing*, vol. 2013, October 2013.

Chapter 4:

P4 ©2010 IEEE. Reprinted, with permission, from M. Caus, A.I. Pérez-Neira, "Optimal MISO pre-equalization for filter bank based multicarrier systems," *Forty Fourth Asilomar Conference on Signals, Systems and Computers (ASILOMAR)*, pp.1521-1525, 7-10 November 2010.

P5 ©2011 IEEE. Reprinted, with permission, from M. Caus, A.I. Pérez-Neira, "Transmit and receive filters for MISO FBMC systems subjected to power constraints," *IEEE International*

Conference on Acoustics, Speech and Signal Processing (ICASSP), pp.2660-2663, 22-27 May 2011.

P6 ©EURASIP 2011. Reprinted, with permission, from M. Caus, A.I. Pérez-Neira, "Power Balancing in FBMC-MISO Systems". *19th European Signal Processing Conference (EUSIPCO)*, pp. 1608-1612, August 2011.

Chapter 5:

P6 ©EURASIP 2011. Reprinted, with permission, from M. Caus, A.I. Pérez-Neira, "Power Balancing in FBMC-MISO Systems". *19th European Signal Processing Conference (EUSIPCO)*, pp. 1608-1612, August 2011.

P7 ©2012 IEEE. Reprinted, with permission, from M. Caus, A.I. Pérez-Neira, "A suboptimal power allocation algorithm for FBMC/OQAM," *IEEE 13th International Workshop on Signal Processing Advances in Wireless Communications (SPAWC)*, pp.189-193, 17-20 June 2012.

P8 ©2012 IEEE. Reprinted, with permission, from M. Caus, A.I. Pérez-Neira, A. Garcia-Armada, "A Discrete Bit Loading Algorithm for FBMC/ OQAM," *IEEE Signal Processing Letters*, vol.19, no.6, pp.324-327, June 2012.

P9 ©EURASIP 2012. Reprinted, with permission, from M. Caus, A.I. Pérez-Neira, "Subcarrier allocation and power loading strategies for multi-user broadcast FBMC/OQAM systems," *20th European Signal Processing Conference (EUSIPCO)*, pp. 1364-1368, August. 2012.

Chapter 6:

P10 ©2013 IEEE. Reprinted, with permission, from M. Caus, A.I. Pérez-Neira, "Multi-stream transmission in MIMO-FBMC systems", *IEEE International Conference on Acoustics, Speech and Signal Processing (ICASSP)*, May 2013.

P11 ©2013 IEEE. Reprinted, with permission, from M. Caus, A. I. Pérez-Neira, "SDMA for filterbank with Tomlinson Harashima precoding", *IEEE International Conference on Communications (ICC)*, June 2013.

P12 ©2013 IEEE. Reprinted, with permission, from M. Caus, A.I. Pérez-Neira, M. Moretti "SDMA for FBMC with block diagonalization," *13th International Workshop on Signal Processing Advances in Wireless Communications (SPAWC)*, June 2013."

P13 ©VDE VERLAG GMBH. Berlin, Offenbach, Germany 2013. Reprinted, with permission, from M. Caus, A. I. Pérez-Neira, "Comparison of linear and widely linear processing in MIMO-FBMC systems". *International Symposium on Wireless Communication Systems (ISWCS)*, August 2013.

Chapter 7:

P14 ©2012 IEEE. Reprinted, with permission, from M. Caus, A.I. Pérez-Neira, "Transmitter-Receiver Designs for Highly Frequency Selective Channels in MIMO FBMC Systems," *IEEE Transactions on Signal Processing*, vol.60, no.12, pp.6519-6532, December 2012.

P15 ©2013 IEEE. Reprinted, with permission, from M. Caus, A.I. Pérez-Neira, "Multi-stream transmission for highly frequency selective channels in MIMO-FBMC/OQAM systems," accepted for publication in *IEEE Transactions on Signal Processing*.

Other contributions: The publications listed below are not included in this dissertation but have also been elaborated during my research stage.

- M. Caus, A.I. Pérez-Neira, "Multi-antenna diversity techniques for FBMC/OQAM systems in wireless communications", *Barcelona Forum on Ph.D. Research in Information and Communication Technologies*, pp. 63-64, 15 Oct. 2012.
- A.I. Pérez-Neira, B. Devillers, M.A. Lagunas, M. Caus, "MIMO for satelite communications", *SatnexIII Summer School*, 5-9 Sep. 2011.
- A.I. Pérez-Neira, C. Ibars, J. Serra, A del Coso, J. Gómez, M. Caus, K.P. Liolis, "MIMO channel modeling and transmission techniques for multi-satellite and hybrid satellite–terrestrial mobile networks", *Physical Communication*, Vol. 4, Issue 2, pp 127-130, June 2011.

Chapter 2

FBMC/OQAM system model

2.1 SISO architecture

This section formulates a pure digital FBMC/OQAM system that works in the TMUX configuration. This means that the output of the synthesis filter bank (SFB) is connected to the input of the analysis filter bank (AFB). This is the usual configuration in multicarrier communications. In this regard, consider the discrete-time baseband model for the single-input-single-output (SISO) communication system depicted in Figure 2.1. The block diagram shows that there are M input signals that are added to form the superimposed signal $s[n]$. Note that the spectrum of the OQAM symbols, which are obtained after staggering in-phase and quadrature components of the complex-valued QAM symbols $\{x_m^c[l]\}$, is first compressed and next the upsampled version is frequency multiplexed to the corresponding subcarrier. To do so, each branch is filtered with the well-frequency localized pulses $\{f_m[n]\}$. To recover the M low-rate signals $\{x_m^c[l]\}$, the synthesized signal $s[n]$ is fed into a bank of matched filters and then the outputs are downsampled to perform the rate conversion.

It is worth emphasizing that the SFB portrayed in Figure 2.1 sets the same upsampling factor among subcarriers. As a consequence, the pulses deployed in the SFB and the AFB have equal bandwidth. This particular case, which is known as uniform FBMC, is very interesting because it allows generating $\{f_m[n]\}$ by applying frequency shifts to a given prototype lowpass filter. In the most general case the rate of the subcarrier signals may not be the same, giving rise to a multirate system, [24, 54]. Nevertheless, it must be mentioned that this work is focused on the study of uniform FBMC schemes based on the transmission of OQAM symbols.

The starting point of this dissertation is the TMUX efficient implementation proposed in [21]. In the literature we can find other schemes based on different structures. In this regard, the exponentially-modulated filter bank (EMFB) scheme also enables shaping subcarrier signals with

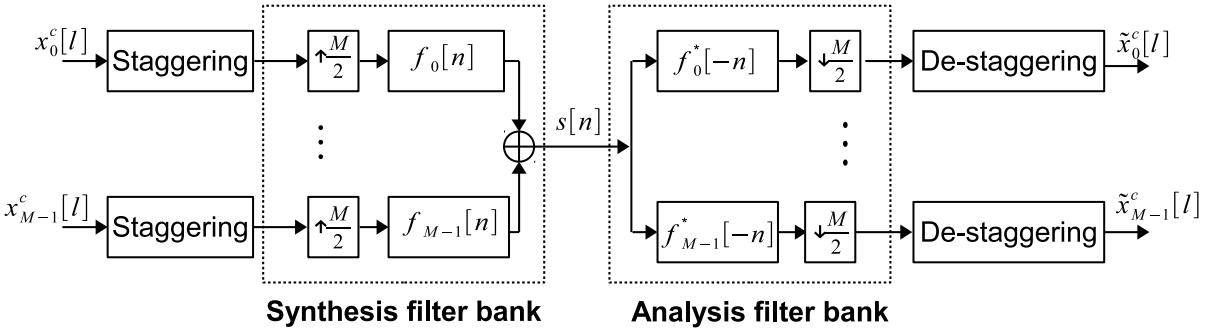

Figure 2.1: Block diagram of the FBMC/OQAM transceiver.

very spectral efficient waveforms, [55–57]. Although EMFB and the FBMC/OQAM follow different approaches, the authors in [58] demonstrate that it is possible to modify the EMFB structure with special operations so that the subcarrier signals obtained by both schemes coincide. Sticking to the FBMC/OQAM case, the block diagram shown in Figure 2.1 can be transformed into the schemes depicted in Figure 2.2 and Figure 2.5 so that the complexity burden is reduced while the processing keeps unchanged. In other words, Figure 2.1 is equivalent to Figures 2.2 and 2.5. The bank of filters given by $\{A_m(z)\}$ correspond to the polyphase components that allow the following representation

$$P(z) = \sum_{l=0}^{M-1} z^{-l} A_l(z^M), \tag{2.1}$$

where $P(z)$ is the z-transform of $p[n]$, which is the prototype pulse that is used to generate the subcarrier pulses $\{f_m[n]\}$. The closed-form expressions of $\{f_m[n]\}$ and $\{\beta_m\}$ are formulated hereinafter. Note that in Figure 2.2 and Figure 2.5 the notation used to refer to the input of the AFB is not matched with the output of the SFB because, in general, the output of the SFB is altered before it reaches the input of the AFB. This happens for instance in wireless communications where the received signal is affected by multipath propagation and is contaminated with additive noise.

As Figure 2.2 indicates the input sequences are pre-processed to generate the OQAM symbols. The pre-processing consists in staggering between the in-phase and quadrature components of the complex-valued QAM symbols. This is tantamount to delaying half the symbol period of either the real or the imaginary part of the complex-valued sequences $\{x_m^c[l]\}$. It is important to remark that on the even subcarriers the quadrature component is delayed with respect to the in-phase component, while on odd subcarriers is the real part that is delayed. Figure 2.3 illustrates this way of performing. It worth emphasizing that the OQAM symbols are modulated at twice the rate of the QAM symbols, but the OQAM symbols only carry information in a single dimension. Based on this, any point in the OQAM constellation diagram can be obtained by multiplying a real-valued

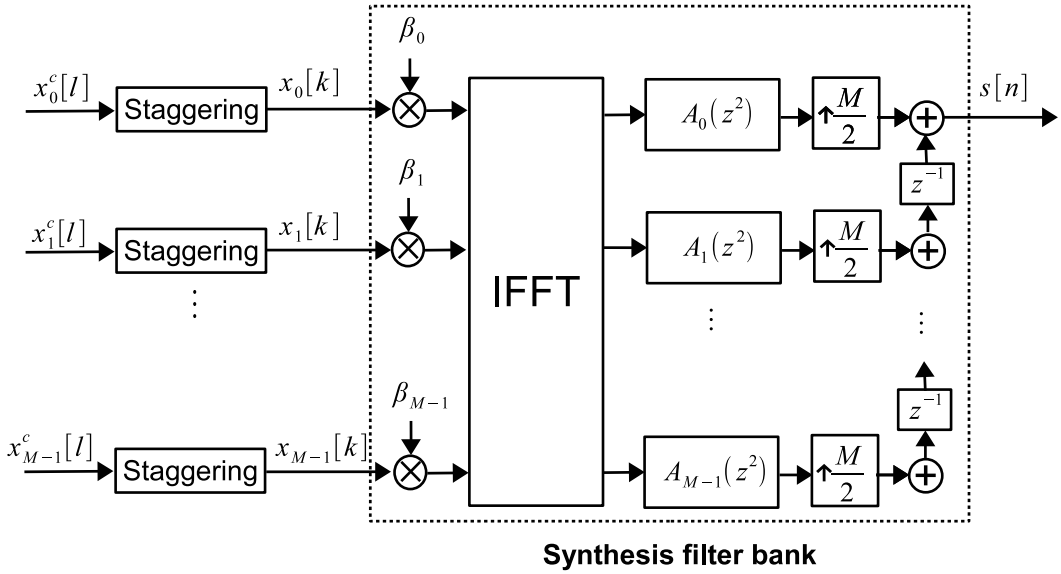

Figure 2.2: Efficient implementation of the transmitter.

pulse amplitude modulated (PAM) symbol with a term that controls the phase. In this sense, the sequence that is fed into the SFB can expressed as $x_m[k] = d_m[k]\theta_m[k]$, where $d_m[k]$ is the PAM symbol and the phase term can be defined as follows:

$$\theta_m[k] = \begin{cases} 1 & m+k \text{ even} \\ j & m+k \text{ odd} \end{cases} . \tag{2.2}$$

Another possibility is to set $\theta_m[k] = j^{m+k}$, which is equivalent to (2.2) aside from the sign. The idea is to ensure that the PAM symbols that are transmitted in adjacent positions in the time-frequency grid are frequency shifted by a factor of $\frac{\pi}{2}$. In this proposal we have favoured the notation written in (2.2). Without loss of generality the transmitted signal is given by

$$\begin{aligned} s[n] &= \sum_{k=-\infty}^{\infty} \sum_{m=0}^{M-1} d_m[k]\theta_m[k] p\left[n - k\frac{M}{2}\right] e^{j\frac{2\pi}{M}m\left(n-k\frac{M}{2}-D\right)} \\ &= \sum_{k=-\infty}^{\infty} \sum_{m=0}^{M-1} d_m[k]\theta_m[k] f_m\left[n - k\frac{M}{2}\right] \end{aligned} \tag{2.3}$$

where

$$f_m[n] = p[n]\, e^{j\frac{2\pi}{M}m(n-D)}. \tag{2.4}$$

Notice that the sample index k is used by low-rate signals while the high-rate signals utilize

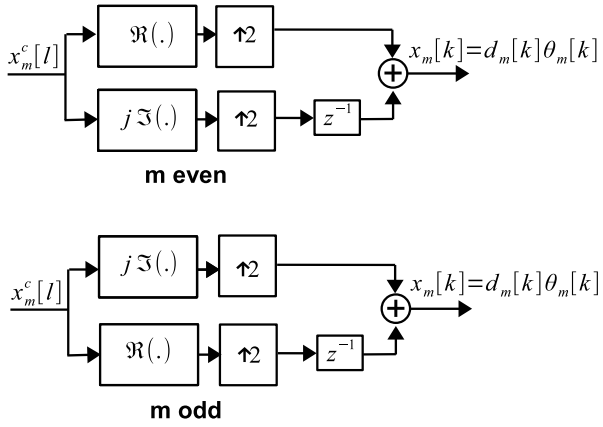

Figure 2.3: Staggering process.

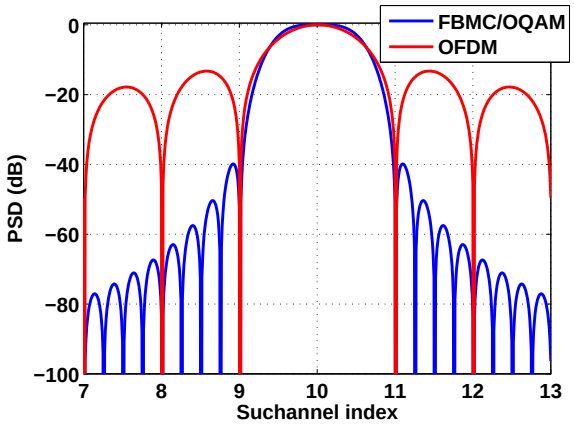

Figure 2.4: Power spectral density corresponding to the signal transmitted in the tenth subchannel when the air-interface is based on FBMC/OQAM and OFDM.

the sample index n. Bearing in mind the phase term choice in (2.2) together with the efficient implementation of [21], it follows that $\beta_m = e^{-j\frac{2\pi}{M}mD}$. The prototype pulse $p[n]$ is a unit-energy finite impulse response (FIR) filter of order $L-1$, i.e. $\sum_{n=0}^{L-1}|p[n]|^2 = 1$. The delay D appears as a consequence of forcing the prototype pulse to be causal, thus its value depends on the pulse length. The authors in [21] have proposed to fix $D = (L-1)/2$. It is customary to select a length that is close to a multiple of the number of subbands, that is $L \in \{KM-1, KM, KM+1\}$. The coefficient K controls how many multicarrier symbols overlap in the time domain. For this reason it is called the overlapping factor. To illustrate the good spectral containment exhibited by the subcarrier signals, Figure 2.4 shows the power spectral density (PSD) of the signal transmitted on the tenth subchannel when the air-interface is based on OFDM and FBMC/OQAM. The PSD is

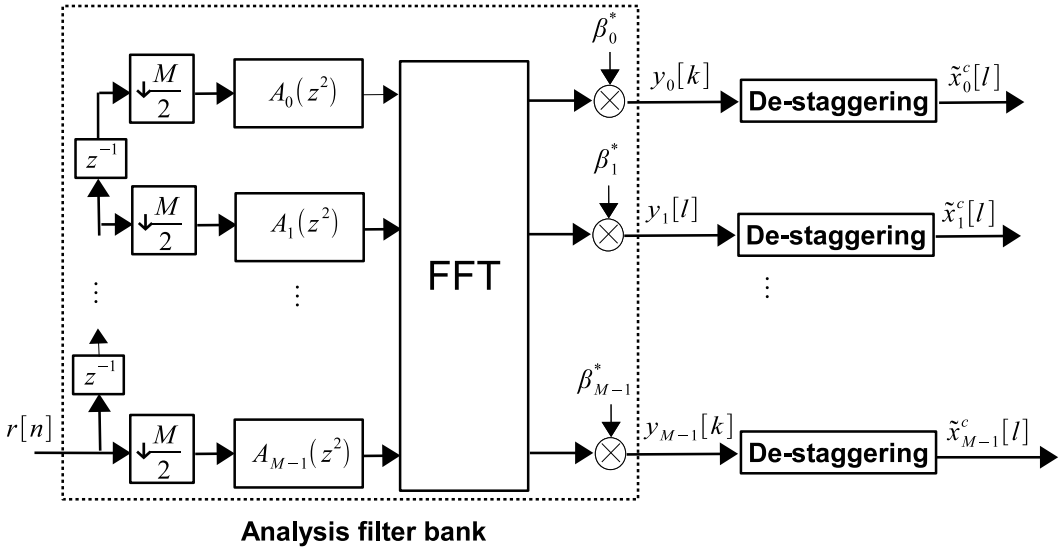

Figure 2.5: Efficient implementation of the receiver.

normalized so that the gain in the passband region is 0 dB.

Denoting $r[n]$ the signal to be fed to the AFB, the information conveyed on each subchannel is obtained by filtering $r[n]$ through a bank of filters, which are matched to the transmit subband filters. Hence, the qth demodulated signal at the kth time instant is given by

$$y_q[k] = \sum_{n=k\frac{M}{2}}^{L-1+k\frac{M}{2}} r[n] p\left[n - k\frac{M}{2}\right] e^{-j\left(\frac{2\pi}{M} q\left(n-k\frac{M}{2}-D\right)\right)}. \tag{2.5}$$

Defining $(.)_{\downarrow x}$ as the downsampling operation by a factor of x, the signal $y_q[k]$ can be reformulated as

$$y_q[k] = \left(y[n] * f_q^*[-n]\right)_{\downarrow M/2}, \tag{2.6}$$

which brings about the following compact model

$$y_q[k] = \sum_{m=0}^{M-1} \left(d_m[k]\,\theta_m[k]\right) * \alpha_{qm}[k] \tag{2.7}$$

$$\alpha_{qm}[k] = \left(f_m[n] * f_q^*[-n]\right)_{\downarrow M/2} \tag{2.8}$$

as long as $r[n] = s[n]$. Finally the symbols are estimated by de-staggering the AFB outputs. The processing is summarized in Figure 2.6. On the qth subband the PAM symbols are obtained after compensating the phase term and extracting the real component, i.e. $\tilde{d}_q[k] = \Re\left\{\theta_q^*[k] y_q[k]\right\}$. As it is pointed out in [21] if the prototype filter is designed such that the perfect reconstruction (PR)

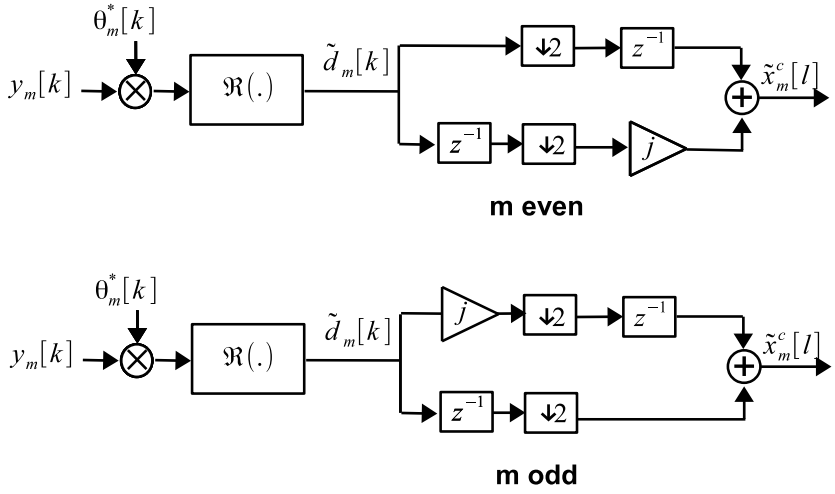

Figure 2.6: De-staggering process.

property is satisfied, that is

$$\Re\left\{\sum_{n=-\infty}^{\infty} f_m\left[n-l\frac{M}{2}\right] f_q^*\left[n-v\frac{M}{2}\right]\theta_m[l]\theta_q^*[v]\right\}=\delta_{m,q}\delta_{l,v}, \tag{2.9}$$

then $\tilde{d}_q[k]=d_q[k]$ in the absence of noise and multipath fading. In wireless communications, the received signal is affected by multipath fading and contaminated by additive white Gaussian noise (AWGN). Denoting $h[n]$ the channel impulse response (CIR) and $\bar{w}[n]$ the noise samples, it follows that $r\,[n]=h\,[n]*s\,[n]+\bar{w}\,[n]$. With that, (2.7) is transformed into

$$\begin{aligned} y_q\,[k] &= \sum_{m=q-1}^{q+1}\left(d_m\,[k]\,\theta_m\,[k]\right)*g_{qm}\,[k]+w_q[k] \\ &= d_q[k]\theta_q[k]g_{qq}[0]+\underbrace{\sum_{\substack{m=q-1\\ m\neq q}}^{q+1}\sum_{\tau=-\infty}^{\infty} d_m[k-\tau]\theta_m[k-\tau]g_{qm}[\tau]}_{ICI}+\underbrace{\sum_{\substack{\tau=-\infty\\ \tau\neq 0}}^{\infty} d_q[k-\tau]\theta_q[k-\tau]g_{qq}[\tau]}_{ISI} \\ &\quad + w_q[k], \end{aligned} \tag{2.10}$$

where

$$g_{qm}\,[k]=\left(f_m\,[n]*h[n]*f_q^*\,[-n]\right)_{\downarrow M/2} \tag{2.11}$$

$$w_q[k] = \left(\bar{w}[n] * f_q^*[-n]\right)_{\downarrow M/2}. \tag{2.12}$$

The definition of (2.11) highlights that the channel destroys the orthogonality properties and, thus the AFB outputs are not free of ISI and ICI. In (2.10) we have assumed that the prototype pulse exhibits a good spectral containment so that ICI mainly comes from the immediate adjacent neighbors. This implies that the frequency response of $p[n]$ is confined within $\left[-\frac{2\pi}{M} \quad \frac{2\pi}{M}\right]$ and, therefore, the mth subcarrier signal occupies this band $B_m = \left[(m-1)\,\frac{f_s}{M} \quad (m+1)\,\frac{f_s}{M}\right]$, where f_s is the sampling frequency. Based on this, the subcarrier spacing is defined as $\Delta_f = \frac{f_s}{M}$. All these assumptions hold true for several pulse-shape designs, see e.g. [21, 59–61].

Provided that the channel frequency selectivity and the subcarrier spacing are such that the channel frequency response (CFR) is flat within the interval B_q, then we can use one of these two definitions

$$g_{qm}[k] = H\left(e^{j\frac{2\pi}{M}m}\right)\alpha_{qm}[k] \tag{2.13}$$

$$g_{qm}[k] = H\left(e^{j\frac{2\pi}{M}q}\right)\alpha_{qm}[k], \tag{2.14}$$

instead of (2.11). Let $H\left(e^{j\frac{2\pi}{M}m}\right)$ denote the CFR evaluated on $\frac{2\pi}{M}m$. It must be mentioned that the models in (2.13) and (2.14) are preferable over the model in (2.11) because they offer a better analytical tractability. However, the system parameters and the propagation conditions will determine its validity. From this point on we will use the term: low frequency selective channels, to refer to those scenarios where (2.13) and (2.14) are valid. Otherwise, we will use the term: highly frequency selective channels. Channel models that do not satisfy (2.13) and (2.14) usually have large delay spreads. The typical urban and the highly terrain scenarios are two examples where (2.13) and (2.14) do not hold true, [62]. If the channel frequency response is flat within subchannels, then we can indistinctly adopt model (2.13) or (2.14). In the subsequent chapters, it will be demonstrated that the system is more robust against the frequency selectivity of the channel when beamformers are designed assuming (2.14) rather than (2.13). To illustrate that the processing is simpler when the flat fading condition is satisfied, let us assume that (2.14) is valid. Then we could restore the orthogonality on the real field by filtering the demodulated data by a single-tap equalizer. If the PR property is satisfied and the subbands are processed as follows:

$$\tilde{d}_q[k] = \Re\left(\frac{\theta_q^*[k]y_q[k]}{H\left(e^{j\frac{2\pi}{M}q}\right)}\right), \tag{2.15}$$

then the PAM symbols are perfectly estimated except from the noise, i.e. $\tilde{d}_q[k] = d_q[k] + \Re\left(w_q[k]/H\left(e^{j\frac{2\pi}{M}q}\right)\right)$. However if the channel cannot be modeled flat at each subchannel the

Table 2.1: Intrinsic interferences for q even.

	k=-3	k=-2	k=-1	k=0	k=1	k=2	k=3
$\alpha_{qq-1}[k]$	-j0.0429	-0.1250	j0.2058	0.2393	-j0.2058	-0.1250	j0.0429
$\alpha_{qq}[k]$	-0.0668	0	0.5644	1	0.5644	0	-0.0668
$\alpha_{qq+1}[k]$	j0.0429	-0.1250	-j0.2058	0.2393	j0.2058	-0.1250	-j0.0429

Table 2.2: Intrinsic interferences for q odd.

	k=-3	k=-2	k=-1	k=0	k=1	k=2	k=3
$\alpha_{qq-1}[k]$	j0.0429	-0.1250	-j0.2058	0.2393	j0.2058	-0.1250	-j0.0429
$\alpha_{qq}[k]$	0.0668	0	-0.5644	1	-0.5644	0	0.0668
$\alpha_{qq+1}[k]$	-j0.0429	-0.1250	j0.2058	0.2393	-j0.2058	-0.1250	j0.0429

single-tap equalizer does not guarantee that the interferences are completely removed. Hence, if leakage is likely to occur, then it is deemed necessary that the prototype pulse exhibits good time and frequency localization properties. In view of this, the PR property is relaxed giving rise to the near perfect reconstruction (NPR) property. On one hand, filters designed according to the NPR property induce marginal amounts of ISI and ICI even in the ideal transmission scenario. On the other hand, they present higher stopband attenuation than their equal-length counterparts designed according to the PR criterion. Hence, the detrimental effects inflicted by the channel can be more effectively counteracted by pulses that fulfil the NPR. In the rest of the chapter, if otherwise stated, the pulse $p[n]$ is designed by following the frequency sampling approach described in [59] with an overlapping factor equal to four. The values of $\{\alpha_{qm}[k]\}$ are gathered in Table 2.1 and Table 2.2. The terms associated with $|k| > 3$ have been neglected since they have a magnitude that is significantly lower than that of the terms corresponding to $|k| \leq 3$.

2.2 MIMO architecture

The objective of this section is to provide a unified formulation for MIMO-FBMC/OQAM systems. In this sense, consider the communication system depicted in Figure 2.7. Note that the transmitter and the receiver are equipped with N_T and N_R antennas respectively. At the transmitter, each subband is able to convey S streams. The symbols to be spatially multiplexed on the mth subband at the kth time instant are gathered in this vector $\mathbf{x}_m[k] = \left[x_m^1[k]...x_m^S[k]\right]^T$, which is defined as $\mathbf{x}_m[k] = \theta_m[k]\mathbf{d}_m[k] = \theta_m[k]\left[d_m^1[k]...d_m^S[k]\right]^T$. Next, the symbols are pre-processed on a per-subcarrier basis so that S sequences are mapped onto N_T antennas. The precoded symbols are defined as $\mathbf{v}_m[k] = \left[v_m^1[k]...v_m^{N_T}[k]\right]^T$. With that, the signal transmitted by the ith antenna becomes

$$s_i[n] = \sum_{k=-\infty}^{\infty} \sum_{m=0}^{M-1} v_m^i[k] f_m \left[n - k\frac{M}{2} \right]. \tag{2.16}$$

At the receive side, the link of each transmit and receive antenna pair is degraded by multipath fading and contaminated with AWGN. Bearing this in mind, the samples received by the jth receive antenna reads as $r_j[n] = \sum_{i=1}^{N_T} s_i[n] * h_{ij}[n] + \bar{w}_j[n]$, where $h_{ij}[n]$ accounts for the channel associated with the ith transmit antenna and the jth receive antenna. The noise that is added at the input of the jth receive antenna chain is denoted $\bar{w}_j[n]$. In the rest of the paper, if otherwise stated, the noise samples are zero-mean circularly symmetric complex Gaussian random variables, i.e $\bar{w}_j[n] \sim \mathcal{CN}(0, N_0), \mathbb{E}\{\bar{w}_j[n]\bar{w}_i^*[k]\} = N_0\delta_{i,j}\delta_{k,n}$. The expression of the demodulated data can be inferred from (2.10), i.e.

$$y_q^j[k] = \sum_{m=q-1}^{q+1} \sum_{i=1}^{N_T} v_m^i[k] * g_{qm}^{ij}[k] + w_q^j[k] \tag{2.17}$$

$$g_{qm}^{ij}[k] = \left(f_m[n] * h_{ij}[n] * f_q^*[-n] \right)_{\downarrow M/2} \tag{2.18}$$

$$w_q^j[k] = \left(\bar{w}_j[n] * f_q^*[-n] \right)_{\downarrow M/2}, \tag{2.19}$$

for $0 \leq q \leq M-1$ and $1 \leq j \leq N_R$. The equivalent channel $g_{qm}^{ij}[k]$ is different from zero for $-L_{g_1} \leq k \leq L_{g_2}$. The limits are computed as $L_{g_2} = \left\lfloor \frac{L-1+L_{ch}}{M/2} \right\rfloor$ and $L_{g_1} = \left\lfloor \frac{L-1}{M/2} \right\rfloor$, where L_{ch} is the maximum channel excess delay. Similarly to the transmit counterpart, the outputs of the AFB are post-processed on a per-subcarrier fashion. This means that this vector $\mathbf{y}_q[k] = \left[y_q^1[k] ... y_q^{N_R}[k] \right]^T$ is further processed to get $\mathbf{z}_q[k] = \left[z_q^1[k] ... z_q^S[k] \right]^T$. Resorting to matrix notation we get

$$\mathbf{y}_q[k] = \sum_{m=q-1}^{q+1} \sum_{\tau=-L_{g_1}}^{L_{g_2}} \mathbf{G}_{qm}[\tau] \mathbf{v}_m[k-\tau] + \mathbf{w}_q[k], \tag{2.20}$$

where

$$\mathbf{G}_{qm}[\tau] = \begin{bmatrix} g_{qm}^{11}[\tau] & \cdots & g_{qm}^{N_T 1}[\tau] \\ \vdots & & \vdots \\ g_{qm}^{1 N_R}[\tau] & \cdots & g_{qm}^{N_T N_R}[\tau] \end{bmatrix} \tag{2.21}$$

$$\mathbf{w}_q[k] = \left[w_q^1[k] \cdots w_q^{N_R}[k] \right]^T. \tag{2.22}$$

The model of Figure 2.7 is sufficiently general to accommodate any type of precoding and equalization technique. It must be mentioned that we have refrained from considering the schemes that jointly process all the subbands since they yield a computational complexity that may render

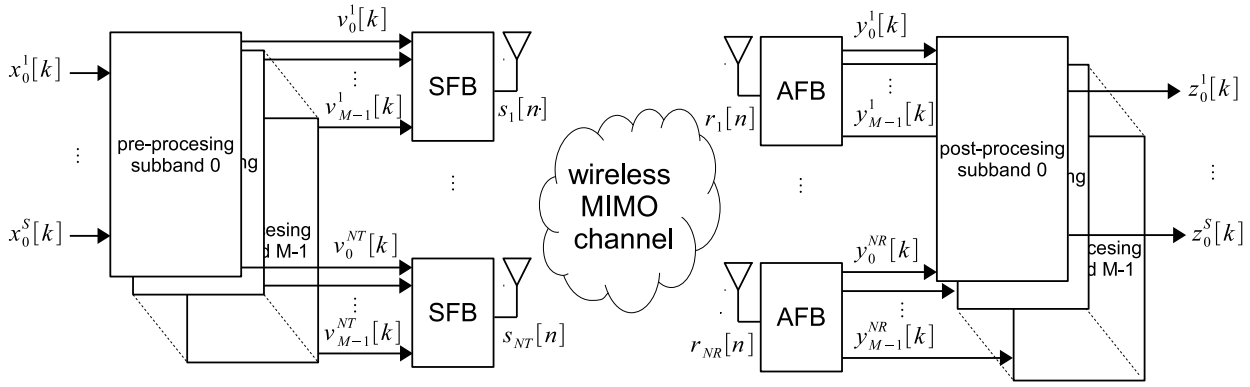

Figure 2.7: FBMC/OQAM application to MIMO communication systems

the solution impractical, especially when the number of carriers is high.

2.3 Study cases

To validate the signal processing techniques that are presented in this dissertation, three different scenarios will be simulated. The details of the system parameters and the propagation conditions are gathered in Table 2.3.

Table 2.3: System parameters and propagation conditions

	Scenario 1	Scenario 2	Scenario 3
Carriers	M=1024	M=1024	M=512
Number of data carriers	M_a=756 or M_a=720	M_a=756 or M_a=720	M_a=378 or M_a=360
Bandwidth	B=10 MHz	B=10 MHz	B=10 MHz
Sampling frequency	f_s=11.2 MHz	f_s=11.2 MHz	f_s=11.2 MHz
Subcarrier spacing	Δ_f=10.94 kHz	Δ_f=10.94 kHz	Δ_f=21.88 kHz
Channel model ([63])	ITU Vehicular A	ITU Pedestrian A	ITU Vehicular B
Expressions for $\{g_{qm}[k]\}$	(2.11),(2.13),(2.14)	(2.11),(2.13),(2.14)	(2.11)

Notice that in Scenario 1 and 2, the coefficients of the equivalent channel $\{g_{qm}[k]\}$ can be formulated using one of these formulas (2.11),(2.13) and (2.14). This implies that the channel frequency response can be approximated flat at the subcarrier level. By contrast, no flatness assumption can be made in Scenario 3 and, therefore, (2.11) is the only expression that is valid to model the equivalent channel. To corroborate it, Figure 2.8 shows the magnitude of the channel frequency response when the ITU Vehicular A (VehA), ITU Pedestrian A (PedA) and the ITU Vehicular B (VehB) models are considered. It is worth noticing that the frequency response associated to PedA is flat in the band that encompasses one subchannel. As for the VehA channel, the response

varies smoothly so that we can still approximate that the channel is flat at the subcarrier level. By contrast, the frequency selectivity of the VehB channel is really severe and the frequency response exhibits sharp variations in the pass band region of each subchannel.

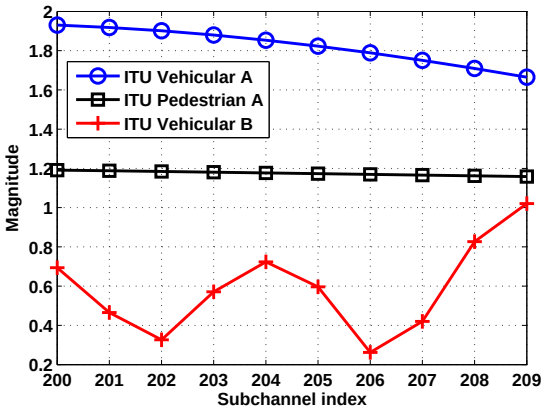

Figure 2.8: Magnitude of the channel frequency response evaluated between subcarrier 200 and subcarrier 209. The subcarrier spacing has been set to 10.94 KHz. The channel realizations obey the ITU Vehicular A, ITU Pedestrian A and the ITU Vehicular B guidelines.

2.3.1 OFDM vs. FBMC/OQAM

It is worth mentioning that Scenarios 1 and 2 are compliant with the WiMAX standard when the number of subcarriers that convey data is set to 720. This configuration guarantees that the out-of-band radiation does not violate the constraint imposed by the spectral mask, provided that the air-interface is based on OFDM. If OFDM is replaced by FBMC/OQAM the emission in the adjacent bands is far below the maximum allowed values. Hence, the number of data carriers can be extended to 756 as proposed in [64]. Hence, FBMC/OQAM can take advantage of pulse shaping techniques to increase the information rate. If otherwise stated, the subcarriers that are switched on when FBMC/OQAM is evaluated is 756 in Scenarios 1 and 2. The parameters in Scenario 3, which are made up, have been obtained from Scenarios 1 and 2 considering that the 10 MHz bandwidth is split into 512 subcarriers rather than 1024. Thus M_a is set to 378 or 360 depending of if FBMC/OQAM or OFDM is implemented.

Since FBMC/OQAM is presented as a potential successor of OFDM, it is worth evaluating the spectral efficiency that is obtained in both cases with the parameters provided in Table 2.3. As it is explained in Section 2.1, in the FBMC/OQAM context M_a symbols drawn from the M_s-QAM constellation are frequency multiplexed with rate $R = \frac{f_s}{M}$ or, equivalently, M_a symbols generated from the $\sqrt{M_s}$-PAM constellation are sent with rate $R = \frac{2f_s}{M}$. In the OFDM case, the symbols are

modulated according to the M_s-QAM constellation and the rate is $R = \frac{f_s}{M+CP}$, where CP denotes the cyclic prefix length. Let η denote the spectral efficiency, which expresses the information rate transmitted over a given bandwidth. In SISO communication systems, we get $\eta = \frac{\log_2\left(\sqrt{M_s}\right)M_a 2f_s}{M \times B}$ bits/s/Hz and $\eta = \frac{\log_2(M_s)M_a f_s}{B(M+CP)}$ bits/s/Hz in FBMC/OQAM and OFDM schemes, respectively. Note that η can be readily obtained from the values computed in the SISO case when multiple streams are allocated in the same frequency resources.

Finally, it is important to remark that in OFDM the energy that is transmitted increases with the length of the cyclic prefix. To carry out a fair comparison between OFDM and FBMC/OQAM we have taken into account the energy devoted to transmit the cyclic prefix.

Chapter 3

Equalization and detection

This chapter tackles the design of signal processing techniques to be used at reception, with the aim of mitigating the negative effects of the channel and the noise. First, the basic concepts of equalization are provided considering a single-input-multiple-output (SIMO) communication system where the receiver is equipped with N_R antennas. Building upon the expressions formulated in (2.17),(2.18) and (2.19), we propose the design of equalization techniques for synchronous PTP communications and for asynchronous multiple access networks. Finally, we undertake research in the design of practical receiver structures for coded FBMC/OQAM systems when the interference is not negligible.

3.1 Equalization in SIMO PTP communications

When channel state information (CSI) is only available at the receiver, the streams are multiplexed over the subcarriers without using any precoding technique, i.e. $v_m[k] = \theta_m[k]d_m[k]$ for all $m \in S_a$, where the set S_a gathers the indices of those subcarriers that are active. Based on this, the demodulated signal by the jth antenna chain is given by

$$y_q^j[k] = \sum_{m=q-1}^{q+1} (\theta_m[k]d_m[k]) * g_{qm}^{1j}[k] + w_q^j[k], \quad 1 \leq j \leq N_R, \quad q \in S_a. \tag{3.1}$$

Bearing in mind that replicas of the desired information are present in all the antennas, we can take advantage of the spatial diversity by filtering (3.1) and combining the filter outputs later on. This translates into performing as follows:

$$z_q[k] = \sum_{j=1}^{N_R} a_{jq}^*[k] * y_q^j[k], \quad q \in S_a. \tag{3.2}$$

In the most general case the linear filters perform a multi-tap filtering, which means that $a_{jq}[k] \neq 0$ for $-L_a \leq k \leq L_a$. Based on this, (3.2) can be formulated in the following matrix way

$$z_q[k] = \sum_{j=1}^{N_R} \mathbf{a}_{jq}^H \mathbf{y}_q^j[k] = \sum_{j=1}^{N_R} \sum_{m=q-1}^{q+1} \sum_{\tau=-L_a-L_{g_1}}^{L_a+L_{g_2}} \mathbf{a}_{jq}^H \mathbf{g}_{qm}^{1j}[\tau]\theta_m[k-\tau]d_m[k-\tau] + \mathbf{a}_{jq}^H \mathbf{w}_q^j[k] \tag{3.3}$$

$$\mathbf{a}_{jq} = [a_{jq}[-L_a] \cdots a_{jq}[L_a]]^T \tag{3.4}$$

$$\mathbf{y}_q^j[k] = \left[y_q^j[k+L_a] \cdots y_q^j[k-L_a]\right]^T \tag{3.5}$$

$$\mathbf{g}_{qm}^{1j}[\tau] = \left[g_{qm}^{1j}[\tau+L_a] \cdots g_{qm}^{1j}[\tau-L_a]\right]^T \tag{3.6}$$

$$\mathbf{w}_q^j[k] = \left[w_q^j[k+L_a] \cdots w_q^j[k-L_a]\right]^T. \tag{3.7}$$

Grouping the signals that are processed by different antennas we get

$$z_q[k] = \sum_{m=q-1}^{q+1} \sum_{\tau=-L_a-L_{g_1}}^{L_a+L_{g_2}} \mathbf{a}_q^H \mathbf{g}_{qm}[\tau]\theta_m[k-\tau]d_m[k-\tau] + \mathbf{a}_q^H \mathbf{w}_q[k], \tag{3.8}$$

where

$$\mathbf{a}_q = \left[\mathbf{a}_{1q}^T \cdots \mathbf{a}_{N_R q}^T\right]^T \tag{3.9}$$

$$\mathbf{g}_{qm}[\tau] = \left[\left(\mathbf{g}_{qm}^{11}[\tau]\right)^T \cdots \left(\mathbf{g}_{qm}^{1N_R}[\tau]\right)^T\right]^T \tag{3.10}$$

$$\mathbf{w}_q[k] = \left[\left(\mathbf{w}_q^1[k]\right)^T \cdots \left(\mathbf{w}_q^{N_R}[k]\right)^T\right]^T. \tag{3.11}$$

3.1.1 MDIR receiver

Regarding the design of the receive filters, the authors in [65–67] have derived solutions under the minimum mean square error (MMSE) criterion. Instead, in [68] the authors have extended the frequency sampling approach proposed in [69] to accommodate multiantenna configurations. The solution provided in [68] performs close to the MMSE receiver while the computational complexity is reduced. In [70] the interference is predicted and cancelled. The approach that is followed in this section consists in appending a maximum likelihood sequence estimator (MLSE) at the output of the space-time processor. In other words, we propose to tailor the matched desired impulse response (MDIR) receiver of [71] to FBMC/OQAM systems. Hence, the broadband combiner is designed to cancel the ICI and reduce the channel length or, equivalently, the equalizer does not try to completely remove all the interference but it allows that some ISI terms can be present

at its output. After applying the broadband combiner, the MLSE deals with the desired impulse response (DIR) and detects the transmitted symbols. Hence, we first have to select which terms will be considered as desired information. Supposing that L_{ISI} terms are allowed, then the optimization problem becomes

$$\begin{aligned} &\underset{\mathbf{a}_q,\mathbf{h}_q}{\operatorname{argmin}}\, \mathbb{E}\left\{\left|\Re\left(z_q[k]\right) - \mathbf{h}_q^T\mathbf{d}_q^d[k]\right|^2\right\} \\ &s.t.\ \ \mathbb{E}\left\{\left|\Re\left(\mathbf{a}_q^H\mathbf{G}_{qq}^k\mathbf{d}_q^d[k]\right)\right|^2\right\} = 1, \end{aligned} \tag{3.12}$$

where $\mathbf{G}_{qq}^k = \left[\theta_q[k]\mathbf{g}_{qq}[0]\cdots\theta_q\left[k-L_{ISI}\right]\mathbf{g}_{qq}[L_{ISI}]\right]$, $\mathbf{d}_q^d[k] = \left[d_q[k]\cdots d_q[k-L_{ISI}]\right]^T$ and $\mathbf{h}_q \in \mathbb{R}^{L_{ISI}+1\times 1}$ denotes the DIR. The constraint has the objective of avoiding the trivial solution and can be understood as an automatic gain control on the desired signal at the equalizer output. Note that solely the real part of the equalized signal is taken into account. The rationale behind this decision has to do with the fact that $\mathbf{d}_q^d[k]$ contains real-valued symbols. Hence, by projecting the desired information on the real dimension we are not forcing the equalizer to remove the undesired part but to project the interference to the imaginary dimension. Somehow we are relaxing the rejection requirements, which may allows us to make a better use of the spatial dimension. In Appendix 3.A it is demonstrated that this strategy allows us to independently equalize real and imaginary parts of the demodulated data. This yields a widely linear processing that brings advantages over the linear processing when the symbols are improper.

The processing to get the optimal duplet $\{\mathbf{a}_q, \mathbf{h}_q\}$ that solves (3.12) is provided in Appendix 3.A. After performing the optimal space-time processing we get $\Re(z_q[k]) = \mathbf{h}_q^T\mathbf{d}_q^d[k] + i_q[k]$. The term $i_q[k]$ accounts for the equalized noise plus the residual interference. We can estimate the sequence $d_q[0], ..., d_q[L_N - 1]$ by feeding $\Re(z_q[0]), ..., \Re(z_q[L_N - 1])$ into the MLSE [72, 73], where L_N is the frame length.

From the mathematical developments of Appendix 3.A, it can be inferred that the duplet $(\mathbf{h}_q, a_{jq}[k])$ obtained for $k + q$ even is different from that computed for $k + q$ odd. As a result, the receiver has to alternate between the two calculated equalizers. In the same manner the MLSE has to take into account the DIR that corresponds to each equalized sample when computing the likelihoods. Figure 3.1 shows the block diagram of the proposed equalization process by using the following notation

$$\begin{aligned} k+q\ \ even &\rightarrow (\mathbf{h}_q^{even}, a_{jq}^{even}[k]) \\ k+q\ \ odd &\rightarrow (\mathbf{h}_q^{odd}, a_{jq}^{odd}[k]). \end{aligned} \tag{3.13}$$

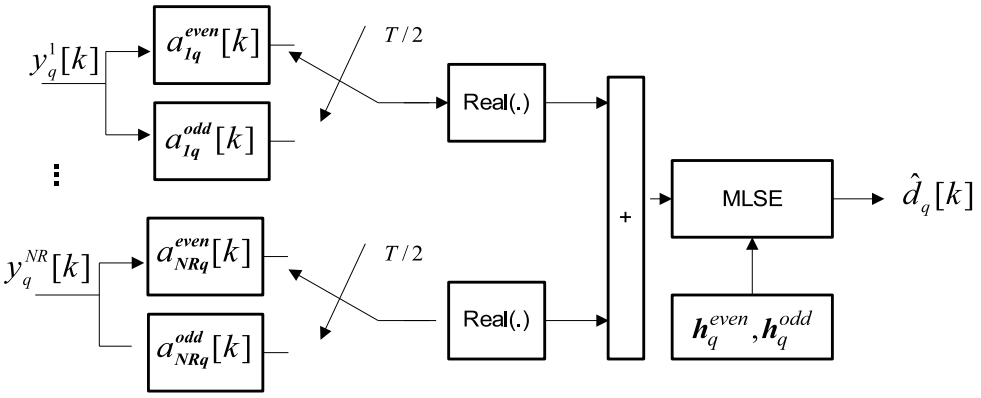

Figure 3.1: MDIR subcarrier receiver adapted to FBMC/OQAM systems.

3.1.2 MDIR impairments

The objective of this section is to point out those aspects that may degrade the MDIR receiver performance when $L_{ISI} > 0$. First of all, note that the noise at the broadband combiner output is coloured. As a result, the complexity that is required to implement the exact MLSE becomes unaffordable. To alleviate the complexity the Viterbi algorithm will be applied although the temporal correlation of the noise negatively impacts on the detection process, [74]. Hence, the receiver is not the optimal one. This problem is addressed in [75] and two solutions based on noise prediction and modification of the Viterbi metrics by grouping the samples in blocks of K are shown to improve the Viterbi results. In consequence, BER plots achieved by the VA could be considered as an upper bound.

The second aspect that will be tackled refers to the Viterbi metrics. The equalized noise plus the residual interference is assumed to be Gaussian distributed with variance σ_q^2 and mean 0, i.e. $i_q[k] \sim \mathcal{N}\left(0, \sigma_q^2\right)$. Provided that $\Re\left(z_q[k]\right)$ is the input sample to the MLSE at kth time instant, the corresponding metrics computed by the Viterbi algorithm consists in calculating $\left|\Re\left(z_q[k]\right) - \mathbf{h}_q^T\mathbf{s}\right|^2$ among all possible data sequences, being $\mathbf{s}$ a candidate sequence. Successful detection depends crucially on the effective signal to noise ratio (SNRe) [71],

$$SNRe_q = \min_{\mathbf{s}_j, \mathbf{s}_i} \frac{\left|\mathbf{h}_q^T\mathbf{s}_j - \mathbf{h}_q^T\mathbf{s}_i\right|}{4\sigma_q^2} \quad i \neq j, \tag{3.14}$$

where $\mathbf{s}_j$ and $\mathbf{s}_i$ are two different candidate sequences. Note that apart from the broadband combiner ability to reject the interferences, the coefficients of the DIR $\mathbf{h}_q^T$ determine the $SNRe_q$. To that end, it would be desirable to avoid the following two situations:

- Two or more coefficients of the DIR have similar magnitude.

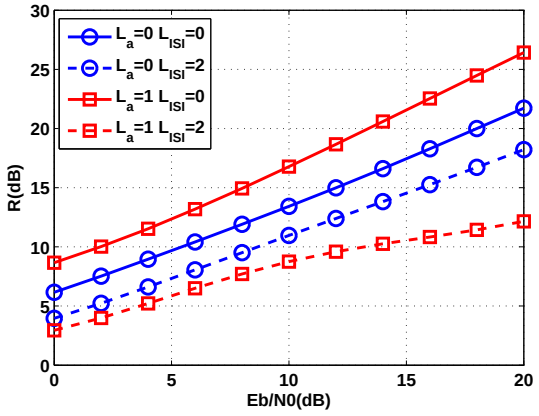

Figure 3.2: R against $\frac{E_b}{N_0}$. The system parameters and the propagations conditions are set according to Scenario 3 (see Table 2.3).

- One coefficient of the DIR is very close to a linear combination of the rest.

3.1.3 Simulation results

In order to illustrate the performance of the MDIR receiver, we set the key features of the system according to the values of Table 2.3 that correspond to the Scenario 1 and 3. The receiver is equipped with 2 antennas yielding a SIMO 2×1 communication system. As a benchmark the OFDM technique is simulated. In the OFDM case, the CP contains $\frac{M}{4}$ samples and the streams are detected on a per-subcarrier basis under the maximum Likelihood criterion. Both in OFDM and FBMC/OQAM the transmitted symbols are drawn from a 4-QAM constellation although in the second case in-phase and quadrature components are staggered so that $\{d_q[k]\}$ are 2-PAM.

MSE assessment

This section aims at demonstrating that focusing on the real part of the equalizer output leads to a better use of the spatial dimension. To that end, we solve these two problems

$$\begin{aligned} \eta_q^1 = \min_{\{\mathbf{a}_q, \mathbf{h}_q\}} & \mathbb{E}\left\{ \left\| z_q[k] - \mathbf{h}_q^H \mathbf{d}_q^d[k] \right\|_2^2 \right\} \\ s.t. \;\; & \mathbb{E}\left\{ \left\| \mathbf{a}_q^H \mathbf{G}_{qq}^k \mathbf{d}_q^d[k] \right\|_2^2 \right\} = 1 \end{aligned} \tag{3.15}$$

$$\begin{aligned} \eta_q^2 = \min_{\{\mathbf{a}_{q,e}, \mathbf{h}_q\}} & \mathbb{E}\left\{ \left\| \Re\left(z_q[k]\right) - \mathbf{h}_q^T \mathbf{d}_q^d[k] \right\|_2^2 \right\} \\ s.t. \;\; & \mathbb{E}\left\{ \left\| \Re\left(\mathbf{a}_q^T \mathbf{G}_{qq}^k \mathbf{d}_q^d[k] \right) \right\|_2^2 \right\} = 1. \end{aligned} \tag{3.16}$$

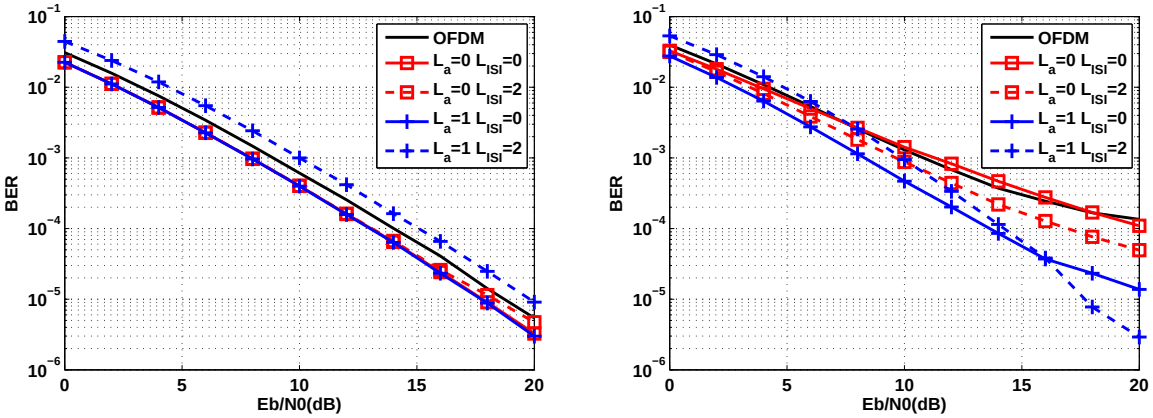

(a) Scenario 1.

(b) Scenario 3.

Figure 3.3: BER against $\frac{E_b}{N_0}$. The simulated systems correspond to FBMC/OQAM with per-subcarrier MDIR receiver and OFDM with CP. System parameters are set according to Scenario 1 and 3 (see Table 2.3).

In order to cast some light on the comparison, Figure 3.2 depicts the ratio $R = \frac{1}{M_a} \sum_{q \in S_a} \frac{\eta_q^1}{\eta_q^2}$ against the energy bit to noise ratio ($\frac{Eb}{N_0}$) for Scenario 3. The set S_a contains the indices of those subcarriers that are not switched off. By analysing the plots we can state that the higher $\frac{E_b}{N_0}$ is, the higher the value of R is regardless of L_a and L_{ISI}. Thus, constraining the equalizer output to be real is well-justified.

BER assessment

In Figure 3.3a and 3.3b the proposed scheme is compared with the OFDM system in terms of BER. Simulation results depicted in Figure 3.3a show that the MDIR receiver is able to outperform OFDM. Note that, the lowest BER curves are achieved when the allowed ISI terms are 0, i.e. $L_{ISI} = 0$. This indicates that in Scenario 1, where the channel frequency response is flat at the subcarrier level, the Viterbi algorithm yields a performance degradation due to the reasons described in Section 3.1.2. Another interesting conclusion is that one tap per-antenna suffices to equalize the channel.

The second part of this section is devoted to evaluate the MDIR receiver when the parameters are set according to Scenario 3. Note that in this case the subcarrier pass band region is two times wider so that the broadband combiner has to face more severe channel frequency responses. By observing Figure 3.3b we can assert that in situation the MDIR receiver can give better performance by setting L_{ISI} and L_a to be different from zero. The plots displayed in Figure 3.3b show that for

low and moderate $\frac{E_b}{N_0}$ the MDR receiver with $L_{ISI} = 0$ and $L_a = 1$ achieves the best performance. However from 16dB on, the lowest BER is obtained by the 3-tap equalizer when the number of allowed ISI terms is 2. It has been empirically observed that increasing L_{ISI} beyond 2 and L_a beyond 1 brings very little improvement but substantially increases the complexity.

3.2 Equalization in the asynchronous SIMO-MAC

In multiple access networks several users send data to the base station (BS) in the uplink. To get the maximum bandwidth efficiency, the users may be allocated on the same time slots and frequency resources. Although this strategy maximizes the bandwidth efficiency, this section focuses on a multiple access channel (MAC) where users are assigned a different set of subcarrier, which drastically simplifies the receive processing to separate the users. In order to identify which subcarriers correspond to a particular user, the indices of the subcarriers are arranged in different sets. In notation terms the set U_i contains the indices of those subcarriers that will be occupied by the ith user. The intersection between two different groups is the null space, i.e. $U_i \cap U_j = 0$, $i \neq j$, $i, j = 1, ..., U$. Hence, the signal transmitted by the ith user can be formulated as follows:

$$s_i[n] = \sum_{k=-\infty}^{\infty} \sum_{m \in U_i} d_m[k] \theta_m[k] f_m \left[n - k\frac{M}{2} \right], \quad 1 \leq i \leq U. \tag{3.17}$$

It has been considered that user terminals are single-antenna. By contrast, the BS is equipped with N_R antennas. In this section we focus on a challenging MAC where each user experiences different time and frequency shifts with respect to a reference point at the BS and undergo independent frequency selective channels. As a result, the signal received by the jth antenna reads as follows:

$$r_j[n] = \sum_{i=1}^{U} \vartheta\left(n, \epsilon_i, \phi_i\right) \left(h_{ij}[n] * s_i[n - \tau_i]\right) + \bar{w}_j[n], \quad 1 \leq j \leq N_R \tag{3.18}$$

$$\vartheta\left(n, \epsilon_i, \phi_i\right) = e^{\left(j\left(\frac{2\pi}{M}\epsilon_i n + \phi_i\right)\right)}. \tag{3.19}$$

With regard to the ith user, the triplet $\epsilon_i, \phi_i, \tau_i$ accounts for the carrier frequency offset (CFO) normalized to the subcarrier spacing, the carrier phase offset (CPO) and the time offset (TO), respectively. Multipath fading between the ith user and the jth receiver antenna is denoted $h_{ij}[n]$. Finally, the samples $\bar{w}_j[n]$ contaminate the jth antenna reception. Provided that the sources of asynchronism are perfectly known by the receiver we can synchronize with the user of interest by performing in this way

$$\begin{aligned} r_j^l[n] &= r_j[n+\tau_l]\vartheta\left(n+\tau_l,\epsilon_l,\phi_l\right)^* \\ &= \sum_{i=1}^{U}\vartheta\left(n+\tau_l,\epsilon_l^i,\phi_l^i\right)\left(h_{ij}[n]*s_i[n-\tau_l^i]\right)+\vartheta\left(n+\tau_l,\epsilon_l,\phi_l\right)^*\bar{w}_j[n+\tau_l], \end{aligned} \tag{3.20}$$

for $1 \leq l \leq U$ and $1 \leq j \leq N_R$. In the rest of the section and without loss of generality we will focus on the lth user detector. For the sake of notation we have defined these terms: $\epsilon_l^i = \epsilon_i - \epsilon_l$, $\phi_l^i = \phi_i - \phi_l$ and $\tau_l^i = \tau_i - \tau_l$. After feeding (3.20) into the analysis filter bank, we can express the qth output, for any $q \in U_l$, in this form

$$y_q^j[k] = \left(r_j^l[n]*f_q^*[-n]\right)_{\downarrow\frac{M}{2}} = \sum_{i=1}^{U}\sum_{m\in U_i}\left(d_m[k]\theta_m[k]e^{j\pi\epsilon_l^i k}\right)*\bar{g}_{qm}^{ilj}[k]+w_{lq}^j[k], \tag{3.21}$$

for $1 \leq j \leq N_R$ and $q \in U_l$, with

$$\bar{g}_{qm}^{ilj}[k] = \left(f_q^*[-n]*\left[\left(f_m[n-\tau_l^i]*h_{ij}[n]\right)\vartheta\left(n+\tau_l,\epsilon_l^i,\phi_l^i\right)\right]\right)_{\downarrow\frac{M}{2}} \tag{3.22}$$

$$w_{lq}^j[k] = \left(f_q^*[-n]*\bar{w}_j[n+\tau_l]\vartheta\left(n+\tau_l,\epsilon_l,\phi_l\right)^*\right)_{\downarrow\frac{M}{2}}. \tag{3.23}$$

The compact formulation written in (3.21) highlights that symbols are rotated as a result of the frequency shifts that the signal transmitted by each user experiences.

3.2.1 MDIR receiver

Thanks to the good spectral containment exhibited by the prototype pulse we can assume that ICI mainly comes from the adjacent subcarriers. This has motivated the design of equalizers that work on a per-subcarrier basis. It must be mentioned that the receive processing devised in this section takes for granted that the channel frequency response is approximately flat at the subcarrier level. Therefore, as it is shown in Section 3.1.3, the channel can be successfully equalized using a single tap per-antenna. Based on that, for $q \in U_l$, the equalized signal can be expressed as follows:

$$z_q[k] = \mathbf{a}_q^H\mathbf{y}_q[k] = \sum_{i=1}^{U}\sum_{m\in U_i}\sum_{\tau=-L_{g_1}}^{L_{g_2}}\mathbf{a}_q^H\bar{\mathbf{g}}_{qm}^{il}[\tau]d_m[k-\tau]\theta_m[k-\tau]e^{j\pi\epsilon_l^i(k-\tau)}+\mathbf{a}_q^H\mathbf{w}_{lq}[k], \tag{3.24}$$

for $q \in U_l$, with

$$\mathbf{y}_q[k] = \left[y_q^1[k]\ldots y_q^{N_R}[k]\right]^T \tag{3.25}$$

$$\mathbf{a}_q = [a_{1q} \dots a_{N_R q}]^T \tag{3.26}$$

$$\mathbf{w}_{lq}[k] = \left[w_{lq}^1[k] \dots w_{lq}^{N_R}[k]\right]^T. \tag{3.27}$$

If the channel coherence bandwidth is wider than the subcarrier spacing, then, similarly to the model formulated in (2.13), we get

$$\bar{\mathbf{g}}_{qm}^{il}[\tau] = \bar{\alpha}_{qm}^{il}[\tau]\left[H_{i1}\left(e^{j\frac{2\pi}{M}m}\right) \dots H_{iN_R}\left(e^{j\frac{2\pi}{M}m}\right)\right]^T = \bar{\alpha}_{qm}^{il}[\tau]\mathbf{H}_{im} \tag{3.28}$$

$$\bar{\alpha}_{qm}^{il}[k] = \left(f_q^*[-n] * \left(f_m[n-\tau_l^i]\right)\vartheta\left(n+\tau_l, \epsilon_l^i, \phi_l^i\right)\right)_{\downarrow\frac{M}{2}}, \tag{3.29}$$

where $H_{ij}\left(e^{j\frac{2\pi}{M}m}\right)$ is the channel frequency response of $h_{ij}[n]$ evaluated on the radial frequency $\frac{2\pi}{M}m$. Note that in those subcarriers where there is no multiple access interference (MAI) i.e. $\bar{\mathbf{g}}_{qm}^{il}[\tau] = \mathbf{0}$ for $i \neq l$, (3.24) coincides with (3.8) if $L_a = 0$. Therefore, the MDIR receiver described in Section 3.1 can be applied in the subcarriers that are free of MAI. Since the sources of asynchronism are known at the receiver, we can determine which bands are only affected by ISI and ICI. In the rest of subcarriers we cannot apply the same MDIR receiver that is proposed for synchronous communications. To illustrate this, suppose that we obtain the duplet $(\{\mathbf{a}_q, h_q\})$ by solving this problem

$$\begin{aligned} &\underset{\{\mathbf{a}_{q,e}, h_q\}}{\operatorname{argmin}}\, \mathbb{E}\left\{\|\Re\left(z_q[k]\right) - h_q d_q[k]\|_2^2\right\} \\ &s.t.\ \ \mathbb{E}\left\{\left\|\Re\left(\mathbf{a}_q^H \bar{\mathbf{g}}_{qq}^{ll}[0] d_q[k]\theta_q[k]\right)\right\|_2^2\right\} = 1. \end{aligned} \tag{3.30}$$

The expression (3.24) reveals that the optimal pair $(\{\mathbf{a}_q, h_q\})$ would depend on the index k because the autocorrelation matrix $\mathbb{E}\left\{\Re\left(\mathbf{y}_q[k]\right)\Re\left(\mathbf{y}_q^T[k]\right)\right\}$ is not stationary. That is, the equalizer and the desired impulse response should be updated with rate $\frac{2f_s}{M}$, regardless of if the channel varies or not. To alleviate the complexity we propose to solve

$$\begin{aligned} &\underset{\{\mathbf{a}_q, h_q\}}{\operatorname{argmin}}\, \mathbb{E}\left\{\|z_q[k] - h_q d_q[k]\|_2^2\right\} \\ &s.t.\ \ \mathbb{E}\left\{\left\|\mathbf{a}_q^H \bar{\mathbf{g}}_{qq}^{ll}[0] d_q[k]\theta_q[k]\right\|_2^2\right\} = 1. \end{aligned} \tag{3.31}$$

From Appendix 3.A, we can deduce that the optimal solution of (3.31) is given by

$$h_q = \mathbf{a}_q^H \bar{\mathbf{g}}_{qq}^{ll}[0] \tag{3.32}$$

$$\begin{aligned} &\lambda_q \bar{\mathbf{g}}_{qq}^{ll}[0]\left(\bar{\mathbf{g}}_{qq}^{ll}[0]\right)^H \mathbf{a}_q = \\ &\left(\sum_{i=1}^{U}\sum_{m\in U_i}\sum_{\tau=-L_{g_1}}^{L_{g_2}} \bar{\mathbf{g}}_{qm}^{il}[\tau]\left(\bar{\mathbf{g}}_{qm}^{il}[\tau]\right)^H - \bar{\mathbf{g}}_{qq}^{ll}[0]\left(\bar{\mathbf{g}}_{qq}^{ll}[0]\right)^H + N_0\mathbf{I}_{N_R}\right)\mathbf{a}_q. \end{aligned} \tag{3.33}$$

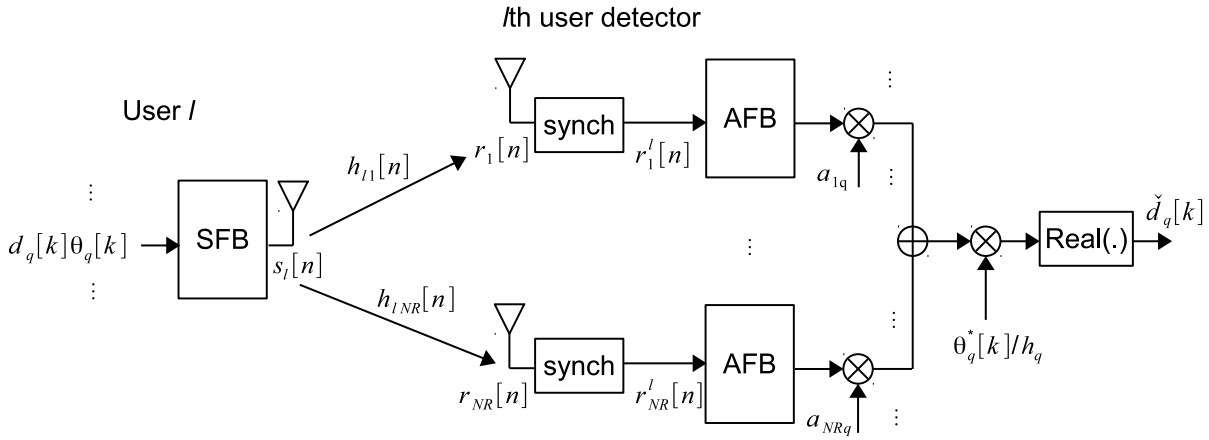

Figure 3.4: FBMC/OQAM-based SIMO multiple access channel.

From the noise autocorrelation matrix derived in Appendix (3.A), it can be readily checked that $\mathbb{E}\left\{\mathbf{w}_{lq}[k]\mathbf{w}_{lq}^{H}[k]\right\} = N_0\mathbf{I}_{N_R}$ The optimization variables in (3.31) have to be recalculated only if the channel varies. With the objective of searching for low complexity architectures we focus on structures that equalize the signal by using a single-tap per-antenna. Then, the equalized signal is processed as follows:

$$\check{d}_q[k] = \Re\left(\theta_q^*[k]\mathbf{a}_q^H\mathbf{y}_q[k]/h_q\right), \quad q \in S_a, \tag{3.34}$$

and next $\check{d}_q[k]$ is fed into the symbol detector, which is much simpler than the MLSE. This means that the equalizer results in a narrowband combiner and the length of the desired impulse response is fixed to one. As it has been shown in Section 3.1.3 this configuration achieves the lowest BER in Scenario 1, where the channel frequency response is approximately flat at the subcarrier level. The proposed architecture is sketched in Figure 3.4.

3.2.2 ZF receiver

The second strategy to cope with the lack of synchronism follows a zero-forcing (ZF) approach with the aim of completely removing the interference. Since it has been considered that subcarriers are distributed among users in a block-wise fashion, MAI will be only caused by a single interfering user. Provided that we focus on the lth user, we can state that solely those subcarriers that are near the edges of the subband assigned to the lth user are sensitive to be interfered by other users. Based on that, we have made two assumptions to devise the ZF receiver. The first one presumes that $\left|\epsilon_l^i\right| \leq 0.5$. The second assumption is based on recasting (3.28) as

$$\bar{\mathbf{g}}_{qm}^{il}[\tau] = \begin{cases} \bar{\alpha}_{qm}^{ll}[\tau]\mathbf{H}_{lq} & i = l \\ \bar{\alpha}_{qm}^{il}[\tau]\mathbf{H}_{im} & i \neq l \end{cases} . \tag{3.35}$$

If the channel coherence bandwidth is wide enough, then (3.28) and (3.35) are equivalent. We stick to the model defined in (3.35) because it allows us to simplify the ZF design. The fact that pulses have a roll-off factor equal to one also contributes to simplify the problem. Let b_l and f_l be the first and the last subcarrier that delimits the bandwidth assigned to the lth user, i.e. $U_l = \{q | b_l \leq q \leq f_l\}$ for $1 \leq l \leq U$. For a given $q \in U_l$ close to b_l that is sensitive to be affected by MAI, (3.24) can be rewritten as follows:

$$\begin{aligned} z_q[k] = \; & \mathbf{a}_q^H \mathbf{H}_{lq} \left(\sum_{m \in U_l \bigcap \{q-1,q,q+1\}} \sum_{\tau=-L_{g_1}}^{L_{g_2}} \alpha_{qm}[\tau] d_m[k-\tau] \theta_m[k-\tau] \right) + \mathbf{a}_q^H \mathbf{w}_{lq}[k] \\ & \underbrace{+ \mathbf{a}_q^H \mathbf{H}_{l-1 f_{l-1}} \left(\sum_{m \in U_{l-1}} \sum_{\tau=-L_{g_1}}^{L_{g_2}} \bar{\alpha}_{qm}^{(l-1)l}[\tau] d_m[k-\tau] \theta_m[k-\tau] e^{j\pi\epsilon_l^{l-1}(k-\tau)} \right)}_{MAI} . \end{aligned} \tag{3.36}$$

Note that $\bar{\alpha}_{qm}^{ll}[\tau]$ defined in (3.29) is equivalent to $\alpha_{qm}[\tau]$ defined in (2.8). The consequence of assuming that $\left|\epsilon_l^i\right| \leq 0.5$ is that the channel seen by those subcarriers that contribute to inter-user interference is the same and is given by $\mathbf{H}_{l-1 f_{l-1}}$. Analogously to (3.36), for a given $q \in U_l$ close to f_l we have

$$\begin{aligned} z_q[k] = \; & \mathbf{a}_q^H \mathbf{H}_{lq} \left(\sum_{m \in U_l \bigcap \{q-1,q,q+1\}} \sum_{\tau=-L_{g_1}}^{L_{g_2}} \alpha_{qm}[\tau] d_m[k-\tau] \theta_m[k-\tau] \right) + \mathbf{a}_q^H \mathbf{w}_{lq}[k] \\ & \underbrace{+ \mathbf{a}_q^H \mathbf{H}_{l+1 b_{l+1}} \left(\sum_{m \in U_{l+1}} \sum_{\tau=-L_{g_1}}^{L_{g_2}} \bar{\alpha}_{qm}^{(l+1)l}[\tau] d_m[k-\tau] \theta_m[k-\tau] e^{j\pi\epsilon_l^{l+1}(k-\tau)} \right)}_{MAI} . \end{aligned} \tag{3.37}$$

By analysing (3.36), we conclude that we can get rid of MAI if the ZF receiver is such that $\mathbf{a}_q^H \mathbf{H}_{l-1 f_{l-1}} = 0$. In other words, the equalizer should lie in the null space of the interfering channel, i.e. $\mathbf{a}_q \in \text{null}\left(\mathbf{H}_{l-1 f_{l-1}}\right)$. Then, ICI and ISI can be removed by performing as (3.34) shows, where now $h_q = \mathbf{a}_q^H \mathbf{H}_{lq}$. In consequence, vector $\mathbf{a}_q$ can be designed to maximize the signal to noise ratio (SNR) of (3.34). This is tantamount to solving this piecewise maximization

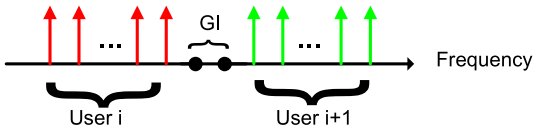

Figure 3.5: Blockwise subcarrier allocation strategy with frequency guards.

$$\begin{aligned} &\underset{\mathbf{a}_q}{\operatorname{argmax}} \left|\mathbf{a}_q^H \mathbf{H}_{lq}\right|^2 \\ &s.t. \quad \mathbf{a}_q \in \operatorname{null}\left(\mathbf{H}_{l-1 f_{l-1}}\right). \end{aligned} \tag{3.38}$$

The processing to be performed on subcarriers close to the boundary that separates users l and $l+1$ relies on solving

$$\begin{aligned} &\underset{\mathbf{a}_q}{\operatorname{argmax}} \left|\mathbf{a}_q^H \mathbf{H}_{lq}\right|^2 \\ &s.t. \quad \mathbf{a}_q \in \operatorname{null}\left(\mathbf{H}_{l+1 b_{l+1}}\right). \end{aligned} \tag{3.39}$$

Still having in mind low complexity architectures, in the rest of subcarriers where MAI is not present, the linear equalizer will be matched to the channel, i.e. $\mathbf{a}_q = \mathbf{H}_{lq}$. It must be highlighted that the system performance depends on: i) the channel coherence bandwidth and ii) the subspaces spanned by $\mathbf{H}_{lq}$, $\mathbf{H}_{l-1 f_{l-1}}$ and $\mathbf{H}_{l+1 b_{l+1}}$. Regarding the first point we can always reduce the subcarrier spacing. Conversely, regarding the second point, there is no way to boost the system performance when subspaces spanned by the interfering and the desired user are aligned.

3.2.3 Simulation results

In this section the MDIR and the ZF receiver are evaluated in terms of BER. Regarding the multi-antenna configuration we have considered a 2x1 SIMO system. The rest of the parameters, which are detailed in Table 2.3, have been selected according to the Scenario 1. In consequence the subcarrier indices assigned to the ith user ($i = 1, ..., U$) are given by $U_i = \{1 + (i-1)\, M_a/U, ..., iM_a/U\}$. In particular we have considered an asynchronous MAC channel with U=4 users. Regarding the simulation results only the second user detector performance has been assessed. It has been considered that the BS has a perfect knowledge of the channel and time and frequency offsets of each user. The input symbols have been drawn from the 16-QAM constellation. The CFO and CPO are generated according to a uniform distribution within the intervals $[-0.5, 0.5]$ and $[0, 2\pi]$, respectively. With regard to the propagation delays they are uniformly distributed between 0 and 100 samples. Aiming at mitigating the detrimental effects that CFO causes a guard interval (GI) between user bursts has been added. This strategy consists of leaving empty those subcarriers whose indices match the first entries of the sets. The idea is illustrated in Figure 3.5.

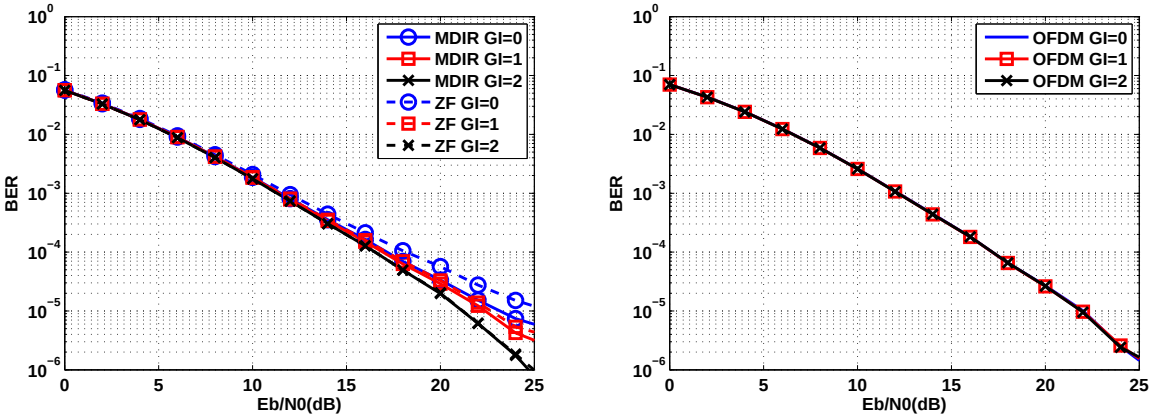

(a) FBMC/OQAM. (b) OFDM.

Figure 3.6: BER against $\frac{E_b}{N_0}$. The simulated systems correspond to OFDM with multi-user MMSE receiver and to FBMC/OQAM with per-subcarrier MDIR receiver and per-subcarrier ZF receiver. System parameters are set according to Scenario 1 (see Table 2.3).

Figure 3.6a depicts the BER plots corresponding to the ZF and MDIR receivers. Regarding the MDIR receiver we have applied the scheme described in Section 3.1.1 in those bands that are free of MAI. In particular we have chosen a receiver that uses 1 tap per antenna and sets the DIR length to 1, thus $L_a = 0$ and $L_{ISI} = 0$. Comparing the plots of Figure 3.6a it is shown that the BER curves virtually match from 0 to 10dB regardless of the GI. Note that by setting GI=2 we completely eliminate MAI. In this scenario the ZF and MDIR receiver achieve the same performance. However, for GI=0 and GI=1 the MDIR receiver outperforms the ZF receiver at high and moderate $\frac{E_b}{N_0}$. Hence, the ZF receiver is more eligible than the MDIR receiver if $\frac{E_b}{N_0} \leq 12$ dB, since the optimization procedure is the simplest under the ZF criterion.

As a benchmark we have considered an OFDM system implementing the multi-user MMSE receiver addressed in [76]. However, it has been slightly modified to accommodate the multi-antenna configuration of the receiver. It can be readily checked that a CP length equal to $\frac{M}{4}$ suffices to ensure that the combined effect of the multipath fading and the time offset between users will not result in IBI. To carry out a fair comparison with respect to FBMC/OQAM, the BER results have been computed solely considering the estimates at the MMSE receiver output corresponding to the second user. By observing the simulation results of Figure 3.6a and Figure 3.6b it is highlighted that the OFDM multi-user receiver and the MDIR nearly coincides when $\frac{E_b}{N_0} \leq 16$ dB. This range is broadened by increasing the GI length. Therefore, there is a trade-off between the robustness against the synchronization errors and the spectral efficiency degradation. By setting GI=2, both ZF and MDIR give the same performance as OFDM. Note that the effect of increasing the GI is

almost negligible in the OFDM case because all subcarriers are jointly processed.

3.2.4 Complexity analysis

In this section we will compute the number of real multiplications that the OFDM multi-user MMSE receiver and the FBMC/OQAM per-subcarrier MDIR receiver perform in the OFDM symbol duration, i.e. during $T = M/f_s$ seconds. We will refer to real multiplications and operations indistinctly.

Regarding the OFDM system the operations computed can be expressed as $N_{MMSE} = N_R \times (N_{FFT} + 4N_tM_a)$. The parameters N_t and N_{FFT} account for the number of taps per subcarrier used by the equalizer and the complexity needed to compute a fast Fourier Transform (FFT), respectively.

In the following we will address the FBMC/OQAM receiver complexity. In particular we will focus on a single user receiver equipped with a single antenna. The initial stage in charge of compensating the frequency offsets takes place with $4M$ operations. Because of the staggering processing the FFT is executed at twice the symbol rate resulting in $2N_{FFT}$ operations. The pulse shaping contributes with additional $8KM$ operations where K is the overlapping factor. Finally the equalization takes place with $4N_tM_a/U$ operations. Therefore, the entire complexity taking into account all the users and the multi-antenna configuration is equal to $N_{MDIR} = N_RU\,(4M + 2N_{FFT} + 8KM + 4N_tM_a/U)$.

As a figure to bring insight into the computational overhead we have considered the ratio $r = N_{MMSE}/N_{MDIR}$. Taking into account the system parameters, the ratio yields a computational overhead of $r = 10.01$. To obtain this ratio, note that we have used the split-radix algorithm to compute the FFT, thus $N_{FFT} = M\,(\log_2(M) - 3) + 4$, [65]. The number of taps in the OFDM case is $N_t = M_a$ whereas in the FBMC/OQAM modulation takes the value $N_t = 1$.

3.3 Interference aware detection

The goal pursued in Sections 3.1 and 3.2 is to devise an equalizer that removes the interference as much as possible before detection. Unfortunately, the residual interference after equalization may not be negligible. If bits are encoded it is crucial not to ignore this interference since the decoding algorithms are very sensitive to the errors yielded by mismatch modeling. In this regard, we study coded FBMC/OQAM systems with the aim of designing interference aware receiver structures that are able to perform a detection that is robust to the residual interference. It is worth mentioning that previous works have studied coded FBMC/OQAM modulations in the presence of severe multipath fading, [77–79]. These studies highlight the importance of characterizing the statistical

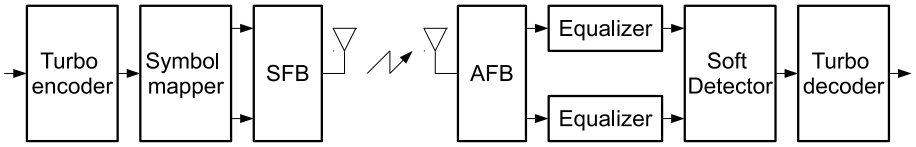

Figure 3.7: Transmitter and receiver block diagram.

information of the signal that corrupts the demodulated data. Building upon the advances made in [77–79] we focus on the design of practical receivers with the objective of reducing the complexity.

By starting we introduce in Figure 3.7 the SISO communication system that it is going to be studied. To protect the information from the detrimental effects caused by multipath fading, the bits are encoded by means of a parallel concatenated coding scheme, which consists of two identical systematic encoders the transfer function of which is $G(D) = \left[1, \frac{1+D^2+D^3}{1+D+D^3}\right]$, [80–83]. Next the coded bits are mapped as Figure 3.7 illustrates. Finally, the sequence of symbols is fed to the SFB, which is in charge of frequency multiplexing the symbols. The symbol mapper and the synthesis filter bank stages will be different depending on the multicarrier modulation to be used. The steps that have to be taken to implement the SFB and the AFB in the FBMC/OQAM case are described in Section 2.1. At the receiver, the AFB is in charge of demodulating the information that is conveyed on each subcarrier. The equalization stage is appended at the AFB output. Let $d_q[k]$ be the PAM symbol conveyed on the qth subcarrier and $a_q[k]$ be the equalizer employed on the qth subcarrier, which is different from zero for $-L_a \leq k \leq L_a$. Then, the signal that is fed into the soft detector is given by

$$\check{d}_q[k] = \frac{\Re\left(\theta_q^*[k]\left(a_q^*[k] * y_q[k]\right)\right)}{h_q} = d_q[k] + i_q[k] \tag{3.40}$$

with

$$h_q = \Re\left(\sum_{\tau=-L_a}^{L_a} g_{qq}[-\tau] a_q[\tau]\right) \tag{3.41}$$

$$\begin{aligned} i_q[k] = \; & \tfrac{1}{h_q} \sum_{\substack{m=q-1 \\ m\neq q}}^{q+1} \sum_{\tau=-L_a-L_{g_1}}^{L_a+L_{g_2}} \Re\left(\theta_q^*[k]\theta_m[k-\tau]\mathbf{a}_q^H \mathbf{g}_{qm}[\tau]\right) d_m[k-\tau] \\ & + \tfrac{1}{h_q} \sum_{\substack{\tau=-L_a-L_{g_1} \\ \tau\neq 0}}^{L_a+L_{g_2}} \Re\left(\theta_q^*[k]\theta_q[k-\tau]\mathbf{a}_q^H \mathbf{g}_{qq}[\tau]\right) d_q[k-\tau] + \frac{1}{h_q}\Re\left(\theta_q^*[k]\mathbf{a}_q^H \mathbf{w}_q[k]\right). \end{aligned} \tag{3.42}$$

The interference plus noise (IN) term in (3.42) is obtained by expanding the expression of the demodulated signal $y_q[k]$ that is formulated in (3.1). Besides, the following column vectors

have been defined $\mathbf{a}_q = [a_q[-L_a] \cdots a_q[L_a]]^T$, $\mathbf{g}_{qm}[\tau] = [g_{qm}[\tau + L_a] \cdots g_{qm}[\tau - L_a]]^T$ and $\mathbf{w}_q[k] = [w_q[k + L_a] \cdots w_q[k - L_a]]^T$. It is important to remark that (3.40) is also valid for OFDM systems if the CP is insufficiently long. However, it has to be taken into account that $d_q[k]$ might correspond to complex-valued symbols. Since the OFDM modulation has been widely studied we refrain from formulating the IN term in the OFDM context. Its expression can be computed as [84] details.

At this point the soft detection can be performed from the output of the equalizers. Bearing in mind (3.40), the a posteriori log-likelihood ratios (LLRs) of the encoded bits c_l, for $l = 1, ..., b$, can be simplified using the Max-Log approximation described in [85] as follows:

$$\mathrm{LLR}\left(c_l|\check{d}_q[k]\right) = \frac{\min\limits_{d:c_l=0} \left|\check{d}_q[k] - d\right|^2 - \min\limits_{d:c_l=1} \left|\check{d}_q[k] - d\right|^2}{2\sigma_q^2}, \tag{3.43}$$

where b is the number of bits that constitutes the transmitted symbols. The expression $d : c_l = 1$ ($d : c_l = 0$) defines the set of symbols whose lth bit is 1 (0). Finally, bits are detected from the soft outputs delivered by the iterative decoder, which is based on the turbo principle.

It is worth emphasizing that it has been assumed that bits are equiprobable and the interference plus noise term is a real-valued random variable that is Gaussian distributed, i.e. $i_q[k] \sim \mathcal{N}(0, \sigma_q^2)$. The same approach is followed in [79]. Note that the mean of the IN term is always zero. For further details check Appendix 3.B. If the statistical information of the noise and the symbols, as well as the instantaneous channel, are perfectly known, it is possible to formulate σ_q^2 in a closed-form expression as follows:

$$\begin{aligned}
\sigma_q^2 = \mathbb{E}\left\{|i_q[k]|^2\right\} = \tfrac{1}{|h_q|^2}\mathbb{E}\left\{\left(\Re\left(\theta_q^*[k]\mathbf{a}_q^H\mathbf{w}_q[k]\right)\right)^2\right\} + \\
\tfrac{1}{|h_q|^2}\sum_{\substack{m=q-1 \\ m\neq q}}^{q+1}\sum_{\tau=-L_a-L_{g_1}}^{L_a+L_{g_2}}\left(\Re\left(\theta_q^*[k]\theta_m[k-\tau]\mathbf{a}_q^H\mathbf{g}_{qm}[\tau]\right)\right)^2 \\
+\tfrac{1}{|h_q|^2}\sum_{\substack{\tau=-L_a-L_{g_1} \\ \tau\neq 0}}^{L_a+L_{g_2}}\left(\Re\left(\theta_q^*[k]\theta_q[k-\tau]\mathbf{a}_q^H\mathbf{g}_{qq}[\tau]\right)\right)^2.
\end{aligned} \tag{3.44}$$

We have assumed that the symbols are zero-mean, independent and uncorrelated with the noise, i.e. $\mathbb{E}\{d_m[k]d_q[n]\} = \delta_{m,q}\delta_{k,n}$ and $\mathbb{E}\{d_m[k]w_q[n]\} = 0$, $\forall m, q, k, n$. Regarding the filtered noise, the analytical expression of its variance can be computed as Appendix 3.A describes. Based on (3.44) we should first calculate the coefficients $\{g_{qm}[k]\}$, which are defined in (2.11), as follows:

$$g_{qm}[k] = \sum_{t=0}^{L_{ch}-1} h[t]e^{j\pi qk}\alpha_{qm}^k[t]e^{-j\frac{2\pi}{M}qt} \tag{3.45}$$

$$\alpha_{qm}^{k}[t] = \sum_{v=0}^{L-1} p[v]\, p\left[v + t - k\frac{M}{2}\right] e^{j\frac{2\pi}{M}(m-q)\left(v-\frac{L-1}{2}\right)}, \tag{3.46}$$

where L_{ch} is the maximum channel excess delay of the channel. Even knowing $\left\{e^{j\pi qk}\alpha_{qm}^{k}[t]\right\}$ beforehand, it can be deduced from (3.45) that the complexity cost in terms of multiplications is $2L_{ch}$. Taking into account which are the values of $g_{qm}[k]$ that are different from zero, the total number of operations is approximately $3\left(L_{g_1} + L_{g_2} + 1\right) 2L_{ch}M_a$. According to the expressions provided in [84], the complexity in the OFDM case is in the order of M_a^3. From the perspective of reducing the complexity, we propose to estimate the power using two different methods.

3.3.1 Direct decision method (DDM)

The first method to estimate (3.44) consists in computing the empirical expectation of $i_q[k]$ over a period, T, in which the channel conditions do not substantially vary. The estimation boils down to compute the following expression

$$\check{\sigma}_q^2 = \frac{1}{T}\sum_{k=0}^{T-1} |i_q[k]|^2 . \tag{3.47}$$

It can be readily verified that the complexity required to compute (3.47) is substantially reduced with respect to that required to obtain the theoretical expression of (3.44). In order to get the instantaneous value of the IN term it is mandatory to subtract the data symbols from the equalized signals, i.e $i_q[k] = \check{d}_q[k] - d_q[k]$. To perfectly compute the term $i_q[k]$, the receiver needs to know the transmitted data beforehand. Hence, this method relies on the transmission of T pilot sequences in the form of a preamble. Nevertheless, this may imply transmitting longer training sequences than those exclusively used for channel estimation and synchronization purposes, which would decrease the spectral efficiency (see e.g. [86–97]). To overcome this drawback the method proposed in this section refrains from using pilots. As a consequence, the IN term is approximated to $\check{i}_q[k] = \check{d}_q[k] - s_q^0[k]$, where $s_q^0[k]$ is an estimation of $d_q[k]$. It must be mentioned that the reliability of the proposed estimator crucially relies on the decisions made from the equalized signals. If the decisions are not correct, the variance estimation will substantially deviate from the real value. In this sense, the simplest option consists in detecting symbols according to the maximum likelihood (ML) criterion, which yields this estimator

$$\check{\sigma}_{q,0}^2 = \frac{1}{T}\sum_{k=0}^{T-1} \min_{s_q^0[k]\in\mathbb{X}} \left|\check{d}_q[k] - s_q^0[k]\right|^2 , \tag{3.48}$$

where $\mathbb{X}$ is the modulation alphabet. One way to evaluate the quality of the estimator is to check

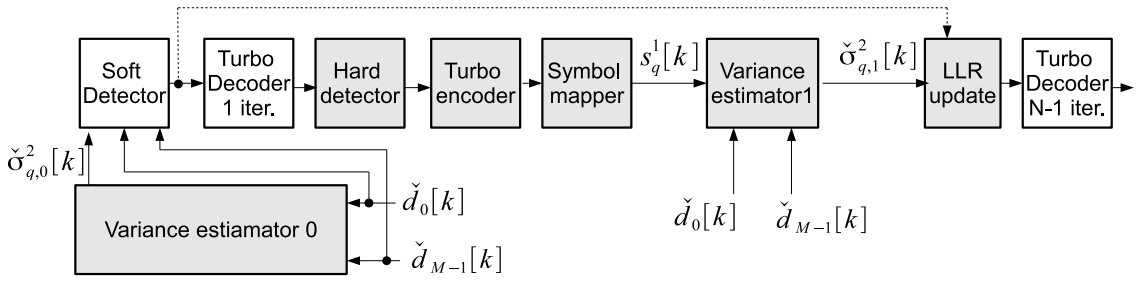

Figure 3.8: Receiver scheme with variance estimation.

if it is unbiased. To this end, we calculate the conditional expectation of $\check{\sigma}^2_{q,0}$ given the event $\left\{s_q^0[0]...s_q^0[T-1]\right\}$, where $s_q^0[k]$, $k=0,...,T-1$, is any symbol of the constellation diagram. That is, $s_q^0[k] \in \mathbb{X}$ for $0 \leq k \leq T-1$. Taking into account that symbols are zero-mean and independent, we can write the expectation in this form

$$\begin{aligned} \mathbb{E}\left\{\check{\sigma}^2_{q,0}|s_q^0[0]...s_q^0[T-1]\right\} &= \tfrac{1}{T}\sum_{k=0}^{T-1}\mathbb{E}\left\{\left|d_q[k]-s_q^0[k]\right|^2\right\}+\mathbb{E}\left\{|i_q[k]|^2\right\} \\ &= \tfrac{1}{T}\sum_{k=0}^{T-1}\mathbb{E}\left\{\left|d_q[k]-s_q^0[k]\right|^2\right\}+\sigma_q^2. \end{aligned} \tag{3.49}$$

Unless the decisions are correct, i.e. $d_q[k] = s_q^0[k]$, the estimator will be biased as (3.49) shows. This highlights the importance of regenerating the message as accurately as possible.

3.3.2 Refined direct decision method (RDDM)

We have empirically observed that the estimator derived in Section 3.3.1 gives satisfactory results when the modulation order is low, e.g. 2PAM. On the contrary for higher order modulations the BER curves exhibit an error floor. To remedy this it is clear that the estimator has to be refined. In this sense the approach that we have followed is based on regenerating the sequence of transmitted symbols from the outputs of the turbo decoder. That is, already detected bits from the initial iteration are fed into the turbo encoder stage and then the coded bits are mapped to obtain the OQAM symbols. From Figure 3.8 it can be inferred that the refined estimation is equivalent to

$$\check{\sigma}^2_{q,1} = \frac{1}{T}\sum_{k=0}^{T-1}\left|\check{d}_q[k]-s_q^1[k]\right|^2. \tag{3.50}$$

Notice that the extrinsic LLRs computed by the first turbo decoder are not directly forwarded to the second turbo decoder to be used as a priori information. That is because the term $\check{\sigma}^2_{q,0}$,

Table 3.1: Complexity order and memory requirements of computing the variance of the IN term in all the subcarriers.

Estimation method	Complexity order	Memory
DDM	$2^b TM_a$	-
RDDM	$TM_a\left(2^b+3b+4\right)$	TM_a

which is computed as (3.48) specifies, may excessively deviate from the real value. If so, errors will propagate on subsequent turbo iterations since the decoding algorithms are sensitive to the variance errors. It is also important to remark that, in contrast to [98], the estimated symbols are not used to cancel out the interferences but to get a more accurate estimation of the transmitted symbols when compared to the approach followed in Section 3.3.1. As (3.49) indicates the lower is the symbol error rate, the lower is the bias. The reason why we have discarded to cancel out the interferences has to do with the complexity burden that is required to calculate the coefficients of the equivalent channels $\{g_{qm}[k]\}$.

It is worth mentioning that the symbols in FBMC/OQAM systems are modulated at rate twice that of the symbols in OFDM. Hence, for a fixed window the number of symbols that are used to calculate (3.47), (3.48) and (3.50) will be $T/2$ in the OFDM case.

3.3.3 Comparison of different estimation techniques

In this section we compare the two estimators described in Sections 3.3.1 and 3.3.2. In this sense, the Table 3.1 summarizes the order of the complexity and the memory that is approximately required by each method. The analysis that has been conducted to get the values of Table 3.1 is detailed hereinafter.

DDM

The direct decision method relies on performing an exhaustive search over all the elements of the modulation alphabet as (3.48) highlights. Provided that b bits are used to represent any point of the constellation diagram, then the number of norms that has to calculated is equal to $2^b TM_a$. On the positive side, the approach followed in section 3.3.1 does not need to store any data.

RDDM

The complexity required to implement the refined direct decision method is tantamount to computing the complexity of the grey blocks in Figure 3.8. Towards this end we first analyse $\check{\sigma}^2_{q,0}$. According to (3.48) the number of norms to be computed is $2^b TM_a$, where b is the number of bits that constitutes the symbols. The next processing that contributes to the increase of the complex-

ity is the conversion from soft bits to binary data. Considering that a single mapping only takes one operation together with the fact that the code rate is set to $r_{code} = 1/3$ implies performing $\frac{b}{3}TM_a$ operations. Then, each bit has to be coded again by concatenating two identical systematic convolutional codes. Then it follows that the turbo code computes $\frac{2b}{3}TM_a$ coded bits and each one is obtained after performing 4 logical operations. To regenerate the message, the coded bits are mapped into OQAM symbols by performing MT_a look up operations. As (3.50) indicates the refined estimation requires computing MT_a norms. In the last step we multiply $\mathrm{LLR}(c_l|\check{d}_q[k])$ by $\frac{\check{\sigma}^2_{q,0}}{\check{\sigma}^2_{q,1}}$, which takes TM_a divisions and TM_a multiplications. According to the values gathered in the Table 3.1, the complexity costs when $b = 2$ results approximately in $14TM_a$ operations. Recall that the number of operations to get the exact value of $\left\{\sigma^2_q\right\}$ is in the order of M_a^3 and $3(1 + L_{g_1} + L_{g_2})2L_{ch}M_a$ when the OFDM and the FBMC/OQAM modulation scheme is considered, respectively. This highlights that although the strategy devised in Section 3.3.2 is the most complex, the method is still interesting because there is a good prospect of L_{ch} and M_a^2 being higher than T. Therefore, the refined direct decision method is likely to be more efficient than the computation of the real variance. Unlike to what happens in the DDM, the regenerated message has to be stored so that it can be loaded later on to estimate the variance. As a result, there should be enough available memory to save TM_a symbols.

A feature that is common to the DDM and the RDDM is that they do not operate on real time. That is, the variance is estimated after receiving T consecutive multicarrier symbols and storing the decision variables $\left\{\check{d}_q[k]\right\}$ for $0 \leq k \leq T-1$ and $q \in S_a$. This observation reveals that in addition to the memory requirements that are summarized in Table 3.1, the receiver has to reserve some additional space to save TM_a equalized symbols.

3.3.4 Application to single frequency networks

It should be noted that unless the interference is significant at the output of the equalizer, the interference aware detection described in Section 3.3 brings no amelioration. In other words, the reception has to be affected by severe multipath fading. We may encounter this situation for single frequency network (SFN) transmission. In a SFN the frequency reuse factor is one and thus the user equipment receives several delayed versions of the same signal, giving rise to an artificial multipath channel that is highly frequency selective. The rationale behind the SFN is to make an efficient use of the spectrum. The transmission scheme that yields a SFN has been considered in [99] for delivering multimedia content to mobile users. The SFN concept has been widely studied also in the DVB-T digital TV context.

In this section we consider the SFN represented in Figure 3.9. Since the synchronization issues are out of the scope of this paper we assume that all the transmitters are perfectly time- and frequency-synchronized. Nevertheless, the signals that come from the first and second-order neigh-

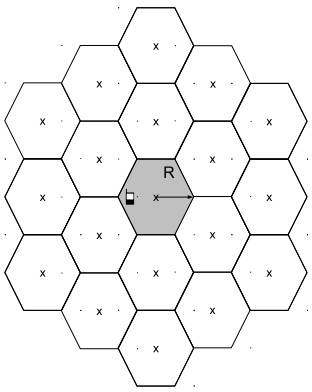

Figure 3.9: Single frequency network with frequency reuse equal to one.

bors will give rise to an artificial multipath. More distant BSs are ignored, so in the considered scenario, 19 BSs are transmitting in the same band.

Assuming that the user terminal is synchronized with the nearest BS, the received signal can be written as function of the virtual channel as $r[n] = h_v[n] * s[n] + \bar{w}[n]$, where

$$r[n] = \sum_{i=1}^{19} \frac{1}{\sqrt{L_i}} s[n - \tau_i] * h_i[n] + \bar{w}[n]. \tag{3.51}$$

Here $s[n]$ is the signal transmitted by all the BSs and $\bar{w}[n]$ is the additive white Gaussian noise. The term τ_i stands for the delay of the ith transmitter with respect to the BS of reference, which can be identified without loss of generality with any index. The propagation conditions between the ith transmitter and the user terminal are modeled by the channel impulse response $h_i[n]$ and by the combined effect of the path loss and the shadowing, which is expressed as $L_i(\text{dB}) = \bar{L}_i(\text{dB}) + X_i(\text{dB})$. The variable $X_i(\text{dB})$ accounts for the shadowing and it follows a Gaussian distribution with zero mean and standard deviation σ_x. By contrast $\bar{L}_i(\text{dB})$ is a distance dependant term given by $\bar{L}_i(\text{dB}) = 128.1 + 37.6\log_{10}(d_i)$, where d_i denotes the distance to the ith transmitter in km [63]. With the aim of studying the most general case, we consider that the user terminal receives several delayed versions of the signal broadcasted by a given transmitter. Therefore, $h_i[n]$ is modeled as a tapped delay line, which indicates that the channel between the receiver and any transmitter is frequency selective.

3.3.5 Numerical results

In this section we compare OFDM and FBMC/OQAM in the SFN scenario depicted in Figure 3.9 where the cell radius is equal to R=1km. Hence, the user is confined in the coverage area of a single transmitter while the exact position randomly varies for each channel realization. The

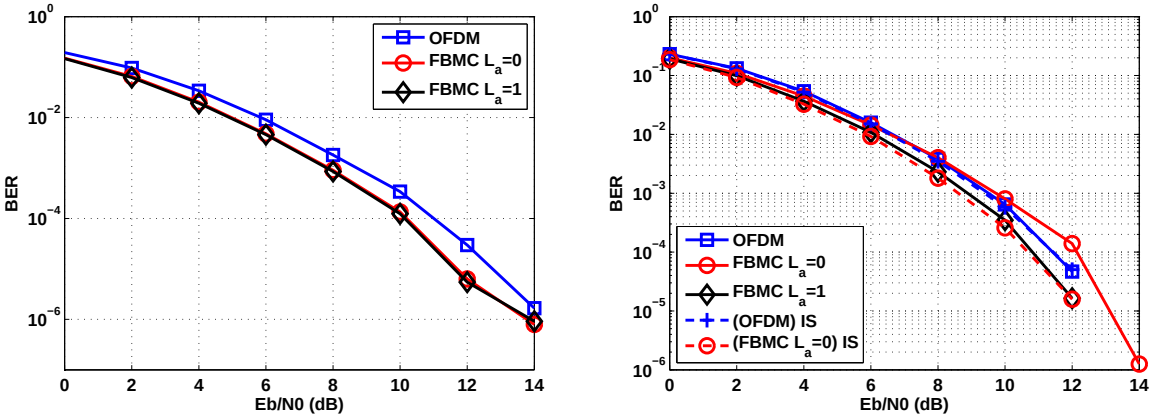

(a) VehA (b) VehB

Figure 3.10: BER vs. $\frac{E_b}{N_0}$ when the receiver is based either on perfect IN variance estimation or on perfect interference cancellation. The propagation conditions obey the VehA and the VehB channel models.

equalizer is designed according to the zero-forcing criterion in both modulations. The design in the FBMC/OQAM case is described in [69]. Regarding the system parameters, the 10 MHz bandwidth is split into M=1024 subbands, out of which 600 are active. The carrier frequency is 2 GHz and the sampling frequency is set to 15.36 MHz. The power delay profile of $\{h_i[n]\}$ obeys the ITU-Vehicular A (VehA) or the ITU-Vehicular B (VehB) models and we assume that the channel is invariant for T=20 consecutive FBMC/OQAM symbols or, equivalently, for T=10 consecutive OFDM symbols. The shadowing standard deviation is $\sigma_x = 8$ dB. As for the decoder, we employ the MAX-LOG-MAP algorithm with N=4 iterations. The symbols belong to 16-QAM, which means that the real symbols $\{d_q[k]\}$ are 4-PAM. The assessment has been made in terms of BER against the energy bit to noise ratio ($\frac{E_b}{N_0}$), which is defined as

$$\frac{E_b}{N_0} = \left(\sum_{i=1}^{19} \frac{1}{L_i}\right) \frac{2\left(\frac{M+\mathrm{CP}}{M}\right)}{4 r_{code} N_0}, \tag{3.52}$$

where the noise samples are generated as follows $\bar{w}[n] \sim \mathcal{CN}(0, N_0)$ and the constant 2 is the symbol energy. The constant 4 accounts for the number of bits that constitutes the 1-6QAM symbols. It is worth mentioning that CP $= 0$ for FBMC/OQAM systems and CP $= \frac{M}{4}$ in the OFDM case.

Benchmark

Before evaluating the impact of the variance estimation methods described in the Sections 3.3.1 and 3.3.2, we depict in Figure 3.10 the BER curves when the variance of $i_q[k]$ is perfectly estimated.

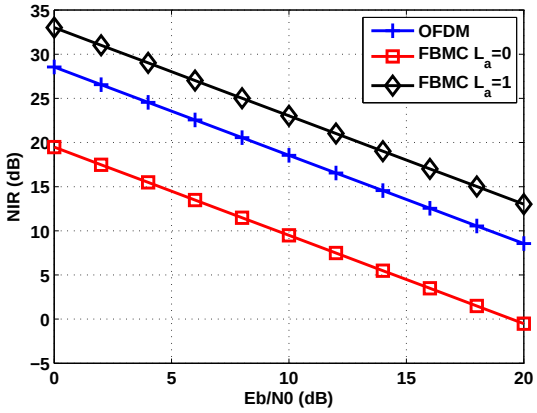

Figure 3.11: Average NIR versus $\frac{E_b}{N_0}$. The propagation conditions obey the VehB channel model.

When the power delay profile of the channel obeys the ITU Vehicular A model, the FBMC/OQAM system does not benefit from performing a multi-tap equalization because the channel frequency response at the subcarrier level is practically flat. With the parameters used in this scenario the maximum channel excess delay satisfies $L_{ch} \leq 216$ and, therefore, the demodulated signals are free of ISI when OFDM is considered. The improvement of FBMC/OQAM with respect to OFDM for $\frac{E_b}{N_0} \leq 14$ dB is consequence of the energy wastage that implies transmitting the CP.

In Figure 3.10b we asses the system performance when the channel is modeled according to the ITU Vehicular B model. Now the gap between the multi-tap and single-tap linear equalization is widened. The reason lies in the fact that the channel coherence bandwidth has reduced since the maximum channel excess delay is upper bounded as follows $L_{ch} \leq 484$. As a result, the transmission based on the OFDM technique does not succeed in avoiding IBI. By setting CP$= \frac{M}{4}$, the IBI is reduced to a higher extend but not enough to give better performance than the FBMC/OQAM modulation that equalizes the channel with 3 taps per-subband. These results reveal that it is of paramount importance to mitigate the residual interference as much as possible. This observation has motivated us to test one alternative receiver that performs a perfect interference suppression (IS). That is, we get rid of the interference from (3.40) before they are fed into the channel decoding stage. Then, the noise is the only source of interference. The curves in Figure 3.10b indicate that the improvement brought by the perfect IS is marginal. As it is pointed out in Section 3.3 the complexity required to estimate the interference may be too high, which provides further arguments in favour of the receiver that is based on estimating the variance.

To further justify the results provided in Fig. 3.10b, we have pictured in Fig. 3.11 the noise to interference ratio (NIR) averaged over all subcarriers. Borrowing the notation from (3.44), the metric in the FBMC/OQAM case is given by

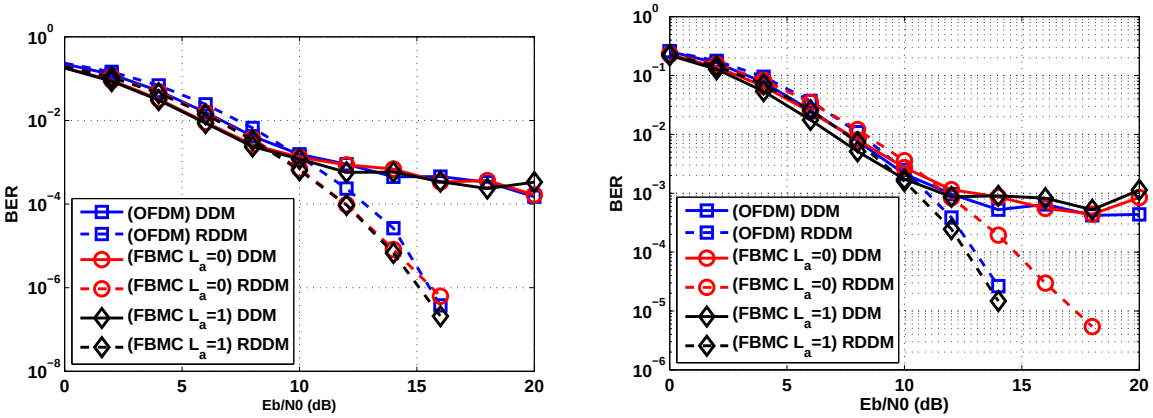

(a) VehA (b) VehB

Figure 3.12: BER versus $\frac{E_b}{N_0}$ when the receiver implements different IN variance estimation methods. The propagation conditions obey the VehA and VehB channel models.

$$NIR = \frac{1}{600} \sum_{q \in S_a} \frac{\mathbb{E}\left\{ \left(\Re \left(\theta_q^*[k] \mathbf{a}_q^H \mathbf{w}_q[k] \right) \right)^2 \right\}}{\sum_{(m,\tau) \neq (q,0)} \left(\Re \left(\theta_q^*[k] \theta_m[k-\tau] \mathbf{a}_q^H \mathbf{g}_{qm}[\tau] \right) \right)^2}, \tag{3.53}$$

where S_a contains the indices of those subcarriers that are active. The Figure 3.11 confirms that multi-tap equalization removes more effectively the interference than the single-tap counterpart in highly frequency selective channels. Hence, the results of Figure 3.11 are in accordance with the coded BER vs. $\frac{E_b}{N_0}$ curves.

The spectral efficiency reaches 1.20 bits/s/Hz for the FBMC/OQAM case. The OFDM counterpart results in 0.96 bits/s/Hz.

Evaluation of the proposed interference aware receiver

In this section we evaluate the performance of the receiver based on the variance estimation. The window used by all the methods described in the Sections 3.3.1 and 3.3.2 encompasses 20 FBMC/OQAM symbols or, equivalently, 10 OFDM symbols. The Figure 3.12a and Fig. 3.12b highlight that the plots obtained when the RDDM is applied are shifted to the right when compared to Figure 3.10a and Figure 3.10b. That is because the turbo decoder performs 3 iterations instead of 4. As Figure 3.8 shows, one iteration is devoted to estimating the variance. Recalling (3.50), we can assert that the degradation also has to do with the errors committed when performing the symbol mapping after reencoding the bits obtained at the output of the initial turbo iteration. By examining Figure 3.12b we can conclude that the degradation in FBMC/OQAM systems is

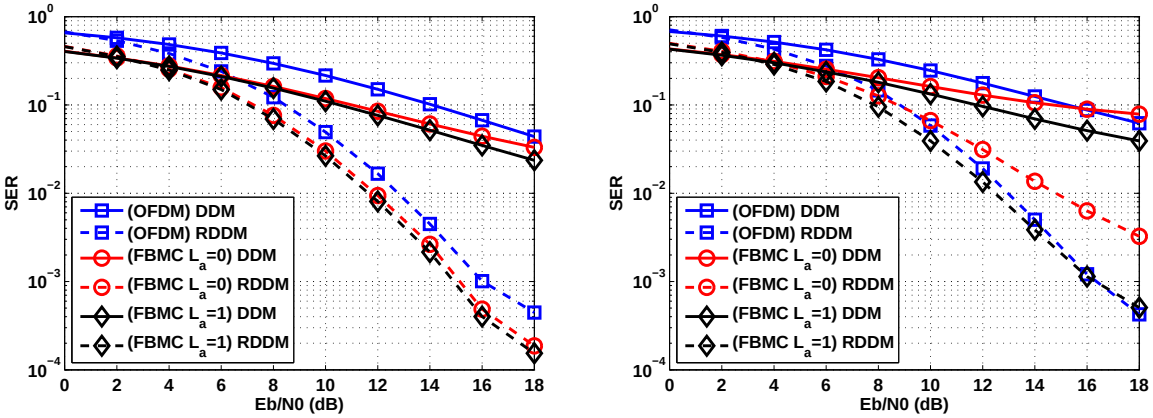

(a) VehA (b) VehB

Figure 3.13: SER before and after performing the initial turbo iteration versus $\frac{E_b}{N_0}$. The propagation conditions obey the VehA aand VehB channel models.

between 1 dB and 2 dB when the equalizers perform a multi-tap filtering. In the single-tap case, the degradation is substantially higher. Taking into consideration Figure 3.11, it seems that the cause is related to the insufficient interference mitigation capabilities exhibited by single-tap equalization in severe propagation conditions. In order to improve the performance the interference has to be more effectively rejected. Notice that the curves associated with the receiver based on the DDM exhibit an error floor. The reason is because the tentative decisions used in (3.48) are too erroneous.

To support the results of Figure 3.12a and Figure 3.12b we plot in Figure 3.13a and Figure 3.13b the symbol error rate (SER) that is observed when the transmitted data is estimated according to the procedure followed by the DDM and the RDDM. Since the decoding algorithms are sensitive to the variance deviations, the coded BER performance relies on the accuracy with which the transmitted message is regenerated as (3.49) demonstrates. The results of Figure 3.13a and Figure 3.13b can be understood as the evaluation of the SER at the input and the output of the initial turbo iteration. In Figure 3.13a the plots associated with the RDDM are equal or less than 1dB apart. Hence, all the techniques suffer a similar deterioration for estimating the variance as Figure 3.12a shows. By contrast, when the selectivity of the channel becomes stronger as it happens in Figure 3.12b, the FBMC/OQAM modulation combined with the single tap zero forcing equalizer do not achieve competitive results when the variance is estimated. By observing Figure 3.13b, it becomes clear that the degradation has to do with the increased SER, which causes less reliable estimation. As it has been previously pointed out, the tentative decisions made when the DDM is applied are not reliable. This is confirmed in Figure 3.13a and Figure 3.13b.

3.4 Chapter summary

This chapter delves into the design of novel receive signal processing techniques, especially devised for FBMC/OQAM systems, with the objective of coping with the interference that is induced by the multipath fading. Indeed, in PTP communications the interference is consequence of losing the orthogonality due to the multipath fading. Therefore, one alternative to get rid of the interference is to counteract the channel. To this end, it has been studied the robustness exhibited by the structure that relies on a feed forward equalizer along with a MLSE. The aim of the equalizer is to reject ICI and shortening the channel that gives rise to ISI. Then the MLSE is able to detect the transmitted symbols dealing with the allowed ISI terms with a reasonably complexity. When the propagation conditions are such that the channel frequency response is flat at the subcarrier level, the best strategy consists in performing a single-tap filtering with the objective of eliminating all ICI and ISI terms. As a consequence, the MLSE operates on a symbol-by-symbol basis. If the flat fading assumption is not satisfied, the equalizer should have at least 3 taps, which means that the temporal diversity comes into play. At low and moderate energy bit to noise ratios, the best performance is achieved if the equalizer is designed to remove ISI and ICI. By contrast, at very low noise regime the lowest BER is achieved if two ISI terms are allowed at the output of the equalizer. In the simulated environments, FBMC/OQAM systems assisted with per-subcarrier MDIR receivers outperform OFDM systems based on ML detection in terms of BER and spectral efficiency.

Fuelled by the good results obtained in PTP communications, the equalization design in multiple access channels has also been covered. In this case, subcarriers are assigned to users in a block-wise fashion so that users do not transmit on the same frequency resources. The analysis has been conducted under the assumption that the channel coherence bandwidth is wider than the subcarrier spacing. Bearing in mind the results obtained in scenarios where there is a single user, the receiver structure that is proposed consists of a single-tap equalizer followed by a ML detector. The idea is to build an equalizer that is able to combat ISI and ICI, which are induced by the channel, along with IUI, which appears due to the time and frequency misalignments between users. Simulation-based results show that FBMC/OQAM based on the MDIR receiver and the OFDM multi-user MMSE receiver give the same performance when $\frac{E_b}{N_0} \leq 16$ dB. With the penalty of marginally reducing the spectral efficiency, the link reliability of FBMC/OQAM can be significantly increased by dropping those subcarriers that are sensitive to suffer from MAI. Thus, the GI length can be adjusted to ensure that there will not be MAI. When this is satisfied the FBMC/OQAM modulation scheme gives the same BER as the OFDM multi-user MMSE receiver but with a complexity 10.01 times lower.

It has been demonstrated that FBMC/OQAM systems that rely on equalization bring compet-

itive results when compared to OFDM. The system performance can be boosted if, in addition to applying equalization techniques, the information bits are protected by means of channel coding. Provided that the channel is highly frequency selective it is very important to not neglect the power of the residual interference at the output of the equalizer when executing the iterative decoding. Otherwise, the performance may significantly degrade. This is especially relevant for single frequency network transmission since the echoes coming form different transmitters are superimposed at the reception, giving rise to an artificial channel the delay spread of which may be very large. This means that the receiver structure has to be aware of interference. The exact characterization of the residual interference may require a complexity that is unaffordable. To keep the complexity low it has been proposed to estimate the variance of the residual interference plus noise term by resorting to data aided algorithms. Simulation-based results reveal that the BER degradation is less than 2 dB when the receiver relies on variance estimation methods. It is also important to highlight that regardless of the method FBMC/OQAM is able to reach or slightly exceed the error performance of CP-OFDM while the spectral efficiency is increased when FBMC/OQAM is considered.

Appendices

3.A Solution of problem 3.12

Let $\mathbf{a}_q$ be either a vector or a matrix, we define this extended notation $\mathbf{a}_{q,e} = \left[\Re\left(\mathbf{a}_q^T\right) \quad \Im\left(\mathbf{a}_q^T\right)\right]^T$. Then, assuming that symbols are independent, i.e. $\mathbb{E}\left\{d_q[k]d_m[n]\right\} = \delta_{q,m}\delta_{k,n}$, we can express the MSE and the constraint as follows:

$$\mathbb{E}\left\{\left|\Re\left(z_q[k]\right) - \mathbf{h}_q^T\mathbf{d}_q^d[k]\right|^2\right\} = \mathbf{a}_{q,e}^T\left(\sum_{m=q-1}^{q+1}\sum_{\tau=-L_a-L_{g_1}}^{L_a+L_{g2}}\bar{\mathbf{g}}_{qm,e}^k[\tau]\left(\bar{\mathbf{g}}_{qm,e}^k[\tau]\right)^T + \mathbf{R}_q\right)\mathbf{a}_{q,e} + \\ \|\mathbf{h}_q\|_2^2 - 2\mathbf{a}_{q,e}^T\bar{\mathbf{G}}_{qq,e}^k\mathbf{h}_q \tag{3.54}$$

$$\mathbb{E}\left\{\left|\Re\left(\mathbf{a}_q^H\mathbf{G}_{qq}^k\mathbf{d}_q^d[k]\right)\right|^2\right\} = \left\|\mathbf{a}_{q,e}^T\bar{\mathbf{G}}_{qq,e}^k\right\|_2^2, \tag{3.55}$$

where $\bar{\mathbf{g}}_{qm}^k[\tau] = \theta_m[k-\tau]\mathbf{g}_{qm}[\tau]$. The autocorrelation matrix can be formulated as follows:

$$\mathbf{R}_q = \mathbb{E}\left\{\mathbf{w}_{q,e}[k]\mathbf{w}_{q,e}^T[k]\right\} = \frac{N_0}{2}\mathbf{I}_{2N_R}\otimes\mathbf{C}_q, \tag{3.56}$$

where (i,j)th element of matrix $\mathbf{C}_q \in \mathbb{R}^{2L_a+1\times 2L_a+1}$ is given by $[\mathbf{C}_q]_{ij} = \Re\left(\alpha_{qq}[i-j]\right)$, for $i,j = 1,...,2L_a+1$. The coefficients $\{\alpha_{qm}[k]\}$ are defined in (2.8). The expression of the autocorrelation

matrix is derived by realizing that if $\bar{w}_j[n] \sim \mathcal{CN}(0, N_0)$ and $\mathbb{E}\left(\bar{w}_j[n]\bar{w}_i^*[k]\right) = N_0\delta_{i,j}\delta_{k,n}$, then $\mathbf{R}_q$ is block diagonal, i.e

$$\begin{aligned}
&\mathbb{E}\left(\Re\left(w_q^j[k-l]\right)\Im\left(w_q^i[k-v]\right)\right) = \mathbb{E}\left(\left\{\sum_{n=(k-l)\frac{M}{2}}^{(k-l)\frac{M}{2}+L-1}\Re\left(\bar{w}_j[n]\right)\Re\left(f_q\left[n-(k-l)\frac{M}{2}\right]\right)+\right.\right.\\
&\left.\Im\left(\bar{w}_j[n]\right)\Im\left(f_q\left[n-(k-l)\frac{M}{2}\right]\right)\right\}\left\{\sum_{t=(k-v)\frac{M}{2}}^{(k-v)\frac{M}{2}+L-1}-\Re\left(\bar{w}_i[t]\right)\Im\left(f_q\left[t-(k-v)\frac{M}{2}\right]\right)+\right.\\
&\left.\left.\Im\left(\bar{w}_i[t]\right)\Re\left(f_q\left[t-(k-v)\frac{M}{2}\right]\right)\right\}\right) =\\
&\sum_{n=\max((k-l),(k-v))\frac{M}{2}}^{\min((k-l),(k-v))\frac{M}{2}+L-1}-\frac{N_0}{2}\delta_{i,j}\Re\left(f_q\left[n-(k-l)\frac{M}{2}\right]\right)\Im\left(f_q\left[n-(k-v)\frac{M}{2}\right]\right)+\\
&\frac{N_0}{2}\delta_{i,j}\Im\left(f_q\left[n-(k-l)\frac{M}{2}\right]\right)\Re\left(f_q\left[n-(k-v)\frac{M}{2}\right]\right),
\end{aligned} \tag{3.57}$$

which is equivalent to

$$\begin{aligned}
\mathbb{E}\left(\Re\left(w_q^j[k-l]\right)\Im\left(w_q^i[k-v]\right)\right) = &\sum_{n=\max((k-l),(k-v))\frac{M}{2}}^{\min((k-l),(k-v))\frac{M}{2}+L-1}\frac{N_0}{2}\delta_{i,j}\Im\left(f_q\left[n-(k-l)\frac{M}{2}\right]\right.\\
&\left.\times f_q^*\left[n-(k-v)\tfrac{M}{2}\right]\right) = \tfrac{N_0}{2}\delta_{i,j}\Im\left(\alpha_{qq}[l-v]\right) = 0.
\end{aligned} \tag{3.58}$$

Following the same approach we get

$$\begin{aligned}
&\mathbb{E}\left(\Re\left(w_q^j[k-l]\right)\Re\left(w_q^i[k-v]\right)\right) = \mathbb{E}\left(\Im\left(w_q^j[k-l]\right)\Im\left(w_q^i[k-v]\right)\right) =\\
&\sum_{n=\max((k-l),(k-v))\frac{M}{2}}^{\min((k-l),(k-v))\frac{M}{2}+L-1}\frac{N_0}{2}\delta_{i,j}\Re\left(f_q\left[n-(k-l)\frac{M}{2}\right]\right)\Re\left(f_q\left[n-(k-v)\frac{M}{2}\right]\right)+\\
&\frac{N_0}{2}\delta_{i,j}\Im\left(f_q\left[n-(k-l)\frac{M}{2}\right]\right)\Im\left(f_q\left[n-(k-v)\frac{M}{2}\right]\right) =\\
&\sum_{n=\max((k-l),(k-v))\frac{M}{2}}^{\min((k-l),(k-v))\frac{M}{2}+L-1}\frac{N_0}{2}\delta_{i,j}\Re\left(f_q\left[n-(k-l)\frac{M}{2}\right]f_q^*\left[n-(k-v)\frac{M}{2}\right]\right) = \frac{N_0}{2}\delta_{i,j}\Re\left(\alpha_{qq}[l-v]\right).
\end{aligned} \tag{3.59}$$

Using the closed-form expressions (3.54) and (3.55), the authors in [100] show that the following equations

$$\mathbf{h}_q^T = \mathbf{a}_{q,e}^T \overline{\mathbf{G}}_{qq,e}^k \tag{3.60}$$

$$\lambda_q \bar{\mathbf{G}}_{qq,e}^k \left(\bar{\mathbf{G}}_{qq,e}^k\right)^T \mathbf{a}_{q,e} = \left(\sum_{m=q-1}^{q+1} \sum_{\tau=-L_a-L_{g_1}}^{L_a+L_{g_2}} \bar{\mathbf{g}}_{qm,e}^k[\tau] \left(\bar{\mathbf{g}}_{qm,e}^k[\tau]\right)^T - \bar{\mathbf{G}}_{qq,e}^k \left(\bar{\mathbf{G}}_{qq,e}^k\right)^T + \mathbf{R}_q \right) \mathbf{a}_{q,e}, \tag{3.61}$$

yield the optimal beamformer and DIR. Among the possible eigenvectors that solve (3.61), if we select the one associated with the minimum eigenvalue, then the SINR is maximized, [100]. Finally the eigenvector is properly scaled so that the constraint in (3.12) is satisfied.

3.B Demonstration that the IN term has zero mean

Under the assumption that symbols have zero mean, we can infer from (3.42) that $\mathbb{E}\{i_q[k]\} = 0$ if

$$\mathbb{E}\left\{\Re\left(\theta_q^*[k]\mathbf{a}_q^H\mathbf{w}_q[k]\right)\right\} = \sum_{\tau=-L_a}^{L_a} \Re\left(\theta_q^*[k]a_q^*[\tau]\right)\mathbb{E}\left\{\Re\left(w_q[k-\tau]\right)\right\} - \Im\left(\theta_q^*[k]a_q^*[\tau]\right)\mathbb{E}\left\{\Im\left(w_q[k-\tau]\right)\right\} \tag{3.62}$$

is equal to zero, which is satisfied if $\mathbb{E}\{\Re(w_q[k-\tau])\} = \mathbb{E}\{\Im(w_q[k-\tau])\} = 0$. To prove it we expand $\mathbb{E}\{\Re(w_q[k-\tau])\}$ and $\mathbb{E}\{\Im(w_q[k-\tau])\}$ as follows:

$$\begin{aligned}\mathbb{E}\left\{\Re\left(w_q[k-\tau]\right)\right\} = & \sum_{n=-L+1}^{0} \Re\left(f_q[-n]\right)\mathbb{E}\left\{\Re\left(\bar{w}\left[(k-\tau)\frac{M}{2}-n\right]\right)\right\} \\ & +\Im\left(f_q[-n]\right)\mathbb{E}\left\{\Im\left(\bar{w}\left[(k-\tau)\frac{M}{2}-n\right]\right)\right\}\end{aligned} \tag{3.63}$$

$$\begin{aligned}\mathbb{E}\left\{\Im\left(w_q[k-\tau]\right)\right\} = & \sum_{n=-L+1}^{0} \Re\left(f_q[-n]\right)\mathbb{E}\left\{\Im\left(\bar{w}\left[(k-\tau)\frac{M}{2}-n\right]\right)\right\} \\ & -\Im\left(f_q[-n]\right)\mathbb{E}\left\{\Re\left(\bar{w}\left[(k-\tau)\frac{M}{2}-n\right]\right)\right\}.\end{aligned} \tag{3.64}$$

Since $\bar{w}[n]$ is modeled as a complex circularly symmetric Gaussian variable with mean 0 and variance N_0, then $\mathbb{E}\{\Re(\bar{w}[n])\} = \mathbb{E}\{\Im(\bar{w}[n])\} = \mathbb{E}\{\Re(\bar{w}[n])\,\Im(\bar{w}[n])\} = 0$. From this definition it follows that (3.63) and (3.64) are zero. With that we conclude the proof that demonstrates that $\mathbb{E}\{i_q[k]\} = 0$.

Chapter 4

Precoding techniques in MISO PTP communications

The task of compensating the channel distortion is of paramount importance in the FBMC/OQAM context to restore the orthogonality. The previous chapter has delved into the receive processing techniques to equalize the channel. Exclusively focusing on MISO synchronous communication systems, this chapter concentrates on signal processing techniques at transmission. The techniques that will be presented in the following exploit the fact that CSI is available at the transmitter to reduce the complexity of the receiver.

4.1 System model

Consider a PTP communication system where the transmitter is equipped with N_T antennas and the receiver has a single antenna. The transmitter is able to take advantage of the spatial dimension since the CSI is available at the transmit side. Based on that, the symbol that is multiplexed on the mth subcarrier and is mapped onto the ith transmit antenna is given by $v_m^i[k] = b_{im}^*[k]*(\theta_m[k]d_m[k])$ for $1 \leq i \leq N_T$ and $m \in S_a$, where the set S_a contains the indices of the active data subcarriers. Note that the OQAM symbols are linearly precoded on a per-subcarrier basis with the multi-tap filters $\{b_{im}[k]\}$, which are different from zero for $-L_b \leq k \leq L_b$. Bearing in mind (2.17), the demodulated signal at the other end of the link is formulated as follows:

$$y_q[k] = \sum_{i=1}^{N_T} \sum_{m=q-1}^{q+1} b_{im}^*[k] * (\theta_m[k]d_m[k]) * g_{qm}^{i1}[k] + w_q[k], \tag{4.1}$$

for $q \in S_a$. To get more tractable expressions, (4.1) is compactly formulated in this way

$$y_q[k] = \sum_{m=q-1}^{q+1} \sum_{\tau=-L_b-L_{g_1}}^{L_b+L_{g_2}} \mathbf{b}_m^H \mathbf{g}_{qm}[\tau]\theta_m[k-\tau]d_m[k-\tau] + w_q[k] \tag{4.2}$$

$$\mathbf{b}_q = \left[\mathbf{b}_{1q}^T \dots \mathbf{b}_{qN_T}^T\right]^T \tag{4.3}$$

$$\mathbf{g}_{qm}[\tau] = \left[\left(\mathbf{g}_{qm}^{11}[\tau]\right)^T \dots \left(\mathbf{g}_{qm}^{N_T 1}[\tau]\right)^T\right]^T, \tag{4.4}$$

where $\mathbf{b}_{iq} = [b_{iq}[-L_b] \dots b_{iq}[L_b]]^T$ and $\mathbf{g}_{qm}^{i1}[\tau] = \left[g_{qm}^{i1}[\tau + L_b] \dots g_{qm}^{i1}[\tau - L_b]\right]^T$. In contrast to (3.8), the linear filtering aimed at equalizing the channel in (4.2) has no influence on the noise. Without loss of generality, precoders can be expressed as function of unit norm vectors. In other words, precoders can be factorized as $\mathbf{b}_q = \sqrt{p_q}\mathbf{u}_q$, where p_q is the power loaded on the qth subcarrier and the vector $\mathbf{u}_q \in \mathbb{C}^{(2L_b+1)N_T \times 1}$ is such that $\|\mathbf{u}_q\|_2^2 = 1$. With the objective of improving the link reliability with a reduced complexity, the demodulated signals are processed with a single-tap equalizer that is real-valued. Then, the symbol estimates to be fed into the detector are obtained by compensating the phase term and extracting the real part, i.e.

$$\begin{aligned}
\check{d}_q[k] &= \Re\left(\theta_q^*[k]a_q y_q[k]\right) = a_q \Re\left(\theta_q^*[k] y_q[k]\right) \\
&= \sum_{m=q-1}^{q+1} \sum_{\tau=-L_b-L_{g_1}}^{L_b+L_{g_2}} a_q \Re\left(\mathbf{b}_m^H \bar{\mathbf{g}}_{qm}^k[\tau]\right) d_m[k-\tau] + a_q \Re\left(\theta_q^*[k] w_q[k]\right) \\
&= a_q \Re\left(\mathbf{b}_q^H \mathbf{g}_{qq}[0]\right) d_q[k] + \sum_{(m,\tau)\neq(q,0)} a_q \Re\left(\mathbf{b}_m^H \bar{\mathbf{g}}_{qm}^k[\tau]\right) d_m[k-\tau] + a_q \Re\left(\theta_q^*[k] w_q[k]\right) \\
&= a_q \Re\left(\mathbf{b}_q^H \mathbf{g}_{qq}[0]\right) d_q[k] + i_q[k], \quad q \in S_a,
\end{aligned} \tag{4.5}$$

where

$$\bar{\mathbf{g}}_{qm}^k[\tau] = \theta_q^*[k]\theta_m[k-\tau]\mathbf{g}_{qm}[\tau] \tag{4.6}$$

and a_q is the coefficient responsible for performing the receive processing on the qth subcarrier. Let $i_q[k]$ denote the interference plus noise term. If we stack real and imaginary parts column-wise the expression that models the global communication system can be formulated in a matrix way. To this end, given the vector $\mathbf{b}_q$ we define this extended notation $\mathbf{b}_{q,e} = \left[\Re\left(\mathbf{b}_q^T\right) \quad \Im\left(\mathbf{b}_q^T\right)\right]^T$. Then (4.5) can be expressed as function of the new vectors as follows:

$$\check{d}_q[k] = a_q \mathbf{b}_{q,e}^T \mathbf{g}_{qq,e}[0] d_q[k] + \sum_{(m,\tau)\neq(q,0)} a_q \mathbf{b}_{m,e}^T \bar{\mathbf{g}}_{qm,e}^k[\tau] d_m[k-\tau] + a_q \Re\left(\theta_q^*[k] w_q[k]\right). \tag{4.7}$$

Splitting (4.7) into the desired and the undesired part will pave the way to formulate the SINR, the signal to leakage plus noise ratio (SLNR) and the MSE. Note that the real-valued representation in (4.7) highlights that precoders perform a widely linear processing since real and imaginary parts are independently processed.

In the whole chapter symbols are assumed to be independent, i.e. $\mathbb{E}\{d_m[k]d_q[n]\} = \delta_{m,q}\delta_{k,n}$ and noise samples follow this distribution $\bar{w}[n] \in \mathcal{CN} \sim (0, N_0)$.

4.2 Precoding with fixed power distribution

In view of (4.5), the problem of designing $\{\mathbf{b}_q, a_q\}$ is definitely challenging due to ICI and ISI terms. By starting, we tackle the design of the transmitter and the receiver having fixed the power distribution. This translates into constraining the maximum allowable power that is allocated on each subcarrier according to a pre-established criterion. When individual power constraints are replaced by a single constraint that accounts for the average transmit power, the system performance can be increased. Nevertheless, when the power coefficients are involved in the optimization procedure, the complexity substantially increases because subcarriers cannot be treated independently. With the emphasis on finding low-complexity solution, the techniques presented in the following refrain from optimizing the power distribution.

4.2.1 ZF transmitter

The first option to devise the transmit processing consists in equalizing the channel frequency response at a given target points. That is, the precoder $b_{iq}[k]$ is designed to equalize $h_{i1}[n]$ in the pass band region of the qth subchannel, i.e. $\left[\frac{2\pi}{M}(q-1) \quad \frac{2\pi}{M}(q+1)\right]$. Following the frequency sampling approach described in [69], the frequency response of $b_{iq}[k]$ is aimed at compensating the channel at these radial frequencies $\left\{\frac{2\pi}{M}(q-1) + \frac{2\pi}{M(L_b+1)}(l+1)\right\}$ for $l = 0, ..., 2L_b$. From (2.18), we can infer that the frequency response of $g_{qm}^{i1}[k]$ is equal to

$$G_{qm}^{i1}\left(e^{jw}\right) = \frac{2}{M} e^{j\frac{2\pi}{M}(q-m)\left(\frac{L-1}{2}\right)} P\left(e^{j\left(\frac{w}{M/2} - \frac{2\pi}{M}m + \frac{2\pi}{M/2}\frac{q}{2}\right)}\right) P\left(e^{j\frac{w}{M/2}}\right) H_{i1}\left(e^{j\left(\frac{w}{M/2} + \frac{2\pi}{M/2}\frac{q}{2}\right)}\right), \quad (4.8)$$

for $w \in (-\pi, \pi)$ when q is even. The term $P(e^{jw})$ denotes the frequency response of the prototype pulse. For the q odd case, the frequency response in this range $w \in (0, 2\pi)$ is

$$G_{qm}^{i1}\left(e^{jw}\right) = \frac{2}{M} e^{j\frac{2\pi}{M}(q-m)\left(\frac{L-1}{2}\right)} P\left(e^{j\left(\frac{w}{M/2} + \frac{2\pi}{M}(q-1-m)\right)}\right) P\left(e^{j\left(\frac{w}{M/2} - \frac{2\pi}{M}\right)}\right) H_{i1}\left(e^{j\left(\frac{w}{M/2} + \frac{2\pi}{M}(q-1)\right)}\right). \quad (4.9)$$

Hence, under the zero forcing criterion the frequency response of $b_{iq}[k]$ at the radial frequency 0 should be proportional to $H_{i1}\left(e^{j\frac{2\pi}{M}q}\right)^{-1}$ for the q even case. In the q odd case, the target point $H_{i1}\left(e^{j\frac{2\pi}{M}q}\right)^{-1}$ should be met when the radial frequency is π. In order to ensure that the power allocated to the qth subband is p_q, we can use this definition $\mathbf{b}_{iq} = \sqrt{p_q}\frac{\bar{\mathbf{u}}_{iq}^*}{\sqrt{N_T}\|\bar{\mathbf{u}}_{iq}\|_2}$. Then, the vector $\bar{\mathbf{u}}_{iq} \in \mathbb{C}^{(1+2L_b)\times 1}$, is designed after solving this system of equations

$$\bar{\mathbf{u}}_{iq} = \mathbf{C}_q^{-1}\mathbf{t}_{iq} \tag{4.10}$$

with

$$\mathbf{t}_{iq} = \left[H_{i1}\left(e^{j\left(\frac{2\pi}{M}(q-1)+\frac{2\pi}{M(L_b+1)}\right)}\right)^{-1}\cdots H_{i1}\left(e^{j\left(\frac{2\pi}{M}(q-1)+\frac{2\pi(1+2L_b)}{M(L_b+1)}\right)}\right)^{-1}\right]^T. \tag{4.11}$$

For q even, the (ith,lth) entry of matrix $\mathbf{C}_q$ is given by $[\mathbf{C}_q]_{il} = e^{-j\left(\frac{\pi}{L_b+1}(i+1)-\pi\right)(l-L_b)}$, for $i, l = 0, ..., 2L_b$. In the q odd case, the (ith,lth) position takes the value $[\mathbf{C}_q]_{il} = e^{-j\frac{\pi}{L_b+1}(i+1)(l-L_b)}$.

As for the receive processing, the equalizers are designed as $a_q = \frac{1}{\Re\left(\mathbf{b}_q^H\mathbf{g}_{qq}[0]\right)}$ with the aim of scaling the symbols after the real part is extracted.

Note that once the precoder on the qth subband is properly scaled, the power p_q is equally split among the antennas. However, it seems that there could be another way to scale the transmit filters that lead to better results. In this sense, we propose a technique that splits the power for the 2-antenna case. Now precoders are given by $\mathbf{b}_{iq} = \sqrt{p_{iq}}\frac{\bar{\mathbf{u}}_{iq}^*}{\|\bar{\mathbf{u}}_{iq}\|_2}$, where $\sum_{i=1}^{N_T} p_{iq} = p_q$. The optimization procedure is based on distributing the power so that the SNR of (4.5) is maximized. The SNR on the qth subcarrier is written in this form

$$SNR_q = \frac{\mathbb{E}\left\{\left|\Re\left(\mathbf{b}_q^H\mathbf{g}_{qq}[0]\right)d_q[k]\right|^2\right\}}{\mathbb{E}\left\{\left|\Re\left(\theta_q^*[k]w_q[k]\right)\right|^2\right\}} = \frac{\left|\sum_{i=1}^{2}\Re\left(\mathbf{b}_{iq}^H\mathbf{g}_{qq}^{i1}[0]\right)\right|^2}{N_0 0.5} = \frac{\left|\sum_{i=1}^{2}\sqrt{p_{iq}}h_{iq}\right|^2}{N_0 0.5}, \tag{4.12}$$

where $h_{iq} = \Re\left(\frac{\bar{\mathbf{u}}_{iq}^T}{\|\bar{\mathbf{u}}_{iq}\|_2}\mathbf{g}_{qq}^{i1}[0]\right)$. The variance of the noise can be derived from the analysis conducted in Appendix 3.A. Then, the power distribution that maximizes the SNR is computed by solving

$$\begin{aligned} &\alpha_q^{opt} = \max_{\alpha_q}\left|\sqrt{\alpha_q}h_{1q} + \sqrt{p_q-\alpha_q}h_{2q}\right|^2 \\ &s.t.\ \ 0 \le \alpha_q \le p_q. \end{aligned} \tag{4.13}$$

Finally we set $p_{1q} = \alpha_q^{opt}$ and $p_{2q} = p_q - \alpha_q^{opt}$. The details to solve (4.13) are provided in

Appendix 4.A. From this point on, we will refer to the ZF precoder that does not balance the power assigned to each antenna as weighted ZF (WZF).

4.2.2 SLNR-based precoding

The transmit beamforming based on the SLNR aims at providing the optimal signal confinement by mitigating the signal that leaks to unintended subcarriers and time slots. The performance metric is given by

$$SLNR_q = \frac{a_q^2 \left|\mathbf{b}_{q,e}^T \mathbf{g}_{qq,e}[0]\right|^2}{\sum\limits_{\substack{m=q-1 \\ m\neq q}}^{q+1} \sum\limits_{\tau=-L_b-L_{g_1}}^{L_b+L_{g_2}} a_m^2 \left|\mathbf{b}_{q,e}^T \bar{\mathbf{g}}_{mq,e}^k[\tau]\right|^2 + \sum\limits_{\substack{\tau=-L_b-L_{g_1} \\ \tau\neq 0}}^{L_b+L_{g_2}} a_q^2 \left|\mathbf{b}_{q,e}^T \bar{\mathbf{g}}_{qq,e}^k[\tau]\right|^2 + a_q^2 0.5N_0}. \tag{4.14}$$

To simplify the processing we have assumed that the magnitude of the equalizers is in the same order in at least three consecutive subcarriers, i.e. $|a_{q-1}| \approx |a_q| \approx |a_{q+1}|$. This supposition allows us to decouple the design of the transmit and the receive processing. This means that in the first step the transmit beamforming is computed as follows:

$$\begin{aligned} &\underset{\{\mathbf{b}_q\}}{\operatorname{argmax}} \frac{\left|\mathbf{b}_{q,e}^T \mathbf{g}_{qq,e}[0]\right|^2}{\sum\limits_{\substack{m=q-1 \\ m\neq q}}^{q+1} \sum\limits_{\tau=-L_b-L_{g_1}}^{L_b+L_{g_2}} \left|\mathbf{b}_{q,e}^T \bar{\mathbf{g}}_{mq,e}^k[\tau]\right|^2 + \sum\limits_{\substack{\tau=-L_b-L_{g_1} \\ \tau\neq 0}}^{L_b+L_{g_2}} \left|\mathbf{b}_{q,e}^T \bar{\mathbf{g}}_{qq,e}^k[\tau]\right|^2 + 0.5N_0 \frac{\|\mathbf{b}_{q,e}\|_2^2}{p_q}} \\ &s.t. \quad \|\mathbf{b}_{q,e}\|_2^2 = p_q, \quad q \in S_a. \end{aligned} \tag{4.15}$$

The solution of (4.15) can be expressed as $\mathbf{b}_{q,e} = \sqrt{p_q}\frac{\mathbf{u}_q}{\|\mathbf{u}_q\|_2}$ [101], where

$$\begin{aligned} \mathbf{u}_q = \Bigg(&\sum_{\substack{m=q-1 \\ m\neq q}}^{q+1} \sum_{\tau=-L_b-L_{g_1}}^{L_b+L_{g_2}} \bar{\mathbf{g}}_{mq,e}^k[\tau] \left(\bar{\mathbf{g}}_{mq,e}^k[\tau]\right)^T + \\ &\sum_{\substack{\tau=-L_b-L_{g_1} \\ \tau\neq 0}}^{L_b+L_{g_2}} \bar{\mathbf{g}}_{qq,e}^k[\tau] \left(\bar{\mathbf{g}}_{qq,e}^k[\tau]\right)^T + \frac{0.5N_0}{p_q}\mathbf{I}_{(2L_b+1)2N_T} \Bigg)^{-1} \mathbf{g}_{qq,e}[0]. \end{aligned} \tag{4.16}$$

Recalling the definition of (2.2), it follows that the entries of this matrix $\bar{\mathbf{g}}_{qq,e}^k[\tau]\left(\bar{\mathbf{g}}_{qq,e}^k[\tau]\right)^T$ do not depend on k. Therefore, the same processing can be applied for k even and k odd. Finally, the

receive processing is designed just to properly scale the symbol. As a consequence, $a_q = \frac{1}{\Re\left(\mathbf{b}_q^H \mathbf{g}_{qq}[0]\right)}$.

4.2.3 MDIR transmitter

Unlike previous designs, the optimization procedure followed in this section jointly designs the transmit and the receive processing. In particular, the criterion employed is based on the minimization of the sum mean square error (MSE). The problem is posed as follows:

$$\begin{aligned} &\underset{\{\mathbf{b}_q, h_q\}}{\operatorname{argmin}} \sum_{q \in S_a} \mathbb{E}\left\{ \left| \Re\left(\theta_q^*[k] y_q[k]\right) - h_q d_q[k] \right|^2 \right\} \\ &s.t. \quad \|\mathbf{b}_q\|_2^2 = p_q, \quad q \in S_a. \end{aligned} \tag{4.17}$$

The problem (4.17) yields a DIR , which is given by h_q, matched to the precoder and the channel. Because of this, the technique described in this section is called MDIR. To comply with the unified notation in (4.5), the equalizer is related with the DIR in this form $a_q = \frac{1}{h_q}$. The details to solve (4.17) are provided in Appendix 4.B.

4.2.4 MMSE transmitter

Similarly to previous section, the approach followed hereinafter to design the transmit and the receive processing is based on the minimization of the sum MSE subject to individual power constraints. However, the problem has been slightly modified as follows:

$$\begin{aligned} &\underset{\{\mathbf{b}_q, a_q\}}{\operatorname{argmin}} \sum_{q \in S_a} \mathbb{E}\left\{ \left| \Re\left(\theta_q^*[k] a_q y_q[k]\right) - d_q[k] \right|^2 \right\} \\ &s.t. \quad \|\mathbf{b}_q\|_2^2 = p_q, \quad q \in S_a. \end{aligned} \tag{4.18}$$

The details to solve (4.18) are provided in Appendix 4.C.

4.2.5 Simulation results

This section evaluates the precoding schemes discussed throughout Section 4.2 in terms of BER against the energy bit to noise ratio ($\frac{E_b}{N_0}$). The transmitter is equipped with 2 antennas, yielding a MISO 1×2 communication system. The system parameters are selected according to the values of Table 2.3 to simulate scenarios 1 and 3. The transmitted streams are generated by staggering in-phase and quadrature components of 16-QAM symbols. As for the power allocation, each subcarrier has been assigned the same power, i.e. $p_q = 1$. It must be mentioned that we have favoured the uniform power allocation (UPA) due to its simplicity, although alternative strategies can be easily applied.

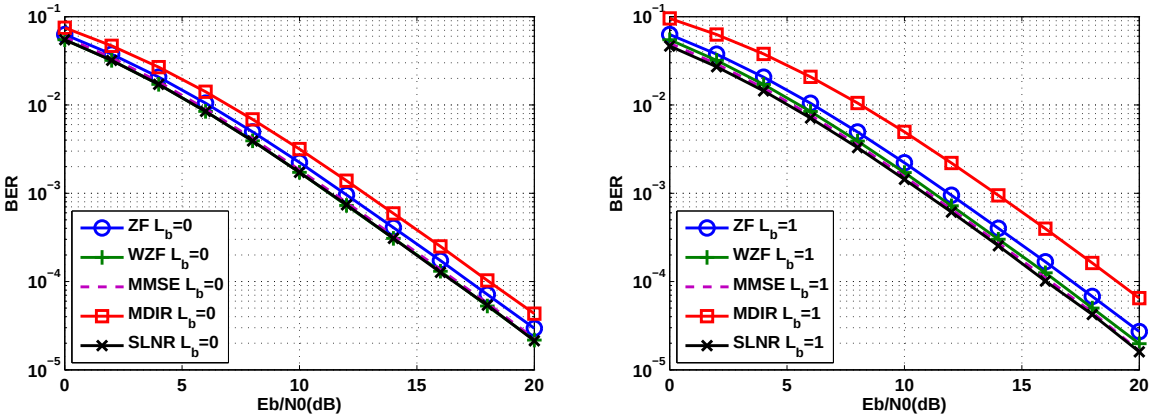

(a) Single-tap precoding.

(b) Three-tap precoding.

Figure 4.1: BER against $\frac{E_b}{N_0}$. The simulated systems correspond to FBMC/OQAM with different precoding schemes. System parameters are set according to Scenario 1 (see Table 2.3).

Figure 4.1 shows that in Scenario 1 the WZF, the MMSE and the SLNR techniques practically achieve the same BER. Moreover, multi-tap precoding brings very little improvement, which confirms that transmit processing techniques based on single-tap precoding suffices to combat multipath fading in Scenario 1. The WZF transmitter does not balance the power among antennas, which is useful to outperform the ZF transmitter. The improvement is around 1 dB. Note that the MDIR transmitter gives the worst performance. By scrutinizing the way MDIR transmitter is designed, it becomes evident that precoding vectors have the objective of mitigating the leakage as much as possible without including $\mathbf{g}_{qq}[0]$ in the equation design. As a result, precoders are not matched with the channel seen by the symbol to be detected. This offers a plausible explanation for the degradation. It is also interesting to remark that single-tap precoding provides better results than the 3-tap alternative when the MDIR is considered. From Section 4.2.3 we know that multi-tap precoding exhibits better interference mitigation capabilities when compared to the single-tap solution. Therefore, the results suggest that the price that has to be paid in exchange of further mitigating the leakage is a reduction of the magnitude of the desired signal. In conclusion, the reduced leakage yielded by the 3-tap precoder does not compensate the degradation that it causes on the desired signal.

When Scenario 3 is simulated, the techniques behave in a different way as Figure 4.2 highlights. Now, multi-tap precoding makes a difference and it provides the lowest BER. This indicates that the channel frequency response is not flat anymore at the subcarrier level. Unlike Figure 4.1, the ZF and WZF techniques exhibit an error floor. Therefore, the ZF criterion does not succeed in effectively removing interference. In this sense, the MDIR transmitter, which aims at mitigating

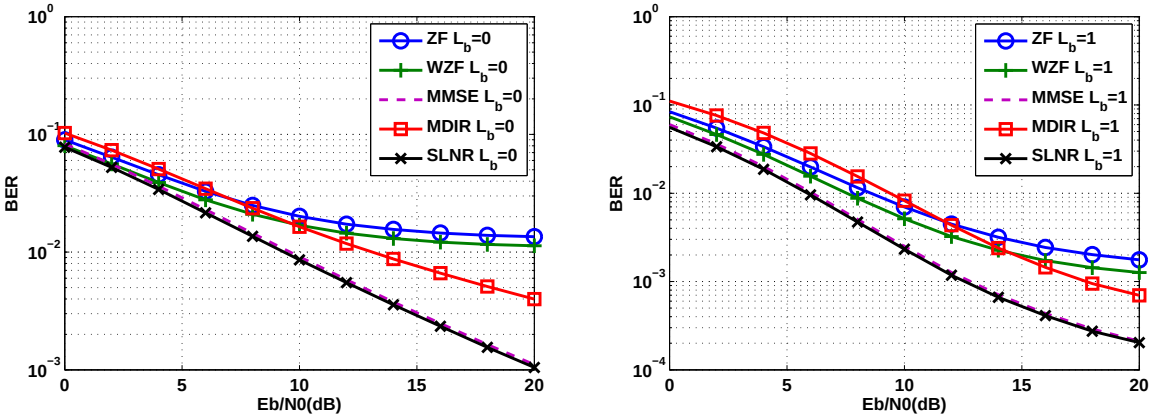

(a) Single-tap precoding.

(b) Three-tap precoding.

Figure 4.2: BER against $\frac{E_b}{N_0}$. The simulated systems correspond to FBMC/OQAM with different precoding schemes. System parameters are set according to Scenario 3 (see Table 2.3).

the leakage, is able to provide an increased robustness at high $\frac{E_b}{N_0}$ where the interference dominates over the noise. Note that in Scenario 3, the MDIR transmitter based on multi-tap filtering offers a better trade-off between leakage mitigation and signal weighting than the single-tap configuration. However, the MMSE and the SLNR techniques use the taps in a more efficient manner than the MDIR scheme and still achieve the lowest BER.

As a benchmark the OFDM technique is simulated in a MISO 1×2 communication system. The transmit processing is based on implementing the transmit Wiener filter on a per-subcarrier basis [102]. The power is equally split among subcarriers. Under the propagation conditions described in Scenario 1, both configurations with CP=$\frac{M}{8}$ and CP=$\frac{M}{4}$ absorb the most delayed echo. Therefore, the ideal choice is to set CP=$\frac{M}{8}$ so that the reduced energy wastage translates into a lower BER. After comparing Figure 4.1 and Figure 4.3a, we can assert that FBMC/OQAM is able to provide the same BER than OFDM when the propagation conditions are modeled as Scenario 1 specifies. In Scenario 3, neither configuration is able to avoid IBI in the OFDM context. As a consequence, demodulated signals are not free of interference, which lead the BER plots to saturate. In this case the largest CP brings substantial improvement. When orthogonality is not restored, the leakage is higher in OFDM than it is in FBMC/OQAM systems. Hence, as Figure 4.3b and Figure 4.2 highlight, the FBMC/OQAM modulation is more resilience than the OFDM technique in highly frequency selective channels.

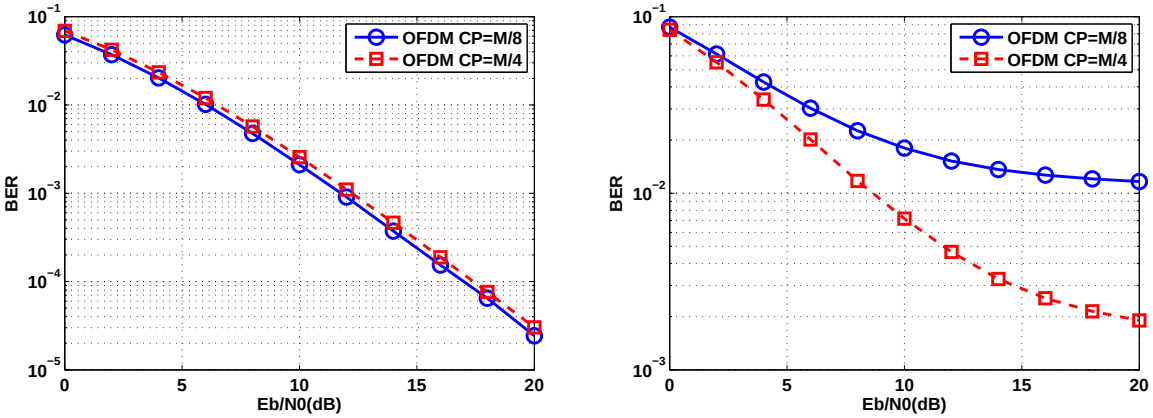

(a) Scenario 1.

(b) Scenario 3.

Figure 4.3: BER against $\frac{E_b}{N_0}$. The simulated systems correspond to OFDM. System parameters are set according to Scenario 1 and 3 (see Table 2.3).

4.3 Precoding with power allocation

In this section the emphasis is not on the complexity but on the performance. For this reason, power allocation is also involved in the optimization of the performance metric. When the power distribution is not fixed, the feasibility set is extended, which should result in performance gains. To validate this idea, we first jointly design precoders and power coefficients to minimize the transmit power given QoS constraints. Secondly, given the precoders, only the power allocation will be optimized.

4.3.1 Optimal precoding

Under the criterion of minimizing the total transmit power while assuring that the received samples attain the QoS requirements, the optimization problem to derive the transmit processing is as follows:

$$\begin{aligned} \text{QP}: \quad & \underset{\{\mathbf{u}_q, p_q\}}{\text{argmin}} \sum_{q \in S_a} p_q \\ & s.t. \;\; SINR_q \geq \alpha_q, \quad \|u_q\|_2^2 = 1, \quad p_q \geq 0, \quad q \in S_a, \end{aligned} \tag{4.19}$$

with

$$SINR_q = \frac{p_q \left|\mathbf{u}_q^T \bar{\mathbf{g}}_{qq,e}^k[0]\right|^2}{\sum\limits_{\substack{m=q-1 \\ m\neq q}}^{q+1} \sum\limits_{\tau=-L_b-L_{g_1}}^{L_b+L_{g_2}} p_m \left|\mathbf{u}_m^T \bar{\mathbf{g}}_{qm,e}^k[\tau]\right|^2 + \sum\limits_{\substack{\tau=-L_b-L_{g_1} \\ \tau\neq 0}}^{L_b+L_{g_2}} p_q \left|\mathbf{u}_q^T \bar{\mathbf{g}}_{qq,e}^k[\tau]\right|^2 + 0.5N_0}. \tag{4.20}$$

The SINR function is independent of the variable k. Hence, the optimal power distribution and beamforming design can be applied regardless of if k is even or k is odd. Resorting to the dual optimization framework, we can solve the problem QP. The details are provided in Appendix 4.D.

4.3.2 Suboptimal precoding

The processing devised in Section 4.3.1 jointly optimizes $\{p_q\}$ and $\{\mathbf{u}_q\}$. Aiming at reducing the complexity, the current section addresses the optimal power allocation strategy among subcarriers for fixed $\{\mathbf{u}_q\}$, thus $\{p_q\}$ and $\{\mathbf{u}_q\}$ are independently devised. In this regard, the first step consists in designing the unit norm vectors. Next, the power coefficients are computed by solving

$$\begin{aligned} \text{QP}: \quad & \underset{\{p_q\}}{\operatorname{argmin}} \sum_{q\in S_a} p_q \\ & s.t. \;\; SINR_q \geq \alpha_q, \;\; p_q \geq 0, \;\; q \in S_a. \end{aligned} \tag{4.21}$$

The optimal power coefficients are computed by solving $(\mathbf{I}_{M_a} - \mathbf{D}\Psi)\,\mathbf{p} = \mathbf{D}\mathbf{n}$ using the definitions in (4.44),(4.45),(4.46) and (4.47). When the optimal precoding is designed the unfeasibility can be detected when problem (4.42) is being solved. In the suboptimal case the set of SINRs is feasible if only if the spectral radius of the matrix $\mathbf{D}\Psi$ is strict lower than 1, [103].

4.3.3 Simulation results

In order to validate the performance of the techniques devised in Sections 4.3.1 and 4.3.2, simulation-based results are provided in the following. In particular, we plot in Figure 4.4 the amount of power that is required to attain the target SINR. Note that the average transmitted power, i.e. $\sum_{q\in S_a} p_q$, is represented in a logarithmic scale and is evaluated versus the inverse of the normalized noise power, which is given by $\frac{N_0}{1mW}$. The optimal precoding scheme, which is obtained after solving problem (4.19), is confronted with the suboptimal technique described in Section 4.3.2. In this regard, when solving problem (4.21) precoders are given beforehand according to the ZF technique, which is devised in Section 4.2.1. The reason why we have discarded other precoding schemes is provided hereinafter. Regarding the key features of the system we consider a MISO 1×2 system. The rest of the parameters are selected according to Table 2.3 to simulate Scenario 1.

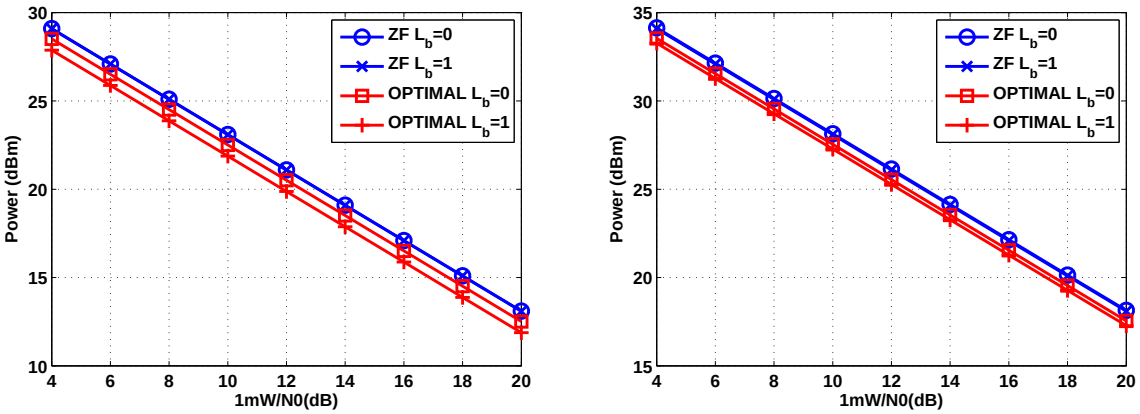

(a) SINR=10 dB.

(b) SINR=15 dB.

Figure 4.4: Average power against the inverse of the normalized noise power. The simulated systems correspond to FBMC/OQAM with different precoding schemes. The target SINR is set to 10 dB and 15 dB. System parameters are set according to Scenario 1 (see Table 2.3).

Regarding optimal and suboptimal schemes, we consider that the same quality of service constraints apply to all active subcarrriers. In Figure 4.4a the SINR is set to 10 dB whereas in Figure 4.4b the SINR has to be at least 15 dB. It must be mentioned that with these constraints we have encountered several cases of unfeasibility for $\frac{1mW}{N_0} < 10^{0.4}$. For this reason, we have refrained from evaluating the results in this region. In Scenario 3, problems (4.19) and (4.21) turn sometimes to be infeasible even at low noise regime. It can be readily checked that in the absence of interference the QoS constraints are always met. Hence, the responsible of the infeasibility is the ISI and the ICI. In Scenario 3 the channel frequency selectivity is especially severe. Because of that, precoders fail to restore the orthogonality. Then, the interference becomes non-negligible, which may explain why the QoS cannot be always attained in Scenario 3. This has been the main argument to only focus on simulating Scenario 1.

The suboptimal scheme based on the ZF precoder needs to transmit the same amount of power to meet the constraints regardless of the number of taps. This is observed in Figure 4.4a and Figure 4.4b. By contrast, the optimal solution does benefit from multi-tap filtering. By setting the number of taps to 3, which is equivalent to set $L_b = 1$, we can save up to 1 dBm when compared to the suboptimal schemes based on the ZF precoding scheme. Obviously, the more demanding are the QoS constraints, the higher is the transmitted power. As a result, it can be concluded that the strategy of jointly optimizing the power distribution and the precoding vectors yields better results than independently designing each parameter.

As it has been pointed out at the beginning of this section, the suboptimal scheme is only

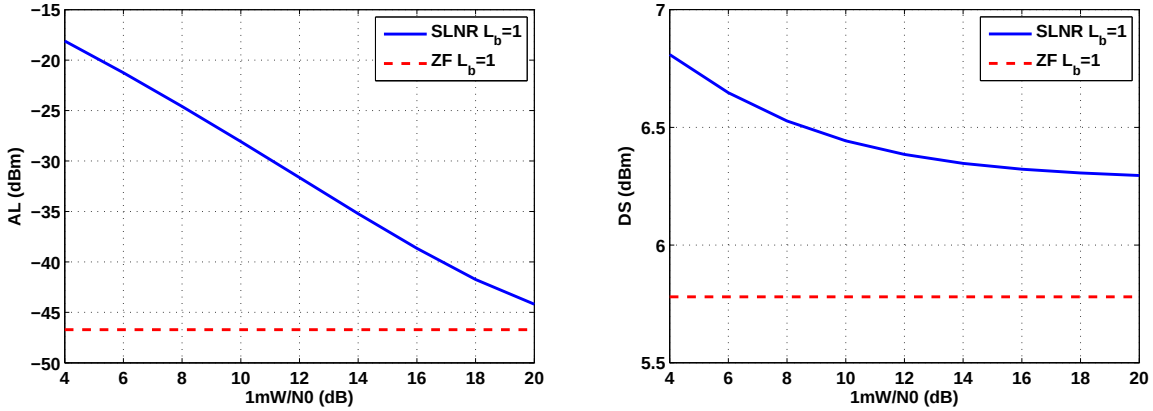

(a) Leakage. (b) Desired signal.

Figure 4.5: Average leakage and desired signal energy against the inverse of the normalized noise power. The simulated systems correspond to FBMC/OQAM with different precoding schemes. System parameters are set according to Scenario 1 (see Table 2.3).

combined with the ZF precoding scheme. The results of Figure 4.1 suggest that the use of the SLNR technique may also come in useful to reduce the transmit power. Unfortunately, the problem (4.21) is infeasible for some channel realizations when the precoding scheme is based on the approach described in Section 4.2.2. The infeasibility has been observed for $\frac{1mW}{N_0} \geq 10^{0.4}$. This seems to contradict the results depicted in Figure 4.1 where the ZF and the SLNR nearly achieve the same performance. Since the infeasibility is related with the magnitude of the interference, one plausible explanation would be that the SLNR technique does not mitigate enough ISI and ICI terms. To corroborate this impression, we compute the leakage that both the ZF and the SLNR inflict on surrounding positions along the time-frequency grid. In particular, the performance metric is the average leakage that is given by

$$AL = \frac{1}{M_a} \sum_{q \in S_a} \sum_{\substack{\tau=-L_b-L_{g_1} \\ \tau \neq 0}}^{L_b+L_{g_2}} \left\| a_q \mathbf{b}_{q,e}^T \bar{\mathbf{g}}_{qq,e}^k[\tau] \right\|_2^2 + \frac{1}{M_a} \sum_{q \in S_a} \sum_{\substack{m=q-1 \\ m \neq q}}^{q+1} \sum_{\tau=-L_b-L_{g_1}}^{L_b+L_{g_2}} \left\| a_m \mathbf{b}_{q,e}^T \bar{\mathbf{g}}_{mq,e}^k[\tau] \right\|_2^2 . \tag{4.22}$$

In addition we have represented the average energy of the desired signal, i.e.

$$DS = \frac{1}{M_a} \sum_{q \in S_a} \left\| a_q \mathbf{b}_{q,e}^T \mathbf{g}_{qq,e}[0] \right\|_2^2 . \tag{4.23}$$

As Figure 4.5 shows, the leakage is constant in the ZF case because the noise is not involved in

the design. On the contrary, the power spectral density of the noise plays a key role in the design of the SLNR technique. When the noise dominates over the interference, the transmit processing coincides with the matched filter. Thus, when the interference is several orders of magnitude below the noise, the degrees of freedom provided by the spatial dimension are used to maximize the magnitude of the desired signal. This way of performing has been proven to yield the lowest BER when the power allocation is fixed. However, the residual interference is sometimes too high, mostly at high noise regime, leading problem (4.21) to be unsolvable.

4.4 Chapter summary

Building upon the FBMC/OQAM scheme this chapter addresses the design of linear precoders to cope with the interference that is induced by the channel. The beauty of processing symbols at the transmit side is that the noise is not enhanced. It is well-known that in PTP communications the channel destroys the perfect reconstruction property exhibited by FBMC/OQAM systems and, therefore, the signals transmitted in the neighbourhood around the position of interest along the time-frequency grid contribute to the interference generation. Since the transmitter may be equipped with multiple antennas giving rise to a MISO architecture, the objective is to design transmit signal processing techniques that take advantage of the spatial dimension to mitigate the leakage while desired symbols are received with the highest energy possible. By starting, the distribution of power among subcarriers and the beamforming design are decoupled. That is, given the power coefficients, linear precoders are optimized with the condition that the transmitted power on each subcarrier complies with the predefined power allocation strategy. Among the possible criteria to design the transmit processing we have considered the SLNR maximization, the sum MSE minimization and the ZF approach. The BER vs. $\frac{E_b}{N_0}$ curves show that precoders driven by the optimization of the sum MSE and the SLNR provide the best trade-off between leakage mitigation and desired symbol enhancement. As a result, these two techniques give the lowest BER. In low frequency selective channels, the performance given by these two techniques coincides with the BER achieved by OFDM when the transmit Wiener filter is applied. It must be mentioned that in highly frequency selective channels FBMC/OQAM outperforms OFDM as long as linear precoders perform a multi-tap linear filtering.

The second part of this chapter is devoted to investigate the joint optimization of precoders and power coefficients. The idea of weighting subcarrier signals according to channel conditions is to overcome the spectral nulls. The criterion that has been followed to design the precoders consists in minimizing the transmit power while the QoS constraints are satisfied. In this sense, it has been demonstrated that the theory developed for the multiuser downlink beamforming problem can also be used when devising the transmit processing in the FBMC/OQAM context. It is worth

emphasizing that QoS constraints may not be met if they are too stringent. Several cases of unfeasibility have been observed in scenarios where the channel frequency response is not flat at the subcarrier level. By contrast, if the channel frequency selectivity is not appreciable in the pass band region of a single subchannel, then the problem can be solved if the power of the noise is sufficiently low. The system performance degradation for independently designing precoders and power coefficients is around 1 dB. In this case unfeasibility is prevented only if precoders are able to effectively mitigate the leakage. Among the techniques described in the first part of this chapter, the ZF transmitter has been proven to be best choice since it provides the highest leakage attenuation.

Appendices

4.A Solution of problem 4.13

The objective function of problem (4.13) has a critical point in the feasible domain. Setting the gradient to zero yields

$$\bar{\alpha}_q = \frac{p_q}{2}\left(1 - \text{sign}\left(\frac{h_{1q}h_{2q}}{(h_{1q})^2 - (h_{2q})^2}\right)\sqrt{\left(\frac{\left((h_{1q})^2 - (h_{2q})^2\right)^2}{4\,(h_{1q}h_{2q})^2 + \left((h_{1q})^2 - (h_{2q})^2\right)^2}\right)}\right). \tag{4.24}$$

Note that second derivative of the cost function must be taken to determine whether $\bar{\alpha}_q$ is a maximum or a minimum. If the second derivative is negative, the optimal point is given by (4.24). Otherwise, the optimal strategy consists in selecting one of the extreme values. Based on this and for the sake of complexity we will weigh the two antennas using one of the following values $\alpha_q^{opt} \in \{0, \bar{\alpha}_q, p_q\}$. Among the three cases we will select the one that maximizes the SNR. It must be mentioned that the expression formulated in (4.24) is only valid if $h_{1q} \neq h_{2q}$. Provided that $h_{1q} = h_{2q}$, then the optimal strategy is to balance the power, i.e. $\alpha_q^{opt} = p_q/2$.

4.B Solution of problem 4.17

Borrowing the extended notation from (4.7), the MSE between the analysis filter bank output and the desired symbol is given by

$$MSE_q = \mathbb{E}\left\{\left|\Re\left(\theta_q^*[k]y_q[k]\right) - h_q d_q[k]\right|^2\right\} = |h_q|^2 + \frac{N_0}{2} + \sum_{m=q-1}^{q+1}\sum_{\tau=-L_b-L_{g_1}}^{L_b+L_{g_2}}\left\|\mathbf{b}_{m,e}^T\bar{\mathbf{g}}_{qm,e}^k[\tau]\right\|_2^2 - 2h_q\mathbf{b}_{q,e}^T\mathbf{g}_{qq,e}[0]. \tag{4.25}$$

With the objective of jointly designing $\mathbf{b}_{q,e}$ and h_q the sum of the MSE has been selected to be the cost function. In order to comply with a predefined power allocation strategy the norm of the precoders is constrained. Thus, the problem can be formulated as follows:

$$\begin{aligned}&\underset{\{\mathbf{b}_q,h_q\}}{\operatorname{argmin}}\sum_{q\in S_a} MSE_q\\ &s.t.\quad \|\mathbf{b}_{q,e}\|_2^2 = p_q \qquad q\in S_a.\end{aligned} \tag{4.26}$$

It is important to remark that (4.25) is invariant with respect to k. Thus the solution of (4.26) for k odd and k even is the same. Following the same approach that is described in [100] we obtain these design equations

$$h_q = \mathbf{b}_{q,e}^T\mathbf{g}_{qq,e}[0] \tag{4.27}$$

$$\left(\sum_{\substack{m=q-1\\ m\neq q}}^{q+1}\sum_{\tau=-L_b-L_{g_1}}^{L_b+L_{g_2}}\bar{\mathbf{g}}_{mq,e}^k[\tau]\left(\bar{\mathbf{g}}_{mq,e}^k[\tau]\right)^T + \sum_{\substack{\tau=-L_b-L_{g_1}\\ \tau\neq 0}}^{L_b+L_{g_2}}\bar{\mathbf{g}}_{qq,e}^k[\tau]\left(\bar{\mathbf{g}}_{qq,e}^k[\tau]\right)^T\right)\mathbf{b}_{q,e} = \lambda_q\mathbf{b}_{q,e}. \tag{4.28}$$

Note that the power of the noise is not included in the solution. This may lead to undesired designs that could weight the desired symbol with a magnitude that is in the same order as the noise power. This problem can be circumvented to some extent if precoders are factorized as $\mathbf{b}_{q,e} = \sqrt{p_q}\mathbf{u}_q$, where $\mathbf{u}_q$ is any unitary singular vector that solves (4.28). Then, among all the candidates we select the one that maximizes the SLNR, which is given by

$$SLNR_q = \frac{p_q\left\|\mathbf{u}_q^T\mathbf{g}_{qq,e}[0]\right\|_2^2}{\lambda_q p_q\|\mathbf{u}_{q,e}\|_2^2 + 0.5N_0} = \frac{p_q\left\|\mathbf{u}_q^T\mathbf{g}_{qq,e}[0]\right\|_2^2}{\lambda_q p_q + 0.5N_0}. \tag{4.29}$$

4.C Solution of problem 4.18

This appendix describes how to solve

$$\begin{aligned}&\underset{\{\mathbf{b}_q,a_q\}}{\operatorname{argmin}}\sum_{q\in S_a} MSE_q\\ &s.t.\quad \|\mathbf{b}_q\|_2^2 = p_q,\quad q\in S_a,\end{aligned} \tag{4.30}$$

where

$$MSE_q = \mathbb{E}\left\{\left|a_q \Re\left(\theta_q^*[k] y_q[k]\right) - d_q[k]\right|^2\right\} = 1+ \\ a_q^2 \frac{N_0}{2} + \sum_{m=q-1}^{q+1} \sum_{\tau=-L_b-L_{g_1}}^{L_b+L_{g_2}} a_q^2 \left\|\mathbf{b}_{m,e}^T \bar{\mathbf{g}}_{qm,e}^k[\tau]\right\|_2^2 - 2a_q \mathbf{b}_{q,e}^T \bar{\mathbf{g}}_{qq,e}^k[0]. \tag{4.31}$$

A similar problem structure can be found in the context of single carrier MIMO communication systems, [102]. It can be readily verified that the cost function of (4.30) does not depend on the time instant k and, therefore, the solution is valid for k odd and k even. To devise the optimal transmit and receive processing we construct the Lagrangian

$$L\left(\{\mathbf{b}_{q,e}, a_q, \lambda_q\}\right) = \sum_{q \in S_a} MSE_q + \lambda_q \left(\|\mathbf{b}_{q,e}\|_2^2 - p_q\right), \tag{4.32}$$

and we set the partial derivatives to zero, yielding

$$\frac{\partial L\left(\{\mathbf{b}_{q,e}, a_q, \lambda_q\}\right)}{\partial a_q} = 0 \rightarrow \mathbf{b}_{q,e}^T \bar{\mathbf{g}}_{qq,e}^k[0] = a_q \frac{N_0}{2} + \sum_{m=q-1}^{q+1} \sum_{\tau=-L_b-L_{g_1}}^{L_b+L_{g_2}} a_q \left\|\mathbf{b}_{m,e}^T \bar{\mathbf{g}}_{qm,e}^k[\tau]\right\|_2^2 \tag{4.33}$$

$$\frac{\partial L\left(\{\mathbf{b}_{q,e}, a_q, \lambda_q\}\right)}{\partial \mathbf{b}_{q,e}} = \mathbf{0} \rightarrow \mathbf{b}_{q,e} = \left(\sum_{m=q-1}^{q+1} \sum_{\tau=-L_b-L_{g_1}}^{L_b+L_{g_2}} \frac{a_m^2}{a_q^2} \bar{\mathbf{g}}_{mq,e}^k[\tau] \left(\bar{\mathbf{g}}_{mq,e}^k[\tau]\right)^T + \frac{\lambda_q}{a_q^2} \mathbf{I}_{(2L_b+1)2N_T}\right)^{-1} \frac{1}{a_q} \bar{\mathbf{g}}_{qq,e}^k[0]. \tag{4.34}$$

Since the complexity required to solve (4.33) and (4.34) becomes unaffordable as the number of carriers increases, several assumptions have been considered: i) the ICI that the qth subcarrier induces on the mth subcarrier and the ICI that the mth subcarrier induces on the qth subcarrier are equal, ii) the receive processing applied on the qth subcarrier is also used by its neighbors. The two simplifications are tantamount to

$$\sum_{\tau=-L_b-L_{g_1}}^{L_b+L_{g_2}} \left\|\mathbf{b}_{m,e}^T \bar{\mathbf{g}}_{qm,e}^k[\tau]\right\|_2^2 = \sum_{\tau=-L_b-L_{g_1}}^{L_b+L_{g_2}} \left\|\mathbf{b}_{q,e}^T \bar{\mathbf{g}}_{mq,e}^k[\tau]\right\|_2^2 \tag{4.35}$$

$$a_{q-1} = a_q = a_{q+1}. \tag{4.36}$$

Note that (4.35) and (4.36) depend on the channel selectivity. In consequence, the more fre-

quency selective is the channel, the higher will be the error yielded by the mismatch modelling. By assuming that (4.35) and (4.36) hold true we can find the optimal solution by following the same steps that [102] describes, which can be formulated by these closed-form expressions

$$\mathbf{b}_{q,e} = \left(\sum_{m=q-1}^{q+1} \sum_{\tau=-L_b-L_{g_1}}^{L_b+L_{g_2}} \bar{\mathbf{g}}_{mq,e}^{k}[\tau] \left(\bar{\mathbf{g}}_{mq,e}^{k}[\tau] \right)^T + \frac{0.5N_0}{p_q} \mathbf{I}_{(2L_b+1)2N_T} \right)^{-1} \frac{1}{a_q} \bar{\mathbf{g}}_{qq,e}^{k}[0] \tag{4.37}$$

$$a_q = \frac{1}{\sqrt{p_q}} \left\| \left(\sum_{m=q-1}^{q+1} \sum_{\tau=-L_b-L_{g_1}}^{L_b+L_{g_2}} \bar{\mathbf{g}}_{mq,e}^{k}[\tau] \left(\bar{\mathbf{g}}_{mq,e}^{k}[\tau] \right)^T + \frac{0.5N_0}{p_q} \mathbf{I}_{(2L_b+1)2N_T} \right)^{-1} \bar{\mathbf{g}}_{qq,e}^{k}[0] \right\|_2 . \tag{4.38}$$

4.D Solution of problem 4.19

In the following we describe the steps that have been taken to solve this optimization problem

$$\begin{aligned} \text{QP}: \quad & \underset{\{\mathbf{u}_q, p_q\}}{\operatorname{argmin}} \sum_{q \in S_a} p_q \\ & s.t. \;\; SINR_q \geq \alpha_q, \;\; \|\mathbf{u}_q\|_2^2 = 1, \;\; p_q \geq 0, \;\; q \in S_a. \end{aligned} \tag{4.39}$$

As (4.20) indicates we write without loss of generality $\mathbf{b}_{q,e} = \sqrt{p_q}\mathbf{u}_q$ where p_q is the power assigned to the qth subcarrier and $\mathbf{u}_q \in \mathbb{R}^{(2L_b+1)2N_T \times 1}$ is a unit norm vector. Note that the $SINR_q$ is monotonically increasing in p_q and monotonically decreasing in p_{q-1} and p_{q+1}. As a result, the constraints have to be active at the optimal point. Otherwise the transmit power could be reduced without violating any constraint. The same kind of problem can be encountered in the context of multi-user downlink beamforming. The main difference lies in the fact that each subcarrier signal transmitted on a given subcarrier is only interfered by those subcarrier signals transmitted on the adjacent subcarriers. The work addressed in [103] investigates under what conditions problem QP is feasible. Since the particular case where there is no complete cross-talk is considered in [103], the results derived therein also hold for our case. Provided that the set of SINRs is feasible, the problem QP is equivalent to the virtual uplink problem [104], which is given by

$$\begin{aligned} \text{VU}: \quad & \underset{\{\mathbf{u}_q, \lambda_q\}}{\operatorname{argmin}} \sum_{q \in S_a} \lambda_q \alpha_q \frac{N_0}{2} \\ & s.t. \;\; \mathbf{u}_q^T \mathbf{Z}_q \mathbf{u}_q = 0, \;\; \|\mathbf{u}_q\|_2^2 = 1, \;\; \lambda_q \geq 0, \;\; q \in S_a, \end{aligned} \tag{4.40}$$

where

$$\begin{aligned}\mathbf{Z}_q = \quad & \mathbf{I}_{2N_T(1+2L_b)} - \lambda_q \bar{\mathbf{g}}^k_{qq,e}[0]\left(\bar{\mathbf{g}}^k_{qq,e}[0]\right)^T + \sum_{\substack{\tau=-L_b-L_{g_1}\\ \tau\neq 0}}^{L_b+L_{g_2}} \lambda_q \alpha_q \bar{\mathbf{g}}^k_{qq,e}[\tau]\left(\bar{\mathbf{g}}^k_{qq,e}[\tau]\right)^T + \\ & \sum_{\substack{m=q-1\\ m\neq q}}^{q+1} \sum_{\tau=-L_b-L_{g_1}}^{L_b+L_{g_2}} \lambda_m \alpha_m \bar{\mathbf{g}}^k_{mq,e}[\tau]\left(\bar{\mathbf{g}}^k_{mq,e}[\tau]\right)^T.\end{aligned} \tag{4.41}$$

It must be highlighted that problem QP is not convex. In this regard, quadratic programs can be lower bounded if the original problem is relaxed. By introducing the matrices $\mathbf{B}_q = \mathbf{b}_{q,e}\mathbf{b}^T_{q,e}$ we can transform QP into the following convex problem

$$\begin{aligned}\text{SDP}: \quad & \underset{\{\mathbf{B}_q\}}{\operatorname{argmin}} \sum_{q\in S_a} \operatorname{tr}(\mathbf{B}_q) \\ & s.t. \;\; c_q = \alpha_q \tfrac{N_0}{2}, \;\; \mathbf{B}_q = \mathbf{B}_q^T, \;\; \mathbf{B}_q \succeq 0, \;\; q \in S_a,\end{aligned} \tag{4.42}$$

where

$$\begin{aligned}c_q = \quad & \operatorname{tr}\left(\bar{\mathbf{g}}^k_{qq,e}[0]\left(\bar{\mathbf{g}}^k_{qq,e}[0]\right)^T \mathbf{B}_q\right) - \sum_{\substack{\tau=-L_b-L_{g_1}\\ \tau\neq 0}}^{L_b+L_{g_2}} \alpha_q \operatorname{tr}\left(\bar{\mathbf{g}}^k_{qq,e}[\tau]\left(\bar{\mathbf{g}}^k_{qq,e}[\tau]\right)^T \mathbf{B}_q\right) \\ & -\alpha_q \sum_{\substack{m=q-1\\ m\neq q}}^{q+1} \sum_{\tau=-L_b-L_{g_1}}^{L_b+L_{g_2}} \operatorname{tr}\left(\bar{\mathbf{g}}^k_{qm,e}[\tau]\left(\bar{\mathbf{g}}^k_{qm,e}[\tau]\right)^T \mathbf{B}_m\right).\end{aligned} \tag{4.43}$$

The authors in [104] have demonstrated that the Lagrange dual of SDP is equivalent to the Lagrange dual of QP and that the duality gap of the problem QP is zero. Taking into account that the Lagrange dual of SDP gives a lower bound to the SDP problem, we can conclude that the same optimal solution is attained by the semidefinite relaxation SDP and the primal problem QP. Therefore the optimal point of QP can be obtained from the SDP problem, which can be efficiently solved using the optimization solver CVX [105]. From the above analysis it can be inferred that strong duality also holds for the problem SDP, thus the KKT conditions have to be satisfied. In this sense, at the optimal point the complementarity conditions between the primal SDP problem and its dual implies that $\operatorname{tr}(\mathbf{B}_q\mathbf{Z}_q) = 0$ has to be fulfilled. In consequence, any vector that spans the matrix $\mathbf{B}_q$ will also be a solution of the virtual uplink problem as (4.40) shows. Once we have obtained the unit norm precoders $\mathbf{u}_q$, we can compute the power associated to each subcarrier by solving the system of linear equations $(\mathbf{I}_{M_a} - \mathbf{D}\Psi)\,\mathbf{p} = \mathbf{D}\mathbf{n}$. The reason why the power can be

computed in this way relies on the fact that the constraints are satisfied with equality. Provided that the problem is feasible the inverse of $(\mathbf{I}_{M_a} - \mathbf{D}\Psi)$ has non-negative elements which implies that vector $\mathbf{p}$ is element-wise non-negative, [103]. Regarding the notation we have used the following definitions

$$\mathbf{D} = \operatorname{diag}\left\{ \frac{\alpha_{S_a(0)}}{\mathbf{u}_{S_a(0)}^T \left(\bar{\mathbf{g}}_{S_a(0)S_a(0),e}^k[0] \left(\bar{\mathbf{g}}_{S_a(0)S_a(0),e}^k[0] \right)^T \right) \mathbf{u}_{S_a(0)}}, \cdots, \right. \\ \left. \frac{\alpha_{S_a(M_a-1)}}{\mathbf{u}_{S_a(M_a-1)}^T \left(\bar{\mathbf{g}}_{S_a(M_a-1)S_a(M_a-1),e}^k[0] \left(\bar{\mathbf{g}}_{S_a(M_a-1)S_a(M_a-1),e}^k[0] \right)^T \right) \mathbf{u}_{S_a(M_a-1)}} \right\} \tag{4.44}$$

$$[\Psi]_{lt} = \begin{cases} \sum\limits_{\substack{\tau=-L_b-L_{g_1} \\ \tau\neq 0}}^{L_b+L_{g_2}} \mathbf{u}_{S_a(t)}^T \left(\bar{\mathbf{g}}_{S_a(l)S_a(t),e}^k[\tau] \left(\bar{\mathbf{g}}_{S_a(l)S_a(t),e}^k[\tau] \right)^T \right) \mathbf{u}_{S_a(t)} & l = t \\ \sum\limits_{\tau=-L_b-L_{g_1}}^{L_b+L_{g_2}} \mathbf{u}_{S_a(t)}^T \left(\bar{\mathbf{g}}_{S_a(l)S_a(t),e}^k[\tau] \left(\bar{\mathbf{g}}_{S_a(l)S_a(t),e}^k[\tau] \right)^T \right) \mathbf{u}_{S_a(t)} & t \in \left\{ \begin{array}{l} \{l-1, l+1\} \cap \\ \{0, ..., M_a - 1\} \end{array} \right\} \\ 0 & \text{otherwise} \end{cases} \tag{4.45}$$

$$\mathbf{p} = \left[p_{S_a(0)}, ..., p_{S_a(M_a-1)} \right]^T \tag{4.46}$$

$$\mathbf{n} = \mathbf{1}_{M_a} \frac{N_0}{2}, \tag{4.47}$$

where $\mathbf{1}_{M_a}$ is a M_a-dimensional column vector with all the elements equal to one. Let $S_a(i)$ the ith element of S_a, which is the set that identifies the active carriers, and $[\Psi]_{lt}$ be the (l,t)th entry of matrix Ψ for $0 \leq l, t \leq M_a - 1$. Alternatively to the semidefinite relaxation approach, the authors in [106] have proposed a specialized iterative algorithm to solve the problem QP.

Chapter 5

Power allocation algorithms

This chapter focuses on solving the problem of distributing the power among subcarriers in the FBMC/OQAM context when the orthogonality between subcarriers is not completely restored. In the broadcast channel (BC), aside from designing power loading strategies, subcarriers have to be assigned to users. In other words, if all the users cannot be allocated on the same frequency resources, then it is deemed necessary to select those users who will transmit on a given subcarrier. With the objective of devising low-complexity solutions, in this chapter the design of precoders and equalizers is decoupled with the power control and the subcarrier assignment. This strategy allows us to benefit from the signal processing techniques described in Sections 3.1 and 4.2. Therefore, given the transmit and the receive processing, the following sections are devoted to devise power loading and user selection strategies. The algorithms presented in this chapter can be regarded as a refinement of the techniques described in Chapters 3 and 4, where the power allocation is fixed. The resource allocation problem for FBMC/OQAM systems has also been examined in [64, 107, 108], although the effect of ISI and ICI induced by the loss of orthogonality is not considered.

5.1 SINR balancing in MISO PTP communications

Likewise OFDM, the BER performance in the FBMC/OQAM modulation crucially depends on the spectral nulls that the channel frequency response may present. One solution to overcome this problem consists in coding the data with a convolutional encoder [109]. Provided that CSI is available at the transmit side, the power can also be smartly distributed among subcarriers with the aim of enhancing the quality of the worst subcarriers. Furthermore, the spatial dimension provides additional degrees of freedom to improve the performance. Concentrating on uncoded FBMC/OQAM systems this section studies how to boost the system reliability by maximizing the minimum SINR given a power budget.

Consider a MISO communication system in a scenario where there is only a single transmitter-receiver pair. Based on this, the input/output relationship on the qth subcarrier is given by (4.7). Since the emphasis of the techniques presented in this section is on the power allocation problem, it is assumed that first precoders are designed according to any criteria described in Section 4.2. The power distribution is initially fixed to comply with the UPA strategy. By setting $p_q = 1$ for $q \in S_a$, we guarantee that precoding vectors are unitary. As a consequence, it is possible to factorize precoders as $\mathbf{b}_{q,e} = \sqrt{p_q}\mathbf{u}_q$, where $\mathbf{u}_q \in \mathbb{R}^{(2L_b+1)2N_T \times 1}$ can be designed to minimize the sum MSE, to maximize the SLNR or according to the ZF approach. In the second step, the power loaded on each subcarrier is designed, given the precoders, as follows:

$$\begin{aligned} &\max_{\{p_q\}} \min_{\{q\}} SINR_q \\ &s.t \quad \sum_{q \in S_a} p_q = P_T, \quad \mathbf{b}_{q,e} = \sqrt{p_q}\mathbf{u}_q, \quad \|\mathbf{u}_q\|_2^2 = 1, \quad p_q \geq 0, \quad q \in S_a, \end{aligned} \tag{5.1}$$

with

$$SINR_q = \frac{p_q h_q}{\sum\limits_{(m,\tau)\neq(q,0)} p_m \left|\mathbf{u}_m^T \bar{\mathbf{g}}_{qm,e}^k[\tau]\right|^2 + 0.5N_0} \tag{5.2}$$

$$h_q = \left|\mathbf{u}_q^T \bar{\mathbf{g}}_{qq,e}^k[0]\right|^2. \tag{5.3}$$

The statistical information considered in Section 4.1 has been used in this section to compute the SINR. The set S_a contains M_a indices that correspond to those subcarriers that are active. It can be verified that $SINR_q$ is monotonically increasing in p_q and monotonically decreasing in p_{q-1}, p_{q+1}. As a result, the optimal solution adjusts the powers to balance $\{SINR_q\}$, [106]. In case one of the subcarriers is suffering from a deep notch, this subcarrier would get all the power leading to performance degradation. Nevertheless this is circumvented to some extent thanks to the spatial diversity, as long as propagation conditions of different links present low-correlation. Then all subcarriers can provide the same quality of service with no need to allocate most of the power on a single subcarrier. The details to solve (5.1) are provided in Appendix 5.A. It is worth emphasizing that cost functions in (5.1) can be expressed as a ratio of affine functions, which is quasi-convex. Provided that denominators of the cost functions are restricted to be strictly positive the max-min problem can be transformed to an equivalent linear program, [110]. However, the algorithm presented in this section does not try to efficiently solve (5.1). By contrast we propose a suboptimal strategy that can substantially reduce the complexity burden. This strategy relies on the assumption that the magnitude of the noise is higher than the magnitude of the interference, i.e.

$$\sum_{(m,\tau)\neq(q,0)} \left|\mathbf{u}_m^T \bar{\mathbf{g}}_{qm,e}^k[\tau]\right|^2 << 0.5N_0. \tag{5.4}$$

Under the assumption that ISI and ICI terms can be neglected, the power can be optimally split as follows:

$$p_q = \frac{P_T}{h_q \sum_{m\in S_a} \frac{1}{h_m}}, \quad q \in S_a. \tag{5.5}$$

This solution was originally formulated for the OFDM technique in the absence of interference [111]. It must be mentioned that (5.5) does not balance $\{SINR_q\}$ unless (5.4) holds true for $q \in S_a$. Hence, the system performance crucially depends on the ability of precoders to remove the interference. We have discarded the approach derived in [106] to iteratively design the power control and the precoders for complexity reasons. Since the algorithm does not stop until the stopping criterion is met, it is required to compute several times the singular value decomposition of a $M_a \times M_a$ matrix, which is demanding in terms of complexity.

5.1.1 Simulation results

For the numerical results, we have chosen the parameters of Table 2.3 that comply with Scenarios 1 and 3. The number of transmit antennas is set to 2 while the receiver is equipped with a single antenna. As for the symbol mapping, we use 16-QAM constellations to generate the real-valued symbols that are frequency multiplexed in the FBMC/OQAM scheme.

It must be mentioned that the design of precoding strategies has not been explored when solving the max-min problem, but only the power allocation is optimized. Precoders are given beforehand according to the ZF, MDIR and SLNR criteria. The details are provided in Section 4.2. Note that when designing the precoders, the power is uniformly split among subcarrier, i.e. $p_q = 1$, for $q \in S_a$.

Figure 5.1 pictures the minimum SINR that is achieved when the power is allocated under the assumption that the interference is practically cancelled. That is, the power coefficients are designed according to (5.5). The minimum SINR has been evaluated for different average energy symbol to noise ratio, which is defined as $\frac{E_s}{N_0} = \frac{M+CP}{M}\frac{2P_T}{MN_0}$. The factor 2 in the numerator accounts for the average energy of symbols that belong to a 16-QAM constellation. As a consequence, the 4-PAM symbols have unit-energy. Figure 5.1a shows that ZF and SLNR techniques present the highest SINR when Scenario 1 is simulated. By contrast, the performance metric drops significantly when the MDIR is implemented. Since this behaviour has also been observed in Section 4.2.5, we can state that the conclusions drawn therein also hold when power is allocated as (5.5) specifies. Note

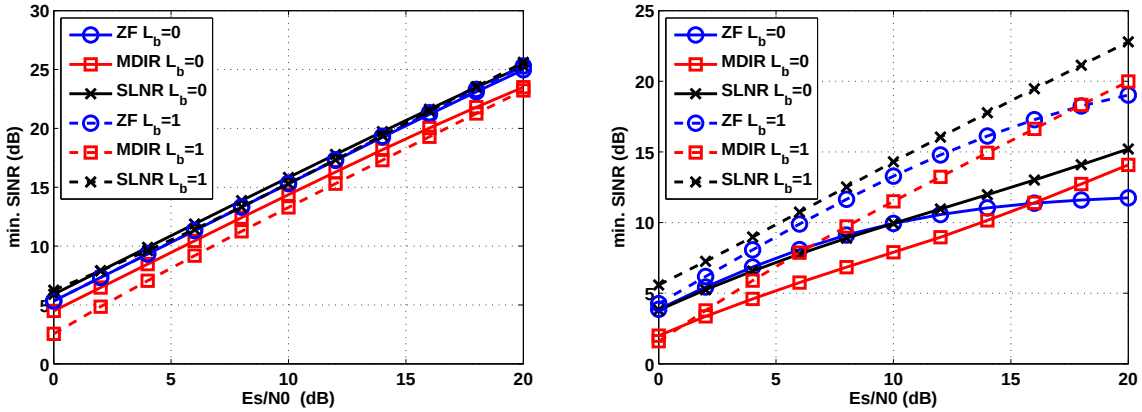

(a) Scenario 1. (b) Scenario 3.

Figure 5.1: Minimum SINR against $\frac{E_s}{N_0}$. The simulated systems correspond to FBMC/OQAM. System parameters are set according to Scenario 1 and 3 (see Table 2.3).

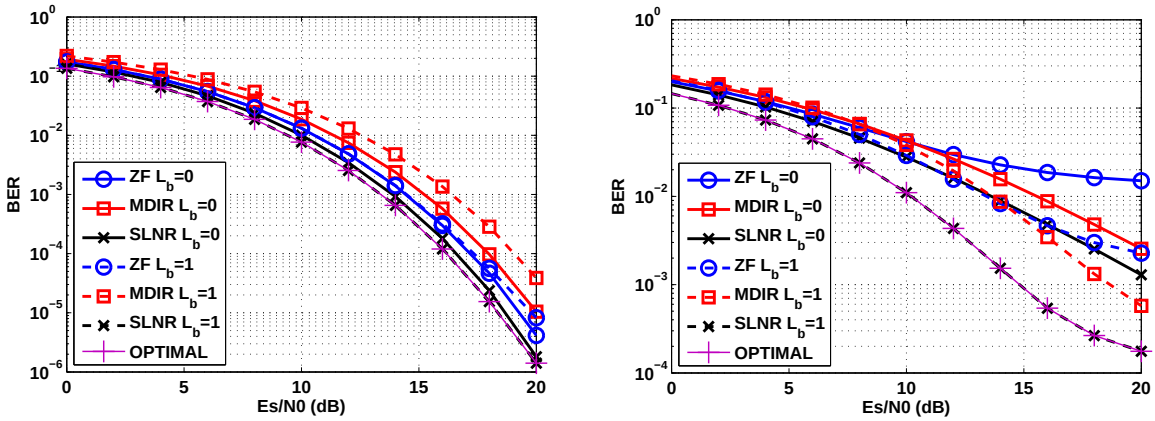

(a) Scenario 1. (b) Scenario 3.

Figure 5.2: BER against $\frac{E_s}{N_0}$. The simulated systems correspond to FBMC/OQAM. System parameters are set according to Scenario 1 and 3 (see Table 2.3).

that the techniques behave differently in Figure 5.1b. Now multi-tap precoding brings substantial improvement. In this sense, the SLNR with 3 taps exhibits the best performance.

Figure 5.2 computes the BER versus the $\frac{E_s}{N_0}$ in Scenarios 1 and 3. Since the BER is determined by the errors that are committed in the worst subcarriers, it follows that the minimum SINR should be related to the BER results. This is confirmed by verifying that the results of Figure 5.2 are in line with the results that are shown in Figure 5.1. That is, the relative behaviour between techniques is the same when the minimum SINR and the BER is evaluated. In order to determine

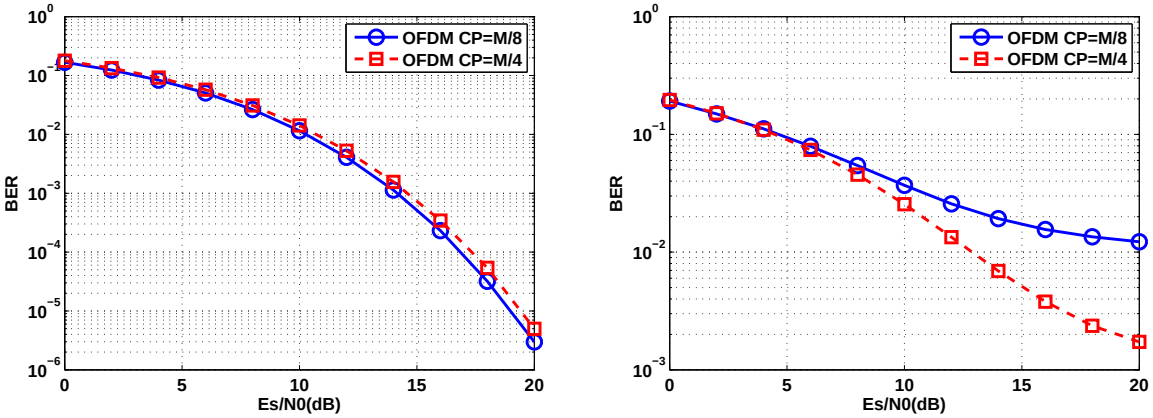

(a) Scenario 1.

(b) Scenario 3.

Figure 5.3: BER against $\frac{E_s}{N_0}$. The simulated systems correspond to OFDM. System parameters are set according to Scenario 1 and 3 (see Table 2.3).

the performance loss for neglecting the interference, we solve the max-min problem posed in (5.1). In particular, we set the number of taps to 3 and we select the SLNR to be the cost function that governs the design of the precoders. This technique is identified in the simulations as optimal. The results of Figure 5.2 indicate that in both scenarios the performance loss as a result of assuming that noise is the dominant source of interference is negligible. This result is very relevant from the complexity point of view, as the number of arithmetic operations is substantially reduced when ICI and ISI terms are ignored.

To determine if FBMC/OQAM is able to remain competitive with OFDM we simulate the OFDM technique in a MISO 1×2 communication system. As for the transmit processing, precoders are based on the transmit Wiener filter fixing the power to comply with the UPA [102]. After fixing the pre-processing strategy, the power is distributed to maximize the minimum SINR [111]. In Scenario 1, the maximum channel excess delay does not exceed $\frac{M}{8f_s}$ seconds, where f_s is the sampling frequency. For this reason, the lowest BER is achieved in Figure 5.3a by the CP$=\frac{M}{8}$ case. In Scenario 1, OFDM and FBMC/OQAM achieve a BER that is in the same order as Figure 5.3a and Figure 5.2a confirms. In Scenario 3, the channel destroys the orthogonality in the OFDM context. Since OFDM exhibits poor stopband attenuation, when compared to the FBMC/OQAM modulation, it follows that OFDM is the most sensible technique to highly frequency selective channels. This justifies why FBMC/OQAM outperforms OFDM in Scenario 3.

5.2 Sum-rate maximization in MISO PTP communications

In this section we tackle the power allocation problem with the aim of maximizing the sum-rate. Since this section studies FBMC/OQAM-based MISO communication systems, we can borrow the expressions from (5.2) and (5.3) to formulate the rate in bits/symbol on the qth subcarrier as

$$r_q = \frac{1}{2}\log_2\left(1 + SINR_q\right), \quad q \in S_a, \tag{5.6}$$

with

$$SINR_q = \frac{h_q p_q}{\alpha_{qq-1}p_{q-1} + \alpha_{qq}p_q + \alpha_{qq+1}p_{q+1} + 0.5N_0} \tag{5.7}$$

$$\alpha_{qm} = \sum_{\tau=-L_b-L_{g_1}}^{L_b+L_{g_2}} \left|\mathbf{u}_m^T \bar{\mathbf{g}}_{qm,e}^k[\tau]\right|^2, \quad m \neq q \tag{5.8}$$

$$\alpha_{qq} = \sum_{\substack{\tau=-L_b-L_{g_1} \\ \tau\neq 0}}^{L_b+L_{g_2}} \left|\mathbf{u}_q^T \bar{\mathbf{g}}_{qq,e}^k[\tau]\right|^2. \tag{5.9}$$

Note that we have assumed that the interference plus noise term is Gaussian distributed. This is a reasonable assumption taking into account that the number of interference terms that appear in (4.5) is quite large. However, even if the number of interference terms is not sufficiently large, the rate in (5.6) can be achieved since the worst case noise is shown to be Gaussian [112]. Note that the factor $\frac{1}{2}$ in (5.6) has to do with the fact that the decision variables in (4.5) are real-valued [113]. In OFDM the factor $\frac{1}{2}$ is dropped because the variables that appear in the input/output relationship belong to the complex field. This observation seems to indicate that if OFDM and FBMC/OQAM achieve the same SINR, the rate is doubled in the OFDM case. However, this is not the case because FBMC/OQAM and OFDM have different symbol periods. As it is explained in section 2.3.1, the symbol period in seconds is $T = \frac{M}{2f_s}$ and $T = \frac{M+CP}{f_s}$ in FBMC/OQAM and OFDM, respectively. We define f_s to be the sampling frequency and CP to be the length of the cyclic prefix. This highlights that if we want to carry out a fair comparison, the rate has to be expressed in bits/s. This means that (5.6) should be recasted as

$$r_q^{FBMC} = r_q \frac{2f_s}{M} = \frac{f_s}{M}\log_2\left(1 + SINR_q\right). \tag{5.10}$$

In the OFDM case, we obtain

$$r_q^{OFDM} = \frac{f_s}{M+CP}\log_2\left(1 + SINR_q^{OFDM}\right), \tag{5.11}$$

where $SINR_q^{OFDM}$ accounts for the signal to interference plus noise ratio that is achieved at the qth output of the demodulator when OFDM is considered. Let $\mathbf{u}_q \in \mathbb{C}^{N_T \times 1}$ be the unit-norm precoder employed by the OFDM modulator on the qth subcarrier and $\mathbf{H}_q \in \mathbb{C}^{N_T \times 1}$ be the channel vector on the radial frequency $\frac{2\pi q}{M}$. Then, we can formulate this expression

$$SINR_q^{OFDM} = \frac{M}{M+CP} \frac{\mathbb{E}\left\{ \left| \mathbf{u}_q^H \mathbf{H}_q \sqrt{p_q} x_q[k] \right|^2 \right\}}{N_0}. \tag{5.12}$$

Unlike the FBMC/OQAM modulation, the symbols $\{x_q[k]\}$ are QAM. The noise is not multiplied by 0.5 because the processing is carried out in the complex-domain. Note also that the noise enhancement factor given by $\frac{M+CP}{M}$ is consequence of the energy wastage that it entails transmitting a cyclic prefix, the length of which is CP. The symbols that are transmitted in the FBM/OQAM case, i.e. $\{d_q[k]\}$, are obtained by staggering half the symbol period the complex-valued symbols $\{x_q[k]\}$. Therefore, the average energy of $\{x_q[k]\}$ is two-fold with respect to the energy of $\{d_q[k]\}$.

Bearing in mind (5.6) and selecting the sum-rate to be the objective function, the problem to be solved can be expressed as follows:

$$\begin{aligned} \mathrm{P}: & \underset{\{p_q\}}{\operatorname{argmax}} \sum_{q \in S_a} \frac{1}{2} \log_2 \left(1 + SINR_q\right) \\ & s.t. \quad \sum_{q \in S_a} p_q \leq P_T, \quad p_q \geq 0, \quad q \in S_a. \end{aligned} \tag{5.13}$$

Note that if precoders are able to restore the orthogonality between subcarrier, then the transmitted data is perfectly recovered except from the noise. With that, the optimal power allocation is computed by executing the water-filling (WF) algorithm [114]. Discarding ideal scenarios we assume that the interference is not negligible. If so, problem P bears resemblance with the sum-rate maximization problem in the interference channel context, where individual power constraints per-transmitter are substituted by a total power constraint. At first glance, problem (5.13) cannot be straightforwardly solved because it is non-concave. One alternative to solve (5.13) is based on resorting to branch and bound methods, which rely on expressing (5.13) as a difference of concave functions [115, 116]. Following this approach it is possible to reach the global optimum. However, the algorithms presented in [115, 116] are very demanding in terms of complexity at high scale problems. That is, since the complexity depends on the number of subcarriers, the solutions proposed in [115, 116] are not practical for FBMC/OQAM systems with large number of subcarriers. Bearing this in mind this section tries to highlight some ideas to reduce the computational load. In this regard, we propose relaxing the original problem by solving the dual problem of (5.13). Hence, we first define the dual objective as

$$g(\lambda) = \max_{\{p_q\}} \sum_{q \in S_a} r_q + \lambda \left(P_T - \sum_{q \in S_a} p_q \right)$$
$$s.t. \;\; p_q \geq 0, \quad q \in S_a, \tag{5.14}$$

where λ is the dual variable. Restricting λ to be positive, the power coefficients are obtained by solving the dual problem

$$\text{DP} : \underset{\lambda}{\text{argmin}} \quad g(\lambda)$$
$$s.t. \;\; \lambda \geq 0. \tag{5.15}$$

Since the objective function in (5.13) is not concave, then the duality gap is not zero [110]. This means that solving (5.13) is not equivalent to solve (5.15). Therefore, the proposed relaxation yields a suboptimal solution.

On the positive side, the dual problem in (5.15) is convex, which means that we can resort to convex optimization theory [110]. On the negative side, even benefiting from convex optimization theory, it is difficult to write the solution of (5.15) in a closed-form expression. This motivates the utilization of iterative methods, as [117] proposes. Note that problem (5.14) is decoupled with M_a disjoint problems if there was no ICI, which would facilitate the solution. In our case the variable p_q appears in r_{q-1}, r_q and r_{q+1}. Consequently, it is mandatory to jointly optimize all the variables when (5.14) is addressed, which results in a complexity that is unaffordable. Thus, even resorting to dual optimization framework the complexity is still too high. In this regard, we propose to split the primal problem into three simpler subproblems, with the aim of alleviating the complexity. In particular, we create these three subsets: $S_1 = \{S_a(0), S_a(2), ..., S_a(M_a - 2)\}$, $S_2 = \{S_a(1), S_a(5), ..., S_a(M_a - 3)\}$ and $S_3 = \{S_a(3), S_a(7), ..., S_a(M_a - 1)\}$. In notation terms $S_a(i)$ denotes the ith element of the set S_a. In accordance with Section 2.3.1, the cardinality of S_a is set to M_a. Note that we have assumed that M_a is a multiple of four. In Scenario 3, this is not satisfied and the indexes are arranged as: $S_1 = \{S_a(0), S_a(2), ..., S_a(M_a - 2)\}$, $S_2 = \{S_a(1), S_a(5), ..., S_a(M_a - 1)\}$ and $S_3 = \{S_a(3), S_a(7), ..., S_a(M_a - 3)\}$. The Figure 5.4 illustrates the idea of grouping subcarriers into three subsets. The key issue is that subcarriers belonging to the same subset do not overlap in the frequency domain. If each subset tries to maximize its own sum-rate we can turn the original problem into three subproblems, which are easier to solve.

It is important to remark that the partition is the result of collecting the indices into the minimum number of subsets while the condition of no ICI between subcarriers in the same subset is satisfied. The reason comes from the intuition that increasing the number of subproblems moves us further away from the original problem. This suggests that we should merge S_2 and S_3. The justification for not doing so is provided in Appendix 5.D.

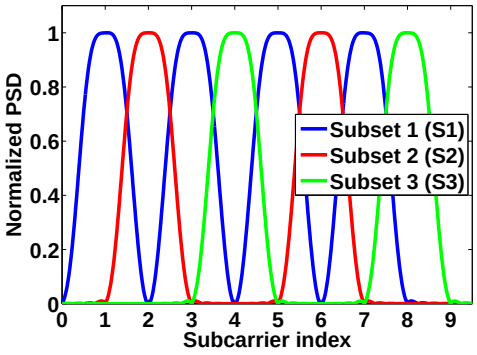

Figure 5.4: Subband partitioning scheme. Subcarrier signals span from the subcarrier index 1 to the index 9.

5.2.1 Step 1

The first step of the algorithm consists in designing the power coefficients that maximize the sum-rate of those subcarriers that belong to S_1. Since the problem of allocating the power to subcarriers associated to S_2 and S_3 has not yet been addressed, the rate maximization problem is simplified as

$$\begin{aligned} \text{P1}: \underset{\{p_q\}}{\text{argmax}} & \sum_{q\in S_1} \frac{1}{2}\log_2\left(1+\frac{p_q h_q}{0.5N_0+p_q\alpha_{qq}}\right) \\ s.t. \quad & \sum_{q\in S_1} p_q \leq \frac{P_T}{\beta}, \quad \beta \geq 1, \quad p_q \geq 0, \quad q \in S_1. \end{aligned} \tag{5.16}$$

Note that we have only used a portion of the total power budget. It is worth emphasizing that P1 is concave. The algorithm that allows us to solve P1 is detailed in Appendix 5.B.

5.2.2 Step 2

In the second step the power coefficients optimized in P1 are fixed. Now ICI terms cannot be neglected anymore. In this sense, we firstly update the interference giving rise to this interference plus noise term

$$W_q = 0.5N_0 + p_{q-1}\alpha_{qq-1} + p_{q+1}\alpha_{qq+1}, \quad q \in S_2, \quad \{q-1, q+1\} \in S_1. \tag{5.17}$$

At this point, the power cannot be computed as Section 5.2.1 proposes. The more power is allocated on a given subcarrier, the higher is the rate on the subcarrier of interest but also the higher is the interference that leaks through adjacent subcarriers, which have already been loaded in the first step. In the following, we describe two unselfish approaches that distribute the power taking into account the degradation inflicted on subcarriers that belong to subset S_1.

Alternative 1

The algorithm described hereinafter controls the degradation inflicted on already optimized subcarriers by upper bounding the power that is to be allocated on each subcarrier. This modification with respect to (5.16) results in this optimization problem

$$\begin{aligned} &\text{P2}: \underset{\{p_q\}}{\text{argmax}} \sum_{q\in S_2} \frac{1}{2}\log_2\left(1+\frac{p_q h_q}{W_q + p_q \alpha_{qq}}\right) \\ &s.t. \quad \sum_{q\in S_2} p_q \leq 0.5\left(P_T - \frac{P_T}{\beta}\right), \quad U_q \geq p_q \geq 0, \quad q \in S_2. \end{aligned} \tag{5.18}$$

A similar problem is formulated in multicarrier-based cognitive radio networks, where the interference to the primary band should not exceed a threshold [118]. The idea of upper bounding the power relies on the fact that r_q, which is defined in (5.6), is monotonically increasing in p_q whereas r_{q-1},r_{q+1} are monotonically decreasing in p_q. Constraining p_q to lie within $[0, U_q]$ we ensure that r_q will be higher than the rate degradation on the adjacent subcarriers. The details to solve P2 and compute U_q are provided in Appendix 5.C and Appendix 5.D, respectively.

Alternative 2

The second alternative to deal with the crosstalk is divided into two steps. At the initial stage, the power is computed as if there was no leakage by executing Algorithm 5. Hence, the power is set after solving this problem

$$\begin{aligned} &\text{P2}: \underset{\{p_q\}}{\text{argmax}} \sum_{q\in S_2} \frac{1}{2}\log_2\left(1+\frac{p_q h_q}{W_q + p_q \alpha_{qq}}\right) \\ &s.t. \quad \sum_{q\in S_2} p_q \leq 0.5\left(P_T - \frac{P_T}{\beta}\right), \quad p_q \geq 0, \quad q \in S_2. \end{aligned} \tag{5.19}$$

Now, power coefficients are allowed to take any positive value. However, it may happen that the rate on a given subcarrier did not compensate the loss of rate that is caused on the adjacent subcarriers. To prevent this from happening, it is mandatory to calculate for all $q \in S_2$ the aggregate given by $r_q + r_{q-1} + r_{q+1}$, before and after solving (5.19). Before computing the argument that maximizes (5.19), the aggregate becomes

$$SR_q(0) = \sum_{\substack{m=q-1 \\ m\neq q}}^{q+1} \frac{1}{2}\log_2\left(1+\frac{h_m p_m}{0.5N_0 + \alpha_{mm} p_m}\right), \quad q \in S_2, \tag{5.20}$$

where $\{q-1, q+1\}$ become part of subset S_1. After executing the power allocation algorithm in the subset S_2, the aggregate is expressed as

$$SR_q(p_q) = \sum_{\substack{m=q-1 \\ m\neq q}}^{q+1} \frac{1}{2}\log_2\left(1+\frac{h_m p_m}{0.5N_0+\alpha_{mm}p_m+\alpha_{mq}p_q}\right) + \frac{1}{2}\log_2\left(1+\frac{h_q p_q}{W_q+\alpha_{qq}p_q}\right), \quad (5.21)$$

for $q \in S_2$. If $SR_q(p_q) < SR_q(0)$ we have to recalculate p_q. In particular, we investigate if reducing the power may bring about a net contribution, i.e. $SR_q(p_q) > SR_q(0)$. The new power is obtained from this piecewise maximization

$$i_q = \underset{0\leq i\leq N_q}{\operatorname{argmax}}\, SR_q(\Delta_q^i). \quad (5.22)$$

That is, the new power is given by $\Delta_q^{i_q}$. We have constrained the power coefficient to lie in a discrete set to reduce the complexity. This simplification is motivated from the difficulty of formulating in a closed-form expression the optimal power that maximizes $SR_q(p_q)$. One option to design the discrete points is to set the power so that the rate is an integer variable. Hence, if the power is equal to

$$\Delta_q^i = \frac{\left(2^{2i}-1\right)W_q}{h_q-\alpha_{qq}\left(2^{2i}-1\right)}, \quad (5.23)$$

then the qth subcarrier conveys i bits. By setting $N_q = \left\lfloor \frac{1}{2}\log_2\left(1+\frac{h_q p_q}{\alpha_{qq}p_q+W_q}\right)\right\rfloor$, we make sure that $\Delta_q^{i_q} < p_q$, where p_q is the power that solves (5.19).

5.2.3 Step 3

After setting the powers associated to S_1 and S_2 according to the outputs of P1 and P2, the subproblem P3 is identical to P2. The interference plus noise term is given by

$$W_q = 0.5N_0 + p_{q-1}\alpha_{qq-1} + p_{q+1}\alpha_{qq+1}, \quad q \in S_3, \quad \{q-1, q+1\} \in S_1. \quad (5.24)$$

The two alternatives described in Section 5.2.2 are slightly modified as follows.

Alternative 1

The power allocation that upper bounds the power coefficients is obtained by solving

$$\begin{aligned} &\text{P3}: \underset{\{p_q\}}{\operatorname{argmax}} \sum_{q\in S_3} \frac{1}{2}\log_2\left(1+\frac{p_q h_q}{W_q + p_q\alpha_{qq}}\right) \\ &s.t. \quad \sum_{q\in S_3} p_q \leq 0.5\left(P_T - \frac{P_T}{\beta}\right), \quad U_q \geq p_q \geq 0, \quad q \in S_3. \end{aligned} \tag{5.25}$$

Alternative 2

Initially the power is distributed as if there was no crosstalk, i.e.

$$\begin{aligned} &\text{P3}: \underset{\{p_q\}}{\operatorname{argmax}} \sum_{q\in S_3} \frac{1}{2}\log_2\left(1+\frac{p_q h_q}{W_q + p_q\alpha_{qq}}\right) \\ &s.t. \quad \sum_{q\in S_3} p_q \leq 0.5\left(P_T - \frac{P_T}{\beta}\right), \quad p_q \geq 0, \quad q \in S_3. \end{aligned} \tag{5.26}$$

The metric that allows us to check if the power allocation is harmful in terms of rate is written as

$$SR_q(p_q) = \sum_{m=q+1}^{q+1} \frac{1}{2}\log_2\left(1+\frac{h_m p_m}{0.5N_0 + \sum_{l=m-1}^{m+1} p_l\alpha_{ml}}\right), \tag{5.27}$$

for $q \in S_3$. If $SR_q(p_q) < SR_q(0)$, the power allocated on the qth subcarrier is equal to $\Delta_q^{i_q}$, where

$$i_q = \underset{0\leq i\leq N_q}{\operatorname{argmax}} SR_q(\Delta_q^i) \tag{5.28}$$

$$\Delta_q^i = \frac{\left(2^{2i}-1\right)W_q}{h_q - \alpha_{qq}\left(2^{2i}-1\right)}. \tag{5.29}$$

The highest index in the discrete set has been fixed as $N_q = \left\lfloor \frac{1}{2}\log_2\left(1+\frac{h_q p_q}{\alpha_{qq}p_q+W_q}\right)\right\rfloor$.

As (5.20) and (5.27) highlight, the odds of having to recalculate the power are the highest in the step 3. The reason lies in the fact that subcarriers grouped in S_1 are more sensitive to ICI after solving (5.26) than after solving (5.19).

5.2.4 Simulation results

In order to test the performance of the proposed algorithms we present in this section some simulation-based results. To highlight the advantages of grouping subcarriers into three subsets

under strong interference conditions, we initially stick to the propagation conditions and the system parameters that correspond to Scenario 3. To make the scenario even more challenging, the precoding scheme is given by the single-tap ZF that is described in section 4.2.1. This precoder gives the worst performance as it is shown in Figure 4.2.

As a benchmark we have allocated the power according to the UPA and the WF algorithm assuming that ICI and ISI terms are negligible [114]. In addition, problem (5.13) has been solved by implementing the iterative algorithm based on the DC interpretation addressed in [119]. Although this method is suboptimal the authors claim that it enables achieving a large portion of the maximum sum-rate.

In Figure 5.5 we evaluate the system performance after performing the three-step algorithm in a 1×2 MISO system. As Sections 5.2.2 and 5.2.3 describe, the power can be distributed according to the alternative 1 or the alternative 2. The two alternatives are compared in Figure 5.5a in terms of sum-rate. In this sense, we have plotted the metric $\sum_{q \in S_a} r_q$, which is expressed in bits/multicarrier symbol. The rate is evaluated for different average energy symbol to noise ratio values, which is defined as $\frac{E_s}{N_0} = \frac{M+CP}{M} \frac{2P_T}{MN_0}$. The factor 2 in the numerator accounts for the average QAM symbol energy. Therefore, the average PAM symbol energy is equal to one. Figure 5.5a shows that the best policy in terms of rate is to set $\beta = 2$. Numerical results show that decreasing β, which means that the power budget used in the step 1 falls, the sum-rate degrades. With $\beta = 2$, both alternatives nearly give the same performance but for $\beta = 4$, the alternative 1 slightly improves the rate. To complement the rate results, we picture in Figure 5.5b the power that is required to achieve the results of Figure 5.5a. Since we have fixed the maximum transmittable power to the practical value $P_T = 1W$, Figure 5.5b can be regarded as the power that each technique should transmit for different noise values. At high noise regime all techniques almost consume all the power. The gap with respect to maximum transmittable power is the result of the stopping criterion that is used when solving problems P1, P2 and P3. At low noise regime we can save additional power for $\beta = 4$ when the alternative 1 is considered. We have observed that as N_0 decreases the maximum allowable power U_q decreases. Since there is no improvement in transmitting beyond the bound, it is obvious that the major savings accour at moderate and low noise regime. The highest savings occur for $\beta = 4$ because reducing the power budget in the step 1, implies that the bound U_q is reduced as well. Nevertheless, the reduction that is achieved in the transmitted power by setting $\beta = 4$ does not compensate the performance loss in terms of rate.

The most efficient techniques simulated in Figure 5.5 are confronted with the benchmarks in Figure 5.6. It can be observed that the highest rate is obtained by the DC solution, which is by far the most demanding in terms of complexity. Ignoring the interference and distributing the power as the WF algorithm specifies, results in a substantial rate degradation, mostly at high $\frac{E_s}{N_0}$. Note that the rate yielded by the UPA coincides with that obtained by the WF. By executing the three-step

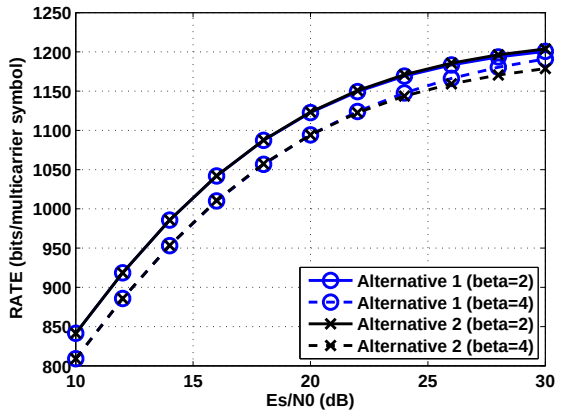

(a) Rate against $\frac{E_s}{N_0}$ fixing $P_T = 1W$.

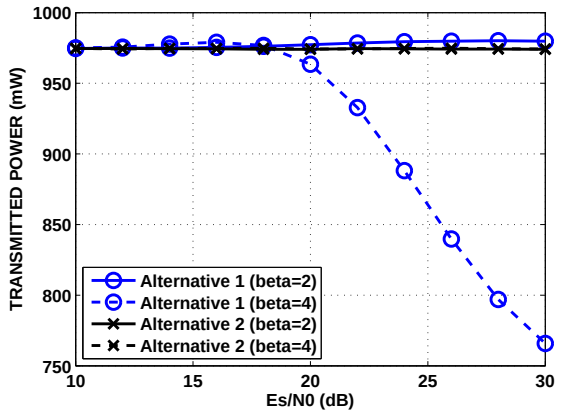

(b) Transmitted power against $\frac{E_s}{N_0}$ fixing $P_T = 1W$.

Figure 5.5: Performance assessment of FBMC/OQAM-based 1×2 MISO systems. The power is distributed according to alternatives 1 and 2. System parameters are set according to the scenario 3 (see Table 2.3).

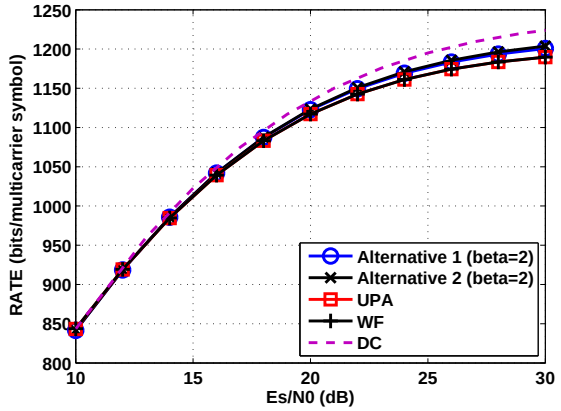

(a) $N_T = 2$.

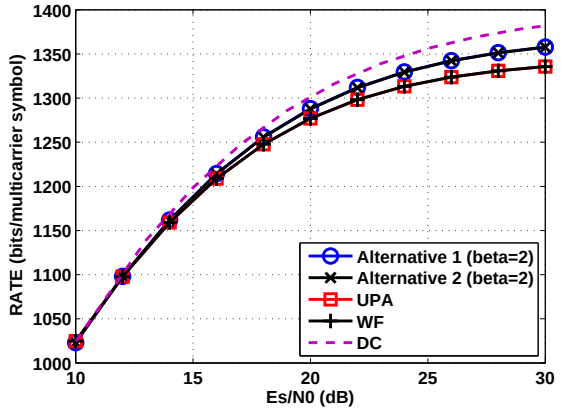

(b) $N_T = 4$.

Figure 5.6: Rate against $\frac{E_s}{N_0}$ fixing $P_T = 1W$. Different power allocation strategies are evaluated in a FBMC/OQAM-based MISO system. System parameters are set according to the scenario 3 (see Table 2.3).

algorithm with $\beta = 2$ we can narrow the gap with respect to DC. Therefore, the proposed technique outperforms the WF and the UPA. However, there is room from improvement since at high $\frac{E_s}{N_0}$ the algorithm based on the DC interpretation achieves the highest rate. In the four transmit antenna case, the rates increase with respect to the two antenna case as a consequence of having more degrees of freedom. Another interesting result is that the gap between the WF and the proposed

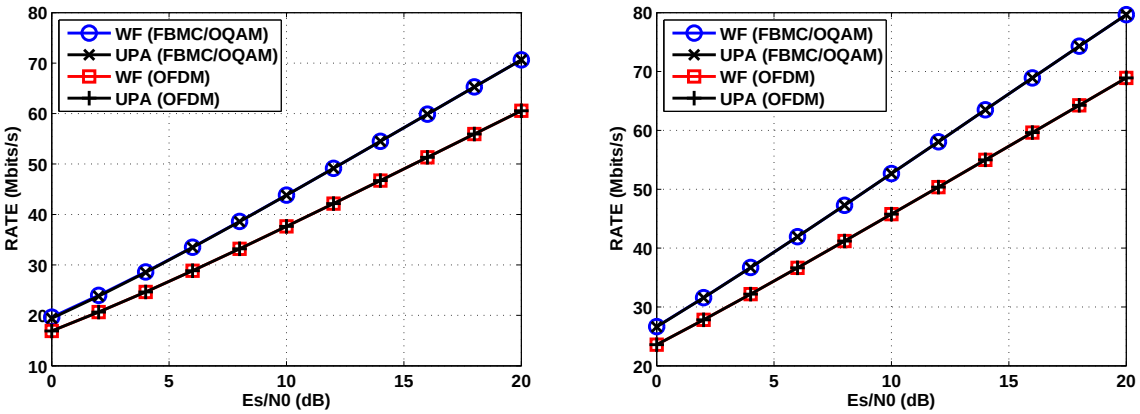

(a) $N_T = 2$. (b) $N_T = 4$.

Figure 5.7: Rate against $\frac{E_s}{N_0}$ fixing $P_T = 1W$. The FBMC/OQAM and the OFDM modulation schemes are evaluated when WF and UPA policies are implemented. System parameters are set according to the scenario a (see Table 2.3).

algorithms is widened by extending the number of transmit antennas from two to four.

In Scenario 3 the orthogonality is also destroyed in the OFDM context, as long as the length of the cyclic prefixed is not allowed to exceed one fourth of the block length. The loss of orthogonality leads to ICI. Due to the poor stopband attenuation exhibited by the rectangular window, ICI not only comes from the adjacent subcarriers. Since the proposed algorithm relies on the fact that only the most immediate neighbors overlap in the frequency domain, in OFDM systems we cannot allocate the power by using the three-step approach. For this reason, the comparison between FBMC/OQAM and OFDM has been made under the conditions of Scenario 1. To carry out a fair comparison, the rate has been evaluated in bits/s as (5.10) and (5.11) detail. In particular, we plot $\sum_{q\in S_a} r_q^{FBMC}$ and $\sum_{q\in S_a} r_q^{OFDM}$. As Table 2.3 specifies, the number of active data carriers is 756 and 720 in FBMC/OQAM and OFDM, respectively. As for the precoding schemes, the FBMC/OQAM relies on the ZF transmitter devised in section 4.2.1. Since the channel is low-frequency selective, the number of taps per-antenna is set to one. In the OFDM case, the transmit processing is based on implementing the transmit Wiener filter on a per-subcarrier basis [102]. The CP length has been set to $\frac{M}{8}$ samples. Regarding the computation of the power coefficients, WF and UPA policies are employed in both systems [114]. Therefore, the interference is ignored in FBMC/OQAM systems when computing the power that is allocated on each subcarrier. However, when the rate is computed in (5.10) no simplifications are made and the interference comes into play. As Figure 5.7 shows, FBMC/OQAM not only achieves competitive results but it outperforms OFDM in the two and the four transmit antenna case, mostly at high $\frac{E_s}{N_0}$. Aspects like the CP

transmission along with the number of active carriers explain the rate figures. Note that the spectral efficiency loss under constant-power water-filling is almost non-existing, which is line with the analysis developed in [120].

5.3 Discrete sum-rate maximization in MISO PTP communications

In this section we tackle the power allocation problem with the aim of maximizing the achievable sum-rate at a given symbol error rate (SER). In addition, we have considered realistic modulation schemes in the sense that the number of bits per-symbol is constrained to be integer. To sum up, we can state that this section delves into the sum-rate maximization at a target SER and imposing integer-bit constraints. In this sense, we first concentrate on the SER expression. Taking into account that the symbols transmitted on the qth subcarrier are generated from the $\sqrt{M_q}$-PAM modulation scheme, the SER of the global communication system that is expressed in (4.5) is given by

$$SER_q^{PAM} = 2\frac{\sqrt{M_q}-1}{\sqrt{M_q}}Q\left(\sqrt{\frac{3p_q h_q}{\sigma_q^2\left(M_q-1\right)}}\right), \quad q \in S_a, \tag{5.30}$$

provided that symbols are equiprobable and that errors only occur between constellation points that are separated with the minimum distance [73]. The term h_q is formulated in (5.3) and

$$\sigma_q^2 = 0.5N_0 + \alpha_{qq}p_q + \alpha_{qq-1}p_{q-1} + \alpha_{qq+1}p_{q+1} \tag{5.31}$$

is obtained from the SINR definition of (5.7). Note that the interference plus noise term is modeled to be Gaussian distributed. At high modulation orders (5.30) can be approximated to

$$SER_q^{PAM} = 2Q\left(\sqrt{\frac{3p_q h_q}{\sigma_q^2\left(M_q-1\right)}}\right), \quad q \in S_a. \tag{5.32}$$

From (5.32) it is possible to obtain the achievable rate that fulfils the target SER. In this sense, it is important to recall that the modulation order $\sqrt{M_q}$ and the number of bits/symbol r_q are related as follows: $\sqrt{M_q} = 2^{r_q}$. Then, the achievable rate can be expressed in bits/symbol as follows:

$$r_q = \frac{1}{2}\log_2\left(1+\frac{p_q h_q}{\sigma_q^2\Gamma_{PAM}}\right), \quad q \in S_a, \tag{5.33}$$

where Γ_{PAM} denotes the signal to noise ratio gap with respect to the capacity in (5.6). Given

the SER, the signal to noise ratio gap is formulated as $\Gamma_{PAM} = \frac{1}{3}\left(Q^{-1}\left(\frac{SER_q^{PAM}}{2}\right)\right)^2$. With this definition, the rate in (5.33) guarantees that the target SER is attained because (5.30) is upper bounded by (5.32). Recalling the expression (5.10), the achievable rate can be expressed in bits/s as

$$r_q^{FBMC} = r_q \frac{2f_s}{M} = \frac{f_s}{M}\log_2\left(1 + \frac{p_q h_q}{\sigma_q^2 \Gamma_{PAM}}\right), \quad q \in S_a. \tag{5.34}$$

The achievable rate in bits/s, when OFDM is considered, is written in this form

$$r_q^{OFDM} = \frac{f_s}{M+CP}\log_2\left(1 + \frac{SINR_q^{OFDM}}{\Gamma_{QAM}}\right), \quad q \in S_a. \tag{5.35}$$

At high rates we can use this definition $\Gamma_{QAM} = \frac{1}{3}\left(Q^{-1}\left(\frac{SER_q^{QAM}}{4}\right)\right)^2$ as shown in [121]. The ratio $SINR_q^{OFDM}$ is expressed in (5.12). If symbols are equiprobable, we can approximate the error rate per-dimension to $\frac{SER_q^{QAM}}{2}$, when the QAM constellation is considered. Assuming that this approximation holds true, OFDM and FBMC/OQAM can be compared by constraining the error rate per-dimension to be the same in both modulations, i.e. $2SER_q^{PAM} = SER_q^{QAM}$. If so, $\Gamma_{PAM} = \Gamma_{QAM}$.

Taking into account that (5.33) is limited to be integer for practicality reasons, the problem that we propose to solve is

$$\begin{aligned} &\mathrm{P}: \underset{p_q}{\operatorname{argmax}} \sum_{q\in S_a} r_q \\ &s.t. \sum_{q\in S_a} p_q \leq P_T, \quad p_q \geq 0, \quad r_q \in \{0,1,...,N_q\}, \quad q \in S_a. \end{aligned} \tag{5.36}$$

Let N_q be the maximum number of transmittable bits on the qth subcarier, which is computed by rounding the value at which r_q saturates. The bound is defined as $N_q = \left\lfloor \lim_{p_q\to\infty} r_q \right\rfloor = \left\lfloor \frac{1}{2}\log_2\left(1 + h_q/(\alpha_{qq}\Gamma_{PAM})\right)\right\rfloor$. Similarly to [122] our approach to solve (5.36) is based on a bit-filling algorithm. The idea is to increase the rate in the subcarrier that exhibits the least incremental power to convey one additional bit. However, the formulation is different since we have made no assumption about the flatness of the channel at each subcarrier. In this sense, provided that on the jth iteration the number of bits loaded so far on the qth subcarrier is denoted $r_q(j)$, the power required on the qth subcarrier is computed from (5.33) and is given by

$$p_q^j = \frac{\Gamma_{PAM}\left(2^{2r_q(j)} - 1\right)\left(0.5N_0 + p_{q-1}^j \alpha_{qq-1} + p_{q+1}^j \alpha_{qq+1}\right)}{h_q - \alpha_{qq}\Gamma_{PAM}\left(2^{2r_q(j)} - 1\right)}. \tag{5.37}$$

From (5.37) it can be inferred that in the next iteration, the additional power required to transmit one more bit on the qth subcarrier, i.e. $\Delta_q^{j+1} = p_q^{j+1} - p_q^j$, reads as follows:

$$\Delta_q^{j+1} = \frac{3\Gamma_{PAM} h_q 2^{2r_q(j)} \left(0.5N_0 + p_{q-1}^j \alpha_{qq-1} + p_{q+1}^j \alpha_{qq+1}\right)}{\left(h_q - \alpha_{qq}\Gamma_{PAM}\left(2^{2r_q(j)} - 1\right)\right)\left(h_q - \alpha_{qq}\Gamma_{PAM}\left(2^{2(r_q(j)+1)} - 1\right)\right)}. \tag{5.38}$$

It is worth emphasizing that (5.33) is monotonically increasing in p_q and monotonically decreasing in p_{q-1} and p_{q+1}. This highlights that the vector of powers $\mathbf{p}(j) = \left[p_{S_a(0)}^j, ..., p_{S_a(M_a-1)}^j\right]^T$ cannot be updated on a per-subcarrier basis. Taking into consideration (5.37) we can use the following matrix notation to compactly formulate the relation between the power coefficients and the bits loaded at each iteration

$$\left(\mathbf{I}_{M_a} - \mathbf{A}\left(j\right)\right)\mathbf{p}\left(j\right) = \mathbf{w}\left(j\right) \tag{5.39}$$

$$\mathbf{w}\left(j\right) = \frac{N_0}{2}\left[\frac{\Gamma_{PAM}\left(2^{2r_{S_a(0)}(j)} - 1\right)}{h_{S_a(0)}}, ..., \frac{\Gamma_{PAM}\left(2^{2r_{S_a(M_a-1)}(j)} - 1\right)}{h_{S_a(M_a-1)}}\right]^T, \tag{5.40}$$

where $\mathbf{I}_{M_a}$ is the M_a-dimensional identity matrix and $\mathbf{A}\left(j\right) \in \mathbb{R}^{M_a \times M_a}$ accommodates ICI and ISI. For $l, t = 0, \cdots, M_a - 1$ the (l,t)th entry of matrix $\mathbf{A}(j)$ is defined as follows:

$$\left[\mathbf{A}\left(j\right)\right]_{lt} = \begin{cases} \alpha_{S_a(l)S_a(t)} \frac{\Gamma_{PAM}\left(2^{2r_{S_a(l)}(j)} - 1\right)}{h_{s_a(l)}} & t \in \{l-1, l, l+1\} \cap \{0, \cdots, M_a - 1\} \\ 0 & \text{otherwise} \end{cases}. \tag{5.41}$$

Note that it is mandatory to compute $\mathbf{C}(j) = (\mathbf{I}_{M_a} - \mathbf{A}(j))^{-1}$ to recalculate the power coefficients if the bit distribution is modified. The complexity is reduced when the matrix inversion lemma comes into action. Provided that at the jth iteration an extra bit is loaded on the lth subcarrier, the matrix $\mathbf{C}(j)$ is given by

$$\mathbf{C}(j) = \left(\mathbf{I}_{M_a} - \mathbf{A}(j-1) + \mathbf{v}_l \mathbf{z}_l^T(j-1)\right)^{-1} = \mathbf{D}(j-1)\mathbf{C}(j-1) \tag{5.42}$$

with

$$\mathbf{D}(j-1) = \left(\mathbf{I}_{M_a} - \frac{\mathbf{C}(j-1)\mathbf{v}_l \mathbf{z}_l^T(j-1)}{1 + \mathbf{z}_l^T(j-1)\mathbf{C}(j-1)\mathbf{v}_l}\right). \tag{5.43}$$

Let $\mathbf{v}_l \in \mathbb{R}^{M_a \times 1}$ be a vector that takes the value one at the lth position whereas it is zero-valued in the rest of positions. The tth element of vector $\mathbf{z}_l(j-1) \in \mathbb{R}^{M_a \times 1}$ is expressed as follows:

$$[\mathbf{z}_l\,(j-1)]_t = \begin{cases} -\alpha_{S_a(l)S_a(t)}\frac{\Gamma_{PAM}2^{2r_{S_a(l)}(j-1)}}{h_{S_a(l)}} & \text{if } \; t \in \{l-1, l, l+1\} \cap \{0, \cdots, M_a-1\} \\ 0 & \text{otherwise} \end{cases}, \quad (5.44)$$

for $0 \leq t \leq M_a - 1$. When updating the power it is crucial that the algorithm makes sure that $\mathbf{p}(j)$ is element-wise positive. From the theory developed in [103], we know that the rates on the jth iteration are achievable if and only if the spectral radius of $\mathbf{A}(j)$ is lower than one. Since the complexity of carrying out a singular value decomposition at each iteration would be unaffordable we can circumvent the problem under the assumption that $\mathbf{C}(j-1)$ is element-wise positive. In other words, the bits loaded in the $j-1$th iteration should be achievable. Initializing the algorithm with $\mathbf{C}(0) = \mathbf{I}_{M_a}$, the condition

$$\mathbf{z}_l^T(j-1)\mathbf{C}(j-1)\mathbf{v}_l \geq -1 \quad (5.45)$$

is sufficient to ensure that the new sum-rate after allocating an extra bit on the lth subcarrier does not violate any power constraint. If the inequality (5.45) is not satisfied, then $\mathbf{D}(j-1)$ is element-wise negative out of the diagonal. Hence, $\mathbf{p}(j)$ is not positive if just a single element in the diagonal of $\mathbf{D}(j-1)$ is negative. To sum up, when (5.45) does not hold true we cannot state that $\mathbf{p}(j) \geq 0$ if

$$1 - \frac{\min\limits_{i=S_a(0),\ldots,S_a(M_a-1)} \left(\left[\mathbf{C}(j-1)\mathbf{v}_l\mathbf{z}_l^T(j-1)\right]_{ii}\right)}{1+\mathbf{z}_l^T(j-1)\mathbf{C}(j-1)\mathbf{v}_l} \leq 0, \quad (5.46)$$

where $\left[\mathbf{C}(j-1)\mathbf{v}_l\mathbf{z}_l^T(j-1)\right]_{ii}$ denotes the (i,i)th entry of $\mathbf{C}(j-1)\mathbf{v}_l\mathbf{z}_l^T(j-1)$. In the rest of cases, i.e. when (5.45) and (5.46) are not fulfilled, the vector $\mathbf{p}(j)$ may be element-wise positive while some positions of $\mathbf{C}(j)$ may contain negative elements. If so, (5.45) does not guarantee the positivity of $\mathbf{p}(j)$, thus the feasibility on subsequent iterations would hinge on checking the spectral radius of $\mathbf{A}(j)$. With the aim of reducing the complexity burden, when (5.45) does not hold true we take for granted that at least one element in the diagonal of $\mathbf{D}(j-1)$ is negative, which implies that the sum-rate is not achievable and as a result the lth subcarrier is removed from the feasible set in subsequent iterations.

5.3.1 Interference aware bit-filling algorithm

As it has been previously stated, we propose to compute the bit and the power allocation by implementing a greedy algorithm. In other words, integer bits are iteratively assigned to subcarriers one at a time. At each iteration the additional bit is assigned to the subcarrier that guarantees

the lowest incremental power. It can be readily verified that bit-filling algorithms converge faster to the solution if the initial bit and power distributions are different from zero. In this regard, we exploit the good spectral confinement of the pulses to set the initial bit and power profiles. The idea consists in collecting the indexes of the subcarriers in two subsets so that subcarrier signals belonging to the same subset do not overlap in the frequency domain. This is achieved by taking one subcarrier out of two, which results in these two subsets: S_1=$\{S_a(0), S_a(2), \cdots, S_a(M_a-2)\}$ and S_2=$\{S_a(1), S_a(3), \cdots, S_a(M_a-1)\}$. Note that we assume that M_a is multiple of two. Based on this partitioning, we first compute bit and power allocations in those subcarriers that belong to S_1. Next, given bit and power distributions computed in the previous step, the discrete rate is maximized considering all active subcarriers. Therefore, we can divide the algorithm into two steps.

Step 1

Algorithm 1 Initial bit loading and power allocation.

Set $\bar{S}_1 = S_1$, $j = 0$, $\mathbf{C}(0) = \mathbf{I}_{M_a}$, $0 \leq \beta \leq 1$
Set $p_q^0 = 0$, $r_q(0) = 0$, for $q \in S_1$
while $\sum_{q \in S_1} p_q^j \leq \beta P_T$ **and** $|\bar{S}_1| \neq \emptyset$ **do**
    $j \leftarrow j + 1$
    Compute Δ_q^j for $q \in \bar{S}_1$ using (5.48)
    $l = \underset{q \in \bar{S}_1}{\operatorname{argmin}} \Delta_q^j$
    $r_l(j) = r_l(j-1) + 1$
    if $r_l(j) = N_l$ **then**
        $\bar{S}_1 = \bar{S}_1 \backslash l$
    end if
    Compute $\mathbf{C}(j)$ using (5.42)
    $p_l^j = p_l^{j-1} + \Delta_l^j$
end while
set $p_q^0 = p_q^j$, $r_q(0) = r_q(j)$, for $q \in S_1$
set $\mathbf{C}(0) = \mathbf{C}(j)$

The resource allocation problem on subset S_1 boils down to solving

$$\begin{aligned} &\text{P1} : \underset{p_q}{\operatorname{argmax}} \sum_{q \in S_1} r_q \\ &s.t. \sum_{q \in S_1} p_q \leq P_T \beta, \quad \beta \leq 1, \quad p_q \geq 0, \quad r_q \in \{0, 1, ..., N_q\}, \quad q \in S_1. \end{aligned} \tag{5.47}$$

The greedy algorithm that allows us to solve (5.47) is detailed in Algorithm 1. It is important to

remark that no power will be assigned to subcarriers that belong to S_2 in the first step. Therefore, (5.38) can be simplified as

$$\Delta_q^{j+1} = \frac{3\Gamma_{PAM} h_q 2^{2r_q(j)} (0.5N_0)}{\left(h_q - \alpha_{qq}\Gamma_{PAM}\left(2^{2r_q(j)} - 1\right)\right)\left(h_q - \alpha_{qq}\Gamma_{PAM}\left(2^{2(r_q(j)+1)} - 1\right)\right)}. \tag{5.48}$$

The absence of ICI allows us to update powers on a per-subcarrier basis as line 12 indicates. As a consequence, we do not have to deal with the infeasibility issue. Note that in the last iteration the parameters $\mathbf{C}(j)$, p_q^j and $r_q(j)$ are stored to be used in the second step to initialize the algorithm.

Step 2

Algorithm 2 Bit loading and power allocation given initial bit and power distributions.

1: Set $\bar{S}_a = S_a$, $j = 0$
2: Given $\mathbf{C}(0)$ and p_q^0, $r_q(0)$ for $q \in S_a$
3: **while** $\sum_{q\in\bar{S}_a} p_q^j \leq P_T$ **and** $|\bar{S}_a| \neq \emptyset$ **do**
4: $j \leftarrow j + 1$
5: Compute Δ_q^j for $q \in \bar{S}_a$ using (5.38)
6: $l = \underset{q\in\bar{S}_a}{\operatorname{argmin}} \Delta_q^j$
7: $r_l(j) = r_l(j-1) + 1$
8: **if** $r_l(j) = N_l$ **then**
9: $\bar{S}_a = \bar{S}_a \backslash l$
10: **end if**
11: **if** $1 + \mathbf{z}_l^T(j-1)\mathbf{C}(j-1)\mathbf{v}_l > 0$ **then**
12: Compute $\mathbf{w}(j)$ and $\mathbf{C}(j)$ using (5.40) and (5.42)
13: $\mathbf{p}(j) = \mathbf{C}(j)\mathbf{w}(j)$
14: **else**
15: $r_l(j) = r_l(j) - 1$, $\bar{S}_a = \bar{S}_a \backslash l$
16: **end if**
17: **end while**
18: Set $p_q = p_q^j$, $r_q = r_q(j)$, for $q \in S_a$

In the second step of the algorithm, the problem (5.36) is iteratively solved. The final bit and power profiles that are computed after solving P1 are regarded as the initial bit and power distribution. Since βP_T out of the total average power P_T has been consumed in the step 1, the remaining power to be allocated amounts to $(1-\beta)P_T$. The details of the greedy algorithm executed in the second step are provided in Algorithm 2.

Algorithm 3 Initial bit loading and power allocation in the absence of interference.

Set $\bar{S}_a = S_a$, $j = 0$
Set $p_q^0 = 0$, $r_q(0) = 0$, for $q \in S_a$
while $\sum_{q \in S_a} p_q^j \leq P_T$ **and** $|\bar{S}_a| \neq \emptyset$ **do**
    $j \leftarrow j + 1$
    Compute Δ_q^j for $q \in \bar{S}_a$ using (5.49)
    $l = \underset{q \in \bar{S}_a}{\operatorname{argmin}} \Delta_q^j$
    $r_l(j) = r_l(j-1) + 1$
    $p_l^j = p_l^{j-1} + \Delta_l^j$
end while
Set $p_q = p_q^j$, $r_q = r_q(j)$, for $q \in S_a$

5.3.2 Ideal bit-filling algorithm

Based on the bit-filling concept, the strategy presented in this section also assigns one bit at a time. However, it is assumed that the signal processing carried out at the transmit side completely restores the orthogonality. Therefore, the residual interference is neglected. As a result, the cost function to determine the least demanding subcarrier is given by

$$\Delta_q^{j+1} = \frac{3\Gamma_{PAM} h_q 2^{2r_q(j)} (0.5N_0)}{h_q^2}. \tag{5.49}$$

Similarly to the algorithm presented in the first step, power coefficients can be individually treated. The proposed algorithm is detailed in Algorithm 3. Note that now all subcarriers come into action.

After executing the low-complexity algorithm we can either recalculate the bit distribution to comply with the SER constraint or keep the bit allocation unchanged. If we decide to satisfy the QoS constraints, we have to modify the bit profile by performing the following rounding step

$$r_q = \left\lfloor \frac{1}{2}\log_2 \left(1 + \frac{p_q h_q}{\left(0.5N_0 + \sum_{m=q-1}^{q+1} \alpha_{qm} p_m \right) \Gamma_{PAM}} \right) \right\rfloor, \quad q \in S_a. \tag{5.50}$$

In the OFDM context, it turns out that the strategy followed in Algorithm 3 is optimal if the cyclic prefix is long enough. If so, we can solve the discrete rate maximization problem by proceeding as Algorithm 4 indicates. It is worth emphasizing that the power budget has been doubled with respect to FBMC/OQAM. With this change FBMC/OQAM and OFDM systems

transmit the same energy except for the cyclic prefix. From (5.2) it can be deduced that the rate is formulated as

$$r_q = \log_2\left(1 + \frac{p_q h_q}{N_0 \frac{M+CP}{M}\Gamma_{QAM}}\right), \quad q \in S_a. \tag{5.51}$$

Since the transmitted symbols are drawn from the QAM constellation, bits can only be even numbers. For this reason bits are assigned to subcarriers two at a time. As a consequence, the incremental power becomes

$$\Delta_q^{j+1} = \frac{3\Gamma_{QAM} h_q 2^{r_q(j)} N_0 (M+CP)}{M h_q^2}. \tag{5.52}$$

Algorithm 4 Bit loading and power allocation in OFDM systems.

Set $\bar{S}_a = S_a$, $j = 0$
Set $p_q^0 = 0$, $r_q(0) = 0$, for $q \in S_a$
while $\sum_{q \in S_a} p_q^j \leq 2P_T$ **and** $|\bar{S}_a| \neq \emptyset$ **do**
    $j \leftarrow j + 1$
    Compute Δ_q^j for $q \in \bar{S}_a$ using (5.52)
    $l = \underset{q \in \bar{S}_a}{\operatorname{argmin}} \Delta_q^j$
    $r_l(j) = r_l(j-1) + 2$
    $p_l^j = p_l^{j-1} + \Delta_l^j$
end while
Set $p_q = p_q^j$, $r_q = r_q(j)$, for $q \in S_a$

5.3.3 Simulation results

This section evaluates the achievable sum-rate when the target SER is set to $SER_{PAM} = 0.5 \times 10^{-4}$ for all active subcarriers. We start by comparing the performance given by the proposed algorithms in a 1×2 MISO system. The system parameters and the propagation conditions that characterize the links are selected according to Scenario 3. As for the transmit processing, we consider the single-tap zero forcing transmitter devised in section 4.2.1. Since this precoding scheme is not able to completely restore the orthogonality, which is highlighted in Figure 4.2, this choice allows us to test the interference aware bit-filling algorithm described in section 5.3.1.

The plots depicted in Figure 5.8a evaluate the achievable sum-rate versus the average energy symbol to noise ratio ($\frac{E_s}{N_0}$), which is defined as $\frac{E_s}{N_0} = \frac{M+CP}{M}\frac{2P_T}{N_0}$. The achievable sum-rate in bits/multicarrier symbol is given by this expression $\sum_{q \in S_a} r_q$. The closed-form expression of r_q is

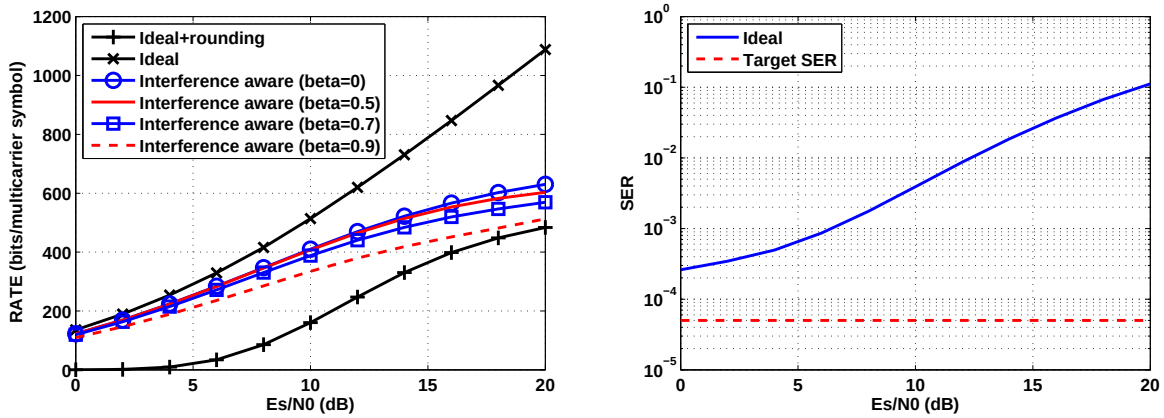

(a) Rate against $\frac{E_s}{N_0}$.

(b) SER against $\frac{E_s}{N_0}$.

Figure 5.8: Assessment of different bit-loading algorithms in FBMC/OQAM systems. System parameters are set according to the scenario 3 (see Table 2.3).

formulated in (5.33). Note that the sum-rate of the interference aware algorithm degrades as β increases. In the step 1 of the algorithm, there is a good prospect of assigning bits to subcarriers with low channel gains if β is too high. Hence, by increasing β it may happen that some subcarriers in subset S_1 are allocated power to the detriment of subcarriers belonging to S_2, which may be more efficient. In this sense, $\beta = 0.5$ and $\beta = 0.7$ offer a good trade-off between complexity reduction and rate degradation. The ideal bit-filling algorithm disregards the interference, giving rise to the least complex algorithm. However, if we want to guarantee the target SER, the achievable rate is substantially reduced when the rounding step is applied. By contrast, if no rounding operation is performed, the achievable rate is the highest. Nevertheless, it is highly likely that the QoS constrains are violated. To confirm this hypothesis, we have pictured in Figure 5.8b the average SER of the ideal bit-filling algorithm. Considering the integer bits and the power coefficients obtained after executing Algorithm 3, the metric is given by

$$SER = \frac{1}{M_a} \sum_{q \in S_a} 2Q\left(\sqrt{\frac{3p_q h_q}{(0.5N_0 + \alpha_{qq-1}p_{q-1} + \alpha_{qq}p_q + \alpha_{qq+1}p_{q+1})\,(2^{2r_q} - 1)}} \right). \tag{5.53}$$

As Figure 5.8b makes evident, the interference cannot be neglected in Scenario 3 and, therefore, the ideal bit-filling algorithm fails to achieve the target SER. As the noise is reduced, the interference becomes gradually the main source of error. As a consequence, the gap with respect to the target SER increases as the $\frac{E_s}{N_0}$ increases as well.

The comparison between FBMC/OQAM and OFDM has been made under the conditions spec-

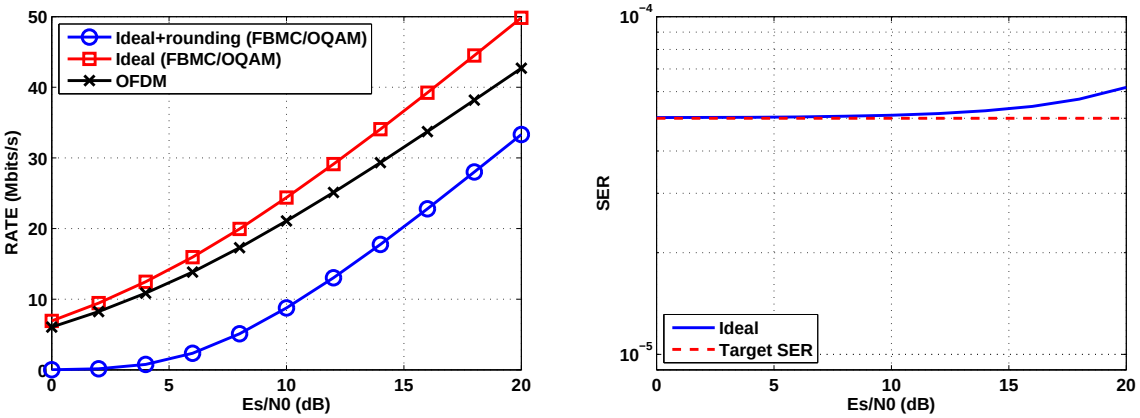

(a) Rate against $\frac{E_s}{N_0}$.

(b) SER against $\frac{E_s}{N_0}$.

Figure 5.9: Assessment of the simple bit-filling algorithm in FBMC/OQAM and OFDM systems. System parameters are set according to the scenario 1 (see Table 2.3).

ified in Scenario 1. By setting the length of the CP to $\frac{M}{8}$ samples, we guarantee that the received signal is free of IBI when OFDM is implemented. In the OFDM case, the resources are allocated as Algorithm 4 indicates. In the FBMC/OQAM counterpart, the Algorithm 3 is implemented. Under the criterion of achieving the same error rate per-dimension regardless of if OFDM or FBMC/OQAM is simulated, we impose this relation $2SER_{PAM} = SER_{QAM}$. In particular we consider these values: $SER_{PAM} = 0.5 \times 10^{-4}$ and $SER_{QAM} = 10^{-4}$. For the sake of fairness the achievable sum-rate is expressed in bits/s. Therefore, we have used expressions (5.34) and (5.35) so that the performance metrics are given by $\sum_{q \in S_a} r_q^{FBMC}$ and $\sum_{q \in S_a} r_q^{OFDM}$. It is important to recall that the cardinality of S_a is 756 and 720 in FBMC/OQAM and OFDM cases, respectively. The precoding scheme used by the FBMC/OQAM modulation in Scenario 3 remains the same in Scenario 1. In OFDM systems, the transmit processing is based on implementing the transmit Wiener filter on a per-subcarrier basis [102]. Just like happens in Scenario 1, Figure 5.9a shows that the rounding step yields a dramatic rate degradation. When Algorithm 3 is implemented, the rate of FBMC/OQAM becomes the highest. In addition, the SER plotted in Figure 5.9b turns out to be really close to the target value. This means that the residual interference is almost cancelled out. The absence of cyclic prefix and the possibility of extending the set of active carriers has lead FBMC/OQAM to outperform OFDM, mostly at high $\frac{E_s}{N_0}$.

5.4 Sum-rate maximization in the SIMO-BC

The sum-rate maximization in the downlink of a SIMO system with U users and a single BS station is studied in this section. Given the set of equalizers, this translates into assigning subcarriers to users and distributing the power among subcarriers for a given power budget. Note that in contrast to previous sections that appear in this chapter, we focus on a SIMO communication system that exclusively relies on the receive processing to combat the multipath fading. In principle, precoding techniques are more attractive than equalization because pre-processing the symbols at the transmit side does not enhance the noise. The reason for discarding the precoding schemes devised in Section 4.2 has to do with their incapability of restoring the orthogonality when adjacent subcarriers are assigned to different users. To illustrate this, imagine that subcarrier q is assigned to user $l \in \{1, ..., U\}$, while the adjacent subcarriers, which are identified with indices $q+1$ and $q-1$, are reserved for user $u \in \{1, ..., U\}$, $u \neq l$. Provided that the study case corresponded to the MISO broadcast channel depicted in Figure 5.10, the symbol that is estimated by the lth user on the qth subcarrier becomes

$$\check{d}_q^l[k] = \sum_{m=q-1}^{q+1} \sum_{\tau=-L_b-L_{g_1}}^{L_b+L_{g_2}} \Re\left(\theta_q^*[k] a_{lq} \theta_m[k-\tau] \mathbf{b}_m^H \mathbf{g}_{qm}^l[\tau]\right) d_m[k-\tau] + \Re\left(\theta_q^*[k] a_{lq} w_{lq}[k]\right) \tag{5.54}$$

with

$$\mathbf{b}_q = [b_{1q}[-L_b] \cdots b_{1q}[L_b] \cdots b_{N_T q}[-L_b] \cdots b_{N_T q}[L_b]]^T \tag{5.55}$$

$$\mathbf{g}_{qm}^l[\tau] = \left[g_{qm}^{1l}[\tau + L_b] \cdots g_{qm}^{1l}[\tau - L_b] \cdots g_{qm}^{N_T l}[\tau + L_b] \cdots g_{qm}^{N_T l}[\tau - L_b]\right]^T \tag{5.56}$$

$$g_{qm}^{il}[k] = \left(f_q^*[-n] * h_{il}[n] * f_m[n]\right)_{\downarrow \frac{M}{2}} \tag{5.57}$$

$$w_{lq}[k] = \left(f_q^*[-n] * \bar{w}_l[n]\right)_{\downarrow \frac{M}{2}}, \tag{5.58}$$

where $h_{il}[n]$ is the channel associated to the receiver l and the transmit antenna i and $\bar{w}_l[n]$ denotes the noise samples that contaminate the reception of the lth user. Using the notation of Chapter 4, equalizers $\{a_{lq}\}$ are scalars and precoders $\{b_{iq}[k]\}$ are different from 0 for $-L_b \leq k \leq L_b$. Suppose that precoders are designed according to the ZF criterion, which is detailed in Section 4.2.1, so that the pre-processing carried out on the qth subcarrier aims at confronting the channel seen by the user allocated on the qth subcarrier. Taking into account that the qth subcarrier signal is intended to user l, the precoder $b_{iq}[k]$ has to pre-cancel the frequency response of $h_{il}[n]$ in this frequency range $\left[\frac{2\pi(q-1)}{M} \quad \frac{2\pi(q+1)}{M}\right]$. Therefore, in the single-tap configuration case the ith ($1 \leq i \leq N_T$) element of $\mathbf{b}_q \in \mathbb{C}^{N_T \times 1}$ is given by

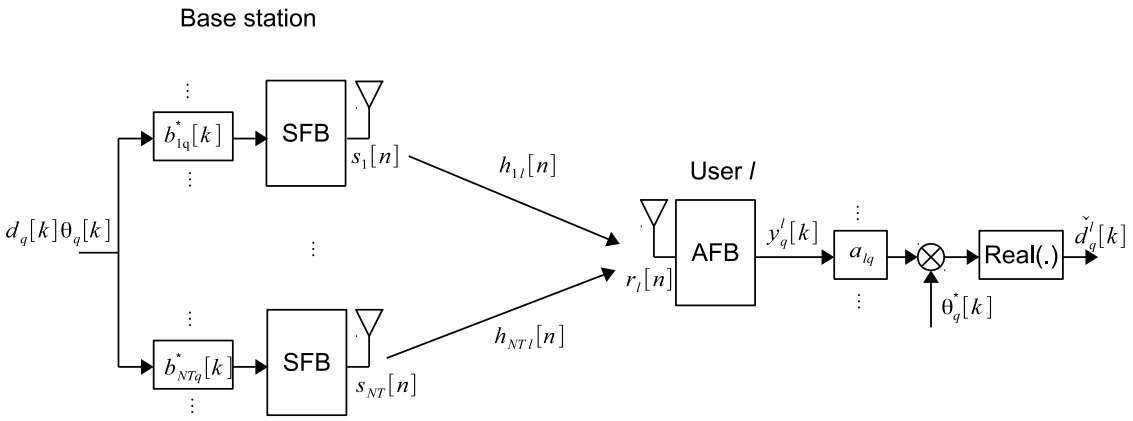

Figure 5.10: FBMC/OQAM-based MISO broadcast channel.

$$b_{iq}[0] = \sqrt{\frac{p_q}{N_T}} \frac{\left| H_{il}\left(e^{j\frac{2\pi q}{M}}\right)\right|}{H_{il}^{*}\left(e^{j\frac{2\pi q}{M}}\right)}. \tag{5.59}$$

We denote $H_{il}\left(e^{j\frac{2\pi q}{M}}\right)$ the frequency response of $h_{il}[n]$ on the radial frequency $\frac{2\pi q}{M}$. Precoders to be applied on subcarriers $q+1$ and $q-1$ can be readily derived from (5.59) knowing that the most immediate neighbors are assigned to user u. Then, we obtain

$$b_{iq-1}[0] = \sqrt{\frac{p_{q-1}}{N_T}} \frac{\left| H_{iu}\left(e^{j\frac{2\pi (q-1)}{M}}\right)\right|}{H_{iu}^{*}\left(e^{j\frac{2\pi (q-1)}{M}}\right)} \tag{5.60}$$

$$b_{iq+1}[0] = \sqrt{\frac{p_{q+1}}{N_T}} \frac{\left| H_{iu}\left(e^{j\frac{2\pi (q+1)}{M}}\right)\right|}{H_{iu}^{*}\left(e^{j\frac{2\pi (q+1)}{M}}\right)}. \tag{5.61}$$

When it comes to designing the precoder vectors we stick to the single-tap configuration for the sake of clarity, i.e. $L_b = 0$. Now, imagine that the channel is low-frequency selective so that (2.13) is satisfied. Then, the ith ($1 \leq i \leq N_T$) component of $\mathbf{g}_{qm}^{l}[\tau] \in \mathbb{C}^{N_T \times 1}$ is expressed as $g_{qm}^{il}[\tau] = \alpha_{qm}[\tau] H_{il}\left(e^{j\frac{2\pi m}{M}}\right)$. With that, (5.54) is recasted as

$$\begin{aligned}\check{d}_q^l[k] = & \sum_{\tau=-L_b-3}^{L_b+3}\sum_{i=1}^{N_T}\Re\left(\theta_q^*[k]a_{lq}\theta_q[k-\tau]\alpha_{qq}[\tau]\sqrt{\frac{p_q}{N_T}}\left|H_{il}\left(e^{j\frac{2\pi q}{M}}\right)\right|\right)d_q[k-\tau]+\\ & \sum_{\substack{m=q-1\\ m\neq q}}^{q+1}\sum_{\tau=-L_b-3}^{L_b+3}\sum_{i=1}^{N_T}\Re\left(\theta_q^*[k]a_{lq}\theta_m[k-\tau]\alpha_{qm}[\tau]\sqrt{\frac{p_m}{N_T}}\left|H_{iu}\left(e^{j\frac{2\pi m}{M}}\right)\right|\frac{H_{il}\left(e^{j\frac{2\pi m}{M}}\right)}{H_{iu}\left(e^{j\frac{2\pi m}{M}}\right)}\right)\\ & \times d_m[k-\tau]+\Re\left(\theta_q^*[k]a_{lq}w_{lq}[k]\right).\end{aligned} \tag{5.62}$$

In general, users suffer from independent multipath fading, thus $H_{iu}\left(e^{j\frac{2\pi m}{M}}\right)\neq H_{il}\left(e^{j\frac{2\pi m}{M}}\right)$. This implies that $\check{d}_q^l[k]$ in (5.62) will be affected by ICI. The analysis that has been derived reveals that the precoding strategies introduced in Section 4.2 cannot be applied in the BC if adjacent subcarriers are likely to be allocated to different users. We can only benefit from the transmit signal processing techniques addressed in Section 4.2 if subcarriers are assigned to users in a block-wise fashion. Then, leaving empty some subcarriers between blocks we would ensure that adjacent subcarriers are assigned to the same user. This strategy avoids ICI but does not exploit user diversity. Conversely, if the channel is confronted at the receive side we can benefit from user diversity. To prove it we also consider that subcarrier q is assigned to user $l\in\{1,...,U\}$, while adjacent subcarriers are given to user $u\in\{1,...,U\}$, $u\neq l$. When the complexity burden is placed at the receiver, the symbol to be estimated on the qth subcarrier is written as

$$\check{d}_q^l[k]=\sum_{m=q-1}^{q+1}\sum_{\tau=-L_a-L_{g_1}}^{L_a+L_{g_2}}\Re\left(\theta_q^*[k]\theta_m[k-\tau]\sqrt{p_m}\mathbf{a}_{lq}^H\mathbf{g}_{qm}^l[\tau]\right)d_m[k-\tau]+\Re\left(\theta_q^*[k]\mathbf{a}_{lq}^H\mathbf{w}_{lq}[k]\right) \tag{5.63}$$

with

$$\mathbf{a}_{lq}=\left[a_{lq}^1[-L_a]\cdots a_{lq}^1[L_a]\cdots a_{lq}^{N_R}[-L_a]\cdots a_{lq}^{N_R}[L_a]\right]^T \tag{5.64}$$

$$\mathbf{g}_{qm}^l[\tau]=\left[g_{qm}^{1l}[\tau+L_a]\cdots g_{qm}^{1l}[\tau-L_a]\cdots g_{qm}^{N_Rl}[\tau+L_a]\cdots g_{qm}^{N_Rl}[\tau-L_a]\right]^T \tag{5.65}$$

$$g_{qm}^{jl}[k]=\left(f_q^*[-n]*h_{jl}[n]*f_m[n]\right)_{\downarrow\frac{M}{2}} \tag{5.66}$$

$$\mathbf{w}_{lq}[k]=\left[w_{lq}^1[k+L_a]\cdots w_{lq}^1[k-L_a]\cdots w_{lq}^{N_R}[k+L_a]\cdots w_{lq}^{N_R}[k-L_a]\right]^T \tag{5.67}$$

$$w_{lq}^j[k]=\left(f_q^*[-n]*\bar{w}_l^j[n]\right)_{\downarrow\frac{M}{2}}. \tag{5.68}$$

Note that (5.63) corresponds to the SIMO communication system represented in Figure 5.11. The parameter L_a indicates that equalizers $\left\{a_{lq}^j[k]\right\}$ are different from zero for $-L_a\leq k\leq L_a$.

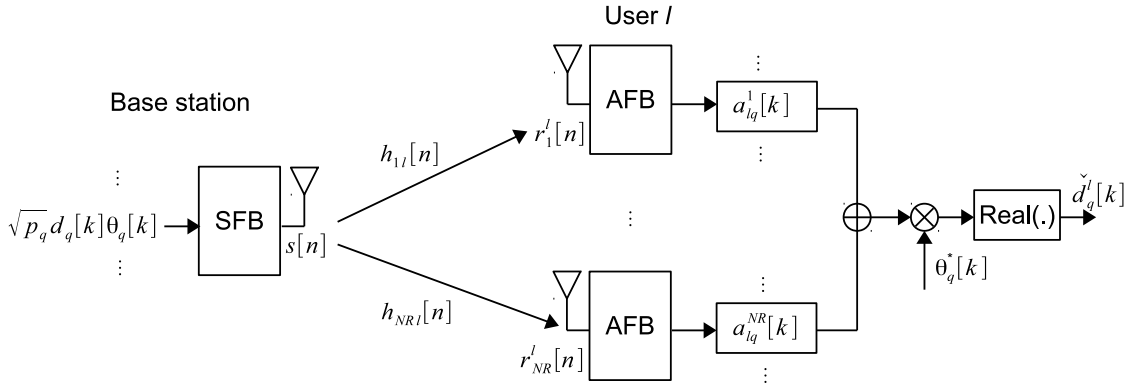

Figure 5.11: FBMC/OQAM-based SIMO broadcast channel.

The term $\bar{w}_l^j[n]$ in (5.68) accounts for the sequence of noise that contaminates the reception of the lth user in the jth receiver chain. For the ease of the analytical tractability, the equalizer is also designed following the zero forcing approach using a single tap per-antenna, i.e. $L_a = 0$. Thus the jth element ($1 \leq j \leq N_R$) is given by

$$a_{lq}^j[0] = \frac{\left|H_{jl}\left(e^{j\frac{2\pi q}{M}}\right)\right|}{H_{jl}^*\left(e^{j\frac{2\pi q}{M}}\right)}. \tag{5.69}$$

Let $H_{jl}\left(e^{j\frac{2\pi q}{M}}\right)$ be the value that the frequency response of $h_{jl}[n]$ takes in the radial frequency $\frac{2\pi q}{M}$. Now, assume that the equivalent channel fulfils (2.14). Then, $g_{qm}^{jl}[\tau] = \alpha_{qm}[\tau]H_{jl}\left(e^{j\frac{2\pi q}{M}}\right)$. Bearing these assumptions in mind, we can expand (5.63) as follows:

$$\begin{aligned}\check{d}_q^l[k] = & \sum_{m=q-1}^{q+1}\sum_{\tau=-L_b-3}^{L_b+3}\sum_{j=1}^{N_R}\Re\left(\theta_q^*[k]\theta_m[k-\tau]\alpha_{qm}[\tau]\sqrt{p_m}\left|H_{jl}\left(e^{j\frac{2\pi q}{M}}\right)\right|\right)d_m[k-\tau] \\ & +\Re\left(\theta_q^*[k]\mathbf{a}_{lq}^H\mathbf{w}_{lq}[k]\right) \\ = & \sum_{j=1}^{N_R}\Re\left(\sqrt{p_q}\left|H_{jl}\left(e^{j\frac{2\pi q}{M}}\right)\right|\right)d_q[k] + \Re\left(\theta_q^*[k]\mathbf{a}_{lq}^H\mathbf{w}_{lq}[k]\right).\end{aligned} \tag{5.70}$$

The second equality follows from the values of $\{\alpha_{qm}[\tau]\}$, which are gathered in Table 2.1 and Table 2.2. The study case that results in (5.70) confirms that if the receive signal processing techniques perfectly equalize the channel, then adjacent subcarriers do not need to be assigned to the same user to avoid ICI. This justifies why we have favoured SIMO architectures. Having said that, the algorithms derived in the following will hinge on this expression

$$\begin{aligned}\check{d}_q^{u(q)}[k] = & \sum_{m=q-1}^{q+1} \sum_{\tau=-L_a-L_{g_1}}^{L_a+L_{g_2}} \Re\left(\theta_q^*[k]\theta_m[k-\tau]\sqrt{p_m}\mathbf{a}_{u(q)q}^H \mathbf{g}_{qm}^{u(q)}[\tau]\right) d_m[k-\tau] \\ & + \Re\left(\theta_q^*[k]\mathbf{a}_{u(q)q}^H \mathbf{w}_{u(q)q}[k]\right),\end{aligned} \tag{5.71}$$

where $u(q) \in \{1, ..., U\}$ unambiguously indicates the user that is allocated on the qth subcarrier, assuming that there are U users connected to the BS. Then, the rate in bits/symbols can be expressed as

$$r_q = \frac{1}{2}\log_2\left(1 + SINR_q^{u(q)}\right), \quad q \in S_a, \quad 1 \leq u(q) \leq U \tag{5.72}$$

with

$$SINR_q^{u(q)} = \frac{h_q^{u(q)} p_q}{\alpha_{qq-1}^{u(q)} p_{q-1} + \alpha_{qq}^{u(q)} p_q + \alpha_{qq+1}^{u(q)} p_{q+1} + \sigma_{u(q)q}^2}. \tag{5.73}$$

$$h_q^{u(q)} = \left|\Re\left(\mathbf{a}_{u(q)q}^H \mathbf{g}_{qq}^{u(q)}[0]\right)\right|^2 \tag{5.74}$$

$$\alpha_{qm}^{u(q)} = \sum_{\tau=-L_a-L_{g_1}}^{L_a+L_{g_2}} \left|\Re\left(\theta_q^*[k]\theta_m[k-\tau]\mathbf{a}_{u(q)q}^H \mathbf{g}_{qm}^{u(q)}[\tau]\right)\right|^2, \quad m \neq q \tag{5.75}$$

$$\alpha_{qq}^{u(q)} = \sum_{\substack{\tau=-L_a-L_{g_1} \\ \tau\neq 0}}^{L_a+L_{g_2}} \left|\Re\left(\theta_q^*[k]\theta_q[k-\tau]\mathbf{a}_{u(q)q}^H \mathbf{g}_{qq}^{u(q)}[\tau]\right)\right|^2 \tag{5.76}$$

$$\begin{aligned}\sigma_{u(q)q}^2 &= \mathbb{E}\left\{\left|\Re\left(\theta_q^*[k]\mathbf{a}_{u(q)q}^H \mathbf{w}_{u(q)q}[k]\right)\right|^2\right\} \\ &= \left[\Re\left(\theta_q[k]\mathbf{a}_{u(q)q}^T\right) \quad \Im\left(\theta_q[k]\mathbf{a}_{u(q)q}^T\right)\right] \mathbf{R}_q \left[\Re\left(\theta_q[k]\mathbf{a}_{u(q)q}^T\right) \quad \Im\left(\theta_q[k]\mathbf{a}_{u(q)q}^T\right)\right]^T.\end{aligned} \tag{5.77}$$

Symbols are assumed to be independent, i.e. $\mathbb{E}\{d_q[k]d_m[n]\} = \delta_{q,m}\delta_{k,n}$. The noise autocorrelation matrix $\mathbf{R}_q$ is defined in Appendix 3.A. Similarly to Sections 5.2 and 5.3, the Gausssian distribution of the interference plus noise term is assumed when formulating the rate. Bearing in mind the multi-user system model, the optimal resource allocation is derived by solving

$$\begin{aligned}&\mathrm{P}: \underset{\{p_q, u(q)\}}{\operatorname{argmax}} \sum_{q\in S_a} r_q \\ &s.t. \sum_{q\in S_a} p_q \leq P_T, \quad p_q \geq 0, \quad u(q) \in \{1, ..., U\}, \quad q \in S_a.\end{aligned} \tag{5.78}$$

Note that for fixed user allocation, (5.78) coincides with (5.13). In the absence of ICI and ISI the optimal subcarrier allocation strategy on a given subband stems from choosing the user who presents the highest SNR [123]. Nevertheless, this section focuses on a more challenging scenario where ICI and ISI terms are not negligible. In this regard, the original problem that jointly designs p_q and $u(q)$ is not convex. In order to overcome this hurdle we propose a suboptimal strategy consisting in partitioning the band into three subsets, followed by a sequential optimization over these subsets. The key issue relies on the fact that subcarrier signals gathered in the same subset do not overlap in the frequency domain. To this end we adopt the partitioning strategy proposed in Section 5.2, which is depicted in Figure 5.4. Provided that the number of active carriers is a multiple of four, the subsets are defined as $S_1 = \{S_a(0), S_a(2), ..., S_a(M_a - 2)\}$, $S_2 = \{S_a(1), S_a(5), ..., S_a(M_a - 3)\}$ and $S_3 = \{S_a(3), S_a(7), ..., S_a(M_a - 1)\}$. By contrast, if M_a is not a multiple of four, the subsets are given by $S_1 = \{S_a(0), S_a(2), ..., S_a(M_a - 2)\}$, $S_2 = \{S_a(1), S_a(5), ..., S_a(M_a - 1)\}$ and $S_3 = \{S_a(3), S_a(7), ..., S_a(M_a - 3)\}$. The ith element of the set S_a, which indicates those subcarriers that are active, is denoted $S_a(i)$.

The problem Pi, which is associated to Si, is given by

$$\begin{aligned} &\text{Pi} : \underset{\{p_q, u(q)\}}{\text{argmax}} \sum_{q \in S_i} r_q \\ &s.t. \sum_{q \in S_i} p_q \leq P_{Ti}, \quad p_q \geq 0, \quad u(q) \in \{1, ..., U\}, \quad q \in S_i. \end{aligned} \tag{5.79}$$

Note that splitting the original problem into three subproblems also entails partitioning the power budget. Therefore, it has to be satisfied that $P_{T1} + P_{T2} + P_{T3} = P_T$. Since problems are executed sequentially, when solving Pi the interference that comes from the subcarriers belonging to S_j (j<i) are treated as noise and that from S_l (l>i) is non-existing because these subsets have not been processed yet.

It is worth mentioning that (5.79) can be solved resorting to the dual optimization framework [124]. Aiming at reducing the complexity we decouple the subcarrier and the power allocation problems. In this sense, we first associate the subcarriers collected in S_1 to users and then the power is distributed among S_1. Subsequently we proceed exactly in S_2 and finally in S_3.

5.4.1 Step 1

By starting, users are assigned to the subcarriers that belong to S_1 and then, the power is distributed to maximize the sum-rate. When subcarriers that belong to S_2 and S_3 have not been loaded, the subcarrier allocation problem is posed as follows:

$$u(q) = \underset{\{1\leq j\leq U\}}{\text{argmax}} \frac{1}{2}\log_2\left(1+\frac{p_q h_q^j}{p_q\alpha_{qq}^j+\sigma_{jq}^2}\right), \quad q\in S_1. \tag{5.80}$$

Since the rate is increasing in p_q, the piecewise maximization in (5.80) is equivalent to

$$u(q) = \underset{\{1\leq j\leq U\}}{\text{argmax}} \left(\frac{p_q h_q^j}{p_q\alpha_{qq}^j+\sigma_{jq}^2}\right), \quad q\in S_1. \tag{5.81}$$

Note that the selection depends on the power to be allocated. This highlights that some assumptions have to be made as for the power coefficients. The strategy that has been followed to solve (5.81) is detailed in 5.E.

Once the subcarrier assignment is addressed, the power allocation is computed by solving

$$\begin{aligned} &\underset{\{p_q\}}{\text{argmax}} \sum_{q\in S_1} \frac{1}{2}\log_2\left(1+\frac{p_q h_q^{u(q)}}{p_q\alpha_{qq}^{u(q)}+\sigma_{u(q)q}^2}\right) \\ &s.t. \sum_{q\in S_1} p_q \leq P_{T1}, \quad p_q\geq 0, \quad q\in S_1. \end{aligned} \tag{5.82}$$

Notice that (5.82) is a concave maximization problem, thus there exists a global optimal point that can be found. The Algorithm that has been used to solve (5.82) is described in Appendix 5.B. Alternatively, we may allocate the power according to the UPA strategy, i.e. $p_q = P_{T1}/|S_1|$ $(q\in S_1)$.

5.4.2 Step 2

In the second step, the variables that are optimized in P1 are fixed. Treating the ICI terms as noise gives rise to the following problem

$$u(q) = \underset{\{1\leq j\leq U\}}{\text{argmax}} \left(\frac{p_q h_q^j}{p_q\alpha_{qq}^j+W_q^j}\right), \quad q\in S_2, \tag{5.83}$$

where

$$W_q^j = \sigma_{jq}^2 + p_{q-1}\alpha_{qq-1}^j + p_{q+1}\alpha_{qq+1}^j, \quad \{q-1, q+1\}\in S_1. \tag{5.84}$$

Once interference is updated, the problem (5.83) is solved as (5.81). Next, the sum-rate maximization problem is exactly the same that is analysed in Section 5.2.2. This observation highlights that any of the two alternatives described therein are valid to distribute the power. Since the alternative 2 is not so demanding in terms of complexity as the alternative 1, we propose to distribute the power among subcarriers by solving

$$\begin{aligned} &\underset{\{p_q\}}{\operatorname{argmax}} \sum_{q\in S_2} \frac{1}{2}\log_2\left(1+\frac{p_q h_q^{u(q)}}{p_q \alpha_{qq}^{u(q)}+W_q^{u(q)}}\right) \\ &s.t. \sum_{q\in S_2} p_q \le P_{T2}, \quad p_q \ge 0, \quad q\in S_2. \end{aligned} \tag{5.85}$$

Problem (5.85) is tackled in the same manner as problem (5.82). However, we have to perform one additional step to prevent the rate of already loaded subcarriers from degrading too much. Following the same steps described in Section 5.2.2, we check for all $q \in S_2$ if $SR_q(p_q) < SR_q(0)$, where $\{p_q\}$ are the power coefficients that maximize the cost function in (5.85) and

$$SR_q(p_q) = \sum_{\substack{m=q-1 \\ m\neq q}}^{q+1} \frac{1}{2}\log_2\left(1+\frac{h_m^{u(m)} p_m}{0.5N_0+\alpha_{mm}^{u(m)} p_m+\alpha_{mq}^{u(m)} p_q}\right) + \frac{1}{2}\log_2\left(1+\frac{h_q^{u(q)} p_q}{W_q^{u(q)}+\alpha_{qq}^{u(q)} p_q}\right). \tag{5.86}$$

If $SR_q(p_q) < SR_q(0)$, the amount of power allocated on the qth subcarrier is given by $\Delta_q^{i_q}$, where the index i_q is obtained from this piecewise maximization

$$i_q = \underset{0\le i\le N_q}{\operatorname{argmax}}\, SR_q(\Delta_q^i), \tag{5.87}$$

with

$$\Delta_q^i = \frac{\left(2^{2i}-1\right) W_q^{u(q)}}{h_q^{u(q)} - \alpha_{qq}^{u(q)}\left(2^{2i}-1\right)} \tag{5.88}$$

$$N_q = \left\lfloor \frac{1}{2}\log_2\left(1+\frac{h_q^{u(q)} p_q}{\alpha_{qq}^{u(q)} p_q + W_q^{u(q)}}\right)\right\rfloor. \tag{5.89}$$

5.4.3 Step 3

Before addressing the third subset, the interference is updated according to the power coefficients calculated in steps 1 and 2. Then, we proceed similarly to step 2. That is, we first solve

$$u(q) = \underset{\{1\le j\le U\}}{\operatorname{argmax}} \left(\frac{p_q h_q^j}{p_q \alpha_{qq}^j + W_q^j}\right), \quad q\in S_3, \tag{5.90}$$

where

$$W_q^j = \sigma_{jq}^2 + p_{q-1}\alpha_{qq-1}^j + p_{q+1}\alpha_{qq+1}^j, \quad \{q-1, q+1\} \in S_1. \tag{5.91}$$

Finally, the remaining power coefficients are computed by solving this maximization problem

$$\begin{aligned} &\underset{\{p_q\}}{\operatorname{argmax}} \sum_{q\in S_3} \frac{1}{2}\log_2\left(1+\frac{p_q h_q^{u(q)}}{p_q \alpha_{qq}^{u(q)} + W_q^{u(q)}}\right) \\ &s.t. \sum_{q\in S_3} p_q \le P_{T3}, \quad p_q \ge 0, \quad q \in S_3. \end{aligned} \tag{5.92}$$

Given

$$SR_q(p_q) = \sum_{m=q-1}^{q+1} \frac{1}{2}\log_2\left(1+\frac{h_m^{u(m)} p_m}{\sigma^2_{u(m)m} + \sum_{l=m-1}^{m+1} p_l \alpha_{ml}^{u(m)}}\right), \tag{5.93}$$

we verify if this is satsified $SR_q(p_q) < SR_q(0)$ for $q \in S_3$. If so, the new power loaded on the qth subcarrier is $\Delta_q^{i_q}$, where

$$i_q = \underset{0\le i\le N_q}{\operatorname{argmax}}\, SR_q(\Delta_q^i) \tag{5.94}$$

$$\Delta_q^i = \frac{\left(2^{2i}-1\right) W_q^{u(q)}}{h_q^{u(q)} - \alpha_{qq}^{u(q)}\left(2^{2i}-1\right)}. \tag{5.95}$$

$$N_q = \left\lfloor \frac{1}{2}\log_2\left(1+\frac{h_q^{u(q)} p_q}{\alpha_{qq}^{u(q)} p_q + W_q^{u(q)}}\right)\right\rfloor. \tag{5.96}$$

5.4.4 Simulation results

In this section we evaluate the sum-rate in the BC when the FBMC/OQAM transmultiplexer is implemented. The system that is simulated corresponds to the block diagram depicted in (5.11) with $N_R = 2$. The proposed techniques assume that the subcarrier spacing and propagation conditions are such that the residual ISI and ICI terms cannot be ignored. For this reason we initially run the simulations under the conditions that give rise to Scenario 3. The post-processing carried out by the equalization stage is given by the single-tap ZF that is formulated in (5.69).

Two variants of the proposed three-step approach are assessed. In the first one, subcarriers that belong to a given set are initially assigned to users by evaluating the SINR funtion and proceeding as Appendix 5.E details. Then, the optimal power allocation (OPA) is performed by solving (5.82),(5.85) and (5.92). This technique is identified as MaxSINR+OPA. As for the second option, subcarriers are assigned to users in the same manner as it is done in the MaxSINR+OPA

technique. The difference lies in the fact that the power is equally split among subcarriers yielding a uniform power allocation. Hence, we spare ourselves the effort of solving (5.82),(5.85) and (5.92). In view of this, the second strategy is called MaxSINR+UPA. In both alternatives, we evaluate the sum-rate formulated in (5.86) and (5.93) to determine if the rate on already allocated subcarriers is not degraded too much. If so, we proceed as Sections 5.4.2 and 5.4.3 detail. Regarding how the power budget is split among subsets we have fixed $P_{T1} = P_T/2$ and $P_{T2} = P_{T3} = P_T/4$. We stick to this configuration based on the results obtained in the Section 5.2.4, which confirms that splitting the power in this way gives satisfactory results and outperforms other configurations.

The first benchmark to compare with is also based on the proposed three-step approach. However, (5.79) is not decoupled into two problems at each step but it is solved in a Lagrange-dual way, [124]. Once (5.79) is solved in subsets S_2 and S_3, we check if the rate degradation on subcarriers belonging to S_1 is too much. If so, we proceed similarly to techniques MaxSINR+OPA and MaxSINR+UPA. The second benchmark refrains from resorting to the three-step approach and instead assigns subcarriers to users by evaluating the SNR as in OFDM, [123]. Next the power loading strategy is driven by this optimization procedure

$$\begin{aligned} &\underset{\{p_q\}}{\operatorname{argmax}} \sum_{q\in S_a} \frac{1}{2}\log_2\left(1+\frac{p_q h_q^{u(q)}}{\sum\limits_{m=q-1}^{q+1} p_m \alpha_{qm}^{u(q)} + \sigma_{u(q)q}^2}\right) \\ &s.t. \sum_{q\in S_a} p_q \leq P_T, \quad p_q \geq 0, \quad q \in S_a. \end{aligned} \tag{5.97}$$

Unlike OFDM, the rate maximization in FBMC/OQAM is not convex due to ICI. However, the objective function in (5.97) can be interpreted as a difference of concave functions (DC), which enables using branch and bounds methods to obtain the global optimal solution, [115]. The suboptimal strategy presented in [119] enables achieving a large portion of the maximum sum-rate with a reduced complexity. Considering the description of the second benchmark, we will refer to it as MaxSNR+DC from here onwards.

The curves of Figure 5.12a show the system performance in terms of sum-rate having fixed the number of users to four, i.e. $U = 4$. The sum-rate is given by this summation $\sum_{q\in S_a} r_q$ and it is computed for different average energy symbol to noise ratio values, which is defined as $\frac{E_s}{N_0} = \frac{M+CP}{M}\frac{2P_T}{MN_0}$. The factor 2 in the numerator accounts for the average energy per QAM symbol. Thus, the components that are delayed half the symbol period have unit energy as it has been assumed in Section 5.4. Note that the plots of the MaxSINR+UPA, MaxSINR+OPA and Lagrange-dual virtually coincide. However, the most interesting result is that the proposed solutions clearly

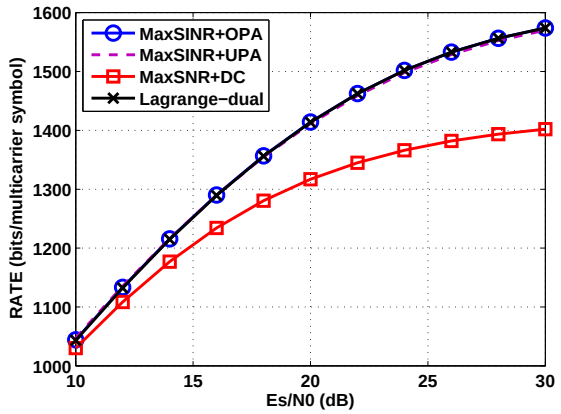

(a) Rate against $\frac{E_s}{N_0}$ fixing $P_T = 1W$ and $U = 4$.

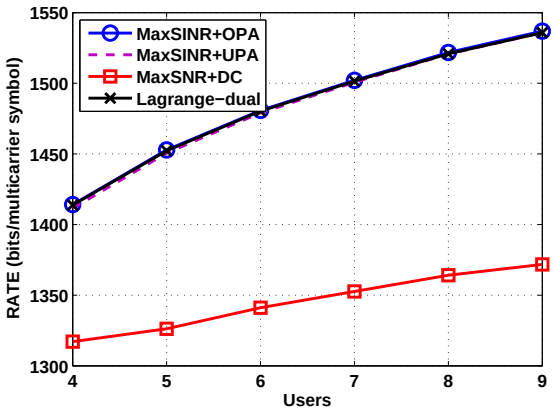

(b) Rate against the number of users fixing $P_T = 1W$ and $\frac{E_s}{N_0}$=20 dB.

Figure 5.12: Evaluation of the sum-rate in the FBMC/OQAM-based 2×1 SIMO broadcast channel. Different power and subcarrier allocation strategies are simulated. System parameters are set according to the scenario 3 (see Table 2.3).

outperform the MaxSNR+DC at the low noise regime. In Figure 5.12b we investigate the impact of the user diversity when $\frac{E_s}{N_0}$=20 dB. As expected the more users are present in the coverage area the higher the rate is. Again MaxSINR+UPA, MaxSINR+OPA and Lagrange-dual techniques nearly give the same performance. Thus, we can conclude that separating the subcarrier and the power allocation results in a marginal rate degradation. Furthermore, the strategy of equally distributing the power performs close to the OPA. Therefore, the solution provided by the MaxSINR+UPA technique becomes the most attractive strategy.

In Figure 5.13 we have computed the sum-rate that is achieved by FBMC/OQAM and OFDM schemes in the BC. It must be highlighted that the proposed subcarrier and power allocation strategies can only be implemented on multicarrier systems where ICI comes at most from the adjacent subcarriers. The slow spectral decay that characterizes the subcarrier signals in OFDM systems prevents us from adapting the three-step approach to OFDM systems when the length of the CP is insufficient. Therefore, the comparison has been made with the system parameters of Scenario 1 so that signals demodulated by the OFDM receiver are free of interference. Then, both in OFDM and FBMC/OQAM systems, subcarriers are assigned to users and power is distributed over subcarriers via the two-step approach described in [123]. While the subcarrier assignment relies on the SNR metric, the power is allocated by following UPA and WF policies [114]. Hence, when distributing the power in the FBMC/OQAM case, it is assumed that the equalizer formulated in (5.69) is able to perfectly restore the orthogonality. These two strategies are identified in the figures with these two acronyms SNR+UPA and SNR+WF. As for the receive processing in the

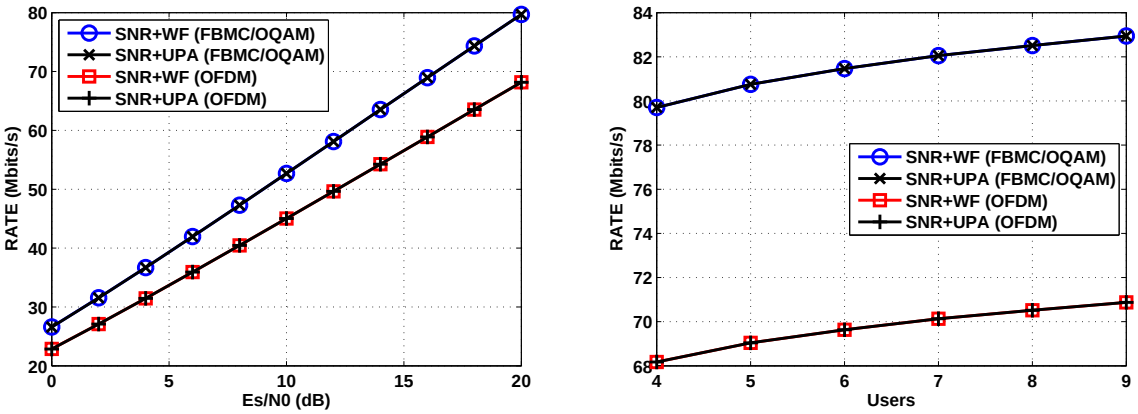

(a) Rate against $\frac{E_s}{N_0}$ fixing $P_T = 1W$ and $U = 4$.

(b) Rate against the number of users fixing $P_T = 1W$ and $\frac{E_s}{N_0}$=20 dB.

Figure 5.13: Evaluation of the sum-rate in the 2×1 SIMO broadcast channel. The FBMC/OQAM and the OFDM modulation schemes are evaluated when the subcarrier allocation is based on the SNR metric and the power is distributed according to WF and UPA policies. System parameters are set according to the scenario 1 (see Table 2.3).

OFDM context, the equalizer is designed according to the MMSE criterion resulting in this vector

$$\mathbf{a}_{lq} = \left(\mathbf{H}_{lq} \mathbf{H}_{lq}^H + \frac{M + CP}{M} N_0 \mathbf{I}_{N_R} \right)^{-1} \mathbf{H}_{lq}, \tag{5.98}$$

where

$$\mathbf{H}_{lq} = \left[H_{1l} \left(e^{j\frac{2\pi}{M}q} \right) \cdots H_{N_R l} \left(e^{j\frac{2\pi}{M}q} \right) \right]^T. \tag{5.99}$$

For the sake of fairness the sum-rate is expressed in terms of bits/s. As a consequence, the metric displayed in Figure 5.13 is given by $\frac{f_s}{M + CP} \sum_{q \in S_a} r_q$. Note that in the FBMC/OQAM case $CP = 0$, while in the OFDM scheme $CP = \frac{M}{8}$. In addition the set S_a, which collects the indices of the active carriers, is different in FBMC/OQAM and OFDM modulation schemes as Section 2.3.1 indicates. As Figure 5.13 pictures, FBMC/OQAM clearly outperforms OFDM mostly at high $\frac{E_s}{N_0}$. The possibility of extending the set of active carriers and the absence of the CP are the attributes that bring about the gain when FBMC/OQAM is used. As in Figure 5.12, the UPA strategy arises as the best solution because achieves competitive results with the lowest computational complexity.

5.5 Chapter summary

The benefits that can be enjoyed in FBMC/OQAM systems if CSI is available at the transmit side have been shown in Chapter 4. Therein, the precoding design is investigated. This chapter further studies the advantages of knowing the state of the channel at transmission. In particular, the effort has been put into the design of power allocation algorithms. The first problem that has been analyzed is the optimization of the power distribution so that the minimum SINR in the whole frequency band is maximized. In this case the attention is centred on point-to-point communications for MISO channels. At the optimal point all the SINRs are the same and, therefore, the power coefficients balance the SINRs. For complexity reasons, precoders are given beforehand and only the power distribution is optimized. If the design of precoders is governed by the SLNR, the max-min problem can be solved with a reduced complexity if noise is considered the dominant source of error. It has been demonstrated that regardless of the frequency selectivity of the channel, the approach based on neglecting the residual interference yields no degradation. In OFDM, the problem of maximizing the minimum SINR has also been tackled having set the precoders according to the transmit Wiener filter approach. When OFDM is confronted with FBMC/OQAM, the BER remains the same if the channel is low frequency selective. Conversely, the lowest BER is achieved by the FBMC/OQAM modulation scheme when the channel frequency response is not flat at the subcarrier level.

The second study case delves into the rate maximization problem for FBMC/OQAM-based MISO channels. Given the precoders, the most general case has been considered. That is, the pre-processing stage is not able to restore the orthogonality at reception. Hence, the conventional WF solution is not the best choice to determine the power loaded on each subcarrier since ICI and ISI are present. This brings a non-concave maximization problem that can be interpreted as the maximization of a difference of concave functions. This reformulation allows us to use DC programming to find the global optimal but the complexity becomes unaffordable when the number of subcarriers is large. Aiming at reducing the complexity we have devised a new suboptimal algorithm. The idea consists in smartly partitioning the frequency band into three subsets so that subcarrier signals belonging to the same subset do not overlap in the frequency domain. If subsets maximize sequentially their own rate the original problem is turned into three simpler problems. It must be underlined that we have followed an unselfish approach when allocating the power. That is, the power loaded on a given subcarrier takes into account the interference that leaks through adjacent subcarriers. Although the proposed solution is suboptimal, it outperforms the UPA and the WF solution in terms of rate at low noise regime. When the estimated symbols are free of interference, the achievable rate in FBMC/OQAM systems is substantially higher than that achieved in OFDM systems. The explanation comes from the fact that in FBMC/OQAM systems

no CP is transmitted as well as the number of active carriers can be extended without violating the spectral mask.

In the third study case the rate maximization problem in FBMC/OQAM systems for point-to-point communications has been revisited imposing QoS and integer-bit constraints. In other words, the problem consists in maximizing the discrete rate for a given power budget while the SER should not exceed a given threshold. The approach that has been followed relies on an iterative bit-filling algorithm. The analysis conducted in this chapter reveals that if precoders do not maintain the orthogonality between subcarrier when signals are demodulated, then some bit distributions should be prohibited. Otherwise the algorithm may diverge. Aiming at avoiding this situation along with reducing the complexity we have devised a novel suboptimal approach, which ensures the convergence. Simulation-based results have shown that under highly frequency selective channels if interference is ignored, then the QoS dramatically degrades. By contrast, if the channel frequency response is flat at least in the frequency range of one subchannel, then the interference incurred by the channel can be omitted while the target SER is preserved. This is very relevant because the complexity required to design power and bit distributions can be substantially alleviated in case symbols are only contaminated by noise. If so, the resulting bit distribution leads to a sum-rate that is higher in FBMC/OQAM than in OFDM. The reason again is related to the number of active carriers and the overhead that represents the CP transmission.

With the objective of maximizing the sum-rate, the last part of this chapter tackles the subcarrier and the power allocation problems for the downlink of multiuser FBMC/OQAM transmission. By using a toy example we have illustrated that if adjacent subcarriers are assigned to different users, then the interference can be more effectively removed when the channel is counteracted at the receive side. For this reason, the utilization of precoding techniques has been discarded. Since the multipath fading is exclusively combated by resorting to equalization techniques, we have focused on the FBMC/OQAM-based SIMO broadcast channel. Given the post-processing techniques that will be applied at the receive side, we have concentrated on devising user selection and power allocation algorithms assuming that there is ISI and ICI. This indicates that the complexity of jointly optimizing the subcarrier assignment and the power allocation may render the solution impractical. As a solution, the band is partitioned into three subsets so that there is no overlapping between the subcarriers of the same subset. Then we propose a low complexity heuristic to carry out the resource allocation over each subset. The key aspects that allow us to reduce the complexity stem from the fact that subsets are sequentially treated. In addition, the algorithm that is executed on each subset separately addresses the subcarrier assignment and the power loading. When allocating the power it has been taken into account that the more power is assigned to a given subcarrier, the higher is the rate on the subcarrier of interest and the lower is the rate on the adjacent subcarriers. Simulation-based results allow us to conclude that the performance in terms of rate strongly relies

on the subcarrier allocation. On the contrary, whether the subcarrier and the power allocation are jointly or independently optimized has a marginal impact on the rate. In this sense the proposed user selection that hinges on the evaluation of the SINR function gives better performance than alternative strategies that are governed by the SNR. When the channel is low frequency selective, equalizers succeed in restoring the orthogonality and the SINR turns out to be very close to the SNR. As a consequence, the resource allocation algorithms used in OFDM systems can be also used in the FBMC/OQAM context. In this case, the highest rate is achieved by the FBMC/OQAM modulation scheme since no redundancy is transmitted and the number of active carriers can be extended.

Appendices

5.A Solution of problem 5.1

Regarding the max-min problem it can be solved by carrying out the singular value decomposition (SVD) of matrix Γ, which is defined as

$$\Gamma = \begin{bmatrix} \mathbf{D}\Psi & (0.5N_0)\,\mathbf{D}\mathbf{1}_{M_a} \\ (1/P_T)\,\mathbf{1}_{M_a}^T\mathbf{D}\Psi & (0.5N_0/P_T)\,\mathbf{1}_{M_a}^T\mathbf{D}\mathbf{1}_{M_a} \end{bmatrix}, \tag{5.100}$$

where

$$\mathbf{D} = \text{diag}\left\{\frac{1}{h_{S_a(0)}}, \cdots, \frac{1}{h_{S_a(M_a-1)}}\right\}. \tag{5.101}$$

Matrix Ψ is defined in (4.45). Let $S_a(i)$ denote the ith element of S_a, which gathers the indices of those subcarriers that are active. The elements of vector $\mathbf{1}_{M_a} \in \mathbb{R}^{M_a \times 1}$ are all identical and equal to one. The solution of (5.1) can be computed from the singular vector associated to the maximum singular value of matrix Γ, [106].

5.B Solution of problem 5.16

The proposed algorithm to solve (5.16) hinges on the dual optimization framework because it poses a problem that it is easier to solve. In (5.16) the objective function and the constraint are concave and convex, respectively, thus the duality gap is zero. In this sense, the power allocation strategy on subset S_1 boils down to solve the dual problem, which is convex. In this regard we formulate the dual function as

$$\begin{aligned} g(\lambda) &= \max_{\{p_q\}} \sum_{q \in S_1} r_q + \lambda \left(\frac{P_T}{\beta} - \sum_{q \in S_1} p_q \right) \\ s.t.\ \ & p_q \geq 0. \end{aligned} \tag{5.102}$$

Finally we express the dual problem in the form

$$\begin{aligned} \text{DP1} : \min_{\lambda} \quad & g(\lambda) \\ s.t.\ \ & \lambda \geq 0. \end{aligned} \tag{5.103}$$

We have opted to solving DP1 similarly to the approach followed in [125], which consists in carrying out an iterative subgradient method since the dual function might not be differentiable. As [110] describes, at each iteration problem (5.102) is solved for a fixed λ and next the dual variable is updated by evaluating the subgradient of $g(\lambda)$. The value of the subgradient allows us to bisect the interval where λ is localized. In order to ensure a fast convergence the algorithm stops when at least 95% of the power is assigned and the total power constraint is not violated. In most of the cases this entails doing less than 10 iterations. The method operates as Algorithm 5 describes.

Algorithm 5 Rate maximization.

1: Set l=λ_{min}, u=λ_{max}
2: **repeat**
3: $\lambda = 0.5(l + u)$
4: evaluate $\partial g(\lambda) = \dfrac{P_T}{\beta} - \sum_{q \in S_1} p_q^*$
5: **if** $\partial g(\lambda) < 0$ **then**
6: l=λ
7: **else**
8: u=λ
9: **end if**
10: **until** $\sum_{q \in S_1} p_q^* \in [0.95\dfrac{P_T}{\beta} \quad \dfrac{P_T}{\beta}]$

In notation terms $\partial g(\lambda)$ corresponds to the subgradient of $g(\lambda)$ at λ, [125]. The power p_q^* is the argument that maximizes $g(\lambda)$ and is computed by setting to zero the partial derivatives of the Lagrange function

$$L(\lambda, \mathbf{p}) = \sum_{q \in S_1} r_q + \lambda \left(\frac{P_T}{\beta} - \sum_{q \in S_1} p_q \right). \tag{5.104}$$

This way of performing enables us to find the candidates that may solve (5.102), since the Lagrange function is differentiable and concave for $p_q \geq 0$, $\lambda \geq 0$. As a result, solving (5.102) is equivalent to computing the powers that satisfy

$$\frac{1}{ln(2)} \frac{h_q \frac{N_0}{2}}{\left(p_q \left(h_q + \alpha_{qq}\right) + \frac{N_0}{2}\right)\left(p_q \alpha_{qq} + \frac{N_0}{2}\right)} = \lambda. \tag{5.105}$$

After several manipulations (5.105) can be transformed into

$$p_q^2 \alpha_{qq} \left(h_q + \alpha_{qq}\right) + p_q \frac{N_0}{2} \left(h_q + 2\alpha_{qq}\right) + \frac{N_0}{2} \left(\frac{N_0}{2} - \frac{h_q}{ln(2)\lambda}\right) = 0, \tag{5.106}$$

which implies finding the roots of a second order polynomial. Since power has to be positive we disregard the negative root. The remaining root may be positive or not. In the positive case we have a maximum due to the concavity of the Lagrange function. In the negative case it can be readily verified that the Lagrange function is monotonically decreasing in p_q for $\lambda \geq 0$, $p_q \geq 0$. As a result the optimal powers are given by

$$p_q^* = max\left(0, p_q^+\right) \tag{5.107}$$

$$p_q^+ = \frac{\left(N_0/2\right)\left(2\alpha_{qq} + h_q\right)}{2\alpha_{qq}\left(\alpha_{qq} + h_q\right)} \left(-1 + \sqrt{1 - \frac{4\alpha_{qq}\left(\alpha_{qq} + h_q\right)}{\left(2\alpha_{qq} + h_q\right)^2} + \frac{4\alpha_{qq}\left(\alpha_{qq} + h_q\right) h_q}{ln(2)\lambda(0.5N_0)\left(2\alpha_{qq} + h_q\right)^2}}\right). \tag{5.108}$$

However, the question of defining the initial interval in Algorithm 5 has not yet been addressed. Obviously, $\lambda_{min} = 0$. The upper bound is set after inferring from (5.107) that the qth subband will be active only if $\lambda < \frac{h_q}{ln(2)0.5N_0}$. Hence, if there are N subcarriers out of M_a that are active, then the following value is an upper bound of the dual variable

$$\lambda_{max} = \frac{\mathbf{h}(N)}{ln(2)}, \tag{5.109}$$

where vector $\mathbf{h}$ gathers the ratios $\frac{h_q}{0.5N_0}$ for all $q \in S_a$ in descending order and $\mathbf{h}$(N) refers to the Nth element. Since it is difficult to predict the number of subcarriers that will be switched off, we have followed a conservative criterion, which assumes that only $N = 0.2M_a$ subcarriers will be assigned power.

5.C Solution of problem 5.18

First we test if $\sum_{q \in S_2} U_q \leq 0.5 \left(P_T - \frac{P_T}{\beta}\right)$. If so, each subcarrier is assigned its maximum allowable power since r_q is monotonically increasing in p_q. Otherwise we proceed as Algorithm 5 describes,

dropping the upper bound on p_q. If the solution does not violate the constraint we are done, i.e. $p_q < U_q$. Otherwise, we set $p_q = U_q$ in those subbands where the bound is exceeded and subtract the power allocated so far to the power budget. Then the process is repeated in the rest of the subbands as Algorithm 6 shows. In notation terms, $\bar{S}_2(i)$ accounts for the ith element of set $\bar{S}_2$.

Algorithm 6 Rate maximization limiting per-subcarrier power.

1: Set $\bar{S}_2 = S_2$, $P_b = 0.5(P_T - \frac{P_T}{\beta})$
2: Apply Algorithm 5 particularizing for $\bar{S}_2$,P_b and W_q that is defined in (5.17)
3: $ITER = |\bar{S}_2|$ (cardinality of $\bar{S}_2$)
4: **for** i=1 to ITER **do**
5: **if** $p_{\bar{S}_2(i)} > U_{\bar{S}_2(i)}$ **then**
6: $p_{\bar{S}_2(i)} = U_{\bar{S}_2(i)}$
7: $\bar{S}_2 = \bar{S}_2 \backslash \bar{S}_2(i)$
8: $P_b = P_b - U_{\bar{S}_2(i)}$
9: **end if**
10: **end for**
11: **if** $|\bar{S}_2| < ITER$ **then**
12: go to 2
13: **end if**

5.D Maximum transmittable power per-subcarrier

The interval $[0, U_q]$ has to be defined to ensure that any power that lies within it yields a rate r_q, which compensates the loss in r_{q-1} and r_{q+1}. This is tantamount to saying that the aggregate

$$SR_q(p_q) = \sum_{m=q-1}^{q+1} \frac{1}{2} \log_2 \left(1 + \frac{h_m p_m}{0.5N_0 + \sum_{l=m-1}^{m+1} \alpha_{ml} p_l} \right) \tag{5.110}$$

has to be monotonically increasing in $p_q \in [0, U_q]$. Assuming that the powers belong to a discrete finite set, that is

$$p_q \in \left\{ 0, \Delta_1^q, ..., \Delta_{N_q}^q \right\}, \tag{5.111}$$

the approach to determine U_q is given by Algorithm 7.

It must be pointed out that the idea of sequentially addressing subsets S_2 and S_3 facilitates the computation of U_q. If we merge S_2 and S_3, Algorithm 7 is not valid to determine the intervals where the sum-rate is increasing, but all the subcarriers gathered in $S_2 \bigcup S_3$ should be jointly processed,

Algorithm 7 Upper bound computation.

1: Set $SR_{q,max} = SR_q(0)$, $i = 0$, $U_q = 0$
2: $i \leftarrow i + 1$
3: **if** $i \leq N_q$ and $SR_q(\Delta_i^q) > SR_{q,max}$ **then**
4: $\quad SR_{q,max} = SR_q(\Delta_i^q)$
5: $\quad U_q = \Delta_i^q$
6: $\quad$ go to 2
7: **end if**

which is much more complex.

Note also that there is a trade-off between the computational complexity and the accuracy with which the transmitter can control the power allocated in each subband. Aiming at implementing a low complexity transmitter, Δ_i^q corresponds to the power required to transmit i bits on the qth subband, thus

$$\Delta_i^q = \frac{(2^{2i}-1)(0.5N_0 + p_{q-1}\alpha_{qq-1} + p_{q+1}\alpha_{qq+1})}{h_q - \alpha_{qq}(2^{2i}-1)}. \tag{5.112}$$

Note that $\Delta_i^q < \Delta_{i+1}^q$. Due to self-interference we cannot transmit any number of bits on the qth subband. Therefore, we define the maximum number of transmittable bits as $N_q = \left\lfloor \frac{1}{2}\log_2\left(1 + \frac{h_q}{\alpha_{qq}}\right)\right\rfloor$.

5.E Solution of problem 5.81

In this appendix we propose to find out the subcarrier allocation in the downlink, which maximizes the data throughput. Provided that we focus on subset S_i, the solution boils down to find the piecewise-maximum of all the SINRs in the corresponding subband as follows:

$$u(q) = \underset{\{1\leq j\leq U\}}{\operatorname{argmax}} \left(\frac{p_q h_q^j}{p_q \alpha_{qq}^j + W_q^j} \right), \quad q \in Si \tag{5.113}$$

$$W_q^j = p_{q+1}\alpha_{qq+1}^j + p_{q-1}\alpha_{qq-1}^j + \sigma_{jq}^2. \tag{5.114}$$

As we have discussed earlier the partitioning strategy shown in Figure 5.4 alleviates the complexity because the term W_q^j can be treated as noise. Note that the selection depends on the power to be allocated. This highlights that some assumptions have to be made as for the power coefficients. In this sense we assume that p_q will lie within this interval $[b_q \;\; a_q]$. Then, the strategy consists in collecting the indexes that solve (5.113) for each value belonging to $[b_q \;\; a_q]$. After checking the set that contains all the indexes we select the user, which SINR function is higher

than the rest with the largest number of points. It is important to remark that the complexity can be dramatically reduced by thoroughly analysing the SINR expression. First note that the fraction $\frac{hp}{W+\alpha p}$ saturates at h/α and takes the value 0 at the origin. Besides it is monotonically increasing for $p > 0$ and concave since the second derivative is negative. Bearing this in mind and supposing that there are only two users (U=2), it can be easily verified that the SINR functions coincide at this point

$$t_q = \frac{W_q^2/h_q^2 - W_q^1/h_q^1}{\alpha_q^1/h_q^1 - \alpha_q^2/h_q^2}. \tag{5.115}$$

As a consequence, if $\alpha_q^1/h_q^1 < \alpha_q^2/h_q^2$ the user selection described above boils down to selecting the user 1 when $t_q < 0.5(a_q + b_q)$ or user 2 when $t_q \geq 0.5(a_q + b_q)$. Conversely, provided that $\alpha_q^1/h_q^1 > \alpha_q^2/h_q^2$ we choose the user 2 when $t_q < 0.5(a_q + b_q)$ or user 1 when $t_q \geq 0.5(a_q + b_q)$. This strategy saves us evaluating the SINRs in the interval $[b_a \;\; a_q]$. Hence the midpoint plays a key role to reduce the complexity. The Algorithm 8 describes how the idea proposed in this appendix can be extended to the case where the number of users is higher than two.

Algorithm 8 Subcarrier allocation.

1: Set the best user to be the first, BU=1
2: **for** $u = 2 : U$ **do**
3: Compute the point where the SINRs of the BUth user and the uth user cross according to (5.115)
4: **if** $t_q < 0.5(a_q + b_q)$ **then**
5: $BU = \underset{u,BU}{\operatorname{argmin}} \left\{\alpha_q^u/h_q^u, \alpha_q^{BU}/h_q^{BU}\right\}$
6: **else**
7: $BU = \underset{u,BU}{\operatorname{argmax}} \left\{\alpha_q^u/h_q^u, \alpha_q^{BU}/h_q^{BU}\right\}$
8: **end if**
9: **end for**

In this case we have assumed that the reduction in the sum-rate, as a consequence of distributing the power according to the UPA strategy, is reasonably small. Hence, we have set the midpoint of $[b_q \;\; a_q]$ to $P_{Ti}/|Si|$, when the ith subset is addressed. Alternatively, the midpoint may be calculated after setting a_q to any given spectral mask constraint and b_q to the minimum power required to transmit one bit on the qth subband.

Chapter 6

MIMO designs for low frequency selective channels

The advent of new services that need high QoS and high data rates will force wireless communication systems to improve the link reliability and increase the system throughput. To satisfy the upcoming needs, the physical layer may rely on multicarrier and MIMO technologies. On one hand, multicarrier techniques are resilient against multipath fading, enable flexible spectrum allocation and can approach the theoretical capacity limits in communications. On the other hand, deploying multiple antennas at both ends of the link has proved to be useful to enhance the link reliability and the throughput with respect to single-antenna configurations [5]. Therefore, the attempt to combine MIMO techniques with multicarrier modulations seems well-justified. So far, most of the efforts have been made at combining MIMO architectures with the OFDM technique. The reason lies in the fact that the global communication system is modeled like a set of parallel flat fading channel in the OFDM context. This facilitates the application of the MIMO concept to multicarrier techniques. Based on the comparison carried out in [31] and the results obtained in previous chapters we can state that the FBMC/OQAM modulation is able to outperform OFDM in some areas. This has motivated us to investigate the application of FBMC/OQAM to MIMO channels. It must be mentioned that most of the existing solutions that combine MIMO techniques with the FBMC/OQAM modulation solely resort to the CSI at the receiver, see e.g. [68, 98, 126–136]. To the best of our knowledge the joint transmit and receive design for FBMC/OQAM systems is only addressed in [137–139]. To make progress towards this direction we further study the design of MIMO precoding and decoding matrices under the assumption that CSI is available at transmission and reception. As for this study cases, MIMO techniques will be investigated in synchronous PTP communications and for the BC, when the channel frequency response is flat at the subcarrier level.

6.1 MIMO designs in PTP communications

Before delving into the design of signal processing techniques in synchronous PTP communications, it is deemed necessary to formulate the expressions that are involved in a MIMO-FBMC/OQAM system. Borrowing the notation from Section 2.2 and bearing in mind Figure 2.7, the demodulated signal on the qth subcarrier and at the kth time instant is given by

$$y_q^j[k] = \sum_{m=q-1}^{q+1} \sum_{i=1}^{N_T} v_m^i[k] * g_{qm}^{ij}[k] + w_q^j[k], \quad 1 \leq j \leq N_R, \tag{6.1}$$

where $g_{qm}^{ij}[k]$ and $w_q^j[k]$ are formulated in (2.18) and (2.19), respectively. The vector of precoded symbols is expressed as $\mathbf{v}_m[k] = \left[v_m^1[k] \cdots v_m^{N_T}[k]\right]^T = \theta_m[k]\mathbf{B}_m\mathbf{d}_m[k]$, where $\theta_m[k]$ is defined in (2.2), $\mathbf{B}_m \in \mathbb{C}^{N_T \times S}$ is the precoding matrix and $\mathbf{d}_m[k] \in \mathbb{R}^{S \times 1}$ is the vector of real-valued symbols that are drawn from the PAM constellation. The transmitted symbols are independent and have unit-energy, that is $\mathbb{E}\left\{\mathbf{d}_q[k]\mathbf{d}_m^T[n]\right\} = \delta_{q,m}\delta_{k,n}\mathbf{I}_S$. Note that matrix $\mathbf{B}_m$ maps S streams onto N_T transmit antennas. The symbols multiplexed on the qth subcarrier are detected after performing the receive processing. When the signal processing techniques applied on the receive side are based on performing a narrowband liner processing, the post-processed vector on the qth subcarrier is written as $\mathbf{z}_q[k] = \left[z_q^1[k] \cdots z_q^S[k]\right]^T = \mathbf{A}_q^H\mathbf{y}_q[k]$, where $\mathbf{y}_q[k] = \left[y_q^1[k] \cdots y_q^{N_R}[k]\right]^T$. The spatial decoding matrix $\mathbf{A}_q \in \mathbb{C}^{N_R \times S}$ is in charge of performing the equalization. Then, it follows that the PAM symbols are estimated by compensating the phase term and extracting the real part of the equalized signals, which boils down to operate as follows:

$$\begin{aligned}
\check{\mathbf{d}}_q[k] = \Re\left(\theta_q^*[k]\mathbf{z}_q[k]\right) = & \sum_{m=q-1}^{q+1} \sum_{\tau=-L_{g_1}}^{L_{g_2}} \Re\left(\theta_q^*[k]\theta_m[k-\tau]\mathbf{A}_q^H\mathbf{G}_{qm}[\tau]\mathbf{B}_m\right)\mathbf{d}_m[k-\tau] + \Re\left(\mathbf{A}_q^H\mathbf{w}_q[k]\right) \\
= & \Re\left(\mathbf{A}_q^H\mathbf{G}_{qq}[0]\mathbf{B}_q\right)\mathbf{d}_q[k] + \Re\left(\mathbf{A}_q^H\mathbf{w}_q[k]\right) + \\
& \sum_{(m,\tau)\neq(q,0)} \Re\left(\theta_q^*[k]\theta_m[k-\tau]\mathbf{A}_q^H\mathbf{G}_{qm}[\tau]\mathbf{B}_m\right)\mathbf{d}_m[k-\tau],
\end{aligned} \tag{6.2}$$

where

$$\mathbf{G}_{qm}[\tau] = \begin{bmatrix} g_{qm}^{11}[\tau] & \cdots & g_{qm}^{N_T 1}[\tau] \\ \vdots & & \vdots \\ g_{qm}^{1N_R}[\tau] & \cdots & g_{qm}^{N_T N_R}[\tau] \end{bmatrix}. \tag{6.3}$$

The noise vector is written as $\mathbf{w}_q[k] = \theta_q^*[k]\left[w_q^1[k] \cdots w_q^{N_R}[k]\right]^T$. As (6.2) highlights, the joint design of precoding and decoding matrices is very challenging because aside from ISI and ICI we

have to deal with inter-stream interference. Inter-stream interference is generated as a consequence of transmitting S streams on the same time slot and frequency resources. It worth emphasizing that this chapter focuses on the design of transmit and receive signal processing techniques when the channel frequency selectivity is not appreciable at the subcarrier level. This means that (2.13) and (2.14) are valid. Then, (6.3) can be replaced by

$$\mathbf{G}_{qm}[\tau] = \alpha_{qm}[\tau] \begin{bmatrix} H_{11}\left(e^{j\frac{2\pi}{M}m}\right) & \cdots & H_{N_T 1}\left(e^{j\frac{2\pi}{M}m}\right) \\ \vdots & & \vdots \\ H_{1N_R}\left(e^{j\frac{2\pi}{M}m}\right) & \cdots & H_{N_T N_R}\left(e^{j\frac{2\pi}{M}m}\right) \end{bmatrix} = \alpha_{qm}[\tau]\mathbf{H}_m, \tag{6.4}$$

or

$$\mathbf{G}_{qm}[\tau] = \alpha_{qm}[\tau] \begin{bmatrix} H_{11}\left(e^{j\frac{2\pi}{M}q}\right) & \cdots & H_{N_T 1}\left(e^{j\frac{2\pi}{M}q}\right) \\ \vdots & & \vdots \\ H_{1N_R}\left(e^{j\frac{2\pi}{M}q}\right) & \cdots & H_{N_T N_R}\left(e^{j\frac{2\pi}{M}q}\right) \end{bmatrix} = \alpha_{qm}[\tau]\mathbf{H}_q. \tag{6.5}$$

Let $H_{ij}\left(e^{j\frac{2\pi}{M}m}\right)$ be the Fourier transform of $h_{ij}[n]$ at the radial frequency $\frac{2\pi}{M}m$. The terms that model the intrinsic interference, i.e. $\{\alpha_{qm}[\tau]\}$, are gathered in Table 2.1 and Table 2.2. At this point, we could use the optimal precoding and decoding matrices that has been originally devised in OFDM [140]. Alternatively, we may take into account the specificities of the FBMC/OQAM modulation to design a new strategy. In the following we review the joint design addressed in [140] as well as analyse the sources of error when the FBMC/OQAM scheme is considered. With the aim of overcoming the limitations of directly applying the OFDM solution to FBMC/OQAM, we devise in Section 6.1.2 a new beamforming design. The novel technique takes into account that the OQAM symbols only convey information in a single dimension. As a result, covariance and pseudo-covariance matrices do not vanish, i.e.

$$\begin{aligned} \mathbb{E}\left\{\left(\mathbf{d}_q[k] - \mathbb{E}\left\{\mathbf{d}_q[k]\right\}\right)\left(\mathbf{d}_q[k] - \mathbb{E}\left\{\mathbf{d}_q[k]\right\}\right)^H\right\} &= \mathbf{I}_S \neq \mathbf{0} \\ \mathbb{E}\left\{\left(\mathbf{d}_q[k] - \mathbb{E}\left\{\mathbf{d}_q[k]\right\}\right)\left(\mathbf{d}_q[k] - \mathbb{E}\left\{\mathbf{d}_q[k]\right\}\right)^T\right\} &= \mathbf{I}_S \neq \mathbf{0}. \end{aligned} \tag{6.6}$$

Therefore, the random vector $\mathbf{d}_q[k]$ is called improper [40]. To exploit the specificities of the FBMC/OQAM modulation, the input/output relationship should be recasted as a real-valued representation. This new formulation opens the door to treat independently in-phase and quadrature components of the signal to be filtered, which can be understood as a special case of WLP, [39]. Since the optimal beamformers devised for OFDM systems perform a linear processing (LP), we use the acronyms WLP and LP to differentiate between the approach presented in [140] and the solution described in Section 6.1.2.

6.1.1 Linear processing design in MIMO-FBMC/OQAM systems

This section reviews the beamforming design described in [140] and, furthermore, analyses the drawbacks of directly implementing this technique to the FBMC/OQAM modulation scheme. If the MIMO precoding and decoding matrices devised in [140] are directly applied to FBMC/OQAM systems, then

$$\mathbf{A}_q = \left(\mathbf{H}_q\mathbf{B}_q\left(\mathbf{H}_q\mathbf{B}_q\right)^H + N_0\mathbf{I}_{N_R}\right)^{-1}\mathbf{H}_q\mathbf{B}_q \tag{6.7}$$

$$\mathbf{B}_q = \frac{1}{N_0}\mathbf{V}_q\Sigma_q, \tag{6.8}$$

where $\mathbb{E}\left\{\mathbf{w}_q[k]\mathbf{w}_q^H[k]\right\} = N_0\mathbf{I}_{N_R}$, $\mathbf{V}_q \in \mathbb{C}^{N_T\times\check{L}_q}$ contains the eigenvectors of $\mathbf{H}_q^H\mathbf{H}_q$ that are associated with the $\check{L}_q$ largest eigenvalues. The noise autocorrelation matrix can be derived from the analysis conducted in Appendix 3.A. The matrix $\Sigma_q \in \mathbb{C}^{\check{L}_q\times S}$ is decomposed as $\Sigma_q = [\mathbf{0}\ \ \mathbf{P}_q]$, where $\mathbf{0} \in \mathbb{R}^{\check{L}_q\times S-\check{L}_q}$ is zero-valued and $\mathbf{P}_q = \text{diag}\left\{\sqrt{p_{\check{L}_q q}}, ..., \sqrt{p_{1q}}\right\} \in \mathbb{R}^{\check{L}_q\times\check{L}_q}$. Whether it is possible or not to spatially multiplex S streams will be given by $\check{L}_q = \min\left(S, \text{rank}\left(\mathbf{H}_q^H\mathbf{H}_q\right)\right)$. As a consequence, $\check{L}_q \leq S$.

By using this equality $\mathbf{A} = \left(\mathbf{HB}\left(\mathbf{HB}\right)^H + \mathbf{R}\right)^{-1}\mathbf{HB} = \mathbf{R}^{-1}\mathbf{HB}\left(\mathbf{I} + \left(\mathbf{HB}\right)^H\mathbf{R}^{-1}\mathbf{HB}\right)^{-1}$ [140], the MIMO decoding matrix can be expressed as

$$\mathbf{A}_q = \mathbf{H}_q\mathbf{B}_q\left(N_0\mathbf{I}_S + \left(\mathbf{H}_q\mathbf{B}_q\right)^H\mathbf{H}_q\mathbf{B}_q\right)^{-1}. \tag{6.9}$$

Supposing that $S \leq \text{rank}\left(\mathbf{H}_q^H\mathbf{H}_q\right)$, the global MIMO channel $\mathbf{A}_q^H\mathbf{H}_q\mathbf{B}_q$ becomes a real-valued diagonal matrix. The (l,l)th entry is given by

$$\left[\mathbf{A}_q^H\mathbf{H}_q\mathbf{B}_q\right]_{ll} = \frac{p_{lq}\beta_{lq}}{N_0 + p_{lq}\beta_{lq}}, \quad 1 \leq l \leq S, \tag{6.10}$$

where β_{lq} is the lth largest eigenvalue of matrix $\mathbf{H}_q^H\mathbf{H}_q$. Now, assume that the channel matrix can be modeled as (6.5). In addition we presume that $\mathbf{H}_{q-1} = \mathbf{H}_q = \mathbf{H}_{q+1}$. Since precoding matrices $\mathbf{B}_{q-1}, \mathbf{B}_{q+1}$ are designed as (6.8) indicates, then

$$\left[\mathbf{A}_q^H\mathbf{H}_q\mathbf{B}_m\right]_{ll} = \frac{p_{lm}\beta_{lq}}{N_0 + p_{lm}\beta_{lq}}, \quad 1 \leq l \leq S, \quad m = \{q-1, q+1\}, \tag{6.11}$$

are also diagonal matrices with real-valued entries. With that, the decision variables are expressed as

$$\begin{aligned}\check{\mathbf{d}}_q[k] = &\ \mathbf{A}_q^H\mathbf{H}_q\mathbf{B}_q\mathbf{d}_q[k] + \Re\left(\mathbf{A}_q^H\mathbf{w}_q[k]\right) + \sum_{(m,\tau)\neq(q,0)} \underbrace{\Re\left(\theta_q^*[k]\theta_m[k-\tau]\alpha_{qm}[\tau]\right)}_{=0}\mathbf{A}_q^H\mathbf{H}_q\mathbf{B}_m\mathbf{d}_m[k-\tau] \\ = &\ \mathbf{A}_q^H\mathbf{H}_q\mathbf{B}_q\mathbf{d}_q[k] + \Re\left(\mathbf{A}_q^H\mathbf{w}_q[k]\right).\end{aligned} \tag{6.12}$$

The second equality hinges on this result $\Re\left(\theta_q^*[k]\theta_m[k-\tau]\alpha_{qm}[\tau]\right) = 0$ for $(m,\tau) \neq (q,0)$, which can be deduced from Tables 2.1 and 2.2 and the definition (2.2). Provided that (6.12) holds true, the mean square error (MSE) and the SINR are related as follows:

$$MSE_q^l = \frac{1}{SINR_q^l + 1} = \frac{1}{\frac{\beta_{lq}p_{lq}}{0.5N_0} + 1}, \tag{6.13}$$

for $1 \leq l \leq S$ and $q \in S_a$. The power coefficients can be designed to minimize different performance metrics. In this section we opt for the sum MSE minimization. Thus, the optimization procedure is given by

$$\begin{aligned}&\underset{\{p_{lq}\}}{\text{argmin}} \sum_{q\in S_a}\sum_{l=1}^{S} \frac{1}{1+\frac{\beta_{lq}p_{lq}}{0.5N_0}} \\ &s.t. \sum_{q\in S_a}\sum_{l=1}^{S} p_{lq} \leq P_T, \quad 0 \leq p_{lq}, \quad 1 \leq l \leq S, \quad q \in S_a.\end{aligned} \tag{6.14}$$

The optimal power distribution is formulated as $p_{lq} = \max\left(\mu^{-0.5}\left(\frac{\beta_{lq}}{0.5N_0}\right)^{-0.5} - \left(\frac{\beta_{lq}}{0.5N_0}\right)^{-1}, 0\right)$, where μ is the Lagrange multiplier that guarantees that $\sum_{q\in S_a}\sum_{l=1}^{S} p_{lq} = P_T$.

6.1.2 Linear processing design in MIMO-OFDM systems

The optimal beamforming design brings about this performance metric

$$SINR_q^l = \frac{1}{MSE_q^l} - 1 = \frac{2\beta_{lq}p_{lq}}{N_0\left(\frac{M+CP}{M}\right)}, \tag{6.15}$$

when the OFDM transmultiplexer is implemented [140]. The power of the noise is not halved when compared to (6.13) because the processing is performed on the complex domain. The factor 2 in the numerator accounts for the average energy symbol, which is two fold with respect to the PAM counterpart. This becomes evident by recalling that PAM symbols in the FBMC/OQAM modulation are obtained by staggering between in-phase and quadrature components of symbols generated from the QAM constellation. The power constrained sum MSE minimization yields

this power distribution $p_{lq} = \max\left(\mu^{-0.5}\left(\frac{\beta_{lq}}{\frac{M+CP}{M}0.5N_0}\right)^{-0.5} - \left(\frac{\beta_{lq}}{\frac{M+CP}{M}0.5N_0}\right)^{-1}, 0\right)$. The term μ guarantees that $\sum_{q\in S_a}\sum_{l=1}^{S} p_{lq} = P_T$.

6.1.3 Widely linear processing design in MIMO-FBMC/OQAM systems

The main drawback of adapting [140] to FBMC/OQAM is that ISI and ICI are not completely removed unless $\mathbf{H}_{q-1} = \mathbf{H}_q = \mathbf{H}_{q+1}$. The authors in [138] have also provided evidence that the orthogonality is destroyed unless the channel frequency response is flat in the neighbourhood around the position of interest in the time-frequency grid. In view of this, we propose one alternative solution that is based on the expression written in (6.4) and, therefore, the supposition that $\mathbf{H}_{q-1} = \mathbf{H}_q = \mathbf{H}_{q+1}$ is not satisfied. Hence, as the channel frequency selectivity becomes stronger, the approximation in (6.5) results in a mismatch with the exact expression that is larger than the mismatch modelling yielded by (6.4). The symbols to be estimated become

$$\begin{aligned}\check{\mathbf{d}}_q[k] = \; & \Re\left(\mathbf{A}_q^H\mathbf{H}_q\mathbf{B}_q\right)\mathbf{d}_q[k] + \Re\left(\mathbf{A}_q^H\mathbf{w}_q[k]\right) + \\ & \sum_{(m,\tau)\neq(q,0)} \Re\left(\theta_q^*[k]\theta_m[k-\tau]\alpha_{qm}[\tau]\mathbf{A}_q^H\mathbf{H}_m\mathbf{B}_m\right)\mathbf{d}_m[k-\tau].\end{aligned} \tag{6.16}$$

It can be verified that the subband processing developed in Section 6.1.1 does not get rid of ISI and ICI from $\check{\mathbf{d}}_q[k]$ if (6.16) is assumed. However, the phase term definition in (2.2) and the values gathered in the Table 2.1 and the Table 2.2 reveal that the terms in (6.16) can be arranged as

$$\begin{aligned}\check{\mathbf{d}}_q[k] = \; & \Re\left(\mathbf{A}_q^H\mathbf{H}_q\mathbf{B}_q\right)\mathbf{d}_q[k] + \Re\left(\mathbf{A}_q^H\mathbf{w}_q[k]\right) - \\ & \sum_{(m,\tau)\neq(q,0)} \operatorname{sign}\left(\theta_q^*[k]\theta_m[k-\tau]\alpha_{qm}[\tau]\right)|\alpha_{qm}[\tau]|\,\Im\left(\mathbf{A}_q^H\mathbf{H}_m\mathbf{B}_m\right)\mathbf{d}_m[k-\tau].\end{aligned} \tag{6.17}$$

The operation sign(.) computes the sign of the argument. From (6.17) we can conclude that the symbols that contribute to ISI and ICI pass through an equivalent communication system that is expressed as $\Im\left(\mathbf{A}_q^H\mathbf{H}_m\mathbf{B}_m\right)$. This observation paves the way to devise the strategy that will remove the undesired terms. In this sense, if $\mathbf{A}_q^H\mathbf{H}_m\mathbf{B}_m$ is restricted to be real-valued for $q-1 \leq m \leq q+1$, then both ISI and ICI terms are cancelled out. If $N_T > N_R$, the zero-forcing condition can be satisfied if the augmented precoder $\mathbf{B}_{m,e} = \left[\Re\left(\mathbf{B}_m\right)^T \quad \Im\left(\mathbf{B}_m\right)^T\right]^T$ belongs to the null space of this matrix

$$\hat{\mathbf{H}}_m = \begin{bmatrix} \Im\left(\mathbf{H}_m\right) & \Re\left(\mathbf{H}_m\right) \\ -\Re\left(\mathbf{H}_m\right) & \Im\left(\mathbf{H}_m\right) \end{bmatrix}, \tag{6.18}$$

which has $2N_R$ rows and $2N_T$ columns. The problem is that (6.18) and the following matrix

$$\check{\mathbf{H}}_m = \begin{bmatrix} \Re\left(\mathbf{H}_m\right) & -\Im\left(\mathbf{H}_m\right) \\ \Im\left(\mathbf{H}_m\right) & \Re\left(\mathbf{H}_m\right) \end{bmatrix} \tag{6.19}$$

span the same subsapce. Then, $\Im\left(\mathbf{A}_q^H \mathbf{H}_m \mathbf{B}_m\right)$=$\Re\left(\mathbf{A}_q^H \mathbf{H}_m \mathbf{B}_m\right)$=0 if $\mathbf{B}_{m,e} \in \text{null}\left(\hat{\mathbf{H}}_m\right)$. With that we would obtain this undesired result $\check{\mathbf{d}}_q[k] = \Re\left(\mathbf{A}_q^H \mathbf{w}_q[k]\right)$. To overcome this hurdle the decoding matrix $\mathbf{A}_q$ is constrained to only have in-phase components. If so, (6.17) is recasted as

$$\begin{aligned} \check{\mathbf{d}}_q[k] = \quad & \mathbf{A}_q^T \Re\left(\mathbf{H}_q \mathbf{B}_q\right) \mathbf{d}_q[k] + \mathbf{A}_q^T \Re\left(\mathbf{w}_q[k]\right) + \\ & \sum_{(m,\tau)\neq(q,0)} \text{sign}\left(\theta_q^*[k]\theta_m[k-\tau]\alpha_{qm}[\tau]\right) |\alpha_{qm}[\tau]|\, \mathbf{A}_q^T \Im\left(\mathbf{H}_m \mathbf{B}_m\right) \mathbf{d}_m[k-\tau] \end{aligned} \tag{6.20}$$

and the ZF condition translates into projecting $\mathbf{B}_{m,e}$ onto the null space of $[\Im\left(\mathbf{H}_m\right) \quad \Re\left(\mathbf{H}_m\right)]$. Now, each subcarrier is able to simultaneously convey up to $\min\left(N_R, 2N_T - N_R\right)$. Stacking real and imaginary parts, we can express the zero forcing condition in this form $\Im\left(\mathbf{H}_m \mathbf{B}_m\right) = [\Im\left(\mathbf{H}_m\right) \quad \Re\left(\mathbf{H}_m\right)]\, \mathbf{B}_{m,e} = \mathbf{0}$. Thus, the precoders should project the input vectors onto the null subspace of $[\Im\left(\mathbf{H}_m\right) \quad \Re\left(\mathbf{H}_m\right)] \in \mathbb{R}^{N_R \times 2N_T}$. Under the assumption that $N_T \geq N_R$, the singular value decomposition of the extended channel matrix is given by

$$[\Im\left(\mathbf{H}_m\right) \quad \Re\left(\mathbf{H}_m\right)] = \mathbf{E}_m \left[\mathbf{D}_m \mathbf{0}\right] \left[\mathbf{F}_m^1 \mathbf{F}_m^0\right]^T, \tag{6.21}$$

where $\mathbf{D}_m \in \mathbb{R}^{N_R \times N_R}$ is a diagonal matrix and $\mathbf{0} \in \mathbb{R}^{N_R \times 2N_T - N_R}$ is zero-valued. As a result, the columns of $\mathbf{F}_m^0 \in \mathbb{R}^{2N_T \times 2N_T - N_R}$ span the null space of $[\Im\left(\mathbf{H}_m\right) \quad \Re\left(\mathbf{H}_m\right)]$. Then, any precoder of the form $\mathbf{B}_{m,e} = \mathbf{F}_m^0 \mathbf{Q}_m$ cancels the interference in the real field. Note that we have freedom to design $\mathbf{Q}_m \in \mathbb{R}^{2N_T - N_R \times S}$. When the ZF condition is satisfied, the estimated symbols are expressed as

$$\check{\mathbf{d}}_q[k] = \mathbf{A}_q^T \bar{\mathbf{H}}_q \mathbf{Q}_q \mathbf{d}_q[k] + \mathbf{A}_q^T \Re\left(\mathbf{w}_q[k]\right) \tag{6.22}$$

with

$$\bar{\mathbf{H}}_q = [\Re\left(\mathbf{H}_m\right) \quad -\Im\left(\mathbf{H}_m\right)]\, \mathbf{F}_q^0. \tag{6.23}$$

Assuming that $\mathbb{E}\left\{\mathbf{d}_q[k]\mathbf{d}_m^H[n]\right\} = \delta_{q,m}\delta_{k,n}\mathbf{I}_S$, the remaining parameters are designed to minimize the sum MSE, which comes down to solve

$$\begin{aligned} &\underset{\{\mathbf{A}_q,\mathbf{Q}_q\}}{\operatorname{argmin}} \sum_{q\in S_a} \mathbb{E}\left\{\left\|\check{\mathbf{d}}_q[k]-\mathbf{d}_q[k]\right\|_2^2\right\} \\ &s.t. \quad \sum_{q\in S_a} \mathbb{E}\left\{\left\|\mathbf{F}_q^0\mathbf{Q}_q\mathbf{d}_q[k]\right\|_2^2\right\} = \sum_{q\in S_a}\left\|\mathbf{Q}_q\right\|_F^2 \leq P_T. \end{aligned} \tag{6.24}$$

The similarity of (6.22) to OFDM allows us to solve (6.24) as [140] describes. Then, (6.22) will present a diagonal structure. Bearing in mind the signal and noise statistics together with the solution of [140], the SINR and MSE figures are given by

$$MSE_q^l = \frac{1}{\mathrm{SINR}_q^l+1} = \frac{1}{\frac{p_{lq}\lambda_{lq}}{0.5N_0}+1}, \quad l=1,...,S, \quad q\in S_a, \tag{6.25}$$

where λ_{lq} is the lth largest eigenvalue of the matrix $\bar{\mathbf{H}}_q^T\bar{\mathbf{H}}_q$ and the optimal power coefficients are computed as $p_{lq}=\max\left(\mu^{-1/2}\left(\frac{\lambda_{lq}}{0.5N_0}\right)^{-1/2}-\left(\frac{\lambda_{lq}}{0.5N_0}\right)^{-1},0\right)$. The constant μ is set to ensure that the power constraint is active.

6.1.4 Widely linear processing versus linear processing

In this section we carry out a comparison between the multi-stream techniques presented in Sections 6.1.1 and 6.1.3. In particular, we focus on the type of designs that minimize the sum MSE. At high SINR or, equivalently, when N_0 tends to 0 the optimal power distribution in the linear and the widely linear case can be respectively approximated as

$$p_{lq}^L \approx P_T\left(\sum_{m\in S_a}\sum_{t=1}^{S}\beta_{tm}^{-0.5}\right)^{-1}\beta_{lq}^{-0.5} \tag{6.26}$$

$$p_{lq}^{WL} \approx P_T\left(\sum_{m\in S_a}\sum_{t=1}^{S}\lambda_{tm}^{-0.5}\right)^{-1}\lambda_{lq}^{-0.5}, \tag{6.27}$$

for $1\leq l\leq S$ and $q\in S_a$, [141]. This simplification allows us derive a theoretical analysis that leads to the following Lemma.

Lemma

$$\begin{aligned} &\sum_{q\in S_a}\sum_{l=1}^{S}\frac{1}{\frac{p_{lq}^{WL}\lambda_{lq}}{0.5N0}+1} \geq \sum_{q\in S_a}\sum_{l=1}^{S}\frac{1}{\frac{p_{lq}^{L}\beta_{lq}}{0.5N0}+1} \\ &\text{if} \quad N_T\geq N_R, \quad S\leq N_R\leq 3. \end{aligned} \tag{6.28}$$

Plugging (6.26) and (6.27) into (6.13) and (6.25), respectively, yields

$$\frac{1}{\frac{p_{lq}^{L}\beta_{lq}}{0.5N0}+1}=\frac{1}{\frac{P_T\left(\sum\limits_{m\in S_a}\sum\limits_{t=1}^{S}\beta_{tm}^{-0.5}\right)^{-1}\beta_{lq}^{0.5}}{0.5N0}+1} \tag{6.29}$$

$$\frac{1}{\frac{p_{lq}^{WL}\lambda_{lq}}{0.5N0}+1}=\frac{1}{\frac{P_T\left(\sum\limits_{m\in S_a}\sum\limits_{t=1}^{S}\lambda_{tm}^{-0.5}\right)^{-1}\lambda_{lq}^{0.5}}{0.5N0}+1}. \tag{6.30}$$

With this result we can conclude that the LP brings a lower sum MSE than the WLP at high SINR if $N_R \leq 3$, $N_T \geq N_R$ and (6.5) holds true. The proof of the Lemma (6.28) is described in Appendix 6.A.

6.1.5 MIMO-FBMC/OQAM versus MIMO-OFDM

When the system parameters and the propagation conditions are such that (6.5) is satisfied, then FBMC/OQAM outperforms OFDM. This becomes obvious by comparing (6.13) and (6.15). However, if we adopt the model in (6.4), then the spatial channel gains in FBMC/OQAM and OFDM may differ. Therefore, at first glance it is not easy to predict which solution will give the best performance. In order to shred some light into this issue, we develop a theoretical analysis that reveals in which multi-antenna configurations the WLP devised in Section 6.1.3 may remain competitive with the MIMO-OFDM design addressed in Section 6.1.2. To do so, it is useful to know how the eigenvalues of these two sets $\{\lambda_{lq}\}$, $\{\beta_{lq}\}$ compare. In addition, it is also important to take into account the negative impact of the CP. In this sense, the following lemmas allow us to determine when MIMO-FBMC/OQAM is superior to MIMO-OFDM.

Lemma

$$\sum_{q\in S_a}\sum_{l=1}^{S}\frac{1}{\frac{\epsilon p_{lq}\beta_{lq}}{0.5N0}+1}\geq\sum_{q\in S_a}\sum_{l=1}^{S}\frac{1}{\frac{p_{lq}\lambda_{lq}}{0.5N0}+1},\quad \text{if}\quad N_T\geq N_R=S=1,\quad \epsilon=\frac{M}{M+CP} \tag{6.31}$$

The Appendix 6.D justifies the Lemma (6.31).

Corollary

The Lemma (6.31) indicates that given a power distribution, the MIMO-FBMC/OQAM scheme achieves the lowest sum MSE. Now, assume that the active carriers in both multicarrier schemes coincide. Let $\left\{p_{lq}^{L}\right\}$ and $\left\{p_{lq}^{WL}\right\}$ denote the optimal power coefficients that are computed as it is

detailed in Sections 6.1.2 and 6.1.3, respectively. From (6.31) it follows that

$$\sum_{q\in S_a}\sum_{l=1}^{1}\frac{1}{\frac{\epsilon p_{lq}^{L}\beta_{lq}}{0.5N0}+1}\geq\sum_{q\in S_a}\sum_{l=1}^{1}\frac{1}{\frac{p_{lq}^{L}\lambda_{lq}}{0.5N0}+1}\geq\sum_{q\in S_a}\sum_{l=1}^{1}\frac{1}{\frac{p_{lq}^{WL}\lambda_{lq}}{0.5N0}+1}. \tag{6.32}$$

This confirms that (6.31) is still valid when the power coefficients are optimized to minimize the sum MSE. The gap in (6.32) is widened if the set that gatheres the active carriers in OFDM is included in the set that indicates which subcarriers transmit data in the FBMC/OQAM case.

Lemma

$$\begin{aligned}&\sum_{q\in S_a}\sum_{l=1}^{S}\frac{1}{\frac{\epsilon p_{lq}\beta_{lq}}{0.5N0}+1}\geq\sum_{q\in S_a}\sum_{l=1}^{S}\frac{1}{\frac{p_{lq}\lambda_{lq}}{0.5N0}+1}\\&\text{if}\quad N_T\geq N_R=S=2,\quad\epsilon=\tfrac{M}{M+CP},\quad\epsilon\leq\min\left\{\frac{\lambda_{lq}^{1}}{\beta_{lq}^{1}}\right\}.\end{aligned} \tag{6.33}$$

Corollary

As Lemma (6.33) states, the MIMO-FBMC/OQAM scheme achieves the lowest sum MSE provided that the eigenvalues obtained in the linear and the widely linear case are sufficiently close. Let us assume that the active carriers in both multicarrier schemes remain the same. We define $\left\{p_{lq}^{L}\right\}$ and $\left\{p_{lq}^{WL}\right\}$ to be the optimal power coefficients computed in Sections 6.1.2 and 6.1.3, respectively. From (6.33) it follows that

$$\sum_{q\in S_a}\sum_{l=1}^{2}\frac{1}{\frac{\epsilon p_{lq}^{L}\beta_{lq}}{0.5N0}+1}\geq\sum_{q\in S_a}\sum_{l=1}^{2}\frac{1}{\frac{p_{lq}^{L}\lambda_{lq}}{0.5N0}+1}\geq\sum_{q\in S_a}\sum_{l=1}^{2}\frac{1}{\frac{p_{lq}^{WL}\lambda_{lq}}{0.5N0}+1}. \tag{6.34}$$

Therefore, when the optimal power distribution comes into play MIMO-FBMC/OQAM still is the optimal choice. The possibility of using pulse shaping techniques in the FBMC/OQAM context, it allows us to increase the number of subcarrier that are switched on, which may widen the gap between OFDM and FBMC/OQAM.

6.1.6 Simulation results

In this section we evaluate the application of FBMC/OQAM and OFDM systems to MIMO channels. The transmit and the receive processing is designed according to Sections 6.1.1, 6.1.2 and 6.1.3. The system performance is measured in terms of BER as function of the average energy symbol to noise ratio, which is defined as $\frac{E_s}{N_0}=\frac{M+CP}{M}\frac{2P_T}{MN_0}$. In OFDM systems the CP encompasses $\frac{M}{4}$ samples and the transmitted symbols are obtained from a 16-QAM constellation. In the FBMC/OQAM case, the information conveyed on each subcarrier is obtained by staggering

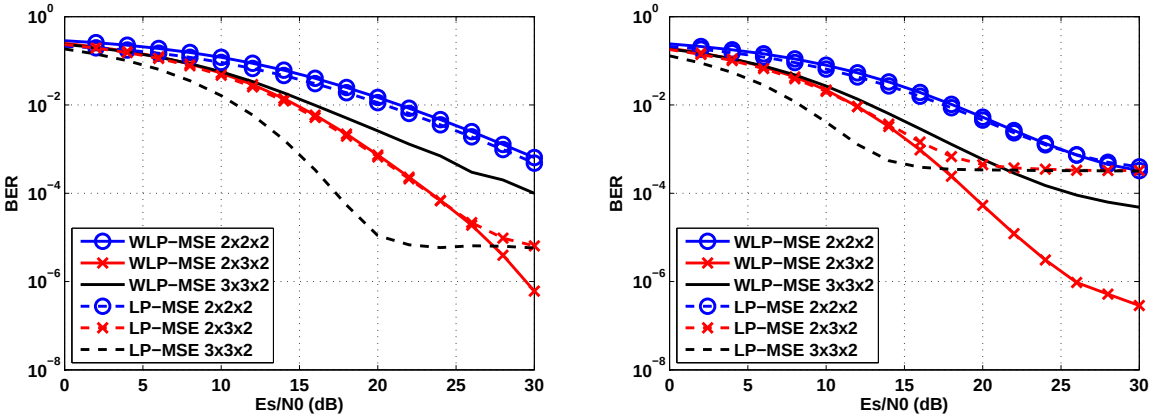

(a) Scenario 2. (b) Scenario 1.

Figure 6.1: BER vs. $\frac{E_s}{N_0}$ for different multi-antenna configurations in FBMC/OQAM systems. System parameters are set according to Scenarios 1 and 2 (see Table 2.3).

in-phase and quadrature components of 16-QAM symbols. To compactly express a given configuration when we use this notation $N_R \times N_T \times S$, it means that S streams are spatially multiplexed on each subcarrier in a communication system where the receiver and the transmitter are equipped with N_R and N_T antennas, respectively.

The validate the conclusions drawn in Section 6.1.4, we simulate in Figure 6.1 the solutions provided in Sections 6.1.1 and 6.1.3. The MIMO architecture is such that $S \leq N_R \leq 3$, $N_T \geq N_R$. Since the BER and the MSE are somehow related, we expect to see that the best performance is given by the linear processing. The Figure 6.1a shows that when the FBMC/OQAM modulation is used, the LP achieves the lowest BER in the $\frac{E_S}{N_0}$ region where plots do not saturate. This observation is in line with the analysis conducted in Section 6.1.4. When $S = N_R$ the LP-MSE and the WLP-MSE technique nearly give the same performance. In the Appendix 6.C it is demonstrated that the channel gains in the N_Rth mode are related as follows: $\lambda_q^{N_R} \geq \beta_q^{N_R}$. In this sense, Figure 6.1 confirms that the gain provided by the WLP in the N_Rth subchannel compensates the loss that may take place in the rest of the spatial subchannels. However, when $S < N_R$ the gap between LP-MSE and WLP-MSE is widened because the N_Rth mode is not active. It is worth emphasizing that at low noise regime the BER plots associated with the LP-MSE technique exhibit an error floor. The mismatch modeling as a result of assuming that the channel frequency response is flat in three consecutive subcarriers brings residual interference. By contrast, the model considered in Section 6.1.3 is more accurate and, thus, there is no saturation. As Figure 6.1b shows, the conclusions drawn from Figure 6.1a are also valid when the Scenario 1 is simulated. Nevertheless, the BER provided by the LP-MSE technique starts saturating at lower $\frac{E_s}{N_0}$ values. As the channel

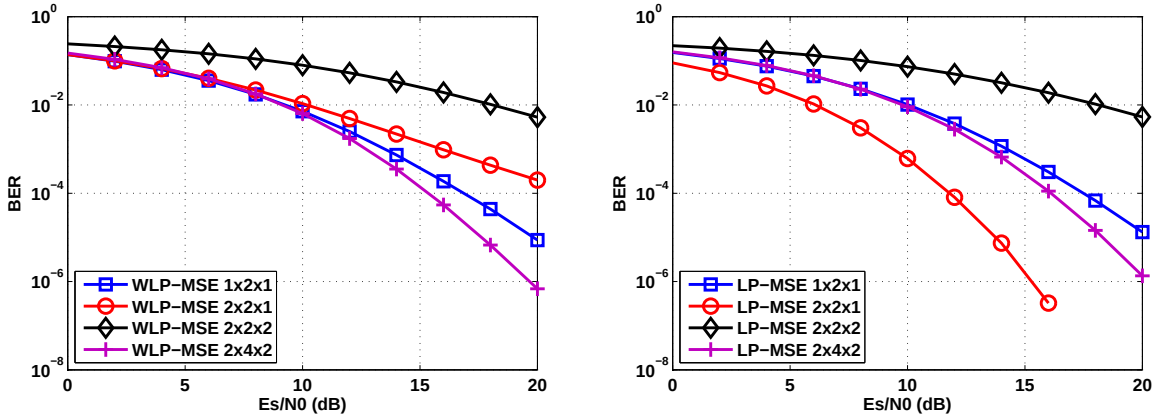

(a) FBMC/OQAM. (b) OFDM.

Figure 6.2: BER vs. $\frac{E_s}{N_0}$ for different multi-antenna configurations in FBMC/OQAM and OFDM systems. System parameters are set according to Scenarios 1 (see Table 2.3).

is more frequency selective the supposition made in Section 6.1.1 is less accurate, which translates into an increased residual interference.

In Figure 6.2 we compare the beamforming designs devised in Sections 6.1.2 and 6.1.3, with the aim of determining if the BER curves are in accordance with the theory developed in Section 6.1.5. Hence, system parameters are related as follows: $S \leq N_R \leq 2$, $N_T \geq N_R$. In the case where $S = N_R = 1$ the FBMC/OQAM outperforms the OFDM, which is in agreement with Lemma 6.31. The results also indicate that OFDM outperforms FBMC only if $S = 1, N_R = 2$. This behaviour indicates that even considering the energy wastage for transmitting the CP the channel gains are the highest in the OFDM context, i.e. $\lambda_{1q} < \beta_{1q}\epsilon$. Conversely if $S = N_R = 2$, both modulations give similar performance. As reported in Lemma 6.33, this observation suggests that the relative difference between λ_{1q} and β_{1q} is less than 25%.

6.2 MIMO designs in the BC

In this section we study how to achieve space-division multiple access (SDMA) in communication systems that are based on the FBMC/OQAM modulation scheme. In particular, we focus on the broadcast channel. The objective is to design MIMO precoding and decoding strategies that allow the base station to simultaneously serve several users in the same frequency resources under the condition that each user does not receive the signal intended for other users, i.e. the zero forcing condition.

As for the system model, consider the block diagram sketched in Figure 6.3 where a single

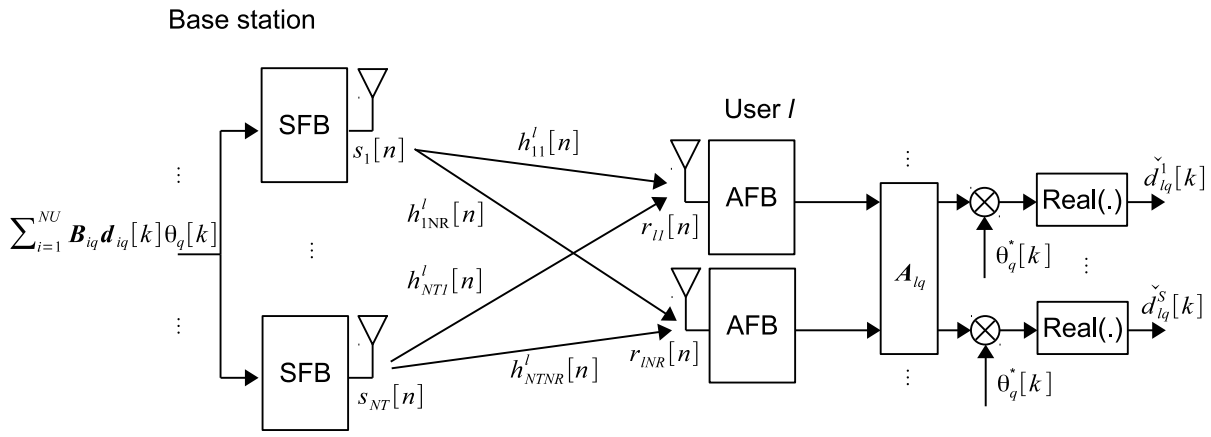

Figure 6.3: FBMC/OQAM-based MIMO broadcast channel.

BS communicates to N_U users. While each user equipment has N_R antennas the BS is equipped with N_T antennas. Extending the expressions formulated in Section 6.1, we can define the symbols estimated by the lth user on the qth subcarrier as follows:

$$\check{\mathbf{d}}_{lq}[k] = \sum_{i=1}^{N_U} \sum_{m=q-1}^{q+1} \sum_{\tau=-3}^{3} \Re\left(\theta_q^*[k]\theta_m[k-\tau]\alpha_{qm}[\tau]\mathbf{A}_{lq}^H\mathbf{H}_{lm}\mathbf{B}_{im}\right)\mathbf{d}_{im}[k-\tau] + \Re\left(\mathbf{A}_{lq}^H\mathbf{w}_{lq}[k]\right), \quad (6.35)$$

for $1 \leq l \leq N_U$. The information conveyed on the mth subcarrier that is intended for the ith user is collected in this vector $\mathbf{d}_{im}[k] \in \mathbb{R}^{S\times 1}$. Note that the symbols that are meant to the user i are linearly precoded and equalized with matrices $\mathbf{B}_{im} \in \mathbb{C}^{N_T\times S}$ and $\mathbf{A}_{im} \in \mathbb{C}^{N_R\times S}$, respectively. The vector $\mathbf{w}_{lq}[k] \in \mathbb{C}^{N_R\times 1}$ accounts for the filtered noise that contaminates the reception of the lth user at the qth output of the FBMC/OQAM demodulator. From (6.35), it can be inferred that the subcarrier spacing is such that the matrix (6.3) can be approximated to (6.4). In notation terms, the (j,i)th entry of $\mathbf{H}_{lm}$ corresponds to the frequency response of $h_{ij}^l[n]$ evaluated on the radial frequency $e^{j\frac{2\pi m}{M}}$.

Bearing in mind the global communication system written in (6.35), we devise in the following two techniques to achieve SDMA in FBMC/OQAM systems. To the best our knowledge [142] is the only work that investigates the precoding design in the FBMC/OQAM context to achieve multiple access in the downlink. To eliminate the interference the transmit processing is based on performing a space-time processing so that the resulting SDMA precoder on a given subcarrier is obtained by computing the inverse of a $12N_T\left(N+L-1\right) \times 10N_RN$ matrix, where L is the channel length and N the number of signals that are jointly processed. The techniques proposed in the following achieve SDMA in the absence of interference by exclusively performing a pure space

processing, which drastically reduces the complexity. With that being said, it is fair to mention that we assume the flat fading condition at the subcarrier level. By contrast, no assumptions are made in [142].

6.2.1 Block diagonalization

SDMA via block diagonalization (BD) allows the base station to serve multiple users while ensuring that the signal intended for a given user does not interfere the reception of the unintended users [143]. The BD is a practical approach that achieves interference-free data multiplexing while offers a good trade-off between complexity and performance. If the channel has memory, the same concept can be performed on a per-subcarrier basis by resorting to the OFDM modulation [144]. Hereinafter we revisit the BD technique so that it can be used in the FBMC/OQAM context. In this regards, it is important to remark that inter-user interference is removed in case precoders are designed as it is proposed in [143]. In other words, if precoders are factorized as $\mathbf{B}_{im} = \mathbf{V}_{im}^{0}\bar{\mathbf{B}}_{im}$, where $\mathbf{V}_{im}^{0} \in \mathbb{C}^{N_T \times N_T-(N_U-1)N_R}$ spans the null space of $\left[\mathbf{H}_{1m}^{T}, \cdots, \mathbf{H}_{(l-1)m}^{T}, \mathbf{H}_{(l+1)m}^{T}, \cdots, \mathbf{H}_{N_U m}^{T}\right]^{T}$ and $\bar{\mathbf{B}}_{im} \in \mathbb{C}^{N_T - N_R(N_U-1)\times S}$ is the inner precoder, then (6.35) is recasted as

$$\check{\mathbf{d}}_{lq}[k] = \sum_{m=q-1}^{q+1} \sum_{\tau=-3}^{3} \Re\left(\theta_q^{*}[k]\theta_m[k-\tau]\alpha_{qm}[\tau]\mathbf{A}_{lq}^{H}\mathbf{H}_{lm}\mathbf{V}_{lm}^{0}\bar{\mathbf{B}}_{lm}\right)\mathbf{d}_{lm}[k-\tau] + \Re\left(\mathbf{A}_{lq}^{H}\mathbf{w}_{lq}[k]\right). \quad (6.36)$$

Now we can deal with ISI and ICI by designing the remaining degrees of freedom given by $\left\{\bar{\mathbf{B}}_{iq}, \mathbf{A}_{lq}\right\}$ according to the WLP described in Section 6.1.3. It must be mentioned that the WLP constraints the equalizers to solely have real components. If $\mathbf{H}_{lq-1} = \mathbf{H}_{lq} = \mathbf{H}_{lq+1}$ we can benefit from the theory developed in [140] by proceeding as Section 6.1.1 proposes. In the linear case, the maximum number of transmittable streams is given by $S \leq \min\left\{N_R, N_T - N_R\left(N_U - 1\right)\right\}$, while in the widely linear counterpart the number of streams that can be multiplexed has to comply with $S \leq \min\left\{N_R, 2N_T - 2N_R\left(N_U - 1\right) - N_R\right\}$. In both cases the number of users and the number of transmit and receive antennas are related as follows: $N_T > N_R(N_U - 1)$.

6.2.2 Spatial Tomlinson Harashima precoder

In this section, as an alternative to the BD technique, we propose to achieve SDMA by applying the spatial Tomlinson Harashima precoder (STHP). The beauty of this technique is that it is able to give better performance than other MIMO precoders that perform a linear processing, [145,146].

The approach used in the original Tomlinson Harashima precoder to combat ISI can be tailored to MIMO architectures to remove the inter-user interference, [145, 146]. In this sense it is required to factorize the channel matrix as the product of a lower triangular matrix and a unitary matrix.

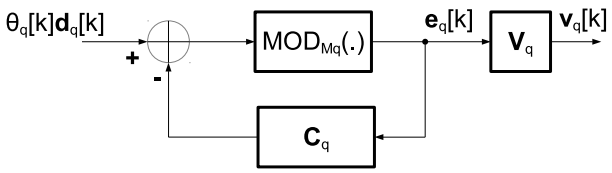

Figure 6.4: Block diagram of the spatial Tomlinson-Harashima precoder.

The same idea can be performed on a per-subcarrier basis in multicarrier systems as long as the channel frequency response is flat at the subcarrier level and there is neither ISI nor ICI. The problem of having ISI and ICI, which arises in FBMC/OQAM systems, may render the original solution impractical. To demonstrate so, we adopt the model written in (6.35) for single-antenna receivers. Then, the estimated symbol by the lth user becomes

$$\check{d}_{lq}[k] = \sum_{m=q-1}^{q+1} \sum_{\tau=-3}^{3} \Re\left(\theta_q^*[k]\theta_m[k-\tau]\alpha_{qm}[\tau]a_{lq}\mathbf{h}_{lm}\mathbf{v}_m[k-\tau]\right) + \Re\left(a_{lq}w_{lq}[k]\right). \tag{6.37}$$

Here $\{a_{lq}\}$ and $w_{lq}[k]$ are scalars and $\mathbf{h}_{lm} \in \mathbb{C}^{1\times N_T}$ is a row vector. The vector $\mathbf{v}_m \in \mathbb{C}^{N_T\times 1}$ maps $\mathbf{d}_m[k] \in \mathbb{R}^{N_U\times 1}$ onto the N_T transmit antennas by carrying out a non-linear processing. The lth element of $\mathbf{d}_m[k]$, i.e. $d_{lm}[k]$, corresponds to the symbol destined to the user l, for $1 \leq l \leq N_U$. If we arrange the symbols estimated by all users as follows: $\check{\mathbf{d}}_q[k] = \left[\check{d}_{1q}[k], \cdots, \check{d}_{N_Uq}[k]\right]^T$, we obtain

$$\check{\mathbf{d}}_q[k] = \sum_{m=q-1}^{q+1} \sum_{\tau=-3}^{3} \Re\left(\theta_q^*[k]\alpha_{qm}[\tau]\mathbf{A}_q\mathbf{H}_m\mathbf{v}_m[k-\tau]\right) + \Re\left(\mathbf{A}_q\mathbf{w}_q[k]\right), \tag{6.38}$$

where $\mathbf{H}_m = \left[\mathbf{h}_{1m}^T \cdots \mathbf{h}_{N_Um}^T\right]^T$ and $\mathbf{A}_q = \operatorname{diag}\{a_{1q}, \cdots, a_{N_Uq}\}$. The noise vector is defined as $\mathbf{w}_q[k] = [w_{1q}[k], \cdots, w_{N_Uq}[k]]^T$. The key feature of the STHP relies on factorizing the channel matrix as $\mathbf{H}_m = \mathbf{L}_m\mathbf{V}_m^H$. Assuming that $N_T \geq N_U$, the $N_U \times N_U$ square matrix $\mathbf{L}_m$ is lower triangular and the columns of $\mathbf{V}_m \in \mathbb{C}^{N_T\times N_U}$ are orthonormal. The transmit nonlinear processing performed on the qth subband is illustrated in Figure 6.4. From the entries located at the main diagonal of $\mathbf{L}_q$ we define the following diagonal matrix $\mathbf{D}_q = \operatorname{diag}\left\{[\mathbf{L}_q]_{11}, \cdots, [\mathbf{L}_q]_{N_UN_U}\right\}$, which enables us to generate the feedback matrix as follows: $\mathbf{C}_q = \mathbf{D}_q^{-1}\mathbf{L}_q - \mathbf{I}_{N_U}$. As for the notation the expression $[\mathbf{A}]_{ij}$ accounts for the entry of matrix $\mathbf{A}$ located at the ith row and jth column. Based on these definitions, the lth element of the N_U-dimensional column vector $\mathbf{e}_q[k]$ is given by this closed-form expression

$$[\mathbf{e}_q[k]]_l = \mathrm{MOD}_{\mathrm{M}_q}\left(\theta_q[k]d_{lq}[k] - \sum_{u=1}^{l-1}[\mathbf{e}_q[k]]_u\,[\mathbf{C}_q]_{lu}\right) = \theta_q[k]d_{lq}[k] - \sum_{u=1}^{l-1}[\mathbf{e}_q[k]]_u\,[\mathbf{C}_q]_{lu} + p_{lq}[k]. \tag{6.39}$$

Provided that $d_{lq}[k]$ has not unit energy and is generated from a M_q-PAM, i.e. $d_{lq}[k] \in \left\{\pm 1, ..., \pm\sqrt{M_q} \mp 1\right\}$, then the modulo arithmetic $\mathrm{MOD}_{\mathrm{M}_q}(x)$ maps the complex number x in this region $R = \left\{x_r + jx_i | x_r, x_i \in \left(-\sqrt{M_q}, \sqrt{M_q}\right)\right\}$, [146]. This means that the modulo arithmetic is equivalent to add multiples of $2\sqrt{M_q}$ to the real and imaginary parts of the argument. Hence, the real and imaginary parts of $p_{lq}[k]$ are multiples of $2\sqrt{M_q}$. The subband processing depicted in Figure 6.4 allows us to recast (6.38) as

$$\check{\mathbf{d}}_q[k] = \sum_{m=q-1}^{q+1}\sum_{\tau=-3}^{3}\Re\left(\theta_q^*[k]\alpha_{qm}[\tau]\mathbf{A}_q\mathbf{L}_m\mathbf{e}_m[k-\tau]\right) + \Re\left(\mathbf{A}_q\mathbf{w}_q[k]\right). \tag{6.40}$$

Since the receivers are not allowed to cooperate the decentralized receive processing that allows each user to recover the desired information consists in setting $a_{lq} = \frac{1}{[\mathbf{L}_q]_{ll}}$. Taking into account that $\mathbf{L}_m$ is a lower triangular matrix, it follows that

$$\begin{aligned}\check{d}_{lq}[k] = &\sum_{m=q-1}^{q+1}\sum_{\tau=-3}^{3}\Re\left\{\theta_q^*[k]\alpha_{qm}[\tau]\frac{[\mathbf{L}_m]_{ll}}{[\mathbf{L}_q]_{ll}}\,[\mathbf{e}_m[k-\tau]]_l\right\} + \\ &\sum_{m=q-1}^{q+1}\sum_{\tau=-3}^{3}\sum_{u=1}^{l-1}\Re\left\{\theta_q^*[k]\alpha_{qm}[\tau]\frac{[\mathbf{L}_m]_{lu}}{[\mathbf{L}_q]_{ll}}\,[\mathbf{e}_m[k-\tau]]_u\right\} + \Re\left\{\frac{w_{lq}[k]}{[\mathbf{L}_q]_{ll}}\right\}.\end{aligned} \tag{6.41}$$

Replacing $\mathbf{e}_m[k]$ with (6.39) yields

$$\begin{aligned}\check{d}_{lq}[k] = &\sum_{m=q-1}^{q+1}\sum_{\tau=-3}^{3}\Re\left\{\theta_q^*[k]\alpha_{qm}[\tau]\frac{[\mathbf{L}_m]_{ll}}{[\mathbf{L}_q]_{ll}}\left(\theta_m[k-\tau]d_{lm}[k-\tau] + p_{lm}[k-\tau]\right)\right\} + \Re\left\{\frac{w_{lq}[k]}{[\mathbf{L}_q]_{ll}}\right\} \\ &+ \sum_{m=q-1}^{q+1}\sum_{\tau=-3}^{3}\sum_{u=1}^{l-1}\Re\left\{\theta_q^*[k]\alpha_{qm}[\tau]\left(\frac{[\mathbf{L}_m]_{lu}}{[\mathbf{L}_q]_{ll}} - \frac{[\mathbf{L}_m]_{ll}}{[\mathbf{L}_q]_{ll}}\,[\mathbf{C}_m]_{lu}\right)[\mathbf{e}_m[k-\tau]]_u\right\}.\end{aligned} \tag{6.42}$$

By observing (6.42) we conclude that the orthogonality is not restored in the real field. If $\mathbf{H}_{q-1} = \mathbf{H}_q = \mathbf{H}_{q+1}$, then $\mathbf{L}_{q-1} = \mathbf{L}_q = \mathbf{L}_{q+1}$ and $\mathbf{C}_{q-1} = \mathbf{C}_q = \mathbf{C}_{q+1}$. As a result, (6.42) becomes

$$\check{d}_{lq}[k] = d_{lq}[k] + \sum_{m=q-1}^{q+1}\sum_{\tau=-3}^{3}\Re\left\{\theta_q^*[k]\alpha_{qm}[\tau]p_{lm}[k-\tau]\right\} + \Re\left\{\frac{w_{lq}[k]}{[\mathbf{L}_q]_{ll}}\right\}. \tag{6.43}$$

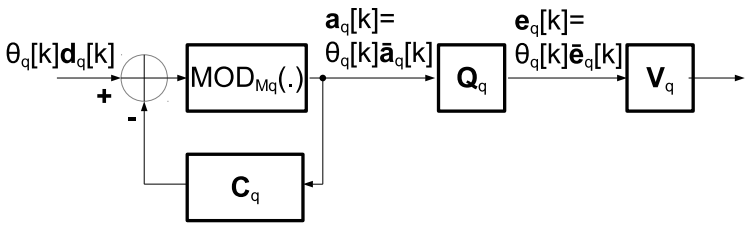

Figure 6.5: Block diagram of the proposed spatial Tomlinson-Harashima precoder.

Since $\Re\left\{\theta_q^*[k]\alpha_{qm}[\tau]p_{lm}[k-\tau]\right\}$ is not a multiple of $2\sqrt{M_q}$ the interference is not removed when (6.43) is modulo reduced. Therefore, we can state that in case the frequency selectivity is not appreciable there is still interference. This observation highlights that the classical STHP does not remove the interference when it is implemented on a per-subcarrier basis in FBMC/OQAM systems. To remedy this problem we have devised a novel subband processing that is illustrated in Figure 6.5. The idea is to design the matrix $\mathbf{V}_q \in \mathbb{C}^{N_T \times 2N_T - N_U}$ with the objective of projecting all the interferences into the same subspace, which should be orthogonal to the subspace where the symbols of interest belong to. To do so, it is deemed necessary that matrices $\mathbf{C}_q, \mathbf{Q}_q$ are restricted to be real-valued. Consequently, since $\theta_q[k]\mathbf{d}_q[k]$ is either real or pure imaginary, the modulo arithmetic will only add multiples of $2\sqrt{M_q}$ in a single dimension. Hence, the vectors $\mathbf{a}_q[k], \mathbf{e}_q[k]$ can be factorized as $\mathbf{a}_q[k] = \theta_q[k]\bar{\mathbf{a}}_q[k]$ and $\mathbf{e}_q[k] = \theta_q[k]\bar{\mathbf{e}}_q[k]$ where $\bar{\mathbf{a}}_q[k] \in \mathbb{R}^{N_U \times 1}$ and $\bar{\mathbf{e}}_q[k] \in \mathbb{R}^{2N_T - N_U \times 1}$. From Figure 6.5 we can deduce that

$$[\bar{\mathbf{a}}_q[k]]_l = \mathrm{MOD}_{\mathrm{M}_q}\left(d_{lq}[k] - \sum_{u=1}^{l-1}[\bar{\mathbf{a}}_q[k]]_u [\mathbf{C}_q]_{lu}\right) = d_{lq}[k] - \sum_{u=1}^{l-1}[\bar{\mathbf{a}}_q[k]]_u [\mathbf{C}_q]_{lu} + p_{lq}[k] \tag{6.44}$$

and $\bar{\mathbf{e}}_q[k] = \mathbf{Q}_q\bar{\mathbf{a}}_q[k]$. Note that $p_{lq}[k]$ is a pure real number multiple of $2\sqrt{M_q}$. Assume that the decentralized receive processing is based on the diagonal matrix $\mathbf{D}_q^{-1}$, whose entries are real. Performing the usual post-processing, the vector of estimated symbols is formulated in this form

$$\check{\mathbf{d}}_q[k] \;=\; \sum_{m=q-1}^{q+1}\sum_{\tau=-3}^{3} \mathbf{D}_q^{-1}\Re\left\{\theta_q^*[k]\theta_m[k-\tau]\alpha_{qm}[\tau]\mathbf{H}_m\mathbf{V}_m\right\}\bar{\mathbf{e}}_m[k-\tau] + \Re\left\{\mathbf{D}_q^{-1}\mathbf{w}_q[k]\right\}. \tag{6.45}$$

It is important to remark that (6.45) bears resemblance with (6.20). And so, if the augmented vector $\mathbf{V}_{q,e} = \left[\Re\left(\mathbf{V}_m\right)^T \quad \Im\left(\mathbf{V}_m\right)^T\right]^T$ spans the null space of $[\Im\left(\mathbf{H}_m\right) \quad \Re\left(\mathbf{H}_m\right)]$ we force the product $\mathbf{H}_m\mathbf{V}_m$ to solely have in-phase components, thus (6.45) will be only affected by multiuser interference leading to this expression

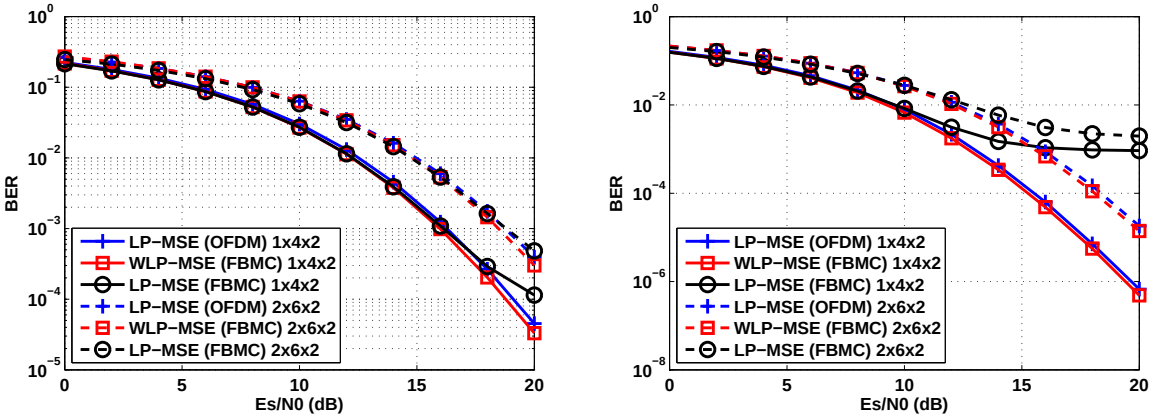

(a) Scenario 2.

(b) Scenario 1.

Figure 6.6: BER vs. $\frac{E_s}{N_0}$ when BD is applied to FBMC/OQAM and OFDM systems. System parameters are set according to Scenarios 1 and 2 (see Table 2.3).

$$\check{\mathbf{d}}_q[k] = \mathbf{D}_q^{-1}\Re\left\{\mathbf{H}_q\mathbf{V}_q\right\}\bar{\mathbf{e}}_q[k] + \Re\left\{\theta_q^*[k]\mathbf{D}_q^{-1}\mathbf{w}_q[k]\right\}. \tag{6.46}$$

Once ISI and ICI are removed, we can cope with inter-user interference by designing the matrices $\mathbf{C}_q, \mathbf{Q}_q$ and $\mathbf{D}_q$ in the same way as the original STHP after computing the QR decomposition of $\Re\{\mathbf{H}_q\mathbf{V}_q\}$. Then, the symbol estimated by the lth receiver on the qth subband is given by

$$\check{d}_{lq}[k] = d_{lq}[k] + p_{lq}[k] + \Re\left\{\frac{w_{lq}[k]}{[\mathbf{L}_q]_{ll}}\right\}. \tag{6.47}$$

Finally $\check{d}_{lq}[k]$ is fed into the modulo device to get rid of the offset $p_{lq}[k]$. Regarding the impact of appending the precoder matrix $\mathbf{V}_q$ we can state that the power will not be boosted if symbols are independent since $\mathrm{tr}\left(\mathbf{V}_q\mathbf{Q}_q\mathbf{Q}_q^T\mathbf{V}_q^H\right) = \mathrm{tr}\left(\mathbf{Q}_q\mathbf{Q}_q^T\Re\left\{\mathbf{V}_q^H\mathbf{V}_q\right\}\right) = \mathrm{tr}\left(\mathbf{Q}_q\mathbf{Q}_q^T\mathbf{V}_{q,e}^T\mathbf{V}_{q,e}\right) = N_U$.

6.2.3 Simulation results

To resolve if the techniques devised in Sections 6.2.1 and 6.2.2 achieve competitive results we have simulated the downlink of a communication system where the BS sends data to N_U users in the same time slots and subcarriers. The transmitted streams in OFDM and FBMC/OQAM systems are generated according to the 16-QAM constellation. However, in the FBMC/OQAM case the real and imaginary parts are delayed half the symbol period. The length of the CP in the OFDM modulation is equal to $\frac{M}{4}$ samples.

The curves portrayed in Figure 6.6 correspond to the BER that is obtained in the BC when

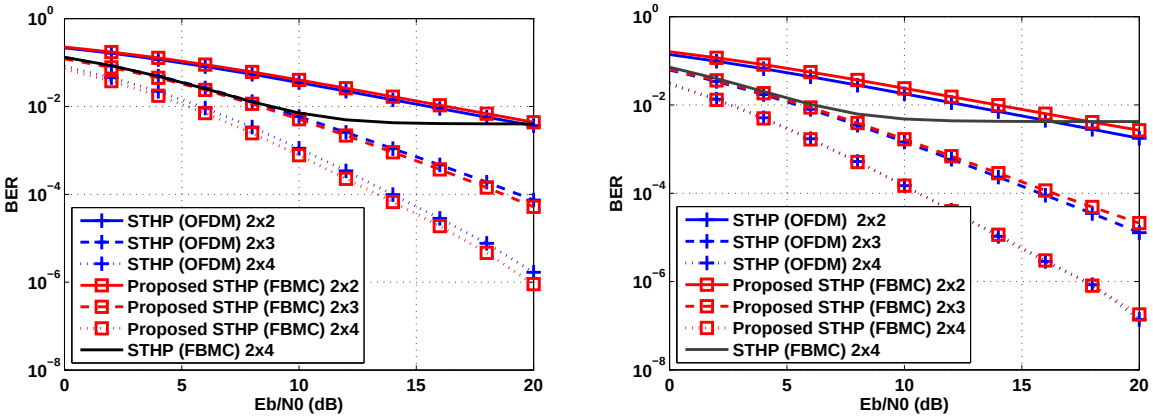

(a) Scenario 2.

(b) Scenario 1.

Figure 6.7: BER vs. $\frac{E_s}{N_0}$ when the TH concept is applied to FBMC/OQAM and OFDM systems. System parameters are set according to Scenarios 1 and 2 (see Table 2.3).

the BD technique is applied. The idea consists in combining the ZF precoder that eliminates inter-user interference [143], with the beamforming design addressed in Sections 6.1.1, 6.1.2 and 6.1.3. The BER has been computed for different energy symbol to noise ratio values $\frac{E_s}{N_0} = \frac{M+CP}{M}\frac{2P_T}{MN_0}$. Regarding the multi-antenna configuration, we have focused on scenarios where $N_T \geq N_U N_R$ and $S = N_R \leq 2$. In this case all the modes are active and, as it has been observed in Section 6.1.6, the conditions of Lemmas 6.31 and 6.33 are likely to be satisfied. If so, it is expected that FBMC/OQAM slightly outperforms OFDM. As for the notation, the compact expression $N_R \times N_T \times N_U$ indicates that each receiver has N_R antennas, the BS is equipped with N_T antennas and the number of users is N_U. The results of Figure 6.6 correspond to a multi-user environment where the number of users is fixed to two, i.e. $N_U = 2$. The WLP, as we have predicted, achieves competitive results with respect to the LP counterpart. Nevertheless, the LP exhibits an error floor when it is applied to FBMC/OQAM systems under the propagation conditions described in Scenario 1.

Next, we evaluate the performance of the proposed STHP. As a benchmark the conventional STHP is directly implemented on a per-subcarrier basis in OFDM and FBMC/OQAM systems. In Figure 6.7 we have depicted the BER against the energy bit to noise ratio (E_b/N_0) when the number of users is equal to two. Since we have selected a 16-ary constellation, the energy bit has been computed as $E_b = \frac{160}{4\times 16} = 2.5$ according to the model used in Section 6.2.2. As for the compact notation, a $N_U \times N_T$ multi-user MISO communication system accounts for a scenario where the number of single-antenna receivers is equal to N_U and the number of antennas deployed at the BS is N_T. Notice that when $N_T = N_U$ the OFDM modulation slightly outperforms the proposed

technique although in Scenario 2 the gap is almost negligible. The performance degradation has to do with the fact that the elements in the diagonal of $\mathbf{L}_q$ have a higher magnitude in the classical STHP than in the proposed STHP. The reason is because we are working with a projected MIMO channel in the proposed technique. However, as the number of the antennas increases we have detected that the difference of the magnitudes is reduced to a higher extent. As a consequence, the FBMC/OQAM gives better performance than OFDM when $N_T = 4$ since no energy is devoted to transmit redundancy. Notice that the STHP (FBMC) technique exhibits an error floor because the classical STHP generates interference when it is directly applied to the FBMC/OQAM modulation.

6.3 Chapter summary

With the aim of making progress in the research of multiantenna and multicarrier techniques this chapter addresses the design of MIMO precoding and decoding strategies for the FBMC/OQAM modulation scheme. The first solution that has been envisaged aims at improving PTP communications and assumes that the channel coherence bandwidth is sufficiently wide so that the frequency selectivity is no perceptible at the subcarrier level. In addition, the proposed beamforming design performs a WLP to benefit from the improperness property of transmitted symbols. The theoretical analysis that has been conducted demonstrates that for some multiantenna configurations, the best strategy is to combine FBMC/OQAM with the MIMO techniques originally devised for OFDM, which is based on the LP. This holds true when the number of streams (S), and the number of transmit antennas (N_T) and receive antennas (N_R) are related as follows: $S \leq N_R \leq 3$, $N_T \geq N_R$. However, when $S = N_R$ the LP slightly outperforms the WLP. It is worth emphasizing that the approach based on combining the MIMO techniques that rely on the LP to FBMC/OQAM systems performs poorly at low noise regime. That is because this technique only offers a good performance if the channel frequency response is flat at least in three consecutive subchannels. In the simulated scenarios this is not satisfied and, therefore, at low noise regime the LP is not suited for FBMC/OQAM because the detection is affected by an error floor. Interestingly, the WLP especially devised for FBMC/OQAM slightly outperforms MIMO-OFDM systems if we stick to the configuration where $S = N_R \leq 2$ and $N_T \geq N_R$. In this scenario the penalty of transmitting redundancy in OFDM systems results in BER degradation when compared to results obtained by MIMO-FBMC/OQAM systems based on the WLP.

In the second part of the chapter we study how to achieve SDMA in the absence of interference in FBMC/OQAM systems. Towards this end, the WLP devised for PTP communications has been revisited so that it can be used in the BC. In this sense, it has been shown that the BD concept can be used in conjunction with the proposed WLP. As a result, several users can be served in the same time slots and frequency resources in the absence of interference. Benefiting from the theory

developed when evaluating the special case where there is only a single user, we have concluded that under some conditions the proposed solution is able to moderately outperform the OFDM technique on the downlink of a multi-user communication system. In particular, if $N_T \geq N_U N_R$ and $S = N_R \leq 2$, where N_T is the number of the transmit antennas, N_U the number of users and S the number of streams intended for each user. It is important to remark that the processing that comes from combing the BD technique with the LP offers a good performance in the FBMC/OQAM context in terms of BER. However, the channel frequency response has to be flat in a region that at least encompasses 3 subchannels. Since this assumption is not accurate, the error floor becomes visible and the BER curves saturate.

The second alternative that has been reviewed to achieve SDMA is based on the Tomlinson Harashima concept. The analytical expressions that we have derived have led us to discard the conventional STHP since it fails to eliminate the interference in the FBMC/OQAM context. The modulo reduction to ensure that the transmitted power does not substantially increases is the main responsible. This has motivated us to design a novel subband processing based on the STHP concept. The proposed solution is inspired by the WLP initially though for PTP communications. Simulation-based results highlight that the proposed solution gives a satisfactory performance because the BER is in the same order as the conventional STHP when it is combined with the OFDM modulation.

Appendices

6.A Demonstration of Lemma 6.28

The demonstration of (6.28) relies on the fact that the vector $\tilde{\boldsymbol{\lambda}}_q = \left[\lambda_{N_R q}^{-1}, ..., \lambda_{1q}^{-1}\right]$ is majorized by $\tilde{\boldsymbol{\beta}}_q = \left[\beta_{N_R q}^{-1}, ..., \beta_{1q}^{-1}\right]$ whenever $N_R \leq 3$ and $N_T \geq N_R$ (see Appendix 6.B). After some manipulations (6.29) and (6.30) are transformed into

$$\frac{1}{\frac{p_{lq}^L \beta_{lq}}{0.5 N_0} + 1} = \frac{\beta_{lq}^{-1}}{\beta_{lq}^{-1} + \frac{2 P_T \beta_{lq}^{-0.5} N_0^{-1}}{S}} \tag{6.48}$$

$$\sum_{m \in S_a} \sum_{t=1} \beta_{tm}^{-0.5}$$

$$\frac{1}{\frac{p_{lq}^{WL} \lambda_{lq}}{0.5 N_0} + 1} = \sum_{l=1}^{S} \frac{\lambda_{lq}^{-1}}{\lambda_{lq}^{-1} + \frac{2 P_T \lambda_{lq}^{-0.5} N_0^{-1}}{S}} \cdot \tag{6.49}$$

$$\sum_{m \in S_a} \sum_{t=1} \lambda_{tm}^{-0.5}$$

The proof consists in showing that

$$\sum_{l=1}^{S}\frac{\beta_{lq}^{-1}}{\beta_{lq}^{-1}+\frac{2P_T\beta_{lq}^{-0.5}N_0^{-1}}{S}\sum\limits_{m\in S_a}\sum\limits_{t=1}\beta_{tm}^{-0.5}}\leq\sum_{l=1}^{S}\frac{\beta_{lq}^{-1}}{\beta_{lq}^{-1}+\frac{2P_T\beta_{lq}^{-0.5}N_0^{-1}}{S}\sum\limits_{m\in S_a}\sum\limits_{t=1}\lambda_{tm}^{-0.5}}\leq\sum_{l=1}^{S}\frac{\lambda_{lq}^{-1}}{\lambda_{lq}^{-1}+\frac{2P_T\lambda_{lq}^{-0.5}N_0^{-1}}{S}\sum\limits_{m\in S_a}\sum\limits_{t=1}\lambda_{tm}^{-0.5}}. \tag{6.50}$$

The first inequality follows from this result

$$\sum_{l=1}^{S}\beta_{lq}^{-0.5}\leq\sum_{l=1}^{S}\lambda_{lq}^{-0.5},\quad 1\leq S\leq N_R\leq 3. \tag{6.51}$$

The above inequality is direct when $S=N_R$ and $\left[\lambda_{N_Rq}^{-1},...,\lambda_{1q}^{-1}\right]$ is majorized by $\left[\beta_{N_Rq}^{-1},...,\beta_{1q}^{-1}\right]$. Proof: since $-x^{0.5}$ is convex, then $\sum_{l=1}^{N_R}x_l^{0.5}$ is Schur-concave. As a result, $\sum_{l=1}^{N_R}x_l^{0.5}\leq\sum_{l=1}^{N_R}y_l^{0.5}$ if $[y_1,...,y_{N_R}]$ is majorized by $[x_1,...,y_{N_R}]$, [147].

The inequality (6.51) is still met for $S<N_R$ because $\lambda_{N_Rq}\geq\beta_{N_Rq}$ and $\lambda_{1q}\leq\beta_{1q}$. The proof is provided in Appendix 6.C.

To show the second inequality in (6.50) we resort again to the majorization theory. The proof is as follows: since $-\frac{x}{x+ax^{0.5}}$ is convex, where a is a positive constant, the function $\sum_{l=1}^{N_R}\frac{x_l}{x_l+ax_l^{0.5}}$ is Schur-concave. Therefore, the second inequality in (6.50) is satisfied when $S=N_R$ because $\left[\lambda_{N_Rq}^{-1},...,\lambda_{1q}^{-1}\right]$ is majorized by $\left[\beta_{N_Rq}^{-1},...,\beta_{1q}^{-1}\right]$. With that being said, it can be checked that the result is also valid for $S<N_R$ since $\lambda_{N_R}\geq\beta_{N_R}$ and $\lambda_1\leq\beta_1$.

With this we conclude the proof that the LP brings a lower sum MSE than the WLP at high SINR if $N_R\leq 3$, $N_T\geq N_R$.

6.B Demonstration that $\tilde{\boldsymbol{\lambda}}_q$ is majorized by $\tilde{\boldsymbol{\beta}}_q$

In this appendix we will demonstrate that the vector $\tilde{\boldsymbol{\lambda}}_q=\left[\lambda_{N_Rq}^{-1},...,\lambda_{1q}^{-1}\right]$ is majorized by $\tilde{\boldsymbol{\beta}}_q=\left[\beta_{N_Rq}^{-1},...,\beta_{1q}^{-1}\right]$ if $N_R\leq 3$ and $N_T\geq N_R$, i.e.

$$\begin{aligned}&\sum_{l=1}^{S}\lambda_{(N_R-l+1)q}^{-1}\leq\sum_{l=1}^{S}\beta_{(N_R-l+1)q}^{-1},\quad 1\leq S\leq N_R-1\\&\sum_{l=1}^{N_R}\lambda_{lq}^{-1}=\sum_{l=1}^{N_R}\beta_{lq}^{-1},\quad N_R\leq 3.\end{aligned} \tag{6.52}$$

It is worth mentioning that the eigenvalues are arranged in descending order. That is, $\beta_{1q}\geq$

$... \geq \beta_{N_R q}$ and $\lambda_{1q} \geq ... \geq \lambda_{N_R q}$. If the equality in (6.52) is satisfied, then the inequality is deduced from this result, $\lambda_{N_R} \geq \beta_{N_R}$ and $\lambda_1 \leq \beta_1$ (see Appendix 6.C). Thus, the proof comes down to demonstrate the second line of (6.52). To this end, we evaluate if

$$\begin{aligned} \operatorname{tr}\left(\left(\mathbf{H}_q\mathbf{H}_q^H\right)^{-1}\right) = \sum_{l=1}^{N_R}\beta_{lq}^{-1} = \quad \operatorname{tr}\Big(\Big(&\left[\Re\left(\mathbf{H}_q\right) \quad -\Im\left(\mathbf{H}_q\right)\right]\left[\Re\left(\mathbf{H}_q\right) \quad -\Im\left(\mathbf{H}_q\right)\right]^T \\ &-j\left[\Re\left(\mathbf{H}_q\right) \quad -\Im\left(\mathbf{H}_q\right)\right]\left[\Im\left(\mathbf{H}_q\right) \quad \Re\left(\mathbf{H}_q\right)\right]^T\Big)^{-1}\Big) \end{aligned} \tag{6.53}$$

and

$$\operatorname{tr}\left(\left(\left[\Re\left(\mathbf{H}_q\right) \quad -\Im\left(\mathbf{H}_q\right)\right]\mathbf{F}_q^0\left(\left[\Re\left(\mathbf{H}_q\right) \quad -\Im\left(\mathbf{H}_q\right)\right]\mathbf{F}_q^0\right)^T\right)^{-1}\right) = \sum_{l=1}^{N_R}\lambda_{lq}^{-1} \tag{6.54}$$

coincide. The row permutation matrix

$$\mathbf{P} = \begin{bmatrix} 0 & 1 \\ -1 & 0 \end{bmatrix} \otimes \mathbf{I}_{N_T} \tag{6.55}$$

allows us to write

$$\begin{aligned} \left[\Im\left(\mathbf{H}_q\right) \quad \Re\left(\mathbf{H}_q\right)\right] &= \left[\Re\left(\mathbf{H}_q\right) \quad -\Im\left(\mathbf{H}_q\right)\right]\mathbf{P} \\ \left[\Im\left(\mathbf{H}_q\right) \quad \Re\left(\mathbf{H}_q\right)\right]\mathbf{P}^T &= \left[\Re\left(\mathbf{H}_q\right) \quad -\Im\left(\mathbf{H}_q\right)\right]. \end{aligned} \tag{6.56}$$

The operation $\otimes$ is the Kronecker product and $\mathbf{I}_a$ is the a-dimensional identity matrix. The inverse in (6.53) and (6.54) can be computed if the channel matrix in not rank deficient. In other words we assume that $\operatorname{rank}\left(\mathbf{H}_q\right) = N_R$ and $N_T \geq N_R$. To show that (6.53) and (6.54) are equivalent we use the following singular value decomposition

$$\left[\Re\left(\mathbf{H}_q\right) \quad -\Im\left(\mathbf{H}_q\right)\right] = \mathbf{U}_q\left[\Sigma_q \mathbf{0}\right]\left[\mathbf{V}_q^1\mathbf{V}_q^0\right]^T. \tag{6.57}$$

This implies that the columns of $\mathbf{F}_q^0 = \mathbf{P}^T\mathbf{V}_q^0 \in \mathbb{R}^{2N_T \times 2N_T - N_R}$ span the null space of matrix $\left[\Im\left(\mathbf{H}_q\right) \quad \Re\left(\mathbf{H}_q\right)\right]$. With that (6.53) and (6.54) can be recasted as follows:

$$\sum_{l=1}^{N_R}\beta_{lq}^{-1} = \operatorname{tr}\left(\left(\mathbf{I}_{N_R} - j\left(\mathbf{V}_q^1\right)^T\mathbf{P}^T\mathbf{V}_q^1\right)^{-1}\Sigma_q^{-2}\right) \tag{6.58}$$

$$\sum_{l=1}^{N_R}\lambda_{lq}^{-1} = \operatorname{tr}\left(\left(\left(\mathbf{V}_q^1\right)^T\mathbf{P}^T\mathbf{V}_q^0\left(\mathbf{V}_q^0\right)^T\mathbf{P}\mathbf{V}_q^1\right)^{-1}\Sigma_q^{-2}\right). \tag{6.59}$$

From the singular value decomposition we know that $\left(\mathbf{V}_q^1\right)^T \mathbf{V}_q^1 = \mathbf{I}_{N_R}$ and $\mathbf{V}_q^1 \left(\mathbf{V}_q^1\right)^T + \mathbf{V}_q^0 \left(\mathbf{V}_q^0\right)^T = \mathbf{I}_{2N_T}$. Hence (6.59) is transformed into

$$\sum_{l=1}^{N_R} \lambda_{lq}^{-1} = \mathrm{tr}\left(\left(\mathbf{I}_{N_R} - \left(\mathbf{V}_q^1\right)^T \mathbf{P}^T \mathbf{V}_q^1 \left(\mathbf{V}_q^1\right)^T \mathbf{P} \mathbf{V}_q^1\right)^{-1} \Sigma_q^{-2}\right), \tag{6.60}$$

which highlights that if the diagonal elements of

$$\mathbf{D}_q^{WL} = \left(\mathbf{I}_{N_R} - \left(\mathbf{V}_q^1\right)^T \mathbf{P}^T \mathbf{V}_q^1 \left(\mathbf{V}_q^1\right)^T \mathbf{P} \mathbf{V}_q^1\right)^{-1} \tag{6.61}$$

and

$$\mathbf{D}_q^{L} = \left(\mathbf{I}_{N_R} - j \left(\mathbf{V}_q^1\right)^T \mathbf{P}^T \mathbf{V}_q^1\right)^{-1} \tag{6.62}$$

are matched, then $\sum_{l=1}^{N_R} \beta_{lq}^{-1} = \sum_{l=1}^{N_R} \lambda_{lq}^{-1}$. It is worth noticing that $\mathbf{C}_q = \left(\mathbf{V}_q^1\right)^T \mathbf{P}^T \mathbf{V}_q^1$ is a real skew-symmetric matrix. As a consequence, the eigenvalues of $\mathbf{C}_q$ are pure imaginary, [148]. In addition if γ_{iq} is an eigenvalue of $\mathbf{C}_q$, so is $-\gamma_{iq}$. This implies that if N_R is an odd number, then 0 is an eigenvalue. In the odd case, we can write this factorization $\mathbf{C}_q = \mathbf{S}\Gamma_q\mathbf{S}^H$, where $\mathbf{S}_q = [\mathbf{s}_{1q}...\mathbf{s}_{N_Rq}] \in \mathbb{C}^{N_R \times N_R}$ is a unitary matrix and the eigenvalues are gathered in this diagonal matrix $\Gamma_q = \mathrm{diag}\left(\gamma_{1q}, -\gamma_{1q}, ..., \gamma_{\frac{N_R-1}{2}q}, -\gamma_{\frac{N_R-1}{2}q}, 0\right) \in \mathbb{C}^{N_R \times N_R}$. The factorization for the N_R even case can be easily deduced from the above discussion. From this point on we assume that N_R is an odd number yet the analysis can be easily adapted to the even case. In this regard, we can write

$$\mathbf{D}_q^{WL} = \mathbf{S}_q \mathrm{diag}\left(\frac{1}{1+|\gamma_{1q}|^2}, \frac{1}{1+|\gamma_{1q}|^2}, \cdots \frac{1}{1+\left|\gamma_{\frac{N_R-1}{2}q}\right|^2}, \frac{1}{1+\left|\gamma_{\frac{N_R-1}{2}q}\right|^2}, 1\right) \mathbf{S}_q^H \tag{6.63}$$

$$\mathbf{D}_q^{L} = \mathbf{S}_q \mathrm{diag}\left(\frac{1+j\gamma_{1q}}{1+|\gamma_{1q}|^2}, \frac{1-j\gamma_{1q}}{1+|\gamma_{1q}|^2}, \cdots, \frac{1+j\gamma_{\frac{N_R-1}{2}q}}{1+\left|\gamma_{\frac{N_R-1}{2}q}\right|^2}, \frac{1-j\gamma_{\frac{N_R-1}{2}q}}{1+\left|\gamma_{\frac{N_R-1}{2}q}\right|^2}, 1\right) \mathbf{S}_q^H. \tag{6.64}$$

One property that can be derived from the fact that $\mathbf{C}_q$ is real-valued and that eigenvalues occur in complex conjugated pairs is that the eigenvectors associated with γ_{iq} and $-\gamma_{iq}$ are related as follows: $\mathbf{s}_{(2i-1)q} = \mathbf{s}_{2iq}^*$, for $1 \leq i \leq 0.5(N_R - 1)$. Let $[\mathbf{D}]_{ij}$ denote the element of matrix $\mathbf{D}$ that is located at the ith row and jth column and $[\mathbf{s}]_i$ denote the ith entry of vector $\mathbf{s}$. With this definition it is possible to check that

$$\left[\mathbf{D}_q^L\right]_{ii} = \left[\mathbf{D}_q^{WL}\right]_{ii} = \left|[\mathbf{s}_{N_Rq}]_i\right|^2 + \sum_{t=1}^{\frac{N_R-1}{2}} \frac{2\left|[\mathbf{s}_{tq}]_i\right|^2}{1+|\gamma_{tq}|^2}, \tag{6.65}$$

which allows us to conclude that the diagonal elements of (6.63) and (6.64) are equal. As it has been discussed, the equality written in (6.65) implies that $\sum_{l=1}^{N_R} \beta_{lq}^{-1} = \sum_{l=1}^{N_R} \lambda_{lq}^{-1}$. This result verifies that $\left[\lambda_{N_Rq}^{-1}, ..., \lambda_{1q}^{-1}\right]$ is majorized by $\left[\beta_{N_Rq}^{-1}, ..., \beta_{1q}^{-1}\right]$ if $N_R \leq 3$.

6.C Demonstration that $\beta_{1q} > \lambda_{1q}$ and $\beta_{N_Rq} < \lambda_{N_Rq}$

Let $\{\lambda_{lq}\}$, $\{\mathbf{u}_{lq}\}$ be respectively the non-zero eigenvalues and the corresponding eigenvectors of matrix $\bar{\mathbf{H}}_q^T \bar{\mathbf{H}}_q$, where $\bar{\mathbf{H}}_q$ is deined in (6.23). The eigenvalues are sorted in descending order, i.e. $\lambda_{1q} > ... > \lambda_{N_Rq}$. It is important to remark that we focus on the case that $N_T \geq N_R$. Furthermore, we assume that $\text{rank}(\mathbf{H}_q^H \mathbf{H}_q) = \text{rank}(\bar{\mathbf{H}}_q^T \bar{\mathbf{H}}_q) = N_R$. Regarding the complex-valued counterpart, the non-zero eigenvalues of matrix $\mathbf{H}_q^H \mathbf{H}_q$ are collected in this set $\{\beta_{1q}, ..., \beta_{N_Rq}\}$. The entries of matrix $\mathbf{H}_q$ are written in (6.5). It is worth noticing that the eigenvalues of $\mathbf{C}_q = \hat{\mathbf{H}}_q^T \hat{\mathbf{H}}_q$, where $\hat{\mathbf{H}}_q$ is formulated in (6.18), are also given by $\{\beta_{lq}\}$ but with multiplicity equal to two. Hence, the eigenvalue β_{lq} is associated to the eigenvectors $\mathbf{c}_{lq}$ and $\bar{\mathbf{c}}_{lq}$. Another interesting results is that

$$\mathbf{C}_q = \left[\Re\left(\mathbf{H}_q\right) \quad -\Im\left(\mathbf{H}_q\right)\right]^T \left[\Re\left(\mathbf{H}_q\right) \quad -\Im\left(\mathbf{H}_q\right)\right] + \left[\Im\left(\mathbf{H}_q\right) \quad \Re\left(\mathbf{H}_q\right)\right]^T \left[\Im\left(\mathbf{H}_q\right) \quad \Re\left(\mathbf{H}_q\right)\right]. \tag{6.66}$$

This result along with (6.21) and (6.56) allows us to state that any column of $\mathbf{C}_q$ is a linear combination of these $2N_R$ column-vectors $\left[\mathbf{F}_q^1 \quad \mathbf{P}\mathbf{F}_q^1\right]$. If $\text{rank}\left(\mathbf{C}_q\right) = 2N_R$, then $\mathbf{C}_q$ and $\left[\mathbf{F}_q^1 \quad \mathbf{P}\mathbf{F}_q^1\right]$ span the same subspace. Under this assumption, the null space of $\mathbf{C}_q$ is orthogonal to the space generated by the columns of $\mathbf{F}_q^1$, i.e. $\left(\text{null}(\mathbf{C}_q) \perp \text{span}(\mathbf{F}_q^1)\right)$. Defining $\mathbf{F}_q = \left[\mathbf{F}_q^1 \mathbf{F}_q^0\right]$, then

$$\mathbf{n}^T \mathbf{s} = \mathbf{n}^T \mathbf{F}_q \mathbf{F}_q^T \mathbf{s} = \mathbf{n}^T \mathbf{F}_q^0 \left(\mathbf{F}_q^0\right)^T \mathbf{s} = 0, \tag{6.67}$$

if $\mathbf{n} \in \text{null}(\mathbf{C}_q)$ and $\mathbf{s} \in \text{span}(\mathbf{C}_q)$. Since $\left(\mathbf{F}_q^0\right)^T \mathbf{C}_q \mathbf{F}_q^0 = \bar{\mathbf{H}}_q^T \bar{\mathbf{H}}_q$, the eigenvectors $\{\mathbf{u}_{lq}\}$ can be expressed as a linear combination of $\left\{\left(\mathbf{F}_q^0\right)^T \mathbf{c}_q^1, \left(\mathbf{F}_q^0\right)^T \bar{\mathbf{c}}_q^1, ..., \left(\mathbf{F}_q^0\right)^T \mathbf{c}_q^{N_R}, \left(\mathbf{F}_q^0\right)^T \bar{\mathbf{c}}_q^{N_R}\right\}$. Knowing that $\text{span}\left(\mathbf{C}_q\right) = \text{span}\left(\left[\mathbf{c}_q^1, \bar{\mathbf{c}}_q^1, ..., \mathbf{c}_q^{N_R}, \bar{\mathbf{c}}_q^{N_R}\right]\right)$, (6.67) becomes $\mathbf{n}^T \mathbf{F}_q^0 \mathbf{u}_{lq} = 0$ if $\mathbf{n} \in \text{null}(\mathbf{C}_q)$. As a result, the N_R unitary vectors given by $\mathbf{e}_{lq} = \mathbf{V}_q^0 \mathbf{u}_{lq}$ satisfy: $\mathbf{e}_q^l \in \text{span}(\mathbf{C}_q)$. With the emphasis on $l = 1$ and $l = N_R$, we obtain these inequalities

$$\begin{aligned} \beta_q^1 &= \max_{\mathbf{c} \in \text{span}(\mathbf{C}_q), \|\mathbf{c}\|_2 = 1} \mathbf{c}^T \mathbf{C}_q \mathbf{c} \geq \left(\mathbf{e}_q^1\right)^T \mathbf{C}_q \mathbf{e}_q^1 = \lambda_q^1 \\ \beta_q^{N_R} &= \min_{\mathbf{c} \in \text{span}(\mathbf{C}_q), \|\mathbf{c}\|_2 = 1} \mathbf{c}^T \mathbf{C}_q \mathbf{c} \leq \left(\mathbf{e}_q^{N_R}\right)^T \mathbf{C}_q \mathbf{e}_q^{N_R} = \lambda_q^{N_R}. \end{aligned} \tag{6.68}$$

6.D Demonstration of Lemma 6.31

The inequality written in (6.31) relies on the fact that $\beta_{1q} = \lambda_{1q}$ if $N_T \geq N_R = 1$. In the linear case, the eigenvalue is related to $\mathbf{H}_q \in \mathbb{C}^{1\times N_T}$ as follows: $\beta_{1q} = \|\mathbf{H}_q\|_2^2$. Note that when the widely linear processing is considered, the interference is cancelled out if the outer precoder is designed as $\mathbf{F}_q^0 = \frac{[\Re(\mathbf{H}_q) \quad -\Im(\mathbf{H}_q)]^T}{\sqrt{\Re\left(\mathbf{H}_q\mathbf{H}_q^H\right)}} \in \mathbb{R}^{2N_T\times 1}$. With that, the magnitude of λ_{1q} is equal to $\Re\left(\mathbf{H}_q\mathbf{H}_q^H\right)$. Since $\Re\left(\mathbf{H}_q\mathbf{H}_q^H\right) = \mathbf{H}_q\mathbf{H}_q^H$, then $\beta_{1q} = \lambda_{1q}$.

6.E Demonstration of Lemma 6.33

From the theory developed in Appendix 6.C, which says that $\lambda_{1q} \leq \beta_{1q}$ and $\lambda_{N_Rq} \geq \beta_{N_Rq}$, it follows that

$$\sum_{l=1}^{k} \lambda_{lq} \leq \sum_{l=1}^{k} \beta_{lq}, \quad k = 1, ..., N_R, \quad N_R \leq 2. \tag{6.69}$$

When $k = N_R = 2$ the expression (6.69) is satisfied if

$$\sum_{l=1}^{N_R} \beta_{lq} = \mathrm{tr}\left(\Re\left(\mathbf{H}_q^H\mathbf{H}_q\right)\right) \geq \sum_{l=1}^{N_R} \lambda_{lq} = \mathrm{tr}\left(\bar{\mathbf{H}}_q^T\bar{\mathbf{H}}_q\right), \tag{6.70}$$

where $\bar{\mathbf{H}}_q$ is formulated in (6.23). Any matrix $\mathbf{H}$ fulfils $\mathrm{tr}\left(\Im\left(\mathbf{H}^H\mathbf{H}\right)\right) = \mathbf{0}$, which confirms the first equality of (6.70). To prove the inequality we resort to this result $\mathrm{tr}\left(\mathbf{AB}\right) \leq \sum_{i=1}^{N} \lambda_i(\mathbf{A})\lambda_i(\mathbf{B})$, where $\mathbf{A}, \mathbf{B}$ are two $N \times N$ positive semidefinite Hermitian matrices. The term $\lambda_i(\mathbf{A})$ denotes the ith largest eigenvalue of $\mathbf{A}$, [148]. Note that all the eigenvalues of $\mathbf{F}_q^0\left(\mathbf{F}_q^0\right)^T$ are equal to one since the columns of $\mathbf{F}_q^0$ are orthonormal. Bearing this in mind we obtain

$$\mathrm{tr}\left(\bar{\mathbf{H}}_q^T\bar{\mathbf{H}}_q\right) \leq \sum_{i=1}^{N_R} \lambda_i\left(\Re\left(\mathbf{H}_q^H\mathbf{H}_q\right)\right)\lambda_i\left(\mathbf{F}_q^0\left(\mathbf{F}_q^0\right)^T\right) = \sum_{i=1}^{N_R} \lambda_i\left(\Re\left(\mathbf{H}_q^H\mathbf{H}_q\right)\right). \tag{6.71}$$

With this we close the demonstration of (6.69).

Another aspect that has to be taken into account when the linear processing is considered is the energy wastage that is implicit in the OFDM scheme. In practice, the eigenvalues obtained in the linear case should be scaled with $\epsilon = \left(1 + \frac{CP}{M}\right)^{-1}$. This highlights that (6.69) may not be satisfied when ϵ comes into play. After considering the negative impact of the CP, the eigenvalues can be related as follows:

$$\lambda_{1q}p_{1q} \leq \epsilon\beta_{1q}p_{1q}, \quad \sum_{l=1}^{2}\lambda_{lq}p_{lq} \geq \epsilon\sum_{l=1}^{2}\beta_{lq}p_{lq}, \tag{6.72}$$

for a given power distribution as long as $N_R = 2$ and

$$LB_{lq} = \frac{\lambda_{1q}}{\beta_{1q}} \leq \epsilon \leq \frac{\lambda_{1q}p_{1q} + \lambda_{2q}p_{2q}}{\beta_{1q}p_{1q} + \beta_{2q}p_{2q}} = UB_{lq}. \tag{6.73}$$

It can be checked that $UB_{lq} > LB_{lq}$ because $\beta_{2q} \leq \lambda_{2q}$ (see Appendix 6.C). Then, we can always generate this set of eigenvalues

$$\lambda'_{1q} = \lambda_{1q}, \quad \lambda'_{2q} = \lambda_{2q} - \frac{1}{p_{2q}}\sum_{l=1}^{2}\left(\lambda_{lq}p_{lq} - \epsilon\beta_{lq}p_{lq}\right), \tag{6.74}$$

which fulfils

$$\lambda'_{1q}p_{1q} \leq \epsilon\beta_{1q}p_{1q}, \quad \sum_{l=1}^{2}\lambda'_{lq}p_{lq} = \epsilon\sum_{l=1}^{2}\beta_{lq}p_{lq}. \tag{6.75}$$

From the majorization theory we can state that $f\left(p_{1q}\lambda'_{1q}, p_{2q}\lambda'_{2q}\right) \leq f\left(\epsilon p_{1q}\beta_{1lq}, \epsilon p_{2q}\beta_{2q}\right)$ if $f(.)$ is Schur-convex, [147]. Since $\frac{1}{1+ax}$ is convex for $a > 0$, then $\sum_{i=1}^{2}\frac{1}{1+ax_i}$ is Schur-convex. Let $\left\{p_{lq}^{WL}\right\}$ and $\left\{p_{lq}^{L}\right\}$ be the optimal power allocation when the channel gains are $\{\lambda_{lq}\}$ and $\{\epsilon\beta_{lq}\}$, respectively. Based on these results, it follows that

$$\sum_{l=1}^{2}\frac{1}{\frac{p_{lq}^{WL}\lambda_{lq}}{0.5N0}+1} \leq \sum_{l=1}^{2}\frac{1}{\frac{p_{lq}^{L}\lambda_{lq}}{0.5N0}+1} \leq \sum_{l=1}^{2}\frac{1}{\frac{p_{lq}^{L}\lambda'_{lq}}{0.5N0}+1} \leq \sum_{l=1}^{2}\frac{1}{\frac{\epsilon p_{lq}^{L}\beta_{lq}}{0.5N0}+1}, \tag{6.76}$$

if $\epsilon \leq LB_{lq}$. Hence, we can state that the WL processing is able to achieve a lower sum MSE and a higher capacity than the linear processing if $N_R = 2$ and $\epsilon \leq \min\{LB_{lq}\}$.

Chapter 7

MIMO designs for highly frequency selective channels

This chapter investigates the application of FBMC/OQAM to MIMO highly frequency selective channels. The analysis is restricted to synchronous PTP communication systems. The signal processing techniques presented hereinafter complement the research carried out in Section 6.1 because no assumptions are made about the flatness of the channel. To combat the frequency selectivity two specific cases have been drawn from the architecture depicted in Figure 2.7. This highlights that it is mandatory to first describe the architecture that is able to accommodate both transmit and receive processing. In order to gain insight into MIMO communications modeling we formulate in detail the two proposed approaches.

7.1 Mathematical model for narrowband precoders and broadband equalizers

In the first case equalizers make use of time and spatial dimensions to decode the symbols whereas at the transmit side the symbols are precoded by carrying out a pure space processing. Having in mind (2.20), this translates into formulating the vector of precoded symbols as $\mathbf{v}_m = \theta_m[k]\mathbf{B}_m\mathbf{d}_m[k]$, where $\theta_m[k]$ is defined in (2.2). The MIMO precoding matrix $\mathbf{B}_m \in \mathbb{R}^{N_T \times S}$ is real-valued and maps the vector of symbols $\mathbf{d}_m[k] = [d_{1m}[k], \cdots, d_{Sm}[k]]^T$ onto the N_T transmit antennas. At the receive side, the broadband processing that allows us to estimate the symbol $d_{lq}[k]$ is summarized as $\check{d}_{lq}[k] = \Re\left(\theta_q^*[k]\left(\sum_{j=1}^{N_R}\left(a_{jq}^l[k]\right)^* * y_q^j[k]\right)\right)$. Equalizers $\left\{a_{jq}^l[k]\right\}$ are different from zero for $-L_a \leq k \leq L_a$. The expression $y_q^j[k]$ is formulated in (2.17). To get a more tractable expression we compactly formulate the estimated symbols in a matrix way using this equality

$$\sum_{i=1}^{N_T}\left(a_{jq}^{l}[k]\right)^{*} * v_{im}[k] * g_{qm}^{ij}[k] = \sum_{\tau=-L_a-L_{g_1}}^{L_a+L_{g_2}} \theta_m[k-t]\left(\mathbf{a}_{jq}^{l}\right)^{H}\mathbf{G}_{qm}^{j}[\tau]\mathbf{B}_m\mathbf{d}_m[k-\tau], \tag{7.1}$$

where $\mathbf{a}_{jq}^{l} = \left[a_{jq}^{l}[-L_a], ..., a_{jq}^{l}[L_a]\right]^T$ and

$$\mathbf{G}_{qm}^{j}[\tau] = \begin{bmatrix} g_{qm}^{1j}[\tau+L_a] & \cdots & g_{qm}^{N_Tj}[\tau+L_a] \\ \vdots & & \vdots \\ g_{qm}^{1j}[\tau-L_a] & \cdots & g_{qm}^{N_Tj}[\tau-L_a] \end{bmatrix}. \tag{7.2}$$

Now, plugging (7.1) into $\check{d}_{lq}[k]$ leads to

$$\check{d}_{lq}[k] = \sum_{m=q-1}^{q+1}\sum_{\tau=-L_a-L_{g_1}}^{L_a+L_{g_2}} \Re\left(\theta_q^{*}[k]\theta_m[k-\tau]\left(\mathbf{a}_q^{l}\right)^{H}\mathbf{G}_{qm}[\tau]\right)\mathbf{B}_m\mathbf{d}_m[k-\tau] + \Re\left(\left(\mathbf{a}_q^{l}\right)^{H}\mathbf{w}_q[k]\right), \tag{7.3}$$

with $\mathbf{w}_q[k] = \theta_q^{*}[k]\left[w_q^1[k+L_a]\cdots w_q^1[k-L_a]\cdots w_q^{N_R}[k+L_a]\cdots w_q^{N_R}[k-L_a]\right]^T$. To get (7.3) we define $\mathbf{a}_q^{l} = \left[\left(\mathbf{a}_{1q}^{l}\right)^T ... \left(\mathbf{a}_{N_Rq}^{l}\right)^T\right]^T$ and $\mathbf{G}_{qm}[\tau] = \left[\left(\mathbf{G}_{qm}^{1}[\tau]\right)^T ... \left(\mathbf{G}_{qm}^{N_R}[\tau]\right)^T\right]^T$. Defining $\mathbf{E}_{qm}^{k}[\tau] = \left(\theta_q^{*}[k]\theta_m[k-\tau]\right)\mathbf{G}_{qm}[\tau]$, then (7.3) becomes

$$\check{d}_{lq}[k] = \sum_{m=q-1}^{q+1}\sum_{\tau=-L_a-L_{g_1}}^{L_a+L_{g_2}} \Re\left(\left(\mathbf{a}_q^{l}\right)^{H}\mathbf{E}_{qm}^{k}[\tau]\right)\mathbf{B}_m\mathbf{d}_m[k-\tau] + \Re\left(\left(\mathbf{a}_q^{l}\right)^{H}\mathbf{w}_q[k]\right). \tag{7.4}$$

Let us define $\mathbf{a}_{q,e}^{l} = \left[\Re\left(\left(\mathbf{a}_q^{l}\right)^T\right) \;\; \Im\left(\left(\mathbf{a}_q^{l}\right)^T\right)\right]^T$, $\mathbf{w}_{q,e} = \left[\Re\left(\mathbf{w}_q^T\right) \;\; \Im\left(\mathbf{w}_q^T\right)\right]^T$ and $\mathbf{E}_{qm,e}^{k}[\tau] = \left[\Re\left(\left(\mathbf{E}_{qm}^{k}[\tau]\right)^T\right) \;\; \Im\left(\left(\mathbf{E}_{qm}^{k}[\tau]\right)^T\right)\right]^T$. This enables us to formulate the estimated real PAM symbols as follows:

$$\check{d}_{lq}[k] = \sum_{m=q-1}^{q+1}\sum_{\tau=-L_a-L_{g_1}}^{L_a+L_{g_2}} \left(\mathbf{a}_{q,e}^{l}\right)^T\mathbf{E}_{qm,e}^{k}[\tau]\mathbf{B}_m\mathbf{d}_m[k-\tau] + \left(\mathbf{a}_{q,e}^{l}\right)^T\mathbf{w}_{q,e}[k]. \tag{7.5}$$

The notation can be simplified as

$$\check{d}_q[k] = \sum_{m=q-1}^{q+1}\sum_{\tau=-L_a-L_{g_1}}^{L_a+L_{g_2}}\sum_{i=1}^{N_T}\mathbf{a}_{q,e}^{T}\mathbf{e}_{qm,e}^{ik}[\tau]b_{im}d_m[k-\tau] + \mathbf{a}_{q,e}^{T}\mathbf{w}_{q,e}[k], \tag{7.6}$$

when a single stream is transmitted. In notation terms the vector $\mathbf{e}_{qm,e}^{ik}[\tau] \in \mathbb{R}^{2N_R(2L_a+1)\times 1}$ corresponds to the ith column of matrix $\mathbf{E}_{qm,e}^{k}[\tau]$.

In order to exploit the non-circular nature exhibited by the OQAM symbols we have adopted a real-valued representation. By examining (7.5) and (7.6) it becomes noticeable that real and imaginary parts are independently processed giving rise to widely linear filtering [39]. In other words, (7.5) and (7.6) depends linearly on the real and the imaginary parts of the equalizer inputs.

7.2 Mathematical model for broadband precoders and narrowband equalizers

In the second approach the precoder is the one that carries out a space-time processing. Based on that the precoded symbol that is transmitted on the mth subcarrier by the ith antenna can be written in the form $v_m^i[k] = \sum_{r=1}^{S} \left(b_{im}^r[k]\right)^* * \left(\theta_m[k] d_{rm}[k]\right)$. Precoders $\{b_{im}^r[k]\}$ are different from zero for $-L_b \leq k \leq L_b$. The narrowband processing carried out at reception results in $\check{d}_{lq}[k] = \Re\left(\sum_{j=1}^{N_R} \theta_q^*[k] a_{jq}^l y_q^j[k]\right)$. It is important to remark that $\left\{a_{jq}^l\right\}$ are represented by real-valued scalars. The expression $y_q^j[k]$ is formulated in (2.17). for the sake of the analytical tractability when formulating the estimated symbols we resort to this equality

$$\sum_{i=1}^{N_T}\sum_{r=1}^{S}\left(\left(b_{im}^r[k]\right)^* * \left(\theta_m[k] d_{rm}[k]\right) * g_{qm}^{ij}[k]\right) = \sum_{r=1}^{S}\sum_{\tau=-L_b-L_{g_1}}^{L_b+L_{g_2}} \left(\mathbf{b}_m^r\right)^H \mathbf{g}_{qm}^j[\tau]\theta_m[k-\tau]d_{rm}[k-\tau]. \quad (7.7)$$

Grouping the coefficients associated to different transmit antennas we get

$$\mathbf{b}_q^r = \left[b_{1q}^r[-L_b]\cdots b_{1q}^r[L_b]\cdots b_{N_Tq}^r[-L_b]\cdots b_{N_Tq}^r[L_b]\right]^T \quad (7.8)$$

$$\mathbf{g}_{qm}^j[\tau] = \left[g_{qm}^{1j}[\tau+L_b]\cdots g_{qm}^{1j}[\tau-L_b]\cdots g_{qm}^{N_Tj}[\tau+L_b]\cdots g_{qm}^{N_Tj}[\tau-L_b]\right]^T. \quad (7.9)$$

Using (7.7) the variables to be detected are written in the form of

$$\begin{aligned}\check{d}_{lq}[k] = & \sum_{m=q-1}^{q+1}\sum_{j=1}^{N_R}\sum_{r=1}^{S}\sum_{\tau=-L_b-L_{g_1}}^{L_b+L_{g_2}} a_{jq}^l \Re\left(\theta_q^*[k]\theta_m[k-\tau]\left(\mathbf{b}_m^r\right)^H \mathbf{g}_{qm}^j[\tau]\right) d_{rm}[k-\tau] \\ & + a_{jq}^l \Re\left(\theta_q^*[k] w_q^j[k]\right).\end{aligned} \quad (7.10)$$

Let us consider this definition $\mathbf{e}_{qm}^{jk}[\tau] = \theta_q^*[k]\theta_m[k-\tau]\mathbf{g}_{qm}^j[\tau]$. Stacking real and imaginary parts

we can define $\mathbf{e}_{qm,e}^{jk}[\tau] = \left[\Re\left(\mathbf{e}_{qm}^{jk}[\tau]\right)^T \quad \Im\left(\mathbf{e}_{qm}^{jk}[\tau]\right)^T\right]^T$ and $\mathbf{b}_{m,e}^{r} = \left[\Re\left(\mathbf{b}_{m}^{r}\right)^T \quad \Im\left(\mathbf{b}_{m}^{r}\right)^T\right]^T$, which allows us us to recast (7.10) as

$$\check{d}_{lq}[k] = \sum_{m=q-1}^{q+1}\sum_{j=1}^{N_R}\sum_{r=1}^{S}\sum_{\tau=-L_b-L_{g_1}}^{L_b+L_{g_2}} a_{jq}^{l}\left(\mathbf{b}_{m,e}^{r}\right)^T \mathbf{e}_{qm,e}^{jk}[\tau] d_{rm}[k-\tau] + \sum_{j=1}^{N_R} a_{jq}^{l}\Re\left(\theta_q^*[k] w_q^j[k]\right), \quad (7.11)$$

The indexes l and r can be dropped when a single stream is transmitted, which yields

$$\check{d}_{q}[k] = \sum_{m=q-1}^{q+1}\sum_{j=1}^{N_R}\sum_{\tau=-L_b-L_{g_1}}^{L_b+L_{g_2}} a_{jq}\mathbf{b}_{m,e}^{T}\mathbf{e}_{qm,e}^{jk}[\tau] d_{m}[k-\tau] + \sum_{j=1}^{N_R} a_{jq}\Re\left(\theta_q^*[k] w_q^j[k]\right). \quad (7.12)$$

7.3 Single-stream transmission

Building upon the architectures described in Sections 7.1 and 7.2 we adopt a new approach to design the transmitter and the receiver, which relies on the two key aspects summarized below:

- Since the problem of jointly designing the transmitter and the receiver is definitely complex, mainly because of the ICI, we have followed a two-step algorithm. Firstly we obtain the narrowband combiners following a new suboptimal method. Details are provided in Sections 7.3.1 and 7.3.2. By contrast, in the second step no simplifications are made. The coefficients of the broadband filters are optimized by setting the narrowband filters to the value computed in the first step. We have empirically observed that the proposed strategy provides lower BER curves when compared to the approach of deriving the narrowband filters having set beforehand the broadband filters.

- Regarding the figures of merit that govern the design, the multiple-tap filters formulated in (7.6) and (7.12) are computed under different criteria: the maximization of the SINR and the maximization of the SLNR, respectively. Note that when the space-time processing is applied at the transmit side the broadband combiners are designed to attenuate the *leakage* that a given symbol induces on surrounding symbol positions. Conversely, if the broadband combiner is deployed at the receive side the coefficients have the objective of mitigating the *interference* that a given symbol is inflicted by symbols transmitted on surrounding positions.

7.3.1 Maximization of the SLNR: space-time processing at transmission

By choosing the SLNR as the objective function we are able to devise a MIMO design particularized for the communication system formulated in (7.12). Provided that we focused on the qth subcarrier, the SLNR expression after extracting the real component at the equalizer output would be written as follows:

$$SLNR_q = \frac{\left|\mathbf{x}_q^T\left(\mathbf{b}_{q,e}\right)\mathbf{a}_q\right|^2}{\sum\limits_{(m,\tau)\neq(q,0)}\left|\sum\limits_{j=1}^{N_R} a_{jm}\mathbf{b}_{q,e}^T\mathbf{e}_{mq,e}^{jk}[\tau]\right|^2 + \dfrac{N_0}{2}\sum\limits_{j=1}^{N_R}|a_{jq}|^2} \tag{7.13}$$

$$\mathbf{x}_q\left(\mathbf{b}_{q,e}\right) = \left[\mathbf{b}_{q,e}^T\mathbf{e}_{qq,e}^{1k}[0]\cdots\mathbf{b}_{q,e}^T\mathbf{e}_{qq,e}^{N_Rk}[0]\right]^T \tag{7.14}$$

$$\mathbf{a}_q = \left[a_{1q}\cdots a_{N_Rq}\right]^T. \tag{7.15}$$

It has been assumed that $\mathbb{E}\left\{d_m\left[k\right]d_q\left[n\right]\right\} = \delta_{m,q}\delta_{k,n}$. The contribution of the noise is calculated by taking the steps described in Appendix 3.A. As (7.13) highlights the problem of jointly optimizing transmit and receive filters is really difficult to be solved. In order to simplify the problem we propose to decouple the design of the precoders with the design of the equalizers. Hence the process can be divided into two steps.

Receiver design

The first part of the algorithm has the objective of designing the coefficients a_{jq}. Since the outcomes of this iteration have to be fed to the next iteration, equalizers cannot be written as function of precoders. Otherwise, we are not able to find a closed-form expression neither for the precoders nor the equalizers. This highlights that the problem has to be relaxed. In this regard we have assumed that the processing carried out on a given subcarrier is also optimal in the adjacent subcarriers, i.e. $a_{jq-1} = a_{jq} = a_{jq+1}$. The idea behind this assumption comes from the fact that the channel frequency response evaluated on adjacent subcarriers is about on the same order. The key aspect of the relaxation is that each subcarrier can be independently processed. However it is still difficult to find the coefficients that maximize the individual SLNR. In order to further simplify the design we substitute the denominator of (7.13) by an upper bound, which is defined according to the following rule

$$\left\|\sum_{j=1}^{N_R} c_j\mathbf{v}_j\right\|_2^2 \leq \left(\sum_{j=1}^{N_R}|c_j|^2\right)\left(\sum_{j=1}^{N_R}\|\mathbf{v}_j\|_2^2\right), \tag{7.16}$$

where c_j is a real-valued scalar and $\mathbf{v}_j$ is a real-valued vector. Bearing in mind (7.16) we define a lower bound of the SLNR that results in the quadratic form

$$LB_q^{slnr} = \frac{\left|\mathbf{x}_q^T\left(\mathbf{b}_{q,e}\right)\mathbf{a}_q\right|^2}{\left(\sum_{j=1}^{N_R}\left|a_{jq}\right|^2\right)\left(\sum_{(m,\tau)\neq(q,0)}\sum_{j=1}^{N_R}\left|\mathbf{b}_{q,e}^T\mathbf{e}_{mq,e}^{jk}[\tau]\right|^2+\frac{N_0}{2}\right)} \leq SLNR_q, \tag{7.17}$$

which facilitates the design since the narrowband combiner that maximizes LB_q^{slnr} is the whitening matched filter

$$\mathbf{a}_q^{opt}\left(\mathbf{b}_{q,e}\right) = \frac{\mathbf{x}_q\left(\mathbf{b}_{q,e}\right)}{\sum_{(m,\tau)\neq(q,0)}\sum_{j=1}^{N_R}\left|\mathbf{b}_{q,e}^T\mathbf{e}_{mq,e}^{jk}[\tau]\right|^2+\frac{N_0}{2}}, \tag{7.18}$$

as [149] demonstrates. Since receive vectors depend on precoders, the design of the optimal receive processing boils down to substituting (7.18) into (7.17) and find the $\mathbf{b}_{q,e}$ that maximizes the SLNR lower bound. The problem consist in solving the Rayleigh quotient

$$\mathbf{b}_{q,e}^{opt} = \underset{\|\mathbf{b}_{q,e}\|_2^2=p_q}{\operatorname{argmax}}\left\{\frac{\mathbf{b}_{q,e}^T\mathbf{T}_q\mathbf{b}_{q,e}}{\mathbf{b}_{q,e}^T\mathbf{Q}_q\mathbf{b}_{q,e}}\right\} \tag{7.19}$$

$$\mathbf{T}_q = \sum_{j=1}^{N_R}\mathbf{e}_{qq,e}^{jk}[0]\left(\mathbf{e}_{qq,e}^{jk}[0]\right)^T \tag{7.20}$$

$$\mathbf{Q}_q = \sum_{(m,\tau)\neq(q,0)}\sum_{j=1}^{N_R}\mathbf{e}_{mq,e}^{jk}[\tau]\left(\mathbf{e}_{mq,e}^{jk}[\tau]\right)^T+\frac{N_0}{2p_q}\mathbf{I}_{2N_T(2L_b+1)}. \tag{7.21}$$

Note that precoders are restricted to comply with the predefined power allocation. Since matrix $\mathbf{Q}_q$ is symmetric, the optimum precoder corresponds to the dominant generalized eigenvector of the matrix pairs $\left(\mathbf{T}_q,\mathbf{Q}_q\right)$. Based on the fact that $\mathbf{Q}_q$ is non-singular the solution reduces to the standard eigenvalue problem

$$\mathbf{Q}_q^{-1}\mathbf{T}_q\mathbf{b}_{q,e}^{opt} = \lambda_q^{MAX}\mathbf{b}_{q,e}^{opt}. \tag{7.22}$$

To comply with the power distribution the eigenvector associated with the maximum eigenvalue is properly scaled. It is worth emphasizing that matrices $\mathbf{T}_q$,$\mathbf{Q}_q$ do not depend on the time index. It can be easily verified that the entries of these matrices are the same for consecutive time instants. As a result in-phase and quadrature components of the transmitted symbols are processed by the same precoders and equalizers. It must be mentioned that the transmit and receive beamformers

computed in this section are overdesigned because they maximize the lower bound of the SLNR albeit some information about the quality of the links is captured by vectors $\mathbf{a}_q^{opt}\left(\mathbf{b}_{q,e}^{opt}\right)$.

Transmitter design

This section aims at getting a better performance by updating the design of the precoders. The method stems from fixing the equalizers in (7.13) and devising the transmit processing that maximizes the real SLNR. If we define the narrowband combiners computed in (7.18) as $\mathbf{c}_q \equiv \mathbf{a}_q^{opt}\left(\mathbf{b}_{q,e}^{opt}\right)$ the solution is equivalent to maximizing the quadratic form

$$\mathbf{b}_{q,e}^{opt} = \underset{\|\mathbf{b}_{q,e}\|_2^2=p_q}{\operatorname{argmax}} \left\{ \frac{\mathbf{b}_{q,e}^T \mathbf{T}_q\left(\mathbf{c}_q\right)\mathbf{b}_{q,e}}{\mathbf{b}_{q,e}^T \mathbf{Q}_q\left(\mathbf{c}_q\right)\mathbf{b}_{q,e}} \right\} \tag{7.23}$$

$$\mathbf{T}_q\left(\mathbf{c}_q\right) = \left(\sum_{j=1}^{N_R} c_{jq}\mathbf{e}_{qq,e}^{jk}[0]\right)\left(\sum_{j=1}^{N_R} c_{jq}\mathbf{e}_{qq,e}^{jk}[0]\right)^T \tag{7.24}$$

$$\mathbf{Q}_q\left(\mathbf{c}_q\right) = \sum_{(m,\tau)\neq(q,0)} \left(\sum_{j=1}^{N_R} c_{jm}\mathbf{e}_{mq,e}^{jk}[\tau]\right)\left(\sum_{j=1}^{N_R} c_{jm}\mathbf{e}_{mq,e}^{jk}[\tau]\right)^T + \left(\frac{N_0}{2p_q}\sum_{j=1}^{N_R}|c_{jq}|^2\right)\mathbf{I}_{2N_T(2L_b+1)}. \tag{7.25}$$

In the same manner as it is done in the receiver design the solution is obtained by selecting the eigenvector associated to the largest eigenvalue that solves

$$\mathbf{Q}_q^{-1}\left(\mathbf{c}_q\right)\mathbf{T}_q\left(\mathbf{c}_q\right)\mathbf{b}_{q,e}^{opt} = \lambda_q^{MAX}\mathbf{b}_{q,e}^{opt}. \tag{7.26}$$

Finally, the transmit beamformer is scaled to satisfy the constraint. At this point it seems reasonable to suggest that the receive vectors may be recalculated by plugging the solution of (7.26) into (7.18). Nevertheless, the maximization of the SLNR lower bound does not guarantee that the real SLNR increases, thus we have discarded to implement an iterative algorithm.

7.3.2 Maximization of the SINR: space-time processing at reception

Adopting the model formulated in (7.6), we have selected the SINR figure to be the cost function. Modeling the statistics of the data in the same manner as it is done in the Section 7.3.1, the SINR expression associated to the qth subcarrier is given by

$$SINR_q = \frac{\left|\mathbf{x}_q^T\left(\mathbf{a}_{q,e}\right)\mathbf{b}_q\right|^2}{\sum_{(m,\tau)\neq(q,0)}\left|\sum_{i=1}^{N_T}\mathbf{a}_{q,e}^T\mathbf{e}_{qm,e}^{ik}[\tau]b_{im}\right|^2 + \mathbf{a}_{q,e}^T\mathbf{R}_q\mathbf{a}_{q,e}} \tag{7.27}$$

$$\mathbf{x}_q\left(\mathbf{a}_{q,e}\right) = \left[\mathbf{a}_{q,e}^T\mathbf{e}_{qq,e}^{1k}[0]\cdots\mathbf{a}_{q,e}^T\mathbf{e}_{qq,e}^{N_Tk}[0]\right]^T \tag{7.28}$$

$$\mathbf{b}_q = \left[b_{1q}\cdots b_{N_Tq}\right]^T. \tag{7.29}$$

Note that the autocorrelation matrix is computed as the Appendix 3.A describes. Again the strategy for alleviating the complexity of jointly computing transmit and receive vectors consists in devising the receive filters for a fixed transmit vector. In the following we describe the processing involved in each step of the algorithm.

Transmitter design

Approximating that $b_{iq-1} = b_{iq} = b_{iq+1}$ and substituting the interference by its upper bound, which follows from the rule written in (7.16), then the SINR lower bound is given by

$$LB_q^{sinr} = \frac{\left|\mathbf{x}_q^T\left(\mathbf{a}_{q,e}\right)\mathbf{b}_q\right|^2}{\mathbf{a}_{q,e}^T\mathbf{R}_q\mathbf{a}_{q,e} + \left(\sum_{i=1}^{N_T}\left|b_{iq}\right|^2\right)\left(\sum_{(m,\tau)\neq(q,0)}\sum_{i=1}^{N_T}\left|\mathbf{a}_{q,e}^T\mathbf{e}_{qm,e}^{ik}[\tau]\right|^2\right)} \leq SINR_q. \tag{7.30}$$

In this regard, we benefit from the lower bound expression to firstly devise the narrowband combiners that solve the following problem

$$\mathbf{b}_q^{opt}\left(\mathbf{a}_{q,e}\right) = \underset{\|\mathbf{b}_q\|_2^2=p_q}{\operatorname{argmax}}\left\{\frac{\left|\mathbf{x}_q^T\left(\mathbf{a}_{q,e}\right)\mathbf{b}_q\right|^2}{\left(\frac{1}{p_q}\mathbf{a}_{q,e}^T\mathbf{R}_q\mathbf{a}_{q,e} + \sum_{(m,\tau)\neq(q,0)}\sum_{i=1}^{N_T}\left|\mathbf{a}_{q,e}^T\mathbf{e}_{qm,e}^{ik}[\tau]\right|^2\right)\mathbf{b}_q^T\mathbf{b}_q}\right\}, \tag{7.31}$$

where the norm of the precoder is given by the power distribution. In this case the solution relies on the normalized whitening matched filter, [149], i.e.

$$\mathbf{b}_q^{opt}\left(\mathbf{a}_{q,e}\right) = \alpha_q\frac{\mathbf{x}_q\left(\mathbf{a}_{q,e}\right)}{\frac{1}{p_q}\mathbf{a}_{q,e}^T\mathbf{R}_q\mathbf{a}_{q,e} + \sum_{(m,\tau)\neq(q,0)}\sum_{i=1}^{N_T}\left|\mathbf{a}_{q,e}^T\mathbf{e}_{qm,e}^{ik}[\tau]\right|^2}. \tag{7.32}$$

The constant α_q is judiciously set to ensure that the power constraint is satisfied with equality. Finally plugging (7.32) into (7.30) yields the following problem

$$\mathbf{a}_{q,e}^{opt} = \text{argmax}\left\{\frac{\mathbf{a}_{q,e}^T \mathbf{T}_q \mathbf{a}_{q,e}}{\mathbf{a}_{q,e}^T \mathbf{Q}_q \mathbf{a}_{q,e}}\right\} \tag{7.33}$$

$$\mathbf{T}_q = \sum_{i=1}^{N_T} \mathbf{e}_{qq,e}^{ik}[0] \left(\mathbf{e}_{qq,e}^{ik}[0]\right)^T \tag{7.34}$$

$$\mathbf{Q}_q = \sum_{(m,\tau)\neq(q,0)} \sum_{i=1}^{N_T} \mathbf{e}_{qm,e}^{ik}[\tau] \left(\mathbf{e}_{qm,e}^{ik}[\tau]\right)^T + \frac{1}{p_q}\mathbf{R}_q. \tag{7.35}$$

Since the matrix $\mathbf{Q}_q$ is non-singular and symmetric, the optimal choice is given by the eigenvalue problem

$$\mathbf{Q}_q^{-1}\mathbf{T}_q\mathbf{a}_{q,e}^{opt} = \lambda_q^{MAX}\mathbf{a}_{q,e}^{opt}. \tag{7.36}$$

Although $\mathbf{b}_q^{opt}\left(\mathbf{a}_{q,e}^{opt}\right)$ does not correspond to the optimal transmit processing it brings about informative figures about the quality of the links.

Receiver design

The second step solely tries to devise the receive vectors that maximize (7.27), given a set of predetermined transmit beamformers. Defining $\mathbf{c}_q \equiv \mathbf{b}_q^{opt}\left(\mathbf{a}_{q,e}^{opt}\right)$ we can formulate the problem as follows:

$$\mathbf{a}_{q,e}^{opt} = \text{argmax}\left\{\frac{\mathbf{a}_{q,e}^T \mathbf{T}_q\left(\mathbf{c}_q\right) \mathbf{a}_{q,e}}{\mathbf{a}_{q,e}^T \mathbf{Q}_q\left(\mathbf{c}_q\right) \mathbf{a}_{q,e}}\right\} \tag{7.37}$$

$$\mathbf{T}_q\left(\mathbf{c}_q\right) = \left(\sum_{i=1}^{N_T} c_{iq}\mathbf{e}_{qq,e}^{ik}[0]\right)\left(\sum_{i=1}^{N_T} c_{iq}\mathbf{e}_{qq,e}^{ik}[0]\right)^T \tag{7.38}$$

$$\mathbf{Q}_q\left(\mathbf{c}_q\right) = \sum_{(m,\tau)\neq(q,0)} \left(\sum_{i=1}^{N_T} c_{im}\mathbf{e}_{qm,e}^{ik}[\tau]\right)\left(\sum_{i=1}^{N_T} c_{im}\mathbf{e}_{qm,e}^{ik}[\tau]\right)^T + \mathbf{R}_q. \tag{7.39}$$

From the results computed in the Section 7.3.1 it can be easily inferred that multi-tap equalizers that maximize the SINR are obtained by solving the following eigen-decomposition problem

$$\mathbf{Q}_q^{-1}\left(\mathbf{c}_q\right)\mathbf{T}_q\left(\mathbf{c}_q\right)\mathbf{a}_{q,e}^{opt} = \lambda_q^{MAX}\mathbf{a}_{q,e}^{opt}. \tag{7.40}$$

Similarly to the Section 7.3.1 we have not favourably considered the implementation of an iterative algorithm since the convergence is not assured. That is, the step in which the solution of

(7.40) should be plugged into (7.32) might moves us further away from the optimal solution.

7.4 Multi-stream transmission

To make progress towards the application of FBMC/OQAM to MIMO channels, we study the design of novel solutions that could simultaneously provide robustness against the channel frequency selectivity and support multi-stream transmission. To this end, two techniques have been devised under the criterion of minimizing the sum MSE. The first technique keeps the complexity at a reasonable level, it is practical from the implementation point of view as it is not iterative, but in exchange the original problem is relaxed, which provides a suboptimal solution. With the objective of performing closer to the optimum solution, the second option iteratively computes precoders and equalizers by resorting to an alternating optimization method, which is much more complex.

7.4.1 Suboptimal subband processing

In this section we study how to jointly design transmit and receive processing adopting the model in (7.5). Regarding the optimization criterion, we opt for the minimization of the sum MSE. Defining the MSE of the lth stream transmitted on the qth subband as $MSE_q^l = \mathbb{E}\left\{\left|d_{lq}[k] - \check{d}_{lq}[k]\right|^2\right\}$, the problem to be solved is

$$\begin{aligned} &\underset{\left\{\mathbf{a}_{q,e}^l, \mathbf{B}_q\right\}}{\operatorname{argmin}} \sum_{q\in S_a}\sum_{l=1}^{S} MSE_q^l \\ &s.t. \sum_{q\in S_a} \mathbb{E}\left\{\|\mathbf{B}_q\mathbf{d}_q[k]\|_2^2\right\} = \sum_{q\in S_a} \|\mathbf{B}_q\|_F^2 \leq P_T, \end{aligned} \tag{7.41}$$

where $\|\mathbf{B}_q\|_F^2 = \operatorname{tr}\left(\mathbf{B}_q\mathbf{B}_q^H\right)$. We use $\operatorname{tr}\left(\mathbf{B}_q\mathbf{B}_q^H\right)$ to denote the trace of $\mathbf{B}_q\mathbf{B}_q^H$. Note that we have assumed that symbols are independent and have unit-energy, i.e. $\mathbb{E}\left\{\left|\mathbf{d}_m[k]\mathbf{d}_q^T[n]\right|^2\right\} = \delta_{m,q}\delta_{n,k}\mathbf{I}_S$. Then, the MSE can be formulated as

$$MSE_q^l = 1 + \sum_{m=q-1}^{q+1}\sum_{\tau=-L_a-L_{g_1}}^{L_a+L_{g_2}} \left\|\left(\mathbf{a}_{q,e}^l\right)^T \mathbf{E}_{qm,e}^k[\tau]\mathbf{B}_m\right\|_2^2 + \left(\mathbf{a}_{q,e}^l\right)^T \mathbf{R}_q\mathbf{a}_{q,e}^l - 2\left(\mathbf{a}_{q,e}^l\right)^T \mathbf{E}_{qq,e}^k[0]\mathbf{B}_q\mathbf{e}_l. \tag{7.42}$$

In notation terms the unitary vector $\mathbf{e}_l$ is zero-valued except in the lth position. The noise correlation matrix is given by $\mathbf{R}_q = \mathbb{E}\left\{\mathbf{w}_{q,e}[k]\mathbf{w}_{q,e}^T[k]\right\}$. The analytical expression can be found in Appendix 3.A. It can be readily checked that the MSE is independent of k and, therefore, the same metric is used for k odd and k even. Due to the ICI we cannot decouple the problem into M_a disjoint problems. This highlights that some relaxation has to be applied if we want to alleviate

the complexity of the optimization procedure. In this sense, we propose substituting the objective function of (7.41) by the following upper bound

$$\begin{aligned} MSE_q^l \;&\leq MSE_{lq}^{UB} = 1 + \sum_{\substack{m=q-1 \\ m\neq q}}^{q+1} \sum_{\tau=-L_a-L_{g_1}}^{L_a+L_{g_2}} \lambda_1\left(\mathbf{B}_m\mathbf{B}_m^T\right) \left\| \left(\mathbf{a}_{q,e}^l\right)^T \mathbf{E}_{qm,e}^k[\tau] \right\|_2^2 + \\ &\sum_{\substack{\tau=-L_a-L_{g_1} \\ \tau\neq 0}}^{L_a+L_{g_2}} \lambda_1\left(\mathbf{B}_q\mathbf{B}_q^T\right) \left\| \left(\mathbf{a}_{q,e}^l\right)^T \mathbf{E}_{qq,e}^k[\tau] \right\|_2^2 + \left\| \left(\mathbf{a}_{q,e}^l\right)^T \mathbf{E}_{qq,e}^k[0]\mathbf{B}_q \right\|_2^2 + \\ &+ \left(\mathbf{a}_{q,e}^l\right)^T \mathbf{R}_q \mathbf{a}_{q,e}^l - 2\left(\mathbf{a}_{q,e}^l\right)^T \mathbf{E}_{qq,e}^k[0]\mathbf{B}_q\mathbf{e}_l. \end{aligned} \tag{7.43}$$

The upper bound (7.43) hinges on the well-known inequality $\mathrm{tr}\left(\mathbf{AB}\right) \leq \sum_{i=1}^{N} \lambda_i\left(\mathbf{A}\right)\lambda_i\left(\mathbf{B}\right)$, where $\mathbf{A}$ and $\mathbf{B}$ are two $N\times N$ positive semidefinite Hermitian matrices, [150]. The terms $\lambda_i\left(\mathbf{A}\right)$ and $\lambda_i\left(\mathbf{B}\right)$ account for the eigenvalues of $\mathbf{A}$ and $\mathbf{B}$, respectively, which are arranged in descending order. Taking into account that $\mathrm{rank} = \left(\mathbf{E}_{qm,e}^k[\tau]\right)^T \mathbf{a}_{q,e}^l \left(\mathbf{a}_{q,e}^l\right)^T \mathbf{E}_{qm,e}^k[\tau] = 1$ along with the invariance of the trace with the order of the multiplication, leads to this result

$$\left\| \left(\mathbf{a}_{q,e}^l\right)^T \mathbf{E}_{qm,e}^k[\tau]\mathbf{B}_m \right\|_2^2 \leq \lambda_1\left(\mathbf{B}_m\mathbf{B}_m^T\right) \left\| \left(\mathbf{a}_{q,e}^l\right)^T \mathbf{E}_{qm,e}^k[\tau] \right\|_2^2. \tag{7.44}$$

With the aim of further simplifying the problem we assume that the dominant eigenvalue of $\mathbf{B}_m\mathbf{B}_m^T$ is upper bounded by the term b_m, i.e. $\lambda_1\left(\mathbf{B}_m\mathbf{B}_m^T\right) \leq b_m$. This assumption opens the door to work with a new performance metric, which is defined as

$$\begin{aligned} UB_q^l \;&= 1 + \sum_{\substack{m=q-1 \\ m\neq q}}^{q+1} \sum_{\tau=-L_a-L_{g_1}}^{L_a+L_{g_2}} b_m \left\| \left(\mathbf{a}_{q,e}^l\right)^T \mathbf{E}_{qm,e}^k[\tau] \right\|_2^2 + \\ &\sum_{\substack{\tau=-L_a-L_{g_1} \\ \tau\neq 0}}^{L_a+L_{g_2}} b_q \left\| \left(\mathbf{a}_{q,e}^l\right)^T \mathbf{E}_{qq,e}^k[\tau] \right\|_2^2 + \left\| \left(\mathbf{a}_{q,e}^l\right)^T \mathbf{E}_{qq,e}^k[0]\mathbf{B}_q \right\|_2^2 + \\ &+ \left(\mathbf{a}_{q,e}^l\right)^T \mathbf{R}_q \mathbf{a}_{q,e}^l - 2\left(\mathbf{a}_{q,e}^l\right)^T \mathbf{E}_{qq,e}^k[0]\mathbf{B}_q\mathbf{e}_l. \end{aligned} \tag{7.45}$$

Then, the new minimization problem becomes

$$\begin{aligned} &\underset{\left\{\mathbf{a}_{q,e}^l, \mathbf{B}_q\right\}}{\mathrm{argmin}} \sum_{q\in S_a} \sum_{l=1}^{S} UB_q^l \\ &s.t. \sum_{q\in S_a} \left\|\mathbf{B}_q\right\|_F^2 \leq P_T \\ &\qquad \lambda_1\left(\mathbf{B}_q\mathbf{B}_q^T\right) \leq b_q, \quad q \in S_a. \end{aligned} \tag{7.46}$$

It is important to remark that the solution of the relaxed problem minimizes an upper bound of the sum MSE. As we show in Appendix 7.A, the expressions that come into play when solving (7.46) offer a good analytical tractability, which is of paramount importance to formulate a solution in a closed-form expression.

Refinement of the subband processing

To perform closer to the optimum, we propose to update the receive matrices so that the exact sum MSE is minimized having fixed the transmit processing. In other words, having computed the precoders with (7.60), the receivers are recalculated to solve (7.42). Therefore it results in

$$\mathbf{A}_{q,e} = \left[\mathbf{a}_{q,e}^{1} ... \mathbf{a}_{q,e}^{S}\right] = \left(\mathbf{R}_q + \sum_{m=q-1}^{q+1} \sum_{\tau=-L_a-L_{g_1}}^{L_a+L_{g_2}} \mathbf{E}_{qm,e}^{k}[t]\mathbf{B}_m \left(\mathbf{E}_{qm,e}^{k}[\tau]\mathbf{B}_m\right)^T\right)^{-1} \mathbf{E}_{qq,e}^{k}[0]\mathbf{B}_q. \quad (7.47)$$

Note that matrix inversion is allowed since it is assumed that the noise autocorrelation matrix is full rank. By using this equality $\mathbf{A} = \left(\mathbf{EB}\left(\mathbf{EB}\right)^H + \mathbf{R}\right)^{-1}\mathbf{EB} = \mathbf{R}^{-1}\mathbf{EB}\left(\mathbf{I} + \left(\mathbf{EB}\right)^H\mathbf{R}^{-1}\mathbf{EB}\right)^{-1}$ [140], the MIMO decoding matrix can be expressed as

$$\mathbf{A}_{q,e} = \bar{\mathbf{C}}_q^{-1}\mathbf{E}_{qq,e}^{k}[0]\mathbf{B}_q\left(\mathbf{I}_S + \left(\mathbf{E}_{qq,e}^{k}[0]\mathbf{B}_q\right)^T\bar{\mathbf{C}}_q^{-1}\mathbf{E}_{qq,e}^{k}[0]\mathbf{B}_q\right)^{-1} \quad (7.48)$$

with

$$\bar{\mathbf{C}}_q = \mathbf{R}_q + \sum_{m=q-1}^{q+1} \sum_{\tau=-L_a-L_{g_1}}^{L_a+L_{g_2}} \mathbf{E}_{qm,e}^{k}[\tau]\mathbf{B}_m \left(\mathbf{E}_{qm,e}^{k}[\tau]\mathbf{B}_m\right)^T - \mathbf{E}_{qq,e}^{k}[0]\mathbf{B}_q\left(\mathbf{E}_{qq,e}^{k}[0]\mathbf{B}_q\right)^T. \quad (7.49)$$

From here onwards we assume that precoders are generated with (7.60) and equalizers are built as (7.48) describes if otherwise stated.

7.4.2 Widely linear vs. linear processing

In this section we analyse the quality of the links after performing the proposed WLP and the LP addressed in [140]. The expressions derived in the WLP case are built on optimistic assumptions for the ease of the tractability. Since the comparison might be unfair, the aim is to find out in which multi-antenna configurations FBMC/OQAM may remain competitive with OFDM.

In the WLP case, the input/output relationship of those symbols transmitted on the qth subband and the time instant of interest will be given by $\mathbf{A}_{q,e}^T\mathbf{E}_{qq,e}^{k}[0]\mathbf{B}_q$. Unless (7.59) and (7.49) coincide, i.e. $\bar{\mathbf{C}}_q = \mathbf{C}_q$, the MIMO channel matrix is not decoupled into independent subchannels.

The diagonal structure can be achieved if the additive noise is the dominant source of interference or in the absence of ISI and ICI. Supposing the latter assumption, the noise correlation matrix is formulated as $\bar{\mathbf{C}}_q = \mathbf{C}_q = \mathbf{R}_q = 0.5N_0\mathbf{I}_{2N_R}$ (see Appendix 3.A), provided that we stick to the case that $L_a = 0$. In order to make expressions analytically tractable, we consider an interference-free scenario and we focus on the case that equalizers have no memory, i.e. $L_a = 0$. Then, we achieve a diagonal structure and the SINR is given by

$$SINR_q^l = \frac{1}{MSE_q^l} - 1 = \frac{p_{lq}\bar{\lambda}_{lq}}{0.5N_0}, \tag{7.50}$$

where $\bar{\lambda}_{lq}$ is the lth largest eigenvalue of matrix $\left(\mathbf{E}_{qq,e}^k[0]\right)^T \mathbf{E}_{qq,e}^k[0]$. We have assumed that $S \leq \text{rank}\left(\left(\mathbf{E}_{qq,e}^k[0]\right)^T \mathbf{E}_{qq,e}^k[0]\right) = \min\left(N_T, 2N_R\right)$. Since (7.50) corresponds to a fictitious scenario that is interference-free, we can conclude that the exact SINR is upper bounded by (7.50). Thoroughly examining $\mathbf{E}_{qq,e}^k[0]$ it is possible to approximate its value by $\mathbf{E}_{qq,e}^k[0] \approx \left[\Re\left(\mathbf{H}_q^T\right) \quad \Im\left(\mathbf{H}_q^T\right)\right]^T = \mathbf{H}_{q,e}$, where $\mathbf{H}_q$ is the frequency response of the MIMO channel matrix evaluated on $\frac{2\pi}{M}q$. To support this statement we first expand this term $g_{qq}^{ij}[0]$, written in (2.18), as follows:

$$g_{qq}^{ij}[0] = \sum_{t=0}^{L_{ch}-1} h_{ij}[t] r_p[t] e^{-j\frac{2\pi}{M}qt} = \sum_{t=0}^{L_{ch}-1} h_{ij}[t] \left(\sum_{v=0}^{L-1} p\left[v\right] p\left[v+t\right]\right) e^{-j\frac{2\pi}{M}qt}. \tag{7.51}$$

It should be mentioned that $p[v] \neq 0$ for $v = 0, ..., L-1$. The maximum channel excess delay is denoted L_{ch} and it is assumed equal for all the links. According to [151], the prototype pulse in the discrete-time domain can be obtained by sampling the analog pulse $p(t)$, i.e. $p[v] = p\left(\left(v - 0.5(L-1)\right)\frac{1}{f_s}\right)$, where f_s is the sampling frequency and the delay $0.5(L-1)$ is chosen to force $p[v]$ to be causal. Then, using the first order Taylor expansion of $p(t)$, we can approximate the samples around the vth sampling instant as $p\left[v+t\right] \approx p[v] + \frac{t}{f_s}d[v]$, [151]. Writing the derivative of the pulse as $p'(t)$ we define $d[v] = p'\left(\left(v - 0.5(L-1)\right)\frac{1}{f_s}\right)$. In the FBMC/OQAM context the pulses follow the Nyquist pulse shaping idea, thus they present an even symmetry, which implies that $p[v] = p[L-1-v]$ as it is stated in [21], and consequently $d[v] = -d[L-1-v]$. The discrete-time signal $d[v]$ will present an odd symmetry with respect to the central sample. As a consequence, $r_p\left[t\right] \approx \sum_{v=0}^{L-1}\left|p\left[v\right]\right|^2$. If the prototype pulse is properly scaled to have unit-energy, the value of $g_{qq}^{ij}[0]$ is approximately the element of matrix $\mathbf{H}_q$ located at the ith column and jth row. This confirms that $\mathbf{E}_{qq,e}^k[0] \approx \mathbf{H}_{q,e}$, as long as the number of carriers is sufficiently large (see [151]). From here onwards we assume that $\mathbf{E}_{qq,e}^k[0] = \mathbf{H}_{q,e}$ holds true.

At this point, it would be interesting to know how the upper bound in (7.50) compares with the solution based on the linear processing [140]. To this end, we formulate the SINR in the OFDM case, which is given by

$$SINR_q^l = \frac{2p_{lq}\beta_{lq}}{\frac{M+CP}{M}N_0}. \tag{7.52}$$

The variance of the noise is not halved because the technique is designed over the complex field. The factor 2 in the numerator highlights that the real PAM symbols are obtained from in-phase and quadrature components of the QAM symbols, which are transmitted in OFDM systems. The coefficients $\{\beta_{1q}\cdots\beta_{Sq}\}$ denote the S largest non-zero eigenvalues of the matrix $\mathbf{H}_q^H\mathbf{H}_q$, so it becomes clear that the power distribution will be different from that of (7.50). In OFDM systems the maximum number of streams that can be spatially multiplexed is given by $\text{rank}\left(\mathbf{H}_q^H\mathbf{H}_q\right) = \min(N_T, N_R)$. To carry out a fair comparison with FBMC/OQAM we exclusively consider the schemes where $S \leq \min(N_T, N_R)$. Also notice that $\mathbf{H}_{q,e}^T\mathbf{H}_{q,e} = \Re\left(\mathbf{H}_q^H\mathbf{H}_q\right)$ and $\Im\left(\mathbf{H}_q^H\mathbf{H}_q\right) = \Re\left(\mathbf{H}_q^T\right)\Im\left(\mathbf{H}_q\right) - \Im\left(\mathbf{H}_q^T\right)\Re\left(\mathbf{H}_q\right)$, which highlights that $\sum_{l=1}^{N_T}\beta_{lq} = \sum_{l=1}^{N_T}\bar{\lambda}_{lq}$. In addition, $\mathbf{c}^T\Im\left(\mathbf{H}_q^H\mathbf{H}_q\right)\mathbf{c} = 0$ for any $\mathbf{c} \in \mathbb{R}^{N_T\times 1}$.

In view of the above discussion we can write these two inequalities

$$\begin{aligned}\beta_{1q} &= \max_{\|\mathbf{c}\|_2=1} \mathbf{c}^H\mathbf{H}_q^H\mathbf{H}_q\mathbf{c} \geq \left(\mathbf{u}_{1q}\right)^H\mathbf{H}_q^H\mathbf{H}_q\mathbf{u}_{1q} = \bar{\lambda}_{1q}\\ \beta_{N_Tq} &= \min_{\|\mathbf{c}\|_2=1} \mathbf{c}^H\mathbf{H}_q^H\mathbf{H}_q\mathbf{c} \leq \left(\mathbf{u}_{N_Tq}\right)^H\mathbf{H}_q^H\mathbf{H}_q\mathbf{u}_{N_Tq} = \bar{\lambda}_{N_Tq},\end{aligned} \tag{7.53}$$

when $\mathbf{u}_{lq}$ corresponds to the real-valued eigenvector of $\mathbf{H}_{q,e}^T\mathbf{H}_{q,e}$ that is associated to the eigenvalue $\bar{\lambda}_{lq}$. With the exception of the two specific cases written in (7.53), we have not been able to establish any inequality for the rest of eigenvalues. With that, we should set $S = N_T \leq N_R$ to ensure that at least in one spatial subchannel, in particular the Sth spatial subchannel, the highest gain will take place when the WL filtering is performed, as long as the interference is removed. With an alternative configuration all the spatial subchannels might present the highest gain when OFDM is considered.

7.4.3 Iterative design

The processing developed in Section 7.4.1 gives priority to find low-complexity solutions, which gives rise to a suboptimal design. Examining (7.41) from a different perspective, that is forgetting about the complexity, we can find a local solution that can be computed via the alternating optimization method. The idea is to independently optimize receive and transmit matrices in an iterative fashion. The resulting design will be used as a benchmark for the results of Section 7.4.1. Without making any relaxation the exact sum MSE is given by

$$MSE\left(\{\mathbf{A}_{q,e},\mathbf{B}_q\}\right)=\sum_{q\in S_a}\mathbb{E}\left\{\left\|\mathbf{d}_q[k]-\check{\mathbf{d}}_q[k]\right\|_2^2\right\}=M_a\times S+$$
$$\sum_{q\in S_a}\sum_{m=q-1}^{q+1}\sum_{\tau=-L_a-L_{g_1}}^{L_a+L_{g_2}}\left\|\mathbf{A}_{q,e}^T\mathbf{E}_{qm,e}^k[\tau]\mathbf{B}_m\right\|_F^2+\sum_{q\in S_a}\mathrm{tr}\left(\mathbf{A}_{q,e}^T\mathbf{R}_q\mathbf{A}_{q,e}-2\mathbf{A}_{q,e}^T\mathbf{E}_{qq,e}^k[0]\mathbf{B}_q\right). \tag{7.54}$$

The cost function in (7.54) is obtained by resorting to this definition $\mathbf{A}_{q,e}=\left[\mathbf{a}_{q,e}^1...\mathbf{a}_{q,e}^S\right]\in\mathbb{R}^{2N_R(1+2L_a)\times S}$. It can be verified that the (lth,lth) element of $\mathbb{E}\left\{\left\|\mathbf{d}_q[k]-\check{\mathbf{d}}_q[k]\right\|_2^2\right\}$ coincides with (7.42).

The receiver design hinges on minimizing (7.54) for fixed MIMO precoding matrices. Then the optimal equalizers are

$$\mathbf{A}_{q,e}=\left(\mathbf{R}_q+\sum_{m=q-1}^{q+1}\sum_{\tau=-L_a-L_{g_1}}^{L_a+L_{g_2}}\mathbf{E}_{qm,e}^k[\tau]\mathbf{B}_m\left(\mathbf{E}_{qm,e}^k[\tau]\mathbf{B}_m\right)^T\right)^{-1}\mathbf{E}_{qq,e}^k[0]\mathbf{B}_q. \tag{7.55}$$

The transmitter design is more challenging than that of the receiver because of the total power constraint. Given the equalizers, the problem becomes

$$\begin{aligned}&\underset{\{\mathbf{B}_q\}}{\mathrm{argmin}}\,MSE\left(\{\mathbf{A}_{q,e},\mathbf{B}_q\}\right)\\&s.t.\quad\sum_{q\in S_a}\|\mathbf{B}_q\|_F^2\le P_T.\end{aligned} \tag{7.56}$$

The solution is detailed in Appendix 7.B. The overall algorithm operates as Algorithm 9 describes.

Algorithm 9 Alternating optimization method

1: Initialize $\mathbf{A}_{q,e},\mathbf{B}_q\ \ 0\le q\le M-1$
2: **for** i=1,...,N **do**
3: Compute $\mathbf{A}_{q,e}$ using (7.55)
4: Compute $\mathbf{B}_q$ executing Algorithm 10
5: **end for**

Note that at each iteration the sum MSE decreases because the design of precoders and equalizers is governed by the same objective function. Hence, Algorithm 9 converges to a minimum point since the sum MSE is lower bounded by zero [152]. However, we cannot state that the solution is a global optimum point because (7.54) is not jointly convex in $\{\mathbf{B}_q\}$ and $\{\mathbf{A}_{q,e}\}$.

7.5 Simulation results

In this section we evaluate the performance of FBMC/OQAM and OFDM systems in terms of uncoded BER. Regarding the configuration of the system we have considered that both the transmitter and the receiver are equipped with multiple antennas. In notation terms a $N_R \times N_T \times S$ communication system accounts for a scenario where S streams are spatially multiplexed in a system that deploys N_R antennas at reception and N_T antennas at the transmit side. In all the cases analysed the symbols are drawn from a 16-QAM constellation, thus $\{d_{lq}[k]\}$ is 4-PAM.

In the case that $S = 1$, beamformers are designed to maximize either the SINR or the SLNR. The models presented in Sections 7.1 and 7.2 allow us to devise transmit and receive strategies that independently process real and imaginary parts resulting in a WLP. As a consequence, the algorithms described in Sections 7.3.1 and 7.3.2 are identified as WLP-SLNR and WLP-SINR, respectively. As a benchmark we have simulated the technique proposed in [101], which performs a LP that maximizes the SINR. So this solution is identified in simulations as LP-SINR. It is important to highlight that the joint transmitter and receiver design analysed in [101] has been applied to OFDM and FBMC/OQAM systems. Regarding the power distribution, we have set $p_q = 1$ for all $q \in S_a$. The BER in the case that a single stream is transmitted per-subcarrier is evaluated as function of the energy bit to noise ratio ($\frac{E_b}{N_0}$).

When multi-stream transmission is studied the system performance of techniques presented in the Section 7.4 are evaluated in terms of BER against the average energy symbol to noise ratio, which is defined as $\frac{E_s}{N_0} = \frac{M+CP}{M}\frac{2\times P_T}{M\times N_0}$. The factor 2 in the numerator accounts for the energy of a complex QAM symbol, since the PAM symbols have unit-energy. As for the benchmark, we have simulated the solution based on the linear processing that minimizes the sum MSE derived in [140]. The solution can be implemented either in an OFDM or in a FBMC/OQAM architecture, as proposed in [138]. To differentiate each case we use these two acronyms: (OFDM) LP-MSE and (FBMC) LP-MSE. Since the non-iterative technique that is described in Section 7.4.3 is based on a WLP, it is identified in the figures as (FBMC) WLP-MSE.

The numerical results depicted in Figure 7.1a show that (FBMC) LP-SINR saturates at high $\frac{E_b}{N_0}$. This justifies the need for devising specific designs for the FBMC/OQAM physical layer. In this sense, the proposed techniques are able to exploit the CSI to outperform the linear processing. Note that at low and moderate $\frac{E_b}{N_0}$ a single tap per antenna suffices to achieve the same results as OFDM. On the contrary, at high $\frac{E_b}{N_0}$ the interference dominates over the noise, which highlights that multiple taps are required to achieve lower BER curves. In Scenario 3 the flatness assumption of the channel at the subcarier level is not realistic. For this reason in Figure 7.1b the (FBMC) LP-SINR saturates at a higher BER when compared to Figure 7.1a. By observing the behaviour of FBMC/OQAM in the Scenario 3 we can conclude that interferences are more effectively mitigated

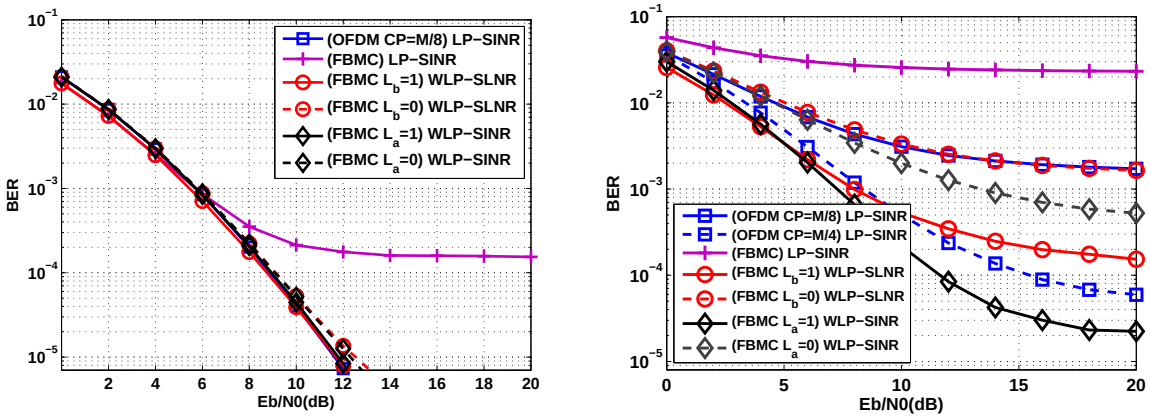

(a) Scenario 1.

(b) Scenario 3.

Figure 7.1: BER vs. $\frac{E_b}{N_0}$ for $2 \times 2 \times 1$ communication systems in OFDM and FBMC/OQAM modulation schemes. System parameters are set according to Scenarios 1 and 3 (see Table 2.3).

when the temporal diversity together with the spatial diversity is considered. It must be pointed out that selecting the SINR expression to be the cost function leads to better results as though we had considered the SLNR. The reason relies on the fact that the BER depends on the SINR as shown in [122]. When the frequency selectivity of the channel is somewhat low, the interferences are almost eliminated and then SLNR and SINR virtually coincide as Figure 7.1a confirms. Conversely, when the variations of the channel become abrupt in the subcarrier pass band region the interferences are not negligible, thus the expressions are far from being equivalent. In OFDM the error is pushed down by increasing the length of the CP. Extending the CP beyond $\frac{M}{4}$ samples we could possibly improve the results. Nevertheless the penalty that should be paid in terms of bandwidth efficiency would be unacceptable. Furthermore, OFDM with CP=$\frac{M}{4}$ is only able to outperform WLP-SLNR technique in the $\frac{E_b}{N_0}$ range [10dB-20dB]. When OFDM is confronted with WLP-SINR, it does not compare favourably. For the sake of clarity in the presentation we have not included the results of those cases where L_a and L_b are larger than one, since they do not substantially improve the results. That might be because the energy of the interference mainly comes from the first-order neighbors.

The plots of Figure 7.2a point out that when the number of receive antennas is higher than the number of transmit antennas the WLP-SLNR technique gives poor results. This happens mainly because the WLP-SLNR restricts the antenna weights on the receive side to be real-valued. Conversely, the coefficients involved in the transmit processing are the ones that are set to be real-valued in the WLP-SINR case. Consequently in a $3 \times 2 \times 1$ configuration, WLP-SLNR uses less degrees of freedom than WLP-SINR, which explains the energy savings provided by WLP-SINR in

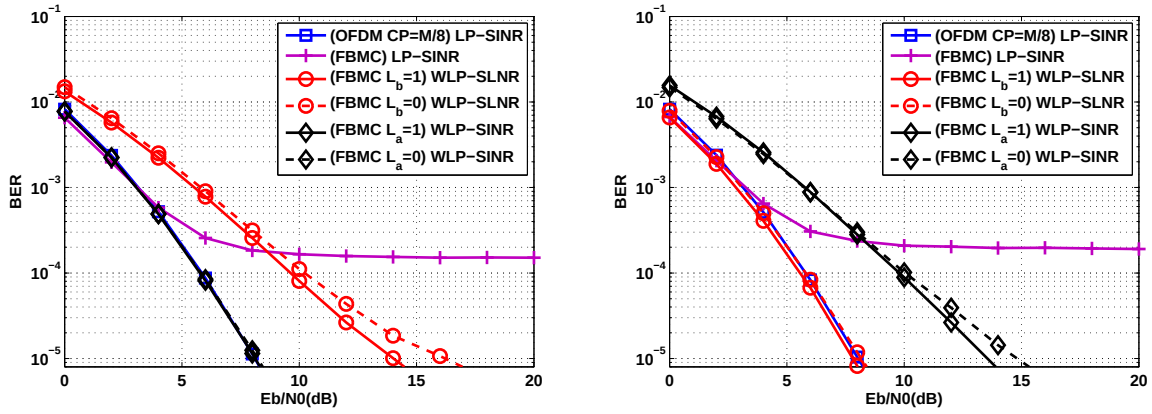

(a) MIMO $3 \times 2 \times 1$.

(b) MIMO $2 \times 3 \times 1$.

Figure 7.2: BER vs. $\frac{E_b}{N_0}$ for different multi-antenna configurations in FBMC/OQAM and OFDM modulation schemes. System parameters are set according to the Scenario 1 (see Table 2.3).

Figure 7.2a. The same argument holds to explain the relative behaviour between WLP-SLNR and WLP-SINR in Figure 7.2b.

In Figure 7.3 we show some results when the number of streams conveyed on each subcarrier is higher than one. The number of streams and the number of transmit and receive antennas are related as follows: $S = N_T \leq N_R$. The justification is provided in Section 7.4.2. In particular, we focus on this configuration $4 \times 2 \times 2$. The results depicted in Figure 7.3a show that the proposed technique slightly outperforms OFDM. This implies that the WLP-MSE technique succeeds in removing the interferences as well as the loss in the first subchannel is compensated by the improvement of the second spatial subchannel. The gap between WLP-MSE and (OFDM) LP-MSE is also due to the energy wastage that implies transmitting the CP. The BER curves of Figure 7.3a also highlight that the proposed technique does not benefit from implementing a multi-tap linear equalizer. Therefore, we can state that the channel frequency response is approximately flat at the subcarrier level. As for the (FBMC) LP-MSE technique, it provides satisfactory results at high and moderate noise regime. However, for $\frac{E_s}{N_0} \geq 14$dB the performance starts degrading because the interferences are not removed and as a consequence the BER plot exhibits an error floor when the noise is not the dominant source of interference. Scenario 3 is very challenging because the CP is not long enough to absorb the maximum channel excess delay. In this sense, as Figure 7.3b shows, the larger is the CP, the lower is the BER. The (FBMC) LP-MSE technique does not compare favourably even at high noise regime. Now, the multi-tap linear equalization does push down the BER curves with respect to the single-tap case. The reason lies in the fact that the channel frequency response cannot be modeled flat at the subcarrier level. We have not increased the number

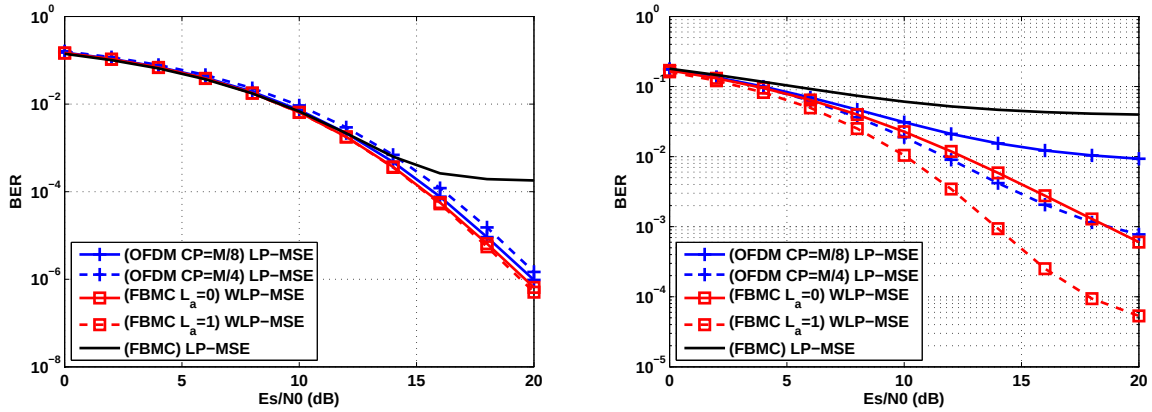

(a) Scenario 1.

(b) Scenario 3.

Figure 7.3: BER vs. $\frac{E_s}{N_0}$ for $4 \times 2 \times 2$ communication systems in OFDM and FBMC/OQAM modulation schemes. System parameters are set according to Scenarios 1 and 3 (see Table 2.3).

of taps beyond 3 because it does not significantly improve the results. The reason is because most of the energy of the interferences comes from the first order neighbours. Under the conditions of Scenario 3, the WLP-MSE technique provides the best results because it is interference aware, which means that it can cope with the loss of orthogonality between subcarriers.

To evaluate how close the designs addressed in Sections 7.4.1 and 7.4.3 perform, we have tested in Figure 7.4 both schemes in Scenarios 1 and 3. In particular, we focus on a $4\times2\times2$ communication system fixing $\frac{E_s}{N_0}$=20 dB. The number of taps of the equalizers is set to 3 and the iterative design is initialized with random matrices. As Figure 7.4 shows, the BER achieved by the iterative design decreases as the number of iterations increase. It only outperforms the one-shot design after performing 100 iterations. Beyond that point the improvement is marginal, thus we can conclude that the non-iterative design almost gives the same BER when compared to the value at which the alternating optimization method converges.

7.6 Chapter summary

This chapter studies the application of FBMC/OQAM systems to low coherence bandwidth MIMO channels in PTP communications. Under these conditions the channel frequency response cannot be modeled flat at a subcarrier level. This implies that the WLP devised in Chapter 6 does not restore the orthogonality. Aiming at circumventing this problem we propose the design of new signal processing techniques. The WLP comes naturally when FBMC/OQAM is analysed since the transmitted symbols are improper. The figures of merit that govern the design when a single

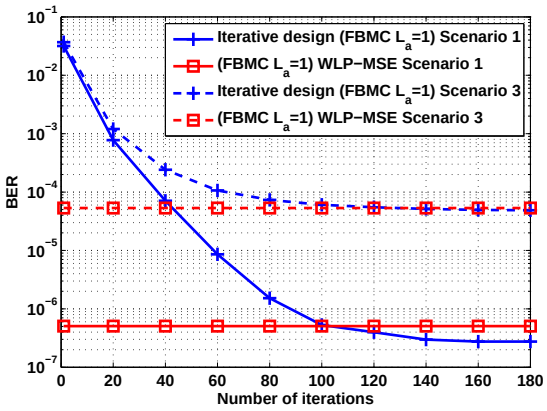

Figure 7.4: BER for a $4 \times 2 \times 2$ communication system having fixed $\frac{E_s}{N_0}$=20dB.

stream is transmitted over each subcarrier are the SLNR and the SINR. In both cases precoders and equalizers work on a per-subcarrier basis and may have multiple taps. If the objective function is given by the SLNR, the precoding is based on a multi-tap linear filtering structure whereas the equalizers utilize a single tap. When the beamforming design is driven by the SINR maximization, the complexity burden is placed on the receive side. That is, precoders employ a single tap while equalizers rely on the multi-tap filtering. The simulation-based results allow us to conclude that under highly frequency selective channels the proposed designs are able to exploit the richness in scattering of the environment to significantly increase the link reliability when compared to MIMO-OFDM systems. The optimal beamforming originally devised in MIMO-OFDM systems does not provide competitive results if it is tailored to the MIMO-FBMC/OQAM modulation scheme.

In the MIMO-FBMC/OQAM scheme it is definitely challenging to simultaneously provide robustness against the channel frequency selectivity and support multi-stream transmission. To this end, the design of MIMO precoding and decoding techniques has been investigated. The processing that comes from tackling the FBMC/OQAM application to MIMO channels can be considered as an improvement with respect to of those solutions that are only able to accommodate a single stream per-subcarrier. Under the criterion of minimizing the sum MSE, two different techniques have been devised. The first technique keeps the complexity at a reasonable level, which is practical from the implementation point of view, but in exchange the original problem is relaxed yielding a suboptimal solution. With the objective of performing closer to the optimum solution, the second option iteratively computes precoders and equalizers by resorting to an alternating optimization method, which is much more complex. In both cases the improperness of transmitted symbols has been exploited resulting in the WLP. We have demonstrated via simulations that the first technique nearly achieves the same results as the iterative design. The numerical results also show that the

multi-stream solution derived for MIMO-FBMC/OQAM systems compares favourably to MIMO-OFDM in terms of BER. However, the number of streams (S) transmitted over each subcarrier and the number of antennas deployed at transmit (N_T) and receive side (N_R) should satisfy this relation: $S = N_T \leq N_R$, which has been theoretically justified. The resulting scheme of combining FBMC/OQAM with the optimal beamforming derived in the OFDM context does not remain competitive because of the error floor appearance at low noise regime.

Appendices

7.A Solution of problem 7.46

To solve (7.46) we propose to apply the two-step algorithm described in [140] to obtain the precoding matrices $\{\mathbf{B}_q\}$ and the receive vectors $\left\{\mathbf{a}_{q,e}^l\right\}$. The first problem to be solved is given by

$$\underset{\left\{\mathbf{a}_{q,e}^l\right\}}{\operatorname{argmin}} \sum_{q\in S_a} \sum_{l=1}^{S} UB_q^l. \tag{7.57}$$

For a fixed transmit processing the problem (7.57) is convex, thus the optimal equalizers are written in this form

$$\mathbf{a}_{q,e}^l = \left(\mathbf{C}_q + \mathbf{E}_{qq,e}^k[0]\mathbf{B}_q \left(\mathbf{E}_{qq,e}^k[0]\mathbf{B}_q\right)^T\right)^{-1} \mathbf{E}_{qq,e}^k[0]\mathbf{B}_q\mathbf{e}_l \tag{7.58}$$

with

$$\mathbf{C}_q = \sum_{\substack{m=q-1\\ m\neq q}}^{q+1} \sum_{\tau=-L_a-L_{g_1}}^{L_a+L_{g_2}} b_m \mathbf{E}_{qm,e}^k[\tau]\left(\mathbf{E}_{qm,e}^k[\tau]\right)^T + \sum_{\substack{\tau=-L_a-L_{g_1}\\ \tau\neq 0}}^{L_a+L_{g_2}} b_q \mathbf{E}_{qq,e}^k[\tau]\left(\mathbf{E}_{qq,e}^k[\tau]\right)^T + \mathbf{R}_q. \tag{7.59}$$

In the second step of the algorithm, the receive vectors in (7.45) are particularized for (7.58) and the transmit matrices are optimized so that the upper bound on the sum MSE is minimized. Thus, the problem reduces to

$$\begin{aligned} &\underset{\{\mathbf{B}_q\}}{\operatorname{argmin}} \sum_{q\in S_a} \sum_{l=1}^{S} UB_q^l \\ &s.t. \sum_{q\in S_a} \|\mathbf{B}_q\|_F^2 \leq P_T \\ &\quad \lambda_1\left(\mathbf{B}_q\mathbf{B}_q^T\right) \leq b_q, \quad q \in S_a, \end{aligned} \tag{7.60}$$

where the objective function can be written as

$$\begin{aligned}\sum_{l=1}^{S} UB_q^l &= \mathrm{tr}\left(\mathbf{I}_S - \left(\mathbf{E}_{qq,e}^k[0]\mathbf{B}_q\right)^T \left(\mathbf{C}_q + \mathbf{E}_{qq,e}^k[0]\mathbf{B}_q \left(\mathbf{E}_{qq,e}^k[0]\mathbf{B}_q\right)^T\right)^{-1} \mathbf{E}_{qq,e}^k[0]\mathbf{B}_q\right) \\ &= \mathrm{tr}\left(\left(\mathbf{I}_S + \left(\mathbf{E}_{qq,e}^k[0]\mathbf{B}_q\right)^T \mathbf{C}_q^{-1}\mathbf{E}_{qq,e}^k[0]\mathbf{B}_q\right)^{-1}\right).\end{aligned} \tag{7.61}$$

Although the new problem does not match the minimization of the exact sum MSE, it allows us to benefit from the framework developed in [140]. In this regard, we can state that if the constraints on the dominant eigenvalues are ignored, the solution of (7.60) has the structure $\mathbf{B}_q = \mathbf{U}_q\Sigma_q$, where $\mathbf{U}_q \in \mathbb{R}^{N_T \times \check{L}_q}$ contains the eigenvectors of $\left(\mathbf{E}_{qq,e}^k[0]\right)^T \mathbf{C}_q^{-1}\mathbf{E}_{qq,e}^k[0] \in \mathbb{R}^{N_T \times N_T}$ that are associated with the $\check{L}_q$ largest eigenvalues. The matrix $\Sigma_q \in \mathbb{C}^{\check{L}_q \times S}$ is decomposed as $\Sigma_q = [\mathbf{0} \;\; \mathbf{P}_q]$, where $\mathbf{0} \in \mathbb{R}^{\check{L}_q \times S - \check{L}_q}$ is zero valued and $\mathbf{P}_q = \mathrm{diag}\left\{\sqrt{p_{\check{L}_q q}}, ..., \sqrt{p_{1q}}\right\} \in \mathbb{R}^{\check{L}_q \times \check{L}_q}$. Whether it is possible or not to spatially multiplex S streams will be given by $\check{L}_q = \min\left(S, \mathrm{rank}\left(\left(\mathbf{E}_{qq,e}^k[0]\right)^T \mathbf{C}_q^{-1}\mathbf{E}_{qq,e}^k[0]\right)\right)$. As a consequence, $\check{L}_q \leq S$. From the precoding structure described above, the constraint on the dominant eigenvalue becomes $\lambda_1\left(\mathbf{B}_q\mathbf{B}_q^T\right) = \max\left\{p_{1q}, ..., p_{\check{L}_q q}\right\} \leq b_q$. Then, all the power coefficients should comply with this inequality $p_{lq} \leq b_q$, for $l = 1, ..., \check{L}_q$. Since the additional constraints are linear with the power coefficients, the upper bounds on the dominant eigenvalues do not affect the solvability of the problem (see [140]). Hence, we can state that the precoder that solves (7.60) is also given by $\mathbf{B}_q = \mathbf{U}_q\Sigma_q$. As a consequence, the power coefficients are obtained by solving

$$\begin{aligned} &\underset{\{p_{lq}\}}{\mathrm{argmin}} \sum_{q \in S_a} \sum_{l=1}^{\check{L}_q} \frac{1}{1 + \lambda_{lq} p_{lq}} \\ &s.t. \sum_{q \in S_a} \sum_{l=1}^{\check{L}_q} p_{lq} \leq P_T \\ &\qquad 0 \leq p_{lq} \leq b_q, \quad 1 \leq l \leq \check{L}_q, \quad q \in S_a. \end{aligned} \tag{7.62}$$

Let λ_{lq} be the lth largest eigenvalue of matrix $\left(\mathbf{E}_{qq,e}^k[0]\right)^T \mathbf{C}_q^{-1}\mathbf{E}_{qq,e}^k[0]$. Since the problem (7.62) is convex, the power coefficients can be formulated as follows:

$$p_{lq} = \min\left(\left(\mu^{-1/2}\left(\lambda_{lq}\right)^{-1/2} - \left(\lambda_{lq}\right)^{-1}\right)^+, b_q\right), \tag{7.63}$$

where μ is the Lagrange multiplier that guarantees that the total power constraint is active and $(x)^+ = \max(0, x)$. One option to compute (7.63) is to proceed similarly to the cap-limited water-filling algorithm [114].

In order to find a low-complexity solution we have forced per-stream powers to be lower than

$\{b_q\}$, i.e. $p_{lq} \leq b_q$. If the coefficients that delimit the allowed values are too high both the transmit and receive matrices are overdesigned since the exact MSE will lie far below with respect to (7.45). Conversely, if the parameters $\{b_q\}$ take small values, the streams transmitted on the worst subchannels may not receive enough power to overcome the spectral nulls, which may have an effect on the reliability of the communication. In this regard, we have empirically observed that when the values of b_q are around $\frac{P_T}{M}$, we achieve a good trade-off. The problem of finding tight upper bounds that rely on analytical expressions is not fully explored in Section 7.4.1 and, therefore, it remains open.

7.B Solution of problem 7.56

Notice that (7.56) is convex and satisfies the Slater's constraint qualification [110], thus we can resort to the dual optimization framework to solve the primal problem. Based on that, we first generate the Lagrangian function as follows:

$$L\left(\lambda, \{\mathbf{A}_{q,e}, \mathbf{B}_q\}\right) = MSE\left(\{\mathbf{A}_{q,e}, \mathbf{B}_q\}\right) + \lambda \left(\sum_{q \in S_a} \|\mathbf{B}_q\|_F^2 - P_T \right), \tag{7.64}$$

where λ accounts for the Lagrange multiplier. The dual function is obtained by solving the following unconstrained minimization

$$g\left(\lambda\right) = \min_{\{\mathbf{B}_q\}} L\left(\lambda, \{\mathbf{A}_{q,e}, \mathbf{B}_q\}\right), \tag{7.65}$$

which allows us to pose the dual problem in this form

$$\begin{aligned} g(\lambda_{opt}) = \quad & \max_{\lambda} g(\lambda) \\ & s.t. \;\; \lambda \geq 0. \end{aligned} \tag{7.66}$$

The MIMO precoding matrix that solves (7.65) is given by

$$\mathbf{B}_q^*(\lambda) = \left(\sum_{m=q-1}^{q+1} \sum_{t=-L_a-L_{g_1}}^{L_a+L_{g_2}} \left(\mathbf{E}_{mq,e}^k[t]\right)^T \mathbf{A}_{m,e} \mathbf{A}_{m,e}^T \mathbf{E}_{mq,e}^k[t] + \lambda \mathbf{I}_{N_T} \right)^{-1} \left(\mathbf{E}_{qq,e}^k[0]\right)^T \mathbf{A}_{q,e}. \tag{7.67}$$

Plugging λ_{opt} into (7.67) yields the optimal precoder. In this sense, we propose to compute the optimal Lagrange multiplier by performing a bisection search assuming that $\lambda \in [0 \;\; \lambda_{max}]$. The criterion to bisect the plane is based on evaluating the supragradient of the dual function since it might not be differentiable [117]. The authors in [125] have demonstrated that the dual function

Algorithm 10 Precoder design

1: **if** $\partial g(0) < 0$ **then** $\lambda = 0$
2: **else**
3: Set l=0, u=λ_{max}
4: **repeat**
5: $\lambda = 0.5(l+u)$
6: **if** $\partial g(\lambda) < 0$ **then** u $= \lambda$ **else** l $= \lambda$
7: **until** $\sum_{q \in S_a} \left\| \mathbf{B}_q^*(\lambda) \right\|_F^2 \in [\delta P_T \quad P_T], \quad 0 < \delta < 1$
8: **end if**
9: $\mathbf{B}_q = \mathbf{B}_q^*(\lambda), \quad q \in S_a$

can be upper bounded as follows:

$$g(\bar{\lambda}) \leq g(\lambda) + (\bar{\lambda} - \lambda) \left(\sum_{q \in S_a} \left\| \mathbf{B}_q^*(\lambda) \right\|_F^2 - P_T \right). \tag{7.68}$$

From (7.68) it is easy to identify the supragradient of the dual function, which is given by $\partial g(\lambda) = \sum_{q \in S_a} \left\| \mathbf{B}_q^*(\lambda) \right\|_F^2 - P_T$. At this point, we should define the initial interval where the Lagrange multiplier lies. Since the strong duality holds, the complementary slackness has to be satisfied [110]. Hence, if $\lambda_{opt} > 0$ the total power constraint is active. By contrast, if the constraint is not satisfied with equality then $\lambda_{opt} = 0$. Bearing the complementary slackness in mind along with the trace inequality $\left(\mathrm{tr}\left(\mathbf{AB}\right) \leq \sum_{i=1}^{N} \lambda_i\left(\mathbf{A}\right) \lambda_i\left(\mathbf{B}\right) \right)$, yields

$$P_T = \sum_{q \in S_a} \left\| \mathbf{B}_q^*(\lambda_{opt}) \right\|_F^2 \leq \sum_{q \in S_a} \sum_{i=1}^{N_T} \frac{\alpha_q^i}{\left(\lambda_{opt} + \gamma_q^{N_T+1-i} \right)^2} \leq \sum_{q \in S_a} \sum_{i=1}^{N_T} \frac{\alpha_q^i}{\lambda_{opt}^2}, \tag{7.69}$$

for $\lambda_{opt} > 0$. Therefore

$$0 \leq \lambda_{opt} \leq \sqrt{\frac{\sum_{q \in S_a} \left\| \mathbf{A}_{q,e}^T \mathbf{E}_{qq,e}^k[0] \right\|_F^2}{P_T}} = \lambda_{max}. \tag{7.70}$$

This result follows from defining the eigenvalues of matrices $\left(\mathbf{E}_{qq,e}^k[0] \right)^T \mathbf{A}_{q,e} \mathbf{A}_{q,e}^T \mathbf{E}_{qq,e}^k[0]$ and

$$\sum_{m=q-1}^{q+1} \sum_{\tau=-L_a-L_{g_1}}^{L_a+L_{g_2}} \left(\mathbf{E}_{mq,e}^k[\tau] \right)^T \mathbf{A}_{m,e} \mathbf{A}_{m,e}^T \mathbf{E}_{mq,e}^k[\tau], \tag{7.71}$$

as $\left\{ \alpha_q^1, ..., \alpha_q^{N_T} \right\}$ and $\left\{ \gamma_q^1, ..., \gamma_q^{N_T} \right\}$, respectively. The eigenvalues collected in both sets are arranged

in descending order. Setting the upper bound according to (7.70) certifies that the optimal Lagrange multiplier is confined in the selected interval. The authors have demonstrated in [152] that $\mathbf{B}_q^*(\lambda)$ decreases monotonically with λ. Hence, if $\partial g(0) < 0$, then $\partial g(\lambda) < 0$ for any $\lambda \in [0 \quad \lambda_{max}]$. Consequently $\lambda_{opt} = 0$ if $\partial g(0) < 0$. Taking this result into account, Algorithm 10 enables us to perform as close to the optimal value as desired. The algorithm stops when the desired precision is reached. In particular we fix $\delta = 0.99$. It is important to remark that through a different reasoning we have arrived at the same result as [152].

Chapter 8

Conclusions and future work

This chapter summarizes the conclusions that can be drawn from the numerical results and the mathematical developments that are included in this thesis. In addition, some ideas are given to continue the work that has been initiated in this dissertation.

8.1 Conclusions

The air-interface of 5th generation wireless systems will have to be designed to meet ambitious throughput goals and to be spectrally agile. Many state-of-the-art communication standards rely on combining MIMO architectures with the OFDM modulation, which is the most prominent multicarrier technology. The popularity of OFDM stems from the fact that the transmission link can be modeled like a set of parallel flat fading channels. As a consequence subbands can be independently processed and thus, OFDM can benefit from the advances made in single carrier systems. Nevertheless, this is achieved in exchange of inserting a CP and shaping subcarrier signals with the rectangular pulse, which exhibits poor stopband attenuation. This highlights the need to go beyond OFDM and push the research for alternative multicarrier modulations. In view of this, the FBMC/OQAM modulation scheme is gaining momentum since it does not transmit redundancy and takes advantage of pulse shaping techniques. Chapter 1 reviews this technology and provides evidence to favourably consider FBMC/OQAM as an eligible technology for future wireless communications. However, the research is not as mature as it is in the OFDM context and there are still some topics that need to be further investigated. In this sense, how to fully exploit the potentials of MIMO communications in the FBMC/OQAM context is on progress. In this sense, this thesis casts some light into the design of multiantenna and multicarrier techniques based on OQAM.

Chapter 2 introduces a unified formulation that is sufficiently general to accommodate any

pre- and post-processing technique for MIMO PTP communication systems in the FBMC/OQAM context. The system model reveals that the multipath fading destroys the orthogonality properties. Therefore, unless the channel is counteracted, the reception will be affected by ISI and ICI. This interference is induced by the modulation. For this reason this type of disturbance is called intrinsic interference. When multiple antennas are placed at both ends of the link, the multiantenna-induced interference comes into play making the FBMC/OQAM extension to MIMO architectures definitely challenging.

The first problem that has been tackled is the design of signal processing techniques to deal with the channel at the receive side. To this end, the receiver structure that consists of a feedforward filter followed by a MLSE has been examined in SIMO PTP communications. The feedforward filter has the objective of reducing the length of the channel. This means that a reduced number of undesired symbols are allowed at the filter output. The residual interference is treated as noise and the MLSE is responsible to cope with the allowed interference terms. The best strategy when it comes to set the number of taps and the number of allowed interference terms depends on the propagation conditions. The good spectral confinement exhibited by the subcarrier signals is harnessed by the receiver to equalize the signals in a per-subcarrier basis even in the MAC in presence of synchronization errors. The subcarrier-wise processing alleviates the complexity with respect to multi-user detectors that jointly process all the subcarriers. Another conclusion that has been drawn when delving into the equalization design is that the residual interference at the equalizer output should not be ignored in the detection stage, if coded FBMC/OQAM systems are employed. Since the exact characterization of the residual inference is computationally demanding, two low-complexity estimation methods have been developed.

When the detrimental effects of the channel are combated at transmission it is deemed necessary to follow an unselfish approach. That is, linear precoders have to take into account the signal that leaks through unintended positions along the time-frequency grid. Behind this rationale several criteria have been proposed to design the transmit strategies for a fixed power allocation, which rely on having CSI knowledge at transmission. The techniques can be refined if the power distribution is optimized given the precoders. We have concentrated on cases where the channel is highly frequency selective, so that precoders are not able to remove the interference. In particular, three different problems have been reviewed. The first and second aim at maximizing the sum-rate for PTP communications given a total power budget. The second problem imposes integer-bit and QoS constraints in addition to the power constraint. Finally, the third problem focuses on the downlink of a multi-user communication system. In this situation subcarriers can only be occupied by a single user. Therefore, the resource allocation problem comes down to allocate the power among subcarriers and assign subcarriers to users. The optimal solution of all the problems that are analysed is difficult to attain with a reduced complexity because adjacent subcarriers

are coupled. However, we can break up the original problem into several simpler subproblems by smartly grouping subcarriers. Then, each subproblem can be independently solved, which drastically reduces the complexity. Although this strategy is suboptimal, the solution performs reasonably close to the optimal.

The last area that is studied in this thesis focuses on the joint transmitter and receiver design for FBMC/OQAM-based MIMO channels. The scenarios that have been analysed cover multiantenna point-to-point as well as multinatenna point-to-multipoint communications. In the most general case, the signal at the output of the AFB is degraded by modulation-, multi-stream-, multiantenna and multi-user-induced interference. In some cases, the linear processing intended for OFDM systems can successfully cope with the interference. By contrast, in other situations it is required to take into account the characteristics of the FBMC/OQAM modulation. Then, real and imaginary parts are independently treated, giving rise to the widely linear processing, which is able to achieve interference-free data multiplexing. The theoretical analysis that is conducted in this dissertation allows us to infer for which multiantenna configurations the WLP remains competitive with the LP. In other words, the relation between the number of streams, transmit and receive antennas determines when WLP may be successfully applied.

In almost all the proposed study cases the signal processing techniques initially though for OFDM come in useful to restore the orthogonality in FBMC/OQAM systems, as long as the channel frequency response is almost flat within subchannels. Then, FBMC/OQAM outperforms OFDM in terms of BER and rate. The reason lies in the fact that the FBMC/OQAM modulation does not resort to the CP transmission, which leads to an increased bandwidth efficiency and a reduced energy wastage. The spectral efficiency can be further improved by extending the number of active data carriers. Since pulses decay faster in FBMC/OQAM systems, the subcarriers that are switched off at the edges of the band can be reduced without increasing the out-of-band radiation. Provided that the flat fading assumption is not satisfied, then the improperness of the transmitted symbols and the intrinsic interference come into play when addressing the design of FBMC/OQAM systems. Interestingly, the best performance is still given in this case by FBMC/OQAM if the maximum channel excess delay is longer than the CP in OFDM systems. The most interesting conclusion that can be drawn from this thesis is that the FBMC/OQAM modulation scheme can benefit from the spatial dimension to boost the system performance when compared to the OFDM counterpart, for some multiantenna configurations and propagation conditions.

8.2 Future lines of research

The results presented in this thesis bridge the gap between FBMC/OQAM and OFDM mainly because of the progress that has been made in the application of multiantenna diversity techniques

to FBMC/OQAM systems. However, we have localized some areas of research that are not fully explored. Some examples are given below.

8.2.1 Resource allocation

From the perspective of marginally degrading the system performance while reducing the complexity, the beamforming design and the resource allocation strategy can be independently and sequentially devised. In this regard, it may happen that the transmit and receive beamformers can just partially remove the interference. If so, ISI and ICI terms cannot be neglected. As a consequence, the resource allocation strategies originally devised for OFDM have to be revisited since they will lose the optimality in the FBMC/OQAM context. This highlights that new algorithms have to be designed. In Chapter 5 the rate maximization is investigated in presence of interference. However, there are alternative interesting criteria that have not been reviewed in this thesis, mostly for multi-user multicarrier systems. As a consequence, it would be worth studying if existing power and subcarrier allocation strategies should be modified to deal with residual ISI and ICI. The most relevant rata adaptation and the margin adaptive problems in the downlink of a communication system with multiple users include:

- Max-min rate allocation [153, 154].
- Sum-rate maximization with proportional rate constraints [155–157].
- Transmit power minimization subject to users' rate constraints [158, 159].

The problem is even more challenging when several users are allowed to transmit on the same subcarriers. Then, the user scheduling, the power allocation and subcarrier assignment have to be optimized [144, 160, 161].

8.2.2 Design of MIMO precoding and decoding matrices

If multiple antennas are incorporated at both ends of the link, MIMO techniques can be designed to boost the system performance. Nonetheless, how to reach the full potentials of these schemes in the context of FBMC/OQAM is still an active research topic. In this sense, the advances made in this thesis can be considered as a starting point, yet there is room for improvement in many areas. The future lines of research that have been identified as for the joint transmitter and receiver design are detailed in the following.

Resorting to majorization theory we have been able to compare analytically the performance given by the proposed WLP, which is especially designed for FBMC/OQAM, and the LP, which can be applied to OFDM and FBMC/OQAM platforms. Nevertheless, the comparison is only valid for

some limited multiantenna configurations. Therefore, further studies are required to determine how compare the WLP and the LP for any number of streams, transmit antennas and receive antennas. Besides, the performance metric that governs the design of transmit and receive beamformers is the sum MSE. It would be interesting to consider other objective functions than the sum MSE.

The MIMO techniques addressed in Chapters 6 and 7 have to be aware of inter-symbol, inter-carrier, inter-antenna and inter-user interference. The inter-carrier interference is by far the most harmful effect because it couples subcarriers. This prevents us from independently processing subcarriers and benefiting from the convex optimization. Some ideas have been highlighted to reduce the complexity such as the utilization of bounds to convexity the problem. Unfortunately, this results in suboptimal solutions. This reveals the difficulty of attaining the optimum with a reduced complexity, which remains as an open problem. Another important aspect regarding the suboptimal designs is that all the degrees of freedom are not used. At least the precoder or the equalizer is restricted to be real-valued. Thus, it is left as future work the joint design of MIMO precoding and decoding matrices that use real and imaginary dimensions.

Bibliography

[1] International Telecommunication Union Radiocommunication, "Assessment of the global mobile broadband deployments and forecasts for international mobile telecommunications." ITU-R. R. M.2243, 2011.

[2] "Evolved Universal Terrestrial Radio Access (E-UTRA); LTE physical - General Description (Release 10)." 3GPP TR 36.201.

[3] "Mobile system profile; (Release 10 approved specification, revision 1.7.1)." WiMAX Forum.

[4] "IEEE Draft Standard for IT - Telecommunications and Information Exchange Between Systems - LAN/MAN - Specific Requirements - Part 11: Wireless LAN Medium Access Control and Physical Layer Specifications - Amd 4: Enhancements for Very High Throughput for operation in bands below 6GHz," *IEEE P802.11ac/D3.0, June 2012*, pp. 1–385, 2012.

[5] A. Paulraj, D. Gore, R. Nabar, and H. Bolcskei, "An overview of mimo communications - a key to gigabit wireless," *Proceedings of the IEEE*, vol. 92, no. 2, pp. 198 – 218, feb 2004.

[6] G. J. Foschini and M. J. Gans, "On limits of wireless communications in a fading environment when using multiple antennas," *Wireless Personal Communications*, vol. 6, pp. 311–335, 1998.

[7] V. Tarokh, N. Seshadri, and A. Calderbank, "Space-time codes for high data rate wireless communication: performance criterion and code construction," *Information Theory, IEEE Transactions on*, vol. 44, no. 2, pp. 744 –765, mar 1998.

[8] I. E. Telatar, "Capacity of multi-antenna gaussian channels," *European Transactions on Telecommunications*, vol. 10, pp. 585–595, 1999.

[9] D. Gesbert, M. Shafi, D. shan Shiu, P. Smith, and A. Naguib, "From theory to practice: an overview of MIMO space-time coded wireless systems," *Selected Areas in Communications, IEEE Journal on*, vol. 21, no. 3, pp. 281 – 302, apr 2003.

[10] H. Sari, G. Karam, and I. Jeanclaude, "Transmission techniques for digital terrestrial tv broadcasting," *Communications Magazine, IEEE*, vol. 33, no. 2, pp. 100–109, 1995.

[11] Z. Wang and G. Giannakis, "Wireless multicarrier communications," *Signal Processing Magazine, IEEE*, vol. 17, no. 3, pp. 29 –48, may 2000.

[12] D. Falconer, S. Ariyavisitakul, A. Benyamin-Seeyar, and B. Eidson, "Frequency domain equalization for single-carrier broadband wireless systems," *Communications Magazine, IEEE*, vol. 40, no. 4, pp. 58–66, 2002.

[13] A. Czylwik, "Comparison between adaptive ofdm and single carrier modulation with frequency domain equalization," in *Vehicular Technology Conference, 1997, IEEE 47th*, vol. 2, 1997, pp. 865–869 vol.2.

[14] H. Myung, J. Lim, and D. Goodman, "Single carrier fdma for uplink wireless transmission," *Vehicular Technology Magazine, IEEE*, vol. 1, no. 3, pp. 30–38, 2006.

[15] S. Premnath, D. Wasden, S. Kasera, N. Patwari, and B. Farhang-Boroujeny, "Beyond OFDM: Best-Effort Dynamic Spectrum Access Using Filterbank Multicarrier," *Networking, IEEE/ACM Transactions on*, vol. 21, no. 3, pp. 869–882, 2013.

[16] R. W. Chang, " Synthesis of Band-Limited orthogonal signals for multichannel data transmission," *Bell Systems Technical Journal*, vol. 45, pp. 1775 – 1796, Dec. 1966.

[17] B. Saltzberg, "Performance of an efficient parallel data transmission system," *Communication Technology, IEEE Transactions on*, vol. 15, no. 6, pp. 805 –811, december 1967.

[18] M. G. Bellanger and J. L. Daguet, "TDM-FDM Transmultiplexer; Digital Polyphase and FFT," *IEEE Trans. Communications*, vol. 22, no. 9, pp. 1199 – 1205, Sept. 1974.

[19] B. Hirosaki, "An Orthogonally Multiplexed QAM System Using the Discrete Fourier Transform," *IEEE Trans. Communications*, vol. 29, no. 7, pp. 982 – 989, Jul. 1981.

[20] G. Cariolaro and F. Vagliani, "An OFDM scheme with a half complexity," *Selected Areas in Communications, IEEE Journal on*, vol. 13, no. 9, pp. 1586 – 1599, Dec. 1995.

[21] P. Siohan, C. Siclet, and N. Lacaille, "Analysis and design of OFDM/OQAM systems based on filterbank theory," *Signal Processing, IEEE Transactions on*, vol. 50, no. 5, pp. 1170 –1183, may 2002.

[22] H. Bölcskei, "Orthogonal frequency division multiplexing based on offset QAM," *Chapter in: Advances in Gabor Analysis, H. G. Feichtinger and T. Strohmer, eds., Birkhäuser*, pp. 321–352, 2003.

[23] M. Vetterli, "Perfect transmultiplexers," in *Acoustics, Speech, and Signal Processing, IEEE International Conference on ICASSP '86.*, vol. 11, apr 1986, pp. 2567 – 2570.

[24] P. P. Vaidyanathan, *Multirate systems and filter banks.* Upper Saddle River, NJ, USA: Prentice-Hall, Inc., 1993.

[25] T. Karp and N. Fliege, "Modified DFT filter banks with perfect reconstruction," *Circuits and Systems II: Analog and Digital Signal Processing, IEEE Transactions on*, vol. 46, no. 11, pp. 1404 –1414, nov 1999.

[26] C. Y. Wong, R. Cheng, K. Lataief, and R. Murch, "Multiuser OFDM with adaptive subcarrier, bit, and power allocation," *Selected Areas in Communications, IEEE Journal on*, vol. 17, no. 10, pp. 1747 –1758, oct 1999.

[27] G. Cherubini, E. Eleftheriou, and S. Ölçer, "Filtered multitone modulation for VDSL," in *Global Telecommunications Conference, 1999. GLOBECOM '99*, vol. 2, 1999, pp. 1139–1144 vol.2.

[28] G. Fettweis, M. Krondorf, and S. Bittner, "GFDM - Generalized Frequency Division Multiplexing," in *Vehicular Technology Conference, 2009. VTC Spring 2009. IEEE 69th*, 2009, pp. 1–4.

[29] N. Michailow, R. Datta, S. Krone, M. Lentmaier, and G. Fettweis, "Generalized Frequency Division Multiplexing: A Flexible Multi-Carrier Modulation Scheme for 5th Generation Cellular Networks," in *German Microwave Conference (GeMiC)*, 2012.

[30] B. Farhang-Boroujeny and C. (George) Yuen, "Cosine Modulated and Offset QAM Filter Bank Multicarrier Techniques: A Continuous-Time Prospect," *EURASIP Journal on Advances in Signal Processing*, vol. 2010, no. 1, p. 16, 2010.

[31] B. Farhang-Boroujeny, "OFDM versus filter bank multicarrier," *Signal Processing Magazine, IEEE*, vol. 28, no. 3, pp. 92 –112, may 2011.

[32] M. Faulkner, "The effect of filtering on the performance of OFDM systems," *Vehicular Technology, IEEE Transactions on*, vol. 49, no. 5, pp. 1877–1884, 2000.

[33] T. Weiss and F. Jondral, "Spectrum pooling: an innovative strategy for the enhancement of spectrum efficiency," *Communications Magazine, IEEE*, vol. 42, no. 3, pp. S8–S14, 2004.

[34] T. Weiss, J. Hillenbrand, A. Krohn, and F. Jondral, "Mutual interference in OFDM-based spectrum pooling systems," in *Vehicular Technology Conference, 2004. VTC 2004-Spring. 2004 IEEE 59th*, vol. 4, 2004, pp. 1873–1877 Vol.4.

[35] Z. Yuan and A. M. Wyglinski, "On Sidelobe Suppression for Multicarrier-Based Transmission in Dynamic Spectrum Access Networks," *Vehicular Technology, IEEE Transactions on*, vol. 59, no. 4, pp. 1998–2006, 2010.

[36] H.-M. Chen, W.-C. Chen, and C.-D. Chung, "Spectrally Precoded OFDM and OFDMA with Cyclic Prefix and Unconstrained Guard Ratios," *Wireless Communications, IEEE Transactions on*, vol. 10, no. 5, pp. 1416–1427, 2011.

[37] E. Bala, J. Li, and R. Yang, "Shaping Spectral Leakage: A Novel Low-Complexity Transceiver Architecture for Cognitive Radio," *Vehicular Technology Magazine, IEEE*, vol. 8, no. 3, pp. 38–46, 2013.

[38] B. Le Floch, M. Alard, and C. Berrou, "Coded orthogonal frequency division multiplex," *Proceedings of the IEEE*, vol. 83, 1995.

[39] B. Picinbono and P. Chevalier, "Widely linear estimation with complex data," *Signal Processing, IEEE Transactions on*, vol. 43, no. 8, pp. 2030 –2033, aug 1995.

[40] F. Neeser and J. Massey, "Proper complex random processes with applications to information theory," *Information Theory, IEEE Transactions on*, vol. 39, no. 4, pp. 1293–1302, 1993.

[41] R. Schober, W. Gerstacker, and J. Huber, "Improving differential detection of MDPSK by noise prediction," in *Global Telecommunications Conference, 1998. GLOBECOM 1998. The Bridge to Global Integration. IEEE*, vol. 1, 1998, pp. 567–572.

[42] S. Buzzi, M. Lops, and A. Tulino, "A generalized minimum-mean-output-energy strategy for CDMA systems with improper MAI," *Information Theory, IEEE Transactions on*, vol. 48, no. 3, pp. 761–767, 2002.

[43] A. Lampe, R. Schober, W. Gerstacker, and J. Huber, "A novel iterative multiuser detector for complex modulation schemes," *Selected Areas in Communications, IEEE Journal on*, vol. 20, no. 2, pp. 339–350, 2002.

[44] W. Gerstacker, R. Schober, and A. Lampe, "Equalization with widely linear filtering," in *Information Theory, 2001. Proceedings. 2001 IEEE International Symposium on*, 2001, pp. 265–.

[45] W. Gerstacker, F. Obernosterer, R. Schober, A. Lehmann, A. Lampe, and P. Gunreben, "Widely linear equalization for space-time block-coded transmission over fading ISI channels," in *Vehicular Technology Conference, 2002. Proceedings. VTC 2002-Fall. 2002 IEEE 56th*, vol. 1, 2002, pp. 238–242.

[46] ——, "Symbol-by-symbol and trellis-based equalization with widely linear processing for space-time block-coded transmission over frequency-selective fading channels," in *Global Telecommunications Conference, 2002. GLOBECOM '02. IEEE*, vol. 1, 2002, pp. 365–369.

[47] P. Chevalier and F. Pipon, "New insights into optimal widely linear array receivers for the demodulation of BPSK, MSK, and GMSK signals corrupted by noncircular interferences-application to SAIC," *Signal Processing, IEEE Transactions on*, vol. 54, no. 3, pp. 870–883, 2006.

[48] J. Olivier and W. Kleynhans, "Single antenna interference cancellation for synchronised GSM networks using a widely linear receiver," *Communications, IET*, vol. 1, no. 1, pp. 131–136, 2007.

[49] F. Sterle, "Widely Linear MMSE Transceivers for MIMO Channels," *Signal Processing, IEEE Transactions on*, vol. 55, no. 8, pp. 4258–4270, 2007.

[50] D. Darsena, G. Gelli, L. Paura, and F. Verde, "Widely-linear beamforming/combining techniques for MIMO wireless systems," in *Communications Control and Signal Processing (ISCCSP), 2012 5th International Symposium on*, 2012, pp. 1–5.

[51] P. Chevalier and F. Dupuy, "Widely Linear Alamouti Receiver for the Reception of Real-Valued Constellations Corrupted by Interferences-The Alamouti-SAIC/MAIC Concept," *Signal Processing, IEEE Transactions on*, vol. 59, no. 7, pp. 3339–3354, 2011.

[52] Z. Ho and E. Jorswieck, "Improper Gaussian Signaling on the Two-User SISO Interference Channel," *Wireless Communications, IEEE Transactions on*, vol. 11, no. 9, pp. 3194–3203, 2012.

[53] "Physical layer for dynamic access and cognitive radio," *European Project ICT 211887, PHYDYAS, http://www.ictphydyas.org.*

[54] M. Renfors and F. Harris, "Highly adjustable multirate digital filters based on fast convolution," in *Circuit Theory and Design (ECCTD), 2011 20th European Conference on*, 2011, pp. 9–12.

[55] A. Viholainen, T. Stitz, J. Alhava, T. Ihalainen, and M. Renfors, "Complex modulated critically sampled filter banks based on cosine and sine modulation," in *Circuits and Systems, 2002. ISCAS 2002. IEEE International Symposium on*, vol. 1, 2002, pp. I–833 – I–836.

[56] J. Alhava and M. Renfors, "Exponentially-modulated filter bank-based transmultiplexer," in *Circuits and Systems, 2003. ISCAS '03. Proceedings of the 2003 International Symposium on*, vol. 4, may 2003, pp. IV–233 – IV–236.

[57] A. Viholainen, J. Alhava, and M. Renfors, "Efficient implementation of 2x oversampled exponentially modulated filter banks," *Circuits and Systems II: Express Briefs, IEEE Transactions on*, vol. 53, no. 10, pp. 1138 –1142, oct. 2006.

[58] A. Viholainen and M. Renfors, "Alternative subband signal structures for complex modulated filter banks with perfect reconstruction," in *Circuits and Systems, 2004. ISCAS '04. Proceedings of the 2004 International Symposium on*, vol. 3, may 2004, pp. III – 525–8.

[59] M. Bellanger, "Specification and design of a prototype filter for filter bank based multicarrier transmission," in *Acoustics, Speech, and Signal Processing, 2001. Proceedings. (ICASSP '01). 2001 IEEE International Conference on*, vol. 4, 2001, pp. 2417 –2420 vol.4.

[60] A. Viholainen, T. Ihalainen, T. H. Stitz, M. Renfors, and M. Bellanger, "Prototype filter design for filter bank multicarrier transmission," in *in Proceedings of the European Signal Processing Conference (EUSIPCO 2009)*, august 2009.

[61] D. Chen, D. Qu, T. Jiang, and Y. He, "Prototype Filter Optimization to Minimize Stopband Energy With NPR Constraint for Filter Bank Multicarrier Modulation Systems," *Signal Processing, IEEE Transactions on*, vol. 61, no. 1, pp. 159–169, 2013.

[62] "3GPP TR 25.943 V11.0.0 Technical Specification Group Radio Access Network; Deployment aspects (Release 11)," Sep. 2012.

[63] International Telecommunication Union Radiocommunication, "Guidelines for the evaluation of radio transmission technologies for IMT-2000." ITU-R M.1225, 1997.

[64] Q. Bai, N. Passas, and J. Nossek, "Scheduling and resource allocation in OFDM and FBMC systems: An interactive approach and performance comparison," in *Wireless Conference (EW), 2010 European*, 2010, pp. 1042–1050.

[65] D. Waldhauser, L. Baltar, and J. Nossek, "MMSE subcarrier equalization for filter bank based multicarrier systems," in *Signal Processing Advances in Wireless Communications, 2008. SPAWC 2008. IEEE 9th Workshop on*, july 2008, pp. 525 –529.

[66] L. Baltar, D. Waldhauser, and J. Nossek, "MMSE subchannel decision feedback equalization for filter bank based multicarrier systems," in *IEEE International Symposium on Circuits and Systems*, may 2009, pp. 2802 –2805.

[67] A. Ikhlef and J. Louveaux, "An enhanced MMSE per subchannel equalizer for highly frequency selective channels for FBMC/OQAM systems," in *Signal Processing Advances in Wireless Communications, 2009. SPAWC '09. IEEE 10th Workshop on*, june 2009, pp. 186 –190.

[68] T. Ihalainen, A. Ikhlef, J. Louveaux, and M. Renfors, "Channel Equalization for Multi-Antenna FBMC/OQAM Receivers," *Vehicular Technology, IEEE Transactions on*, vol. 60, no. 5, pp. 2070–2085, 2011.

[69] T. Ihalainen, T. H. Stitz, M. Rinne, and M. Renfors, "Channel equalization in filter bank based multicarrier modulation for wireless communications," *EURASIP J. Appl. Signal Process.*, vol. 2007, January 2007.

[70] G. Ndo, H. Lin, and P. Siohan, "FBMC/OQAM equalization: Exploiting the imaginary interference," in *Personal Indoor and Mobile Radio Communications (PIMRC), 2012 IEEE 23rd International Symposium on*, 2012, pp. 2359–2364.

[71] M. Lagunas, A. Perez-Neira, and J. Vidal, "Optimal array combiner for sequence detectors," in *Acoustics, Speech and Signal Processing, 1998. Proceedings of the 1998 IEEE International Conference on*, vol. 6, may 1998, pp. 3341 –3344.

[72] Forney, G.D., "Maximum-likelihood sequence estimation of digital sequences in the presence of intersymbol interference," *Information Theory, IEEE Transactions on*, vol. 18, no. 3, pp. 363–378, 1972.

[73] J. Proakis, *Digital Communications*, 4th ed. McGraw-Hill Science/Engineering/Math, 2000.

[74] Forney, G.D., Jr., "The viterbi algorithm," *Proceedings of the IEEE*, vol. 61, no. 3, pp. 268–278, 1973.

[75] S. Altekar and J. Wolf, "Improvements in detectors based upon colored noise," *Magnetics, IEEE Transactions on*, vol. 34, no. 1, pp. 94–97, 1998.

[76] M. Morelli, C.-C. Kuo, and M.-O. Pun, "Synchronization Techniques for Orthogonal Frequency Division Multiple Access (OFDMA): A Tutorial Review," *Proceedings of the IEEE*, vol. 95, no. 7, pp. 1394 –1427, july 2007.

[77] T. Ihalainen, T. Stitz, A. Viholainen, and M. Renfors, "Performance comparison of LDPC-coded FBMC and CP-OFDM in beyond 3G context," in *Circuits and Systems, 2006. ISCAS 2006. Proceedings. 2006 IEEE International Symposium on*, may 2006.

[78] G. Ndo, P. Siohan, and M. Hamon, "A Comparison between Coded OFDM/OQAM and CP-OFDM Modulations over Multipath Channels," in *Vehicular Technology Conference Fall (VTC 2010-Fall), 2010 IEEE 72nd*, sept. 2010, pp. 1 –5.

[79] G. Ndo, P. Siohan, and M.-H. Hamon, "Performances of coded OFDM/OQAM over PLC impaired by impulsive and colored noise," in *Advanced Technologies for Communications (ATC), 2010 International Conference on*, oct. 2010, pp. 1 –6.

[80] C. Berrou, A. Glavieux, and P. Thitimajshima, "Near Shannon limit error-correcting coding and decoding: Turbo-codes. 1," in *Communications, 1993. ICC '93 Geneva. Technical Program, Conference Record, IEEE International Conference on*, vol. 2, 1993, pp. 1064–1070.

[81] P. Robertson, "Illuminating the structure of code and decoder of parallel concatenated recursive systematic (turbo) codes," in *Global Telecommunications Conference, 1994. GLOBECOM '94. Communications: The Global Bridge., IEEE*, vol. 3, 1994, pp. 1298–1303.

[82] J. Hagenauer, E. Offer, and L. Papke, "Iterative decoding of binary block and convolutional codes," *Information Theory, IEEE Transactions on*, vol. 42, no. 2, pp. 429–445, 1996.

[83] X. Li and J. Ritcey, "Bit-interleaved coded modulation with iterative decoding," in *Communications, 1999. ICC '99. 1999 IEEE International Conference on*, vol. 2, 1999.

[84] X. Sun, Q. Wang, L. Cimini, L. Greenstein, and D. Chan, "ICI/ISI-Aware Beamforming for MIMO-OFDM Wireless Systems," *Wireless Communications, IEEE Transactions on*, vol. 11, no. 1, pp. 378 –385, january 2012.

[85] P. Robertson, E. Villebrun, and P. Hoeher, "A comparison of optimal and sub-optimal MAP decoding algorithms operating in the log domain," in *Communications, 1995. ICC '95 Seattle, 'Gateway to Globalization', 1995 IEEE International Conference on*, vol. 2, 1995, pp. 1009–1013.

[86] C. Lele, J.-P. Javaudin, R. Legouable, A. Skrzypczak, and P. Siohan, "Channel estimation methods for preamble-based OFDM/OQAM modulations," *European Transactions on Telecommunications*, vol. 19, no. 7, pp. 741–750, 2008.

[87] C. Lele, P. Siohan, and R. Legouable, "2 dB Better Than CP-OFDM with OFDM/OQAM for Preamble-Based Channel Estimation," in *Communications, 2008. ICC '08. IEEE International Conference on*, 2008, pp. 1302–1306.

[88] T. Stitz, T. Ihalainen, and M. Renfors, "Practical issues in frequency domain synchronization for filter bank based multicarrier transmission," in *Communications, Control and Signal Processing, 2008. ISCCSP 2008. 3rd International Symposium on*, 2008, pp. 411–416.

[89] T. Fusco, A. Petrella, and M. Tanda, "Data-aided symbol timing and CFO synchronization for filter bank multicarrier systems," *Wireless Communications, IEEE Transactions on*, vol. 8, no. 5, pp. 2705–2715, 2009.

[90] ——, "Joint symbol timing and CFO estimation in multiuser OFDM/OQAM systems," in *Signal Processing Advances in Wireless Communications, 2009. SPAWC '09. IEEE 10th Workshop on*, 2009, pp. 613–617.

[91] J. Du and S. Signell, "Novel Preamble-Based Channel Estimation for OFDM/OQAM Systems," in *Communications, 2009. ICC '09. IEEE International Conference on*, 2009, pp. 1–6.

[92] D. Katselis, E. Kofidis, A. Rontogiannis, and S. Theodoridis, "Preamble-Based Channel Estimation for CP-OFDM and OFDM/OQAM Systems: A Comparative Study," *Signal Processing, IEEE Transactions on*, vol. 58, no. 5, pp. 2911–2916, 2010.

[93] D. Mattera and M. Tanda, "Preamble-based Synchronization for OFDM/OQAM Systems," in *European Signal Processing Conference (EUSIPCO 2011)*, 2011.

[94] D. Katselis, M. Bengtsson, C. Rojas, H. Hjalmarsson, and E. Kofidis, "On preamble-based channel estimation in OFDM/OQAM systems," in *European Signal Processing Conference (EUSIPCO 2011)*, 2011.

[95] C. Thein, M. Fuhrwerk, and J. Peissig, "Frequency-domain processing for synchronization and channel estimation in OQAM-OFDM systems," in *Signal Processing Advances in Wireless Communications (SPAWC), 2013 IEEE 14th Workshop on*, 2013, pp. 634–638.

[96] H. Saeedi-Sourck, S. Sadri, Y. Wu, and B. Farhang-Boroujeny, "Near Maximum Likelihood Synchronization for Filter Bank Multicarrier Systems," *Wireless Communications Letters, IEEE*, vol. 2, no. 2, pp. 235–238, 2013.

[97] E. Kofidis, D. Katselis, A. Rontogiannis, and S. Theodoridis, "Preamble-based channel estimation in OFDM/OQAM systems: A review," *Signal Processing*, vol. 93, no. 7, pp. 2038 – 2054, 2013.

[98] R. Zakaria and D. Le Ruyet, "On spatial data multiplexing over coded filter-bank multicarrier with ML detection," in *Personal Indoor and Mobile Radio Communications (PIMRC), 2011 IEEE 22nd International Symposium on*, sept. 2011, pp. 1391 –1395.

[99] 3GPP TS 25.346, "Introduction of the Multimedia Broadcast Multicast Service (MBMS) in the Radio Access Network (RAN); Stage 2 (Release 11)," august 2012.

[100] M. Lagunas, J. Vidal, and A. Perez-Neira, "Joint array combining and MLSE for single-user receivers in multipath Gaussian multiuser channels," *Selected Areas in Communications, IEEE Journal on*, vol. 18, no. 11, pp. 2252–2259, 2000.

[101] K.-K. Wong, R.-K. Cheng, K. Letaief, and R. Murch, "Adaptive antennas at the mobile and base stations in an OFDM/TDMA system," *Communications, IEEE Transactions on*, vol. 49, no. 1, pp. 195 –206, jan 2001.

[102] M. Joham, W. Utschick, and J. Nossek, "Linear transmit processing in MIMO communications systems," *IEEE Trans. on Signal Process.*, vol. 53, pp. 2700–2005, 2005.

[103] H. Boche and M. Schubert, "A general duality theory for uplink and downlink beamforming," in *Proceedings. VTC 2002-Fall.*, vol. 1, 2002, pp. 87 – 91.

[104] M. Bengtsson and B. Ottersten, "Optimal and Suboptimal Transmit Beamforming," in *Handbook of Antennas in Wireless Communications.* CRC Press, 2001, pp. 18–1–18–33.

[105] M. Grant and S. Boyd, "CVX: Matlab Software for Disciplined Convex Programming, version 2.0 beta," http://cvxr.com/cvx, Sep. 2012.

[106] M. Schubert and H. Boche, "Solution of the multiuser downlink beamforming problem with individual SINR constraints," *Vehicular Technology, IEEE Transactions on*, vol. 53, no. 1, pp. 18–28, 2004.

[107] Q. Bai and J. Nossek, "An energy efficient downlink resource allocation strategy for multiuser CP-OFDM and FBMC systems," in *Modeling and Optimization in Mobile, Ad Hoc and Wireless Networks (WiOpt), 2010 Proceedings of the 8th International Symposium on*, 2010, pp. 481–487.

[108] M. Payaro, A. Pascual-Iserte, A. Garcia-Armada, and M. Sanchez-Fernandez, "Resource Allocation in Multi-Antenna MAC Networks: FBMC vs OFDM," in *Vehicular Technology Conference (VTC Spring), 2011 IEEE 73rd*, 2011, pp. 1–5.

[109] L. G. Baltar, A. Mezghani, and J. A. Nossek, "MLSE and MMSE Subchannel Equalization for Filter Bank based Multicarrier Systems: Coded and Uncoded Results," in *European Signal Processing Conference (EUSIPCO 2010)*, 2010.

[110] S. Boyd and L. Vandenberghe, *Convex optimization.* Cambridge University Press, 2004.

[111] A. Pascual-Iserte, A. Perez-Neira, and M. Lagunas, "On power allocation strategies for maximum signal to noise and interference ratio in an OFDM-MIMO system," *Wireless Communications, IEEE Transactions on*, vol. 3, no. 3, pp. 808 – 820, may 2004.

[112] S. Diggavi and T. Cover, "The worst additive noise under a covariance constraint," *Information Theory, IEEE Transactions on*, vol. 47, no. 7, pp. 3072–3081, 2001.

[113] T. M. Cover and J. A. Thomas, *Elements of information theory.* Wiley-Interscience, 1991.

[114] N. Papandreou and T. Antonakopoulos, "Bit and Power Allocation in Constrained Multicarrier Systems: The Single-User Case," *EURASIP Journal on Advances in Signal Processing*, 2008.

[115] K. Eriksson, S. Shi, N. Vucic, M. Schubert, and E. Larsson, "Globally optimal resource allocation for achieving maximum weighted sum rate," in *Global Telecommunications Conference (GLOBECOM 2010), 2010 IEEE*, dec. 2010, pp. 1 –6.

[116] H. Al-Shatri and T. Weber, "Achieving the Maximum Sum Rate Using D.C. Programming in Cellular Networks," *Signal Processing, IEEE Transactions on*, vol. 60, no. 3, pp. 1331–1341, 2012.

[117] S. Boyd, "Ee364b: Lecture slides and notes." [Online]. Available: http://www.stanford.edu/class/ee364b/.

[118] M. Shaat and F. Bader, "Computationally efficient power allocation algorithm in multicarrier-based cognitive radio networks: OFDM and FBMC systems," *EURASIP J. Adv. Signal Process*, vol. 2010, pp. 5:1–5:11, Jan. 2010.

[119] N. Vucic, S. Shi, and M. Schubert, "DC programming approach for resource allocation in wireless networks," in *The 6th Workshop on Resource Allocation in Wireless Networks*, june 2010, pp. 380 –386.

[120] W. Yu and J. Cioffi, "On constant power water-filling," in *Communications, 2001. ICC 2001. IEEE International Conference on*, vol. 6, 2001, pp. 1665–1669 vol.6.

[121] G. Forney and M. Eyuboglu, "Combined equalization and coding using precoding," *Communications Magazine, IEEE*, vol. 29, no. 12, pp. 25–34, 1991.

[122] K. El Baamrani, V. Jimenez, A. Armada, and A. Ouahman, "Multiuser Subcarrier and Power Allocation Algorithm for OFDM/Offset-QAM," *Signal Processing Letters, IEEE*, vol. 17, no. 2, pp. 161 –164, feb 2010.

[123] J. Jang and K. B. Lee, "Transmit power adaptation for multiuser OFDM systems," *Selected Areas in Communications, IEEE Journal on*, vol. 21, no. 2, pp. 171 – 178, feb 2003.

[124] J. Huang, V. Subramanian, R. Agrawal, and R. Berry, "Downlink scheduling and resource allocation for OFDM systems," *Wireless Communications, IEEE Transactions on*, vol. 8, no. 1, pp. 288 –296, Jan. 2009.

[125] W. Yu and R. Lui, "Dual methods for nonconvex spectrum optimization of multicarrier systems," *Communications, IEEE Transactions on*, vol. 54, no. 7, pp. 1310 –1322, july 2006.

[126] M. El Tabach, J.-P. Javaudin, and M. Helard, "Spatial Data Multiplexing Over OFDM/OQAM Modulations," in *Communications, 2007. ICC '07. IEEE International Conference on*, june 2007, pp. 4201 –4206.

[127] A. Ikhlef and J. Louveaux, "Per subchannel equalization for MIMO FBMC/OQAM systems," in *Communications, Computers and Signal Processing, 2009. PacRim 2009. IEEE Pacific Rim Conference on*, aug. 2009, pp. 559 –564.

[128] R. Zakaria, D. Le Ruyet, and M. Bellanger, "Maximum likelihood detection in spatial multiplexing with FBMC," in *Wireless Conference (EW), 2010 European*, april 2010, pp. 1038 –1041.

[129] R. Zakaria and D. Le Ruyet, "A novel FBMC scheme for Spatial Multiplexing with Maximum Likelihood detection," in *Wireless Communication Systems (ISWCS), 2010 7th International Symposium on*, sept. 2010, pp. 461 –465.

[130] ——, "On Maximum Likelihood MIMO detection in QAM-FBMC systems," in *Personal Indoor and Mobile Radio Communications (PIMRC), 2010 IEEE 21st International Symposium on*, sept. 2010, pp. 183 –187.

[131] E. Kofidis and A. Rontogiannis, "Adaptive BLAST decision-feedback equalizer for MIMO-FBMC/OQAM systems," in *Personal Indoor and Mobile Radio Communications (PIMRC), 2010 IEEE 21st International Symposium on*, sept. 2010, pp. 841 –846.

[132] R. Zakaria and D. Le Ruyet, "Partial ISI cancellation with viterbi detection in MIMO filter-bank multicarrier modulation," in *Wireless Communication Systems (ISWCS), 2011 8th International Symposium on*, nov. 2011, pp. 322 –326.

[133] ——, "A Novel Filter-Bank Multicarrier Scheme to Mitigate the Intrinsic Interference: Application to MIMO Systems," *Wireless Communications, IEEE Transactions on*, vol. 11, no. 3, pp. 1112 –1123, march 2012.

[134] R. Zakaria, D. L. Ruyet, and Y. Medjahdi, "On ISI cancellation in MIMO-ML detection using FBMC/QAM modulation," in *ISWCS*, 2012, pp. 949–953.

[135] R. Zakaria and D. Le Ruyet, "On interference cancellation in Alamouti coding scheme for filter bank based multicarrier systems," in *Wireless Communication Systems (ISWCS), 2013 10th International Symposium on*, June 2013, p. 5.

[136] Y. Cheng and M. Haardt, "Widely Linear Processing in MIMO FBMC/OQAM Systems," in *Wireless Communication Systems (ISWCS), 2013 10th International Symposium on*, June 2013, p. 5.

[137] M. Payaró and, A. Pascual-Iserte, and M. Nájar, "Performance comparison between FBMC and OFDM in MIMO systems under channel uncertainty," in *Wireless Conference (EW), 2010 European*, april 2010, pp. 1023 –1030.

[138] I. Estella, A. Pascual-Iserte, and M. Payaró and, "OFDM and FBMC performance comparison for multistream MIMO systems," in *Future Network and Mobile Summit, 2010*, june 2010, pp. 1 –8.

[139] M. Payaró, A. Pascual-Iserte, A. García-Armanda, and M. Sánchez, "Resource Allocation in Multi-Antenna MAC Networks: FBMC vs OFDM," in *Vehicular Technology Conference (VTC Spring), 2011 IEEE 73rd*, may 2011, pp. 1 –5.

[140] D. Palomar, J. Cioffi, and M. Lagunas, "Joint Tx-Rx beamforming design for multicarrier MIMO channels: a unified framework for convex optimization," *Signal Processing, IEEE Transactions on*, vol. 51, no. 9, pp. 2381 – 2401, sept. 2003.

[141] H. Sampath and A. Paulraj, "Joint transmit and receive optimization for high data rate wireless communication using multiple antennas," in *Signals, Systems, and Computers. Conference Record of the Thirty-Third Asilomar Conference on*, vol. 1, 1999, pp. 215–219.

[142] F. Horlin, J. Fickers, T. Deleu, and J. Louveaux, "Interference-free SDMA for FBMC-OQAM," *EURASIP Journal on Advances in Signal Processing*, vol. 2013, no. 1, p. 46, 2013.

[143] Q. H. Spencer, A. L. Swindlehurst, and M. Haardt, "Zero-forcing methods for downlink spatial multiplexing in multiuser MIMO channels," *Signal Processing, IEEE Transactions on*, vol. 52, no. 2, Feb. 2004.

[144] M. Moretti and A. Perez-Neira, "Efficient Margin Adaptive Scheduling for MIMO-OFDMA Systems," *Wireless Communications, IEEE Transactions on*, vol. 12, no. 1, pp. 278–287, 2013.

[145] R. Fischer, C. Windpassinger, A. Lampe, and J. Huber, "MIMO precoding for decentralized receivers," in *Information Theory, 2002. Proceedings. 2002 IEEE International Symposium on*, 2002, p. 496.

[146] ——, "Space-Time Transmission using Tomlinson-Harashima Precoding," in *4th Int. ITG Conf.*, 2002, pp. 139–147.

[147] A. Marshall and I. Olkin, *Inequalities: Theory of Majorization and Its Applications.* New York: Academic, 1979.

[148] R. A. Horn and C. R. Johnson, *Matrix analysis.* Cambridge University Press, 1990.

[149] R. Monzingo and T. Miller, *Introduction to Adaptive Arrays.* New York: Wiley, 1980.

[150] C. R. Horn, R. A.; Johnson, *Matrix Analysis.* Cambridge University Press, 1985.

[151] X. Mestre, M. Sanchez-Fernandez, and A. Pascual-Iserte, "Characterization of the distortion of OFDM/OQAM modulations under frequency selective channels," in *Signal Processing Conference (EUSIPCO), 2012 Proceedings of the 20th European*, aug. 2012, pp. 1598 –1602.

[152] H. Park, S.-H. Park, H.-B. Kong, and I. Lee, "Weighted Sum MSE Minimization under Per-BS Power Constraint for Network MIMO Systems," *Communications Letters, IEEE*, vol. 16, no. 3, pp. 360 –363, march 2012.

[153] W. Rhee and J. Cioffi, "Increase in capacity of multiuser OFDM system using dynamic subchannel allocation," in *Vehicular Technology Conference Proceedings, 2000. VTC 2000-Spring Tokyo. 2000 IEEE 51st*, vol. 2, 2000, pp. 1085 –1089.

[154] I. Kim, I.-S. Park, and Y. H. Lee, "Use of linear programming for dynamic subcarrier and bit allocation in multiuser OFDM," *Vehicular Technology, IEEE Transactions on*, vol. 55, no. 4, pp. 1195–1207, 2006.

[155] I. Wong, Z. Shen, B. Evans, and J. Andrews, "A low complexity algorithm for proportional resource allocation in OFDMA systems," in *Signal Processing Systems, 2004. SIPS 2004. IEEE Workshop on*, oct. 2004, pp. 1 – 6.

[156] Z. Shen, J. Andrews, and B. Evans, "Adaptive resource allocation in multiuser OFDM systems with proportional rate constraints," *Wireless Communications, IEEE Transactions on*, vol. 4, no. 6, pp. 2726 – 2737, nov. 2005.

[157] C. Mohanram and S. Bhashyam, "A sub-optimal joint subcarrier and power allocation algorithm for multiuser OFDM," *Communications Letters, IEEE*, vol. 9, no. 8, pp. 685 – 687, aug. 2005.

[158] C. Y. Wong, R. Cheng, K. Lataief, and R. Murch, "Multiuser OFDM with adaptive subcarrier, bit, and power allocation," *Selected Areas in Communications, IEEE Journal on*, vol. 17, no. 10, pp. 1747–1758, 1999.

[159] D. Kivanc, G. Li, and H. Liu, "Computationally efficient bandwidth allocation and power control for OFDMA," *Wireless Communications, IEEE Transactions on*, vol. 2, no. 6, pp. 1150 – 1158, nov. 2003.

[160] T. Yoo and A. Goldsmith, "On the optimality of multiantenna broadcast scheduling using zero-forcing beamforming," *Selected Areas in Communications, IEEE Journal on*, vol. 24, no. 3, pp. 528–541, 2006.

[161] W. Ho and Y.-C. Liang, "Optimal Resource Allocation for Multiuser MIMO-OFDM Systems With User Rate Constraints," *Vehicular Technology, IEEE Transactions on*, vol. 58, no. 3, pp. 1190–1203, 2009.

Publications in journals

ATENCIÓ ¡

Les pàgines 196 i següents de la tesi contenen el text dels articles citats a continuació, que es poden consultar a les webs dels editors de les revistes.

ATENCIÓN ¡

Las páginas 166 y siguientes de la tesis contienen el texto de los articulos , pueden consultarse en la web del editor de la revista.

ATTENTION ¡

Page 166 and following of the thesis contain the text of the articles are available on the web site editor.

1. Caus, M. ; Perez-Neira, A.I. ; Garcia-Armada, A. *A Discrete Bit Loading Algorithm for FBMC/OQAM* IEEE Signal Processing Letters 2012, vol.19, #6. Doi10.1109/LSP.2012.2192429

2. Caus, M. ; Perez-Neira, A.I. *Transmitter-Receiver Designs for Highly Frequency Selective Channels in MIMO FBMC Systems* IEEE Transactions on Signal Processing vol 60, #12. Doi 10.1109/TSP.2012.2217133

3. Caus,M. ; Perez-Neira, A.I.; Renfors, M. *Low-complexity interference variance estimation methods for coded multicarrier systems: application to SFN.* EURASIP Journal on Advances in Signal Processing 2013, **2013**:163 Doi:10.1186/1687-6180-2013-163

4. Caus, M. ; Perez-Neira, A.I. *Multi-stream transmission for highly frequency selective channels in MIMO-FBMC/OQAM Systems.* IEEE Transactions on Signal Processing, 2014, vol. 62 , Issue: 4 Doi: 10.1109/TSP.2013.2293973